

Design and Development of Planar Lowpass Filters with Sharp Roll-off and Wide Stopband for RF and Wireless Communication Systems

*A thesis submitted to Cochin University of Science and Technology
in partial fulfillment of the requirements
for the award of the degree of*

Doctor of Philosophy
(Faculty of Engineering)

by

Raphika P. M.

Under the guidance of

Prof. Abdulla P.



School of Engineering
Cochin University of Science and Technology, Kochi-22, India.
May 2016

Design and Development of Planar Lowpass Filters with Sharp Roll-off and Wide Stopband for RF and Wireless Communication Systems

Ph.D. Thesis under the Faculty of Engineering

Author

Raphika P. M.

Research Scholar

Electronics and Communication Engineering Division

School of Engineering

Cochin University of Science and Technology

Kochi - 682022

Email: pmraphika@yahoo.co.in

Supervising Guide

Dr. Abdulla P.

Professor

Electronics and Communication Engineering Division

School of Engineering

Cochin University of Science and Technology

Kochi - 682022

Email: abdulla@cusat.ac.in

School of Engineering

Cochin University of Science and Technology

Kochi-22

May 2016

**School of Engineering
Cochin University of Science and Technology
Kochi, India**

Dr. Abdulla P.
Professor




Ph: 9496445235
Email: abdulla@cusat.ac.in

Certificate

This is to certify that the thesis entitled **Design and Development of Planar Lowpass Filters with Sharp Roll-off and Wide Stopband for RF and Wireless Communication Systems** is a bona fide record of research work carried out by Ms. Raphika P. M., under my supervision and guidance at the Electronics and Communication Engineering Division, School of Engineering, Cochin University of Science and Technology, Kochi. The results embodied in this thesis or parts of it have not been presented for any other degree.

I further certify that the corrections and modifications suggested by the audience during the pre-synopsis seminar and recommended by the Doctoral Committee of Ms. Raphika P. M. are incorporated in the thesis.

*Kochi
May 2016*


Dr. Abdulla P.
Professor
School of Engineering
CUSAT, Kochi-22.

Declaration

*I hereby declare that the thesis entitled **Design and Development of Planar Lowpass Filters with Sharp Roll-off and Wide Stopband for RF and Wireless Communication Systems** is a bona fide record of the research work carried out by me, under the supervision of Dr. Abdulla P, Professor, Electronics and Communication Engineering Division, School of Engineering, Cochin University of Science and Technology, Kochi-22. I further declare that this work has not formed the basis for the award of any other Degree, Diploma, Associateship, Fellowship or any other title for recognition.*

Raphika P. M.

Kochi

May 2016

Acknowledgements

First of all, I bow before THE ALMIGHTY for all the blessings. Only with his blessings, I could bring all my efforts to a successful completion.

I deem it a rare privilege to extend my deep sense of gratitude to Dr. Abdulla P., Professor, School of Engineering, Cochin University of Science and Technology for introducing me to the field of radio frequency and microwave filters. His guidance, motivation and constant encouragement throughout the last four years were vital for the completion of my doctoral work. He has kindly provided all the computer software, work station, substrate materials and measuring instruments. I consider it as a great boon to have Dr. Abdulla P., an eminent academician as my research supervisor.

I would also like to thank my Doctoral Committee member, Dr. Binu Paul and Prof. G. Madhu, Principal, School of Engineering for their suggestions and support during the course of this work.

I also extend my sincere thanks to Dr. A. Biju, Principal, M.E.S. College, Maramapally for his constant encouragement and support. I also thank Dr. P.A. Fathima, former Principal, M.E.S. College, Marampally, who encouraged to apply for the Ph.D. course and Faculty Improvement Programme of the UGC for doing the Ph.D. work. Gratitude is also extended to all the management committee members of M.E.S. College, Marampally especially to Dr. Zakariya K.A. for his whole hearted support.

I thank from the bottom of my heart Ms. Jasmine P.M., who had been my work associate at the Department for almost the entire period of my research. We have been complimentary to each other in many ways and this enabled us to work together productively.

I would like to thank my friends Ms. Rekha T.K, Ms. Sindhu Rani and Ms. Bhavana for their support and suggestions while drafting research papers. The arguments and criticism that ensured have greatly contributed in getting this work to the level of fructification and refinement that it has reached.

I am grateful to Dr. Nishamol, Dr. Radhakrishnan and Ms. Bindu C.J., for their valuable contribution and timely help. I remember with gratitude the continues and consistent support from my co-researchers, Ms. Anu A.R., Ms. Jesna Anver, Mr. Ajimsha Moideen and Ms. Ami Iqbal. They remained as the sounding board for ideas.

I would like to thank Dr. Ratheesh, C-MET, Thrissur, Kerala, India for providing low loss dielectric substrate to carry out a part of this work. Sincere thanks are also extended to Dr. Nijas C.M., Dr. Dinesh R. and Mr. Deepak, of the CREMA Lab for their timely help.

I am indebted and thankful to my friend and colleague Ms. Jaseena K.U. for her remarkable way of encouraging and boosting morale. I remember with gratitude all the teaching and nonteaching staffs of M.E.S. College, Marampally for their valuable support and positive strokes.

I am extremely grateful to the University Grants Commission for giving me the opportunity to do the research by availing the Faculty Development Programme of UGC.

Special thanks are also extended to all the staff members of Section A, School of Engineering especially Mr. Ajas, Mr. Nazer, Ms. Anjana and Ms. Indira T.C for their timely help.

My deepest gratitude goes to my mother and family members for their unflagging love and prayers throughout my life. I am obliged to my late father whose dream is fulfilled through this thesis and my brother Mr. Nizar Mohammed for helping with fabrication.

I am really proud of my husband Dr. Naushad K.M. and cherubs Adu and Ami for their spirit of love, patience and encouragement which gave me the courage to persevere.

Raphika P.M.

Preface

Filters are one of the essential components in the RF and wireless communication systems. Small sized planar lowpass filters with good electrical characteristics along with low cost, light weight and ease of fabrication are highly desirable for the front end of modern communication systems to suppress harmonics and spurious signals. Design of compact lowpass filters with improved performance and diverse specifications for numerous applications is a huge challenge.

In this thesis, high performance planar compact lowpass filters using multiple patch resonators on high impedance transmission line are developed. Design techniques of different types of patch resonators and their modifications to enhance the performance of the filters are presented.

Patch resonators are designed by using high impedance short circuited stubs and low impedance open circuited patches. In the first stage of filter realization, compact lowpass filter having sharp roll-off using triangular and funnel patch resonators is presented. The structure is modified further to enhance the relative stopband bandwidth of the filter. In the third stage, another resonator has been introduced near the feed line to achieve sharp roll-off for the same cutoff frequency, stopband bandwidth and suppression level. To obtain compactness, high suppression level and wide stopband in filter design, low thickness substrate is tested and proved in the fourth stage.

Realizations of planar compact lowpass filter with very sharp roll-off near the cutoff frequency have been presented using stepped impedance polygonal patch resonators. By increasing the patch size and number of resonators, the stopband bandwidth and suppression level have to be enhanced to a great extent. Enhancement of performance characteristics of lowpass filter design is continually being extended. By using high value capacitance patch, the stopband suppression level of the filter with sharp roll-off rate is achieved. Elliptic function lowpass filter with ultra-sharp roll-off is also developed using elliptic shaped patch resonators.

Throughout the study, low cost substrate having permittivity 4.4 is used for the filter design. All the designed filters have been fabricated and predicted results are validated by the measurements.

CONTENTS

| | |
|--|-------------|
| List of Illustrations | i |
| List of Tables | xi |
| 1. Introduction | 1-8 |
| 1.1 Motivation..... | 2 |
| 1.2 Objectives of the Study..... | 3 |
| 1.3 Methodology..... | 5 |
| 1.4 Orientation of the Thesis..... | 6 |
| 2. Survey of Literature | 9-42 |
| 2.1 Planar Lowpass Filters..... | 10 |
| 2.2 Performance Characteristics of a Lowpass Filter..... | 10 |
| 2.2.1 Cutoff frequency (f_c)..... | 11 |
| 2.2.2 Insertion Loss (IL)..... | 12 |
| 2.2.3 Return Loss (RL)..... | 12 |
| 2.2.4 Rol-off rate (ξ)..... | 13 |
| 2.2.5 Relative Stoband Bandwidth (RSB)..... | 13 |
| 2.2.6 Normalized Circuit Size (NCS)..... | 14 |
| 2.2.7 Group Delay (τ_d)..... | 14 |
| 2.3 Different types of Lowpass Filters..... | 15 |
| 2.3.1 Butterworth Filters..... | 15 |
| 2.3.2 Chebyshev Filter..... | 16 |
| 2.3.3 Elliptic Function Filter..... | 18 |
| 2.4 Conventional method of Lowass Fiter Design..... | 19 |
| 2.4.1 Lowpass Filter Design using Stepped Impedance Method..... | 19 |

| | |
|---|---------------|
| 2.4.2 Lowpass Filter Design using Open Circuited Stub Method | 22 |
| 2.5 Survey of Literature | 28 |
| 2.5.1 Microstrip Resonators with Defective Ground Structure | 29 |
| 2.5.2 Microstrip resonators without DGS..... | 29 |
| References..... | 35 |
| 3. Compact Lowpass Filter using Funnel and Triangular Patch Resonators..... | 43-102 |
| 3.1 Introduction | 44 |
| 3.2 Basic Characteristics of Microstrip Line..... | 47 |
| 3.3 Filter I- Compact Lowpass Filter using Funnel and Triangular Patch Resonators | 51 |
| 3.3.1 Filter Design Considerations..... | 51 |
| 3.3.2 Design of Patch Resonators..... | 52 |
| 3.3.3 S-Parameter calculations..... | 54 |
| 3.3.4 Design of Symmetrical FPR..... | 57 |
| 3.3.5 Design of Symmetrical TPR..... | 58 |
| 3.3.6 Parametric Analysis of Filter I..... | 62 |
| 3.3.7 L-C Equivalent Circuit Analysis..... | 64 |
| 3.3.8 Equivalent Circuit Parametric Analysis..... | 68 |
| 3.3.8.1 Transmission line inductance, ($L1/L2$) | 68 |
| 3.3.8.2 Inductance of high impedance stub, ($Lr1/Lr2$)..... | 70 |
| 3.3.8.3 Capacitance of low impedance patch, ($Cr1/Cr2$)..... | 71 |
| 3.3.8.4 Coupling Capacitance, (Cc)..... | 74 |
| 3.3.9 Measurement results of Filter I..... | 75 |
| 3.4 Filter II- Compact Planar Lowpass Filter with modified FPR and TPRs..... | 78 |
| 3.4.1 Filter Design Considerations..... | 78 |

| | |
|--|-----|
| 3.4.2 Parametric Analysis of Filter II..... | 81 |
| 3.4.2.1 Stub Height, H1..... | 81 |
| 3.4.2.2 Width of the Transmission Line, (W3)..... | 82 |
| 3.4.2.3 Position of high impedance stub of TPRs relative to the patch, (L4)..... | 84 |
| 3.4.3 Measured Results of Filter II..... | 85 |
| 3.5 Filter III- Compact Lowpass Filter with sharp roll-off and wide stopband using modified FPR and TPRs and suppressing cells..... | 89 |
| 3.5.1 Filter Design Considerations..... | 89 |
| 3.5.2 Simulated and Measured Results of Filter III..... | 90 |
| 3.6 Filter IV-Compact wide stopband lowpass filter with high suppression level..... | 92 |
| 3.6.1 Design of Filter IV | 93 |
| 3.4.2 Simulated and Measured Results of Filter IV..... | 96 |
| 3.7 Conclusions..... | 98 |
| References..... | 100 |

**4. Compact Lowpass Filter with Sharp 20 dB Roll-off Rate and Wide
Stopband using Stepped Impedance Patch Resonators.....103-139**

| | |
|---|-----|
| 4.1 Introduction..... | 104 |
| 4.2 Design of Stepped Impedance Patch Resonators (SI-PRs)..... | 105 |
| 4.2.1 Design of SI-PR1..... | 105 |
| 4.2.2 Design of SI-PR2..... | 110 |
| 4.3 Compact Elliptic Function lowpass Filter Design using SI-PRs..... | 111 |
| 4.3.1 Equivalent Circuit Analysis..... | 113 |
| 4.3.2 Parametric Analysis..... | 115 |
| 4.3.2.1 Stub Position of SI-PR2, (l4)..... | 115 |
| 4.3.2.2 Stub Height, (h2)..... | 117 |
| 4.3.2.3 Width of High Impedance Transmission Line, (w2).... | 117 |

| | |
|---|-----|
| 4.3.3 Simulation and measurement Results of Filter using SI-PRs..... | 119 |
| 4.4 Compact Elliptic Function lowpass Filter Design using modified SI-PRs..... | 123 |
| 4.4.1 Parametric Analysis..... | 124 |
| 4.4.1.1 Height of HIIS of SI-PR1, (h2)..... | 124 |
| 4.4.1.2. Position of HIIS of SI-PR2, (l4)..... | 126 |
| 4.4.2 Simulation and Measurements Results of Compact Lowpass Filter with Modified SI-PR1..... | 127 |
| 4.5 Compact Elliptic Function lowpass Filter Design using SI-PPR..... | 129 |
| 4.6 Compact and Wide Stopband Lowpass Filter Design using SI-PPR..... | 132 |
| 4.7 Conclusions..... | 136 |
| References..... | 138 |

5. Compact Lowpass Filter with High Suppression Level using Octagonal and Heptagonal Patch resonator..... 140-168

| | |
|---|-----|
| 5.1 Introduction..... | 141 |
| 5.2 Compact Lowpass Filter design using Octagonal Patch Resonator..... | 141 |
| 5.3 Compact Lowpass Filter design using Heptagonal Patch Resonator..... | 146 |
| 5.4 Equivalent Circuit Analysis..... | 150 |
| 5.5 Parametric analysis..... | 152 |
| 5.5.1 HPR Parameters..... | 152 |
| 5.5.2 OPR Parameters..... | 155 |
| 5.5.3 Width of Gap Size between HPR and OPR Patches, (g1)..... | 160 |
| 5.5.4 Width of High Impedance Transmission Line, (w2)..... | 160 |
| 5.6 Measurement Results of Filter using OPR and HPR..... | 162 |

| | |
|--|----------------|
| 5.7 Conclusions..... | 165 |
| References..... | 167 |
| 6. Compact Lowpass Filter with Ultra Sharp Roll-Off rate using Elliptical Patch Resonators..... | 169-185 |
| 6.1 Introduction..... | 170 |
| 6.2 Design of Stepped Impedance Patch Resonators..... | 170 |
| 6.2.1 Design of Elliptical Patch Resonator..... | 171 |
| 6.2.2 Design of Modified Rectangular Patch Resonators..... | 174 |
| 6.3 Design of Compact Lowpass Filter with Sharp Roll-off using SI-PRs..... | 176 |
| 6.4 Simulation and Measurement Results of Proposed Filter..... | 179 |
| 6.5 Conclusions..... | 183 |
| References..... | 184 |
| 7. Conclusions and Scope of Future Developments..... | 186-191 |
| 7.1 Summary of Achievements..... | 187 |
| 7.2 Scope of Future Developments..... | 190 |
| List of Publications and Honors..... | 192-195 |

List of Illustrations

| | | |
|------------|---|----|
| Fig. 2.1 | S-Parameter characteristics of a lowpass filter..... | 11 |
| Fig. 2.2 | Butterworth type lowpass filter response..... | 16 |
| Fig. 2.3 | Chebyshev type response of a lowpass filter..... | 17 |
| Fig. 2.4 | Elliptic function type response of a lowpass filter..... | 18 |
| Fig. 2.5 | (a) Geometry of stepped impedance microstrip lowpass filter, (b) L-C equivalent circuit model..... | 20 |
| Fig. 2.6 | (a) Layout of three pole, stepped impedance lowpass filter on a substrate of $\epsilon_r = 10.8$, $t = 1.27$ mm, (b) L-C model equivalent circuit | 21 |
| Fig. 2.7 | Simulated S-Parameter characteristics of three pole stepped impedance lowpass filter..... | 22 |
| Fig. 2.8. | (a) Layout of three pole, open circuited stub lowpass filter on a substrate of $\epsilon_r = 10.8$, $t = 1.27$ mm, (b) L-C model equivalent circuit..... | 23 |
| Fig. 2.9 | Fig. 2.9 Simulated performance of three pole, open circuited lowpass filter on a substrate of $\epsilon_r = 10.8$, $t = 1.27$ mm | 24 |
| Fig. 2.10 | 2.10 Comparison of passband frequency response of filters demonstrated in Fig. 2.6(a) and Fig. 2.8(a)..... | 24 |
| Fig. 2.11 | Comparison of wideband frequency responses of filters demonstrated in Fig. 2.6(a) and Fig. 2.8(a)..... | 25 |
| Fig. 2.12 | (a) Layout of a seven pole open circuited lowpass filter, (b) L-C model equivalent circuit..... | 26 |
| Fig. 2.13. | Comparison of filter performance of the three microstrip designs..... | 27 |
| Fig. 3.1 | General microstrip structure | 47 |

| | | |
|------------|--|----|
| Fig. 3.2 | Impedance characteristics of microstrip line as a function of permittivity, ϵ_r of the substrate for thickness $t= 1.6$ mm | 50 |
| Fig. 3.3 | Impedance characteristics of microstrip line as a function of thickness, t of the substrate for permittivity $\epsilon_r = 4.4$ | 50 |
| Fig. 3.4 | (a) High impedance short circuited stub, (b) Low impedance open circuited patch..... | 51 |
| Fig. 3.5 | (a) Geometry of FPR, (b) L-C model equivalent circuit of FPR..... | 53 |
| Fig. 3.6 | (a) Geometry of TPR, (b) L-C model equivalent circuit of TPR..... | 53 |
| Fig. 3.7 | (a) Layout of FPR on high impedance line, (b) Equivalent Circuit..... | 54 |
| Fig. 3.8 | EM, L-C and MATLAB coded simulated $ S_{21} $ characteristics FPR on high impedance line..... | 56 |
| Fig. 3.9 | Fig. 3.9 Geometry of FPR on transmission line ($W1 = 0.6$ mm, $H1 = 1.6$ mm) | 57 |
| Fig. 3.10. | Simulated S-Parameter characteristics of FPR as a function of $W1$ and $H1$. Optimized dimensions are: $W1 = 0.6$ mm, $H1 = 1.6$ mm | 58 |
| Fig. 3.11 | Geometry of symmetrical TPR on high impedance transmission line ($W2 = 0.2$ mm, $H1 = 1.6$ mm) | 59 |
| Fig. 3.12 | Fig. 3.12 Simulated S-Parameters of symmetrical TPR as a function of position along the transmission line..... | 59 |
| Fig. 3.13 | Simulated S parameters characteristics with two TPRs | 60 |
| Fig. 3.14 | Simulated S parameters with FPR and two TPRs..... | 61 |
| Fig. 3.15 | Simulated $ S_{21} $ characteristics of the Filter I as a function of stub height, $H1$ from the microstrip line..... | 63 |
| Fig. 3.16 | Fig. 3.16. Simulated $ S_{21} $ characteristics of the Filter I as a function of gap size, (W) between the low impedance patches..... | 63 |

| | | |
|------------|--|----|
| Fig. 3.17 | First Null frequency variation of the Filter I as a function of HI and W | 64 |
| Fig. 3.18. | The layout of the proposed Filter I..... | 65 |
| Fig. 3.19 | L-C model equivalent circuit of the Filter I | 65 |
| Fig. 3.20 | (a) Configuration to calculate the capacitance of resonant patch, (b) Equivalent circuit..... | 66 |
| Fig. 3.21 | EM and L-C simulation results of the Filter I..... | 67 |
| Fig. 3.22 | $ S_{21} $ Characteristics of the Filter I as a function of L_1 | 69 |
| Fig. 3.23 | $ S_{21} $ Characteristics of the Filter I as a function of L_2 | 69 |
| Fig. 3.24. | $ S_{21} $ Characteristics of the Filter I as a function of L_{r1} | 70 |
| Fig. 3.25. | $ S_{21} $ Characteristics of the Filter I as a function of L_{r2} | 70 |
| Fig. 3.26 | (a) $ S_{21} $ Characteristics of the Filter I as a function of C_{r1} , (b) passband performance of Filter I as a function of C_{r1} | 72 |
| Fig.3.27 | (a) $ S_{21} $ Characteristics of the Filter I as a function of C_{r2} , (b) passband performance of Filter I as a function of C_{r2} | 73 |
| Fig. 3.28 | $ S_{21} $ Characteristics of the Filter I as a function of coupling capacitance C_c | 74 |
| Fig.3.29 | Measured results of proposed Filter I..... | 75 |
| Fig.3.30 | Measured group delay characteristics of Filter I..... | 76 |
| Fig. 3.31 | Photograph of prototype of Filter I..... | 77 |
| Fig. 3.32 | (a) Layout of Filter I with enhanced length of transmission line and patch size, (b) Simulated S-Parameters..... | 78 |
| Fig. 3.33 | Passband $ S_{21} $ characteristics of modified Filter I..... | 79 |
| Fig. 3.34 | Equivalent relation between TPRs and FPR with modified TPRs FPR..... | 80 |
| Fig. 3.35 | $ S_{21} $ Characteristics of the Filter II as a function of stub height, HI | 81 |
| Fig. 3.36 | $ S_{11} $ Characteristics of Filter II as a function stub height, HI | 82 |

| | | |
|-----------|---|-----|
| Fig. 3.37 | $ S_{21} $ Characteristics of Filter II as a function transmission line width, $W3$ | 83 |
| Fig. 3.38 | $ S_{11} $ Characteristics of Filter II as a function transmission line width, $W3$ | 83 |
| Fig. 3.39 | $ S_{21} $ Characteristics of Filter II as a function of position of high impedance stub TPRs relative to the patch, $L4$ | 84 |
| Fig. 3.40 | $ S_{11} $ Characteristics of Filter II as a function of position of high impedance stub TPRs relative to the patch, $L4$ | 85 |
| Fig. 3.41 | Layout of proposed Filter II..... | 86 |
| Fig. 3.42 | Simulated and measured results of Filter II..... | 87 |
| Fig. 3.43 | Photograph of prototype of Filter II..... | 87 |
| Fig. 3.44 | The measured group delay characteristics of Filter II..... | 88 |
| Fig. 3.45 | The measured VSWR Characteristics of Filter II..... | 88 |
| Fig. 3.46 | Layout of the proposed Filter III..... | 89 |
| Fig. 3.47 | Simulated and measured results of Filter III..... | 90 |
| Fig. 3.48 | Measured group delay characteristics of Filter III..... | 91 |
| Fig. 3.49 | Photograph of prototype of Filter III..... | 91 |
| Fig. 3.50 | (a) Layout of the corrugated high impedance transmission line, (b) Layout of U- shaped high impedance stub of resonator 2..... | 94 |
| Fig. 3.51 | Geometry of unit cell model of modified funnel patch resonator | 95 |
| Fig. 3.52 | Geometry of unit cell model of modified triangular patch resonator..... | 95 |
| Fig. 3.53 | Schematic structure of the proposed Filter IV..... | 96 |
| Fig. 3.54 | Simulated and measured results of of Filter IV..... | 97 |
| Fig. 3.55 | Photograph of prototype Filter IV..... | 97 |
| Fig. 4.1 | Unit cell model of SI-PR1, (a) Structure of unit cell, (b) L-C equivalent circuit..... | 106 |

| | | |
|------------|--|-----|
| Fig. 4.2 | Configuration of the LICP of SI-PR1, (a) Patch 1, (b) Patch 2 (c) Patch 3 (d) Proposed LICP of SI-PR1..... | 107 |
| Fig. 4.3. | Frequency response characteristics of unit cell model of resonator 1 as a function of patch size..... | 108 |
| Fig. 4.4. | Geometry of $\lambda_g/2$ SI-PR 1 with L-C equivalent circuit and performance characteristics. (a) Geometry, (b) L-C equivalent circuit..... | 109 |
| Fig. 4.5. | Simulated S-Parameter characteristics of $\lambda_g/2$ SI-PR1..... | 110 |
| Fig. 4.6 | Unit cell model, geometry and frequency response characteristics of SI-PR2. (a) Unit cell model and L-C equivalent circuit, (b) Geometry of SI-PR2, (c) Frequency response characteristics SI-PR2..... | 111 |
| Fig. 4.7 | Layout of compact lowpass filter with SI-PRs..... | 112 |
| Fig. 4.8 | Simulated transmission characteristics as a function of resonators..... | 113 |
| Fig. 4.9 | Equivalent circuit of compact elliptic function lowpass filter using SI-PRs..... | 114 |
| Fig. 4.10 | Fig. 4.10 EM and L-C model transmission characteristics of compact elliptic function lowpass filter using SI-PRs..... | 114 |
| Fig. 4.11 | Simulated S-Parameters of the proposed filter as a function of the connecting stub position of SI-PR2, (l_4) | 116 |
| Fig. 4.12 | Simulated S-Parameters of the proposed filter as a function of the connecting stub height, (h_2)..... | 116 |
| Fig. 4.13 | The effect of width of HIML w_2 on 3 dB cutoff frequency, f_c and first transmission zero frequency, f_z of the compact filter with SI-PRs | 118 |
| Fig. 4.14 | The effect of characteristic impedance Z_C on 3 dB cutoff frequency f_c and first transmission zero frequency, f_z of the compact filter with SI-PRs..... | 118 |
| Fig. 4.15. | Simulated $ S_{21} $ characteristics of the compact filter with SI-PRs as a function of width, w_2 of HIML..... | 119 |

| | | |
|-----------|---|-----|
| Fig. 4.16 | Simulated and measured result of compact elliptic function lowpass filter with SI-PRs..... | 119 |
| Fig. 4.17 | Measured group delay characteristics of the compact elliptic function lowpass filter with SI-PRs..... | 120 |
| Fig. 4.18 | Measured VSWR characteristics of the compact lowpass filter with SI-PRs..... | 121 |
| Fig. 4.19 | Photograph of the proposed compact lowpass filter with SI-PRs..... | 121 |
| Fig. 4.20 | Layout of compact lowpass filter modified SI-PR1..... | 124 |
| Fig. 4.21 | Transmission characteristics of filter as a function of height of HIIS of SI-PR1, h_2 | 125 |
| Fig. 4.22 | Reflection characteristics of filter as a function of height of HIIS of SI-PR1, h_2 | 125 |
| Fig. 4.23 | Transmission characteristics of filter as a function of position of HIIS of SI-PR2, l_4 | 126 |
| Fig. 4.24 | Reflection characteristics of filter as a function of position of HIIS of SI-PR2, l_4 | 126 |
| Fig. 4.25 | Measured and simulated results of compact filter with modified SI-PRs..... | 128 |
| Fig. 4.26 | Measured group delay characteristics of the filter with modified SI-PRs..... | 128 |
| Fig. 4.27 | A photograph of prototype compact filter with modified SI-PRs..... | 129 |
| Fig. 4.28 | Unit cell model of proposed SI-PPR..... | 129 |
| Fig. 4.29 | Simulated S-Parameters of SI-PPR and SI-PR1..... | 130 |
| Fig. 4.30 | Layout of the proposed Filter with SI-PPR..... | 131 |
| Fig. 4.31 | Photograph of compact lowpass filter with SI-PPR..... | 131 |
| Fig. 4.32 | Simulated and measured result of proposed Filter with SI-PPR..... | 132 |

| | | |
|-----------|--|-----|
| Fig. 4.33 | Layout of the proposed compact and wide stopband lowpass filter design using SI-PPR..... | 133 |
| Fig. 4.34 | The photograph of the proposed filter with SI-PPR..... | 134 |
| Fig.4.35 | Simulated and measured result of proposed compact lowpass filter with wide stopband..... | 134 |
| Fig, 4.36 | Measured group delay characteristics of proposed compact lowpass filter with wide stopband..... | 135 |
| Fig. 5.1 | Geometric structure of the proposed lowpass filter using OPRs... | 142 |
| Fig. 5.2 | Simulated S-Parameters of proposed filter with centre OPR..... | 143 |
| Fig. 5.3 | Simulated S-Parameters of filter response with side OPRs..... | 143 |
| Fig. 5.4 | Simulated S-Parameters characteristics of filter with two types of OPRs..... | 144 |
| Fig. 5.5 | Simulated and measured results of the filter with OPRs..... | 145 |
| Fig. 5.6 | Photograph of the fabricated filter with OPRs..... | 145 |
| Fig. 5.7 | Layout and photograph of compact lowpass filter with HPR and OPRs (a) Layout, (b) Photograph..... | 146 |
| Fig. 5.8 | Measured S-Parameters characteristics of lowpass filter using OPR and HPR discussed in section 5.2 and 5.3..... | 147 |
| Fig. 5.9 | Simulated magnitude response of the lowpass filter with centre HPR and side OPRs designed on FR4 material with loss tangent of 0.02 | |
| Fig. 5.10 | Simulated magnitude response of the lowpass filter with centre HPR and side OPRs designed on C-MET/LK4.3 material with loss tangent of 0.0018..... | 149 |
| Fig. 5.11 | L-C Equivalent circuit model of the filter with HPR and OPRs... | 151 |
| Fig. 5.12 | L-C and EM simulation results of the filter HPR and OPRs..... | 151 |
| Fig. 5.13 | $ S_{21} $ characteristics of the filter as a function of width of high impedance stub of HPR, w_I | 152 |
| Fig. 5.14 | $ S_{21} $ characteristics of the filter as a function of width of high impedance stub of HPR, w_I | 153 |

| | | |
|-----------|--|-----|
| Fig. 5.15 | $ S_{21} $ characteristics of the filter as a function of HPR patch capacitance, C_{r1} | 154 |
| Fig. 5.16 | Passband insertion loss characteristics of the filter as a function of HPR patch capacitance, C_{r1} | 155 |
| Fig. 5.17 | $ S_{21} $ characteristics of the filter as a function of width, w_3 | 156 |
| Fig. 5.18 | $ S_{21} $ characteristics of the filter as a function of OPR patch capacitance, C_{r2} , (a) Passband and stopband characteristics, (b) Passband characteristics..... | 157 |
| Fig. 5.19 | Current distribution characteristics of filter at $T_{Z1} = 2.32\text{GHz}$ | 158 |
| Fig. 5.20 | Current distribution characteristics of filter at $T_{Z2} = 2.9\text{ GHz}$ | 159 |
| Fig. 5.21 | Current distribution characteristics of filter at $T_{Z3} = 7.75\text{ GHz}$ | 159 |
| Fig. 5.22 | $ S_{21} $ Characteristics of the filter as a function of width of the transmission line, w_2 | 161 |
| Fig. 5.23 | $ S_{11} $ Characteristics of the filter as a function of width of the transmission line, w_2 | 161 |
| Fig. 5.24 | Simulated and measured results of the proposed lowpass filter centre HPR and side OPRs..... | 163 |
| Fig. 5.25 | Measured group delay characteristics the filter..... | 163 |
| Fig. 5.26 | Measured VSWR characteristics the filter..... | 164 |
| Fig. 5.27 | Photograph of the proposed filter..... | 164 |
| Fig. 6.1 | (a) Geometry of the unit cell model of EPR, (b) L-C equivalent circuit..... | 171 |
| Fig. 6.2 | Simulated S-Parameters of unit cell model of EPR..... | 172 |
| Fig. 6.3 | (a) Geometry of $\lambda_g/2$ EPR, (b) L-C equivalent circuit..... | 173 |
| Fig. 6.4 | Simulated S-Parameters of $\lambda_g/2$ EPR as a function of the width of high impedance short circuited stub, w_1 | 174 |
| Fig. 6.5 | (a) Geometry of unit cell model of MRPR, (b) L-C equivalent circuit..... | 175 |
| Fig. 6.6 | (a) Geometry of $\lambda_g/2$ MRPR, (b) Simulated S-Parameters..... | 175 |

| | | |
|-----------|---|-----|
| Fig. 6.7 | (a) Configuration of lowpass filter with EPR and MRPR, (b) Simulated S-Parameters characteristics..... | 177 |
| Fig. 6.8 | Passband insertion loss characteristics of the filter as a function of MRPR patch length l_6 | 178 |
| Fig. 6.9 | Layout of the proposed lowpass filter..... | 180 |
| Fig. 6.10 | Photograph of the prototype filter..... | 180 |
| Fig. 6.11 | Measured and simulated transmission characteristics of the filter..... | 181 |
| Fig. 6.12 | Measured and simulated reflection characteristics of the filter..... | 181 |
| Fig. 6.13 | Measured and simulated passband group delay characteristics of the filter..... | 182 |

List of Tables

| | | |
|------------|---|-----|
| Table 2.1. | Three microstrip lowpass filter designs with open circuited stubs..... | 27 |
| Table 3.1. | Comparison between performance of Filter I and other published works in the literature..... | 77 |
| Table 3.2. | IL comparison between filter shown in Fig. 3.32 (a) and filter II..... | 80 |
| Table 3.3. | Table 3.3. Comparison between performance of Filter III and similar reported work..... | 93 |
| Table 3.4. | Comparison between performance of Filter IV and similar work reported in the literature..... | 98 |
| Table 3.5 | Comparison between Proposed Filters using FPR and TPRs..... | 100 |
| Table 4.1 | Response of SI-PR1 related to the size of LICP..... | 108 |
| Table 4.2 | Comparison between performance of filter with SI-PRs and other published work in the literature | 122 |
| Table 4.3 | Performance comparison of proposed filter with SI-PPR and similar published work in the literature..... | 135 |
| Table 4.4 | Performance comparison of compact lowpass filters using SI-PRs and SI-PPR..... | 137 |
| Table 5.1 | Filter characteristics as a function of g_1 | 161 |
| Table 5.2 | Comparison of compact lowpass filter using centre HPR and side OPRs with previous work reported in the literature..... | 165 |
| Table 5.3 | Comparison between performance of the filters discussed in this chapter..... | 167 |
| Table 6.1 | Performance comparison of performance of proposed lowpass filter with previously reported high performance lowpass filters..... | 182 |

Chapter 1

Introduction

This chapter explores the challenges in the design and development of high performance lowpass filters, and motivation for the work along with the design objectives. The chapter concludes with the execution methodology of the works and the details of orientation of the present thesis.

1.1 Motivation

Microwave lowpass filters have been widely used as an important building block in front-end circuitry of various radio frequency and wireless communication systems to suppress harmonics and spurious signals without interfering the desired signals. These elements are in existence for over more than a century. But the standards and technologies currently used in modern RF and wireless communication system applications such as in mobile communications, satellite and space communications and high speed multimedia require lowpass filters with drastically different characteristics. New technologies must be developed to realize lowpass filters which exhibit miniaturization, portability, low cost, and excellent in and out-of band performances. For example, lowpass filters used to integrate with UWB chipless RFID receivers require sharp transition characteristics with wide and high stopband suppression levels. The sharp roll-off rate is difficult to achieve by following the conventional methods of lowpass filter design, which supports only gradual switching characteristics with limited stopband performances. Besides, the slope of transition can be improved by introducing more number of reactive elements, which increases the insertion loss in passband and layout area of the filter. Thus, reducing the filter size with good transition characteristics is a great challenge to researchers. Furthermore, modern high data rate communication systems require additional specifications that introduce fabrication complexity. The suppression rate beyond passband is one of the evaluating criteria for these filters. Due to the restriction of minimizing the dimensions of the filter, it is a challenge to the researchers to design a lowpass filter with sharp roll-off rate and wide stopband with high suppression levels.

Presently, planar transmission lines have much attention compared to coaxial, dielectric and waveguides in modern communication systems due to its practical features including compact size, low cost, light weight, good affinity with active circuit elements and ease of fabrication. Besides, microstrip lowpass filters provide low insertion loss in the passband and high attenuation in the stopband together with good switching characteristics for a wide applicable frequency range, which can be obtained by employing various kinds of substrate materials. Moreover, it is also possible to design planar lowpass filters for the use at higher microwave frequencies. The technique of positioning the transmission zeroes in the stopband in order to selectively suppress the unwanted harmonics and thereby enhancing the stopband bandwidth is relatively possible by using microstrip lowpass filters.

Design and realization of lowpass filter can be challenging for several reasons. There is no single technology or filter topology suitable for all applications in radio frequency and wireless communication systems. There is also a fundamental limitation imposed by the relationship between the filter size, substrate characteristics and frequency of operations. Many of the simpler design procedures can sometimes arrive at the geometries that are unrealizable and the available literature is generally focused on the filter design with high cost material with low value of substrate parameters.

1.2 Objectives of the Study

Several design techniques have been proposed in the literature to enhance the performance characteristics of microstrip lowpass filters. Although most of the suggested methods are good choice in modern communication systems, that suffer deficiencies such as poor selectivity, large layout area,

limited stopband bandwidth, difficulty to integrate with other circuit elements, poor reflection performance and use of high cost materials. The design and development of compact planar lowpass filters with good electrical and mechanical characteristics is an emerging area of research in the national and international level.

This thesis is the outcome of the design methodologies and experimental investigations of high performance, low cost, planar lowpass filters with sharp roll-off rate, wide stopband bandwidth and high stopband suppression level by loading multiple patch resonators on high impedance transmission line. The main objectives of the thesis are:

- Design and development of planar compact lowpass filters with sharp roll-off rate, wide stopband bandwidth and high suppression level using low cost substrates.
- High performance lowpass filter realization by loading multiple patch resonators of semi-lumped element characteristics on a high impedance microstrip transmission line.
- The patch resonators are designed using high impedance short circuited stubs and low impedance open circuited patches.
- Extract the L-C equivalent circuit model of the designed filters and detailed analysis of the circuit to study the dependence of each circuit component on the performance characteristics of the filters.
- Develop prototype for all the designed filters using low cost materials, preferably FR4.
- Study the role of thickness and loss tangent of the substrate material that influences the performance characteristics of the filter.
- Validate the designed results of the filters with experimental results.

1.3 Methodology

High performance and compact lowpass filters are in great demand for present communication systems to suppress harmonics and spurious signals. The works are mainly concentrated on design and development of planar lowpass filters with sharp roll-off and wide stopband. The filters are designed and realized using microstrip transmission media because they possess low insertion loss in the passband and infinite attenuation in the stopband together with compact size, low cost and ease of fabrication. The filter designs are based on loading multiple high impedance stub loaded patch resonators on high impedance transmission line to provide elliptic function response with sharp transition zero near passband. Patch resonators offer high power handling capability and lower conductor loss as compared with the narrow microstrip line resonators. The patch resonators are designed with high impedance short circuited stubs and low impedance open circuited patches. To achieve the goal, various patch shapes (topologies) are investigated with substrate materials having same dielectric constant and different thickness. Initially, unit cell model of centre resonator is designed and the L-C equivalent model of the unit cell is extracted with component values. The results are validated with EM simulation results to prove the elliptic function response of the filter. From the ABCD parameters of the unit cell, the transmission characteristics are analyzed by using MATLAB codes and the obtained results are validated with equivalent L-C model characteristics. The filter structures are optimized using electromagnetic simulation software Zeland IE3D and Ansoft HFSS. IE3D is a full-wave method of moments (MoM) based electromagnetic simulator solving the current distribution on 3D and multilayer structure of general shape and Ansoft HFSS utilises finite element method (FEM) to compute the electrical

behaviour of high frequency and high speed components. Multiple resonators are designed and loaded on high impedance transmission line to provide sharp transmission zeroes at finite frequencies. Rigorous parametric analysis has been conducted and the optimized structures are fabricated using photolithographic process. Finally, the experimental results are validated with simulated results using R&S ZVL13 vector network analyser. The analyzer is calibrated using Through-Open-Short-Match (T-O-S-M) calibration techniques. Power is fed to the filters through microwave coaxial cable and SMA connectors. The transmission and reflection characteristics of the filter structures are analysed using scattering parameters.

1.4. Orientation of the Thesis

The thesis discusses the design and development of various planar compact lowpass filter with sharp roll-off rate and very good in and out-of band performances. The thesis is organized into seven chapters. Chapter one explains the motivation for the present work, objectives and methodology of this study. The remaining chapters of this thesis are organized as follows:

- **Chapter 2**

This chapter explores the brief introduction of planar lowpass filters and its performance characteristics. The conventional methods of lowpass filter design and its shortcomings for the practical applications have been presented in the following sessions. A comprehensive survey of the state of art in lowpass filter design technology and a detailed review of various high performance

lowpass filter design methods using different types of resonators are also discussed.

- **Chapter 3**

The main objective of the work is to design and develop compact lowpass filters with sharp roll-off rate, wide stopband and high suppression level by using low cost substrates. This chapter discusses the basic characteristic of microstrip transmission line and the filter design considerations together with the design of high performance lowpass filter using funnel and triangular patch resonators. A novel technique to extract both the patch capacitance and coupling capacitance between the patches is suggested. The detailed parametric analysis and the methods to enhance the filter performance by modifying the shape of the resonators using low thickness substrate are also discussed.

- **Chapter 4**

In this chapter, methods to enhance the roll-off rate of the filter by using stepped impedance patch resonators are discussed. The equivalent circuit model of the proposed filter is presented and compared with EM model analysis. The method to enhance the stopband performance by introducing suppressing cells and stepped impedance polygonal patch resonators is also discussed.

- **Chapter 5**

In this chapter, the design procedure of a compact lowpass filter with high suppression level on lossy FR4 material (loss tangent 0.02) by octagonal and heptagonal patch resonators is discussed. The role of loss tangent of the substrate to determine the performance

characteristics of the filter is studied and proved the same with a low loss material having same substrate properties such as permittivity and thickness. The designed filter is developed on CMET/LK-4.3. The filter achieves a sharp roll-off and high suppression level and validated the experimental results with EM simulation results.

- **Chapter 6**

In this chapter, a novel compact lowpass filter with ultra sharp roll-off rate and wide stopband bandwidth using elliptical shaped centre patch resonator and modified rectangular patch resonators is designed and demonstrated. The experimental results validated the simulation results.

- **Chapter 7**

This chapter concludes the work with major achievements discussed in the previous chapters and outlined the major obstacles of the design method. The scope of future developments is also discussed.

Chapter 2

Survey of Literature

This chapter explores brief introduction of planar lowpass filters and their performance characteristics. Depending upon the characteristic function, classification of different types of lowpass filters is also presented. The conventional methods of lowpass filter design and its shortcomings for the practical application have been presented in the following sessions. A comprehensive survey of the state of art in lowpass filter design technology and a detailed review of various high performance lowpass filter design methods using different types of resonators are also discussed.

2.1 Planar Lowpass Filters

Filters are the frequency selective circuits used to select one or more frequency bands called its passband and reject or block the other bands called stopband. Depending on the selection of frequencies, the filters are classified into lowpass filter, highpass filter, bandpass filter and band reject filter. For a wide range of microwave frequencies, there exist various kinds of transmission media including the coaxial, dielectric, waveguide, and planar structures for the filter design. Presently, the most common choice for RF and microwave filter design is planar transmission media, preferably microstrip lines. The advantages of planar structures over the others are:

- Low insertion loss in the passband
- High attenuation in the stopband
- Compact size
- Easy to process by photolithography/micromachining
- Low cost
- Light weight
- Good affinity with active circuit elements

2.2 Performance Characteristics of a Lowpass Filter

The amplitude squared transfer function for a two port lossless passive filter network is defined as:

$$|S_{21}(j\omega)|^2 = \frac{1}{1 + k^2 F_n^2(\omega)} \quad (2.1)$$

where k is a parameter related to the amount of ripples, $F_n(\omega)$ represents a filtering or characteristic function, ω is the frequency variable. Depending on the transmission characteristics of the filter, they are classified into lowpass, highpass, bandpass or bandreject filters. Microwave lowpass filters implemented using printed circuit board technologies are in great demand in front-end circuitry of modern radio frequency and wireless communication systems to suppress harmonics and spurious signals. Transmission and reflection characteristics of the lowpass filter are expressed in terms of its S-parameter characteristics [1].

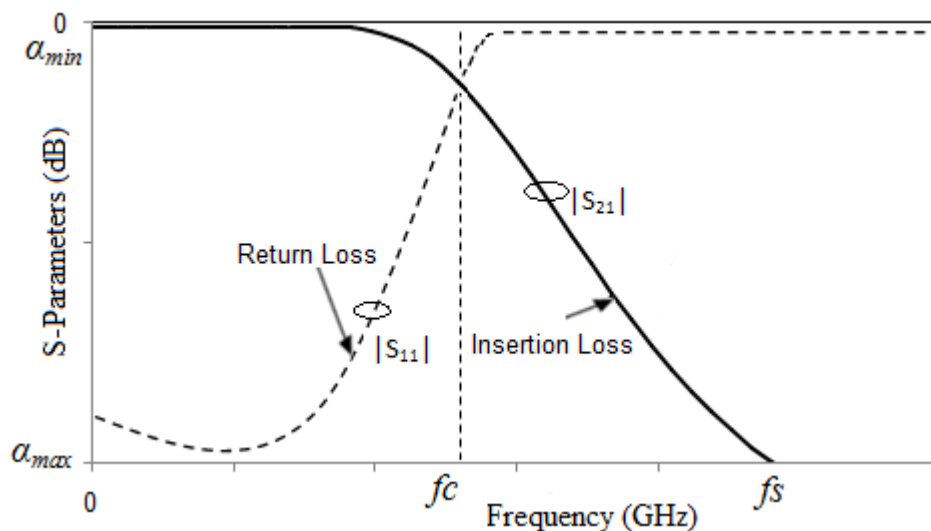


Fig. 2.1 S-Parameter characteristics of a lowpass filter

Fig. 2.1 shows the S-Parameter characteristics of a microwave lowpass filter. The important performance characteristics of these types of filters are:

2.2.1 Cutoff frequency (f_c): Cutoff frequency is the boundary of filter characteristics at which the energy flowing through the system begins to be reduced (attenuated) rather than passing through. It is determined by -3 dB point

frequency from peak passband value at which the transmission gets attenuated or it is the frequency at which the transmitted power becomes half.

2.2.2 Insertion Loss (IL): Insertion loss is often used within the telecommunication designs to determine the terminal attenuation that results from inserting a device into the signal path. It is a measure of loss in the passband of the transmission characteristics.

$$IL = 10 \log \frac{1}{|S_{21}(j\omega)|^2} \text{ dB} \quad (2.2)$$

or

$$IL = -20 \log |S_{21}| \text{ dB} \quad (2.3)$$

For lossless transmission, or an ideal lowpass filter, the insertion loss is 0 dB in the passband and ∞ dB in the stopband. Besides, IL in the stopband is a measure of suppression level of the filter and the frequencies at which the suppression level is measured, which is called the stopband bandwidth.

2.2.3 Return Loss (RL): Return loss is a measure of reflection characteristics of the filter. It is caused due to impedance mismatch between the circuit elements. Since $|S_{11}|^2 + |S_{21}|^2 = 1$ for a lossless, passive two-port network, the return loss response of the filter is characterized by:

$$RL = 10 \log \left[\frac{1}{1 - |S_{21}(j\omega)|^2} \right] \text{ dB} \quad (2.4)$$

or

$$RL = -20 \log |S_{11}| \text{ dB} \quad (2.5)$$

An ideal lowpass filter should provide good impedance matching in passband characteristics. Filter having ∞ dB return loss in the passband and high degree of reflection ($RL = 0$ dB) in stopband is demandable for an ideal lowpass filter.

2.2.4 Roll-off Rate (ξ): The term used to describe the switching characteristics or slope of the filter response in the transition region from the passband to the stopband is defined as the roll-off rate of the filter. The roll-off rate ξ of a lowpass filter is defined as:

$$\xi = \frac{\alpha_{\max} - \alpha_{\min}}{fs - fc} \text{ dB/GHz} \quad (2.6)$$

where α_{\max} is the attenuation level being measured at frequency fs and α_{\min} is the attenuation level at fc . For an ideal lowpass filter it is desirable to have infinite roll-off rate.

2.2.5 Relative Stopband Bandwidth (RSB): One of the important parameter of a lowpass filter is its stopband bandwidth with high suppression level. The stopband bandwidth is always expressed in terms of its stopband centre frequency, as relative stopband bandwidth (RSB). The RSB of a filter is defined as:

$$RSB = \frac{\text{stopband bandwidth}}{\text{stopband centre frequency}} \times 100\% \quad (2.7)$$

or

$$RSB = \frac{2(f_H - f_L)}{f_H + f_L} \times 100\% \quad (2.8)$$

where, f_H is the higher cutoff frequency and f_L is the lower cutoff frequency, that are expressed within the specified suppression level.

2.2.6 Normalized Circuit Size (NCS): The filter component size must be small to realize overall system miniaturization. The size of the filter is expressed in terms of its electrical size, normalized to guided wavelength as:

$$NCS = \frac{\text{physical size (length x width)}}{\lambda_g^2} \quad (2.9)$$

where $\lambda_g = \frac{\lambda}{\sqrt{\epsilon_{re}}}$, is the guided wavelength at cutoff frequency.

2.2.7 Group delay (τ_d): Whenever a signal is transmitted through a frequency selective network such as filter, some delay is introduced into the output with respect to the input signal. The group delay, τ_d is defined as the negative derivative of phase with respect to frequency.

$$\tau_d(\omega) = -\frac{d\phi_{21}(\omega)}{d\omega} \text{ seconds} \quad (2.10)$$

where ϕ_{21} is in radians and ω is in radians per second.

Basically, group delay is a measure of the amount of time required for a signal to propagate through a device. It is also an indicator of the passband dispersion characteristics of the filter. For an ideal filter, group delay should be constant throughout the passband.

2.3 Different types of Lowpass Filters

As demonstrated in the amplitude squared transfer function of a filter in Eq. (2.11), the performance of a lowpass filter is defined in terms of its characteristic function $F_n(\omega)$ [1]. Depending on $F_n(\omega)$, the lowpass filter characteristics are generally classified as Butterworth, Chebyshev and Elliptic function filter.

2.3.1 Butterworth Filter

This type of characteristics is also called binomial or maximally flat response, and it provides flattest possible passband response for a given order of the filter [1-2]. The amplitude squared transfer function of a Butterworth lowpass filter is expressed as:

$$|S_{21}(j\omega)|^2 = \frac{1}{1 + k^2 \left(\frac{f}{fc}\right)^{2N}} \quad (2.11)$$

where N is the order of the filter and fc is the cutoff frequency. The passband of the filter extends from $f = 0$ to $f = fc$. N is a parameter corresponds to the number of reactive elements present in the filter circuit. As depicted in Eq. (2.11), the transfer function of this type of filter has $(2N-1)$ zero derivatives at $f = 0$, and for higher frequencies beyond fc , rolls-off down to zero in the stopband at a rate of $20 N$ dB/decade or $6N$ dB/octave.

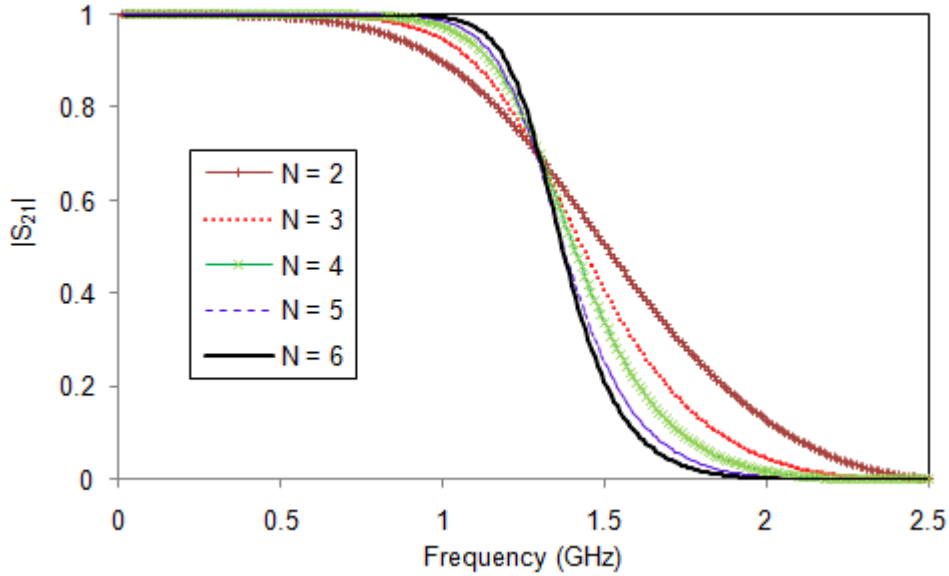


Fig. 2.2 Butterworth type lowpass filter response

One of the main disadvantages of the Butterworth filter is, it achieves flat passband at the expense of a wide transition from passband to stopband. It has also poor phase characteristics. However, higher the value of N , larger the number of cascaded stages required within the filter design, and thus the response approaches to the ideal filter characteristics as shown in Fig. 2.2. In practice, ideal Butterworth frequency response is unattainable as it produces poor passband characteristics and increased layout area.

2.3.2 Chebyshev filter

This type of filter characteristics is also called equal ripple response. The amplitude squared transfer function of an N -order Chebyshev type lowpass filter response is:

$$|S_{21}(j\omega)|^2 = \frac{1}{1 + k^2 T_N^2(\omega)} \quad (2.12)$$

where, $T_N(\omega)$ is a Chebyshev function, which oscillate between ± 1 for $|\omega| \leq 1$.

As demonstrated in Fig. 2.3, the response of this type of filter will have ripples in the passband and as from Eq. (2.12), k^2 determines the passband

ripple levels. For large ω , $T_N(\omega) \approx \frac{1}{2} \left(2 \frac{f}{fc} \right)^N$.

So for $f \gg fc$, the insertion loss becomes

$$IL \approx \frac{k^2}{4} \left(\frac{2f}{fc} \right)^{2N} \quad (2.13)$$

which is also increases at the rate of $20N$ dB/decade. But the insertion loss for the Chebyshev case is $(2^{2N})/4$ greater than the binomial response at any given frequency where $f \gg fc$.

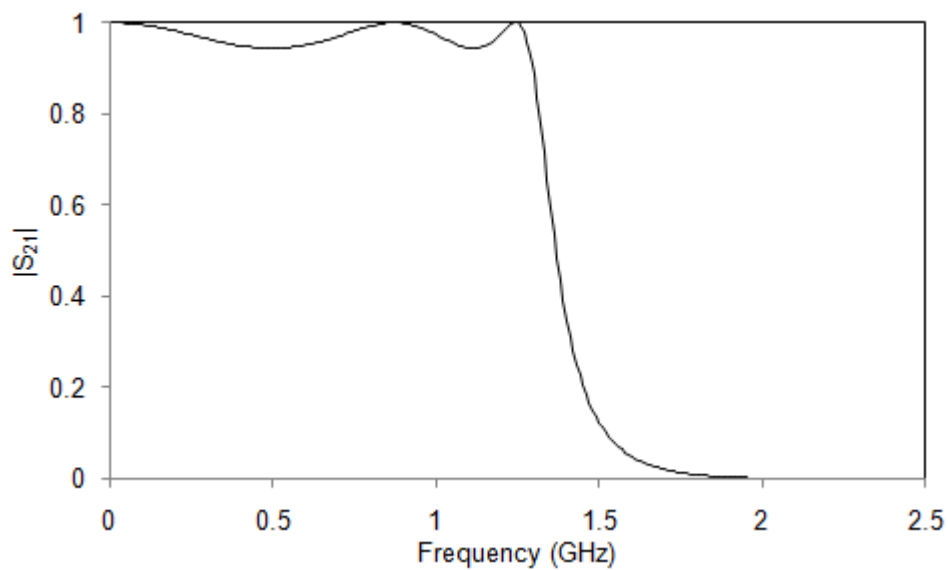


Fig. 2.3 Chebyshev type response of a lowpass filter

2.3.3 Elliptic Function Filter

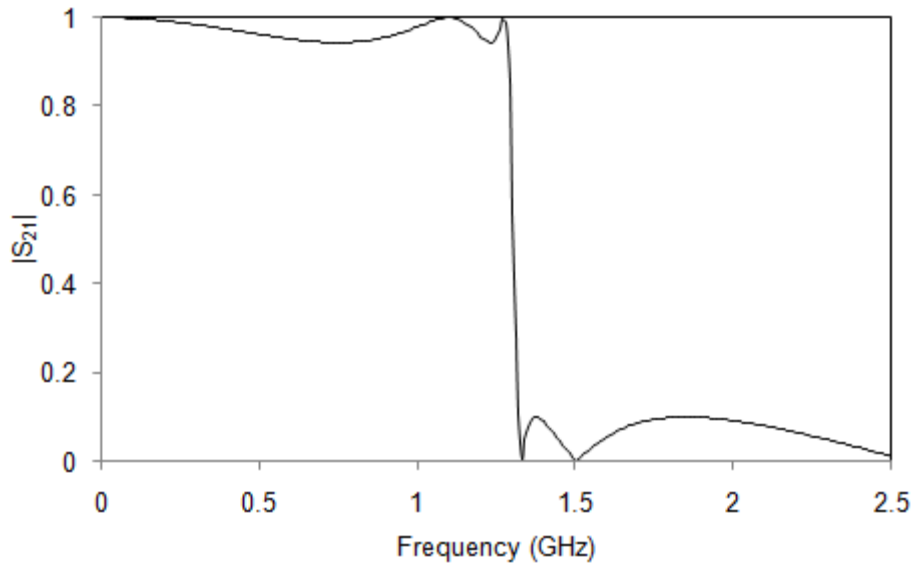


Fig. 2.4 Elliptic function type response of a lowpass filter

The lowpass filter having Butterworth and Chebyshev type responses has monotonically increasing attenuation in the stopband characteristics. Elliptic function filter has sharp cutoff rate with equal ripple in the passband and stopband. The transfer function of an Elliptic function lowpass filter is defined as:

$$|S_{21}(j\omega)|^2 = \frac{1}{1 + k^2 L_N^2(\xi, \omega)} \quad (2.14)$$

where $L_N(\omega)$ is the N^{th} order elliptic rational function and ξ is the selectivity factor of the filter. The value of the ripple factor, k^2 specifies the passband ripple, while the combination of the ripple factor and the selectivity factor specifies the stopband ripple.

Fig. 2.4 shows the response characteristics of an elliptic function lowpass filter. The characteristic function of an elliptic function lowpass filter is complex and the filter has nonlinear phase response characteristics.

2.4 Conventional Method of Lowpass Filter Design

The conventional method of microstrip lowpass filter design is either by using stepped impedance method or by open circuited stub method [1].

2.4.1 Lowpass Filter Design using Stepped Impedance Method

The simple method to design and develop planar lowpass filters is to use alternating section of high and low impedance microstrip transmission line elements. The transmission line acts as stepped impedance lines. Fig. 2.5(a) shows a general structure of stepped impedance lowpass microstrip filters. The filter structure can be approximated as L-C ladder type of lowpass filters as shown in Fig. 2.5(b). The thin and thick microstrip lines offer high and low characteristic impedances respectively. By suitably selecting the physical size of these lines much shorter than the associated guided wavelengths, the high impedance lines act as series inductors and the low impedance lines act as shunt capacitance. Higher the impedance of thin lines, better the approximation of lumped inductance and lower the impedance, better the approximation of lumped capacitance.

The condition for better results is, $Z_{0C} < Z_0 < Z_{0L}$, where Z_{0C} and Z_{0L} denote the characteristic impedances of the low and high impedance lines, respectively, and Z_0 is the source impedance, which is usually 50 Ω . The number of reactive elements decides the pole of the filter.

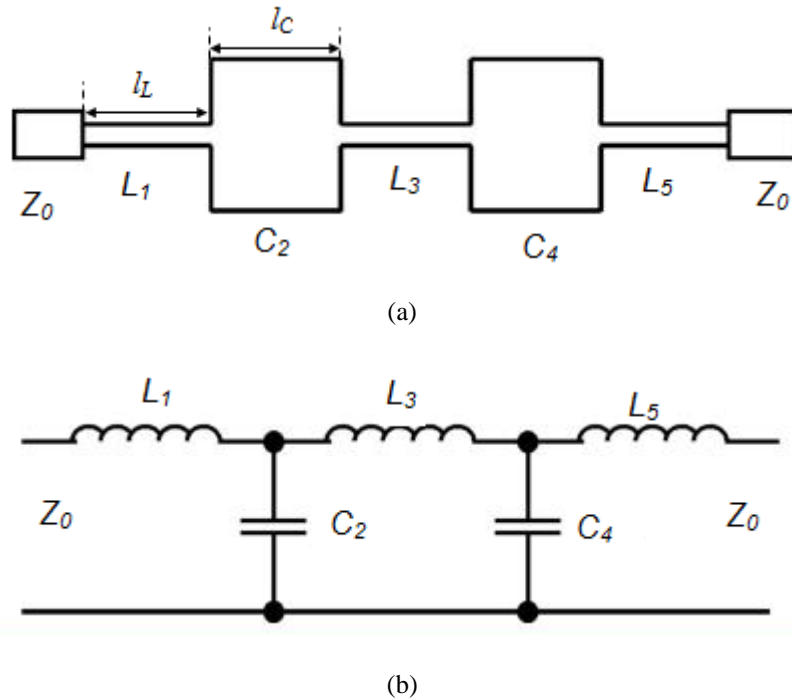


Fig. 2.5 (a) Geometry of stepped impedance microstrip lowpass filter, (b) L-C equivalent circuit model

Fig. 2.6 shows the geometry of three pole, stepped impedance lowpass filter with its L-C model equivalent circuit. The dielectric material used for the filter design is having permittivity, $\epsilon_r = 10.8$, and thickness, $t = 1.27$ mm. The physical length of the high impedance lines l_L and the low impedance lines l_C can be determined by Eqs.(2.15) and (2.16) respectively. The filter dimensions are: $l_1 = 9.8$ mm, $l_2 = 7.1$ mm, $h_1 = 4$ mm and $w_1 = 0.2$ mm. The cutoff frequency of the demonstrated lowpass filter is at 1 GHz. Even though, the filter design method is very simple and it provides good passband performance, the filter shows a gradual roll-off after cutoff frequency as illustrated in Fig. 2.7.

$$l_L = \frac{\lambda_{gL}}{2\pi} \sin^{-1} \left(\frac{\omega_c L}{Z_{0L}} \right) \quad (2.15)$$

and

$$l_C = \frac{\lambda_{gC}}{2\pi} \sin^{-1} (\omega_c C Z_{0C}) \quad (2.16)$$

where λ_{gL} and λ_{gC} are the respective guided wavelengths, L and C are the associated equivalent inductance and capacitance respectively, and ω_c is the cutoff frequency in radians/second [1].

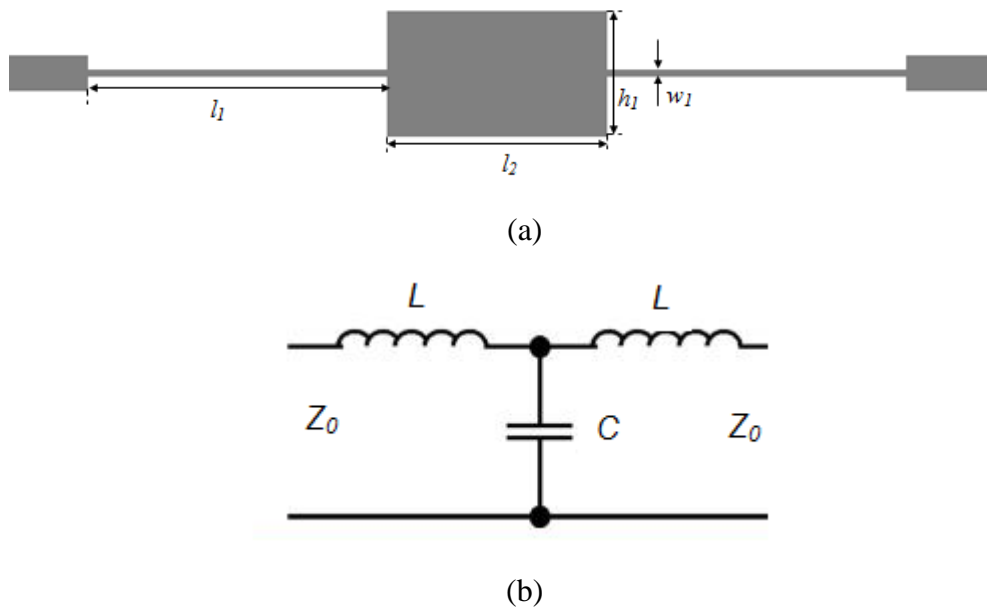


Fig. 2.6 (a) Layout of three pole, stepped impedance lowpass filter on a substrate of $\epsilon_r = 10.8$, $t = 1.27$ mm, (b) L-C model equivalent circuit

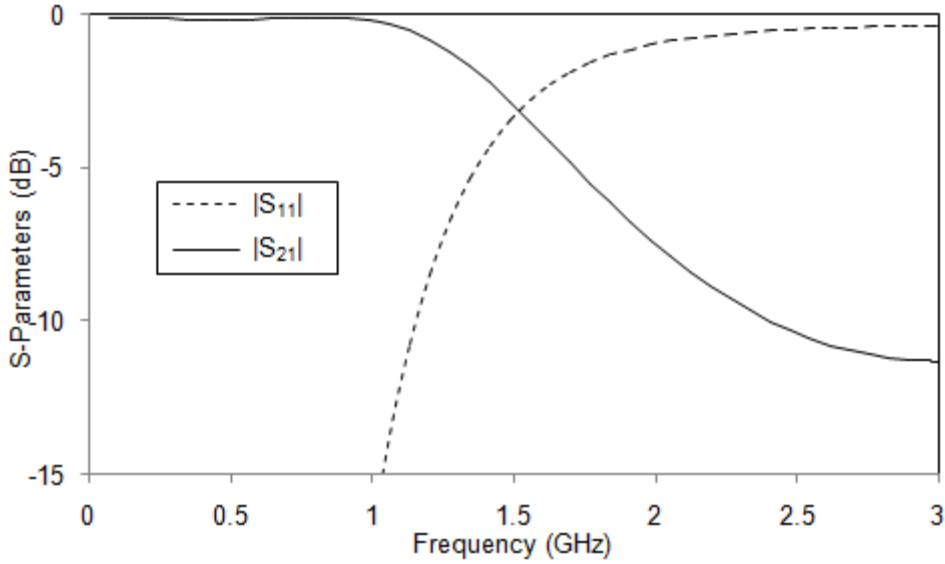


Fig. 2.7 Simulated S-Parameter characteristics of three pole stepped impedance lowpass filter

2.4.2 Lowpass Filter Design using Open Circuited Stub Method

Another method of microstrip lowpass filter design is open circuited stub method, where low impedance open circuited patches are loaded on the high impedance transmission line. Fig. 2.8 shows the layout and L-C equivalent circuit model of three pole lowpass filter using open circuited stub method. The filter dimensions are: $l_1 = 11.35$ mm, $l_2 = 4$ mm, $h_1 = 5.75$ mm, and $w_1 = 0.2$ mm. The open circuited patch acts as lumped capacitance, C and the value of the same can be extracted by using Eq. (2.17).

$$\omega C = \frac{1}{Z_0} \tan\left(\frac{2\pi}{\lambda_g} l_2\right) \text{ for } l_2 < \lambda_g / 4, \quad (2.17)$$

where Z_0 is the characteristic impedance and l_2 is the physical length of the patch, which is smaller than guided wavelength λ_g .

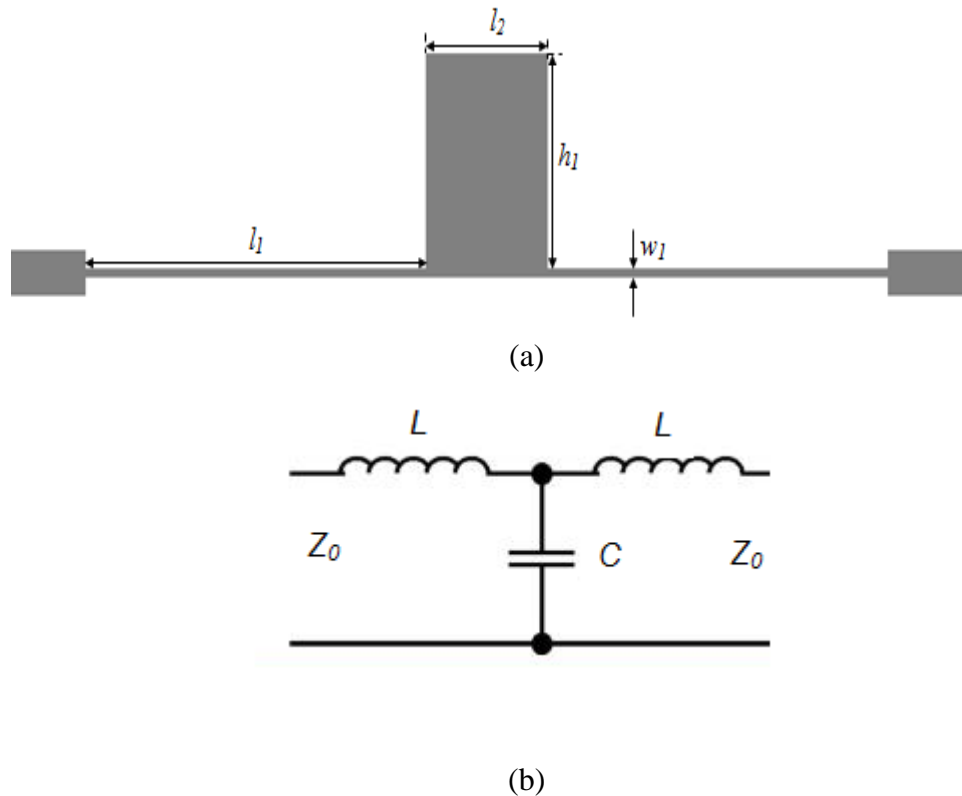


Fig. 2.8. (a) Layout of three pole open circuited stub lowpass filter on a substrate of $\epsilon_r = 10.8$, $t = 1.27$ mm, (b) L-C model equivalent circuit.

As shown in Fig. 2.9, the filter using open circuited stub provides slightly better results than stepped impedance lowpass filter, still the filter suffers from gradual roll-off rate. Fig. 2.10 compares the simulated results of both lowpass filters using stepped impedance method demonstrated in section 2.4.1 and similar filter design using open circuited stub method.

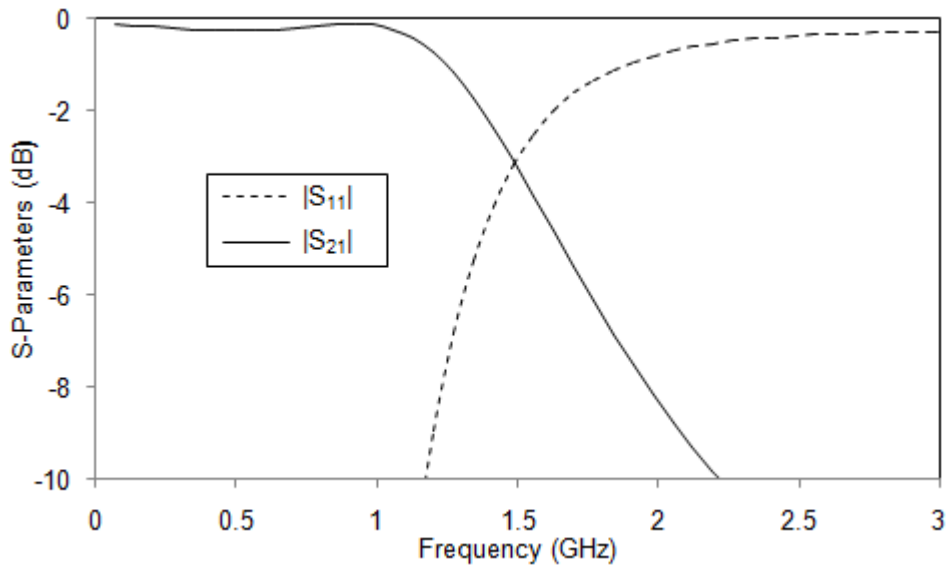
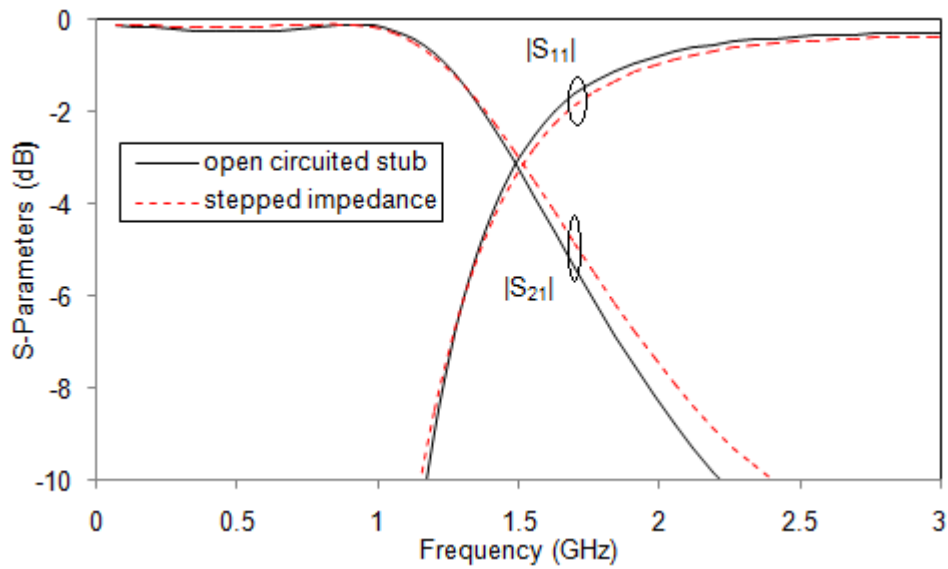
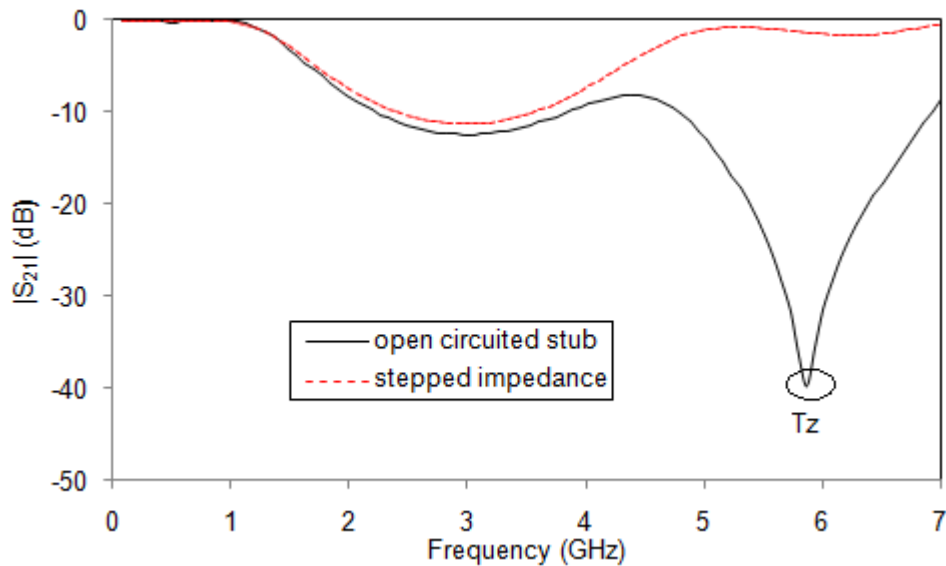


Fig. 2.9 Simulated performance of three pole, open circuited lowpass filter on a substrate of $\epsilon_r = 10.8$, $t = 1.27$ mm



2.10 Comparison of passband frequency response of filters demonstrated in Fig. 2.6(a) and Fig. 2.8(a)

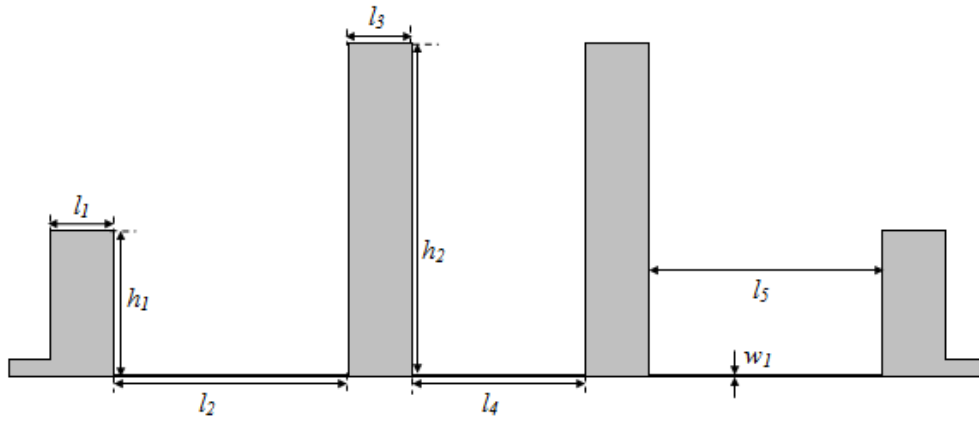
As shown in Fig. 2.10, both filters offer almost similar transmission and reflection characteristics up to the cutoff frequency. However the stopband performances of these filters are different as demonstrated in Fig. 2.11. The filter using an open circuited stub exhibits a transmission zero, Tz at about 5.869 GHz in the stopband. This is because, at this frequency the open circuited stub is about a quarter guided wavelength so as to almost short out the transmission, causes the attenuation peak.



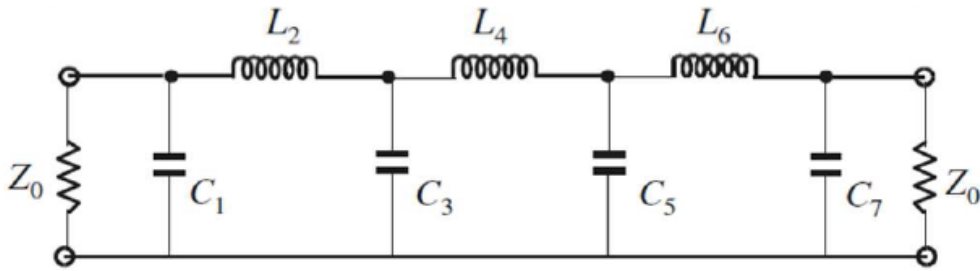
2.11 Comparison of wideband frequency responses of filters demonstrated in Fig. 2.6(a) and Fig. 2.8(a)

The selectivity of the filter can be enhanced to a great extent by increasing the degree of the filter, which can be executed by introducing more number of reactive elements [2–3]. Fig. 2.12 illustrates the layout of a seven pole open circuited stub lowpass filter with its L-C model equivalent circuit. The filter structural parameters are illustrated in Table 2.1. The low impedance

open circuited stubs are approximated as shunt capacitors and high impedance narrow microstrip lines of width w_1 are approximated as series inductors.



(a)



(b)

Fig. 2.12 (a) Layout of a seven pole open circuited lowpass filter, (b) L-C model equivalent circuit

Table 2.1. Three microstrip lowpass filter designs with open circuited stubs

| Substrate ($\epsilon_r = 10.8$, $t = 1.27$ mm) $l_1 = l_3 = 4$ mm | $l_2 = l_5$ (mm) | l_4 (mm) | h_1 (mm) | h_2 (mm) |
|---|---------------------|---------------|---------------|---------------|
| Design A ($w_1 = 0.2$ mm) | 14.7 | 10.9 | 15.75 | 27.5 |
| Design B ($w_1 = 0.2$ mm) | 14.7 | 10.9 | 9.25 | 21 |
| Design C ($w_1 = 0.1$ mm) | 14.7 | 10.9 | 9.15 | 20.85 |

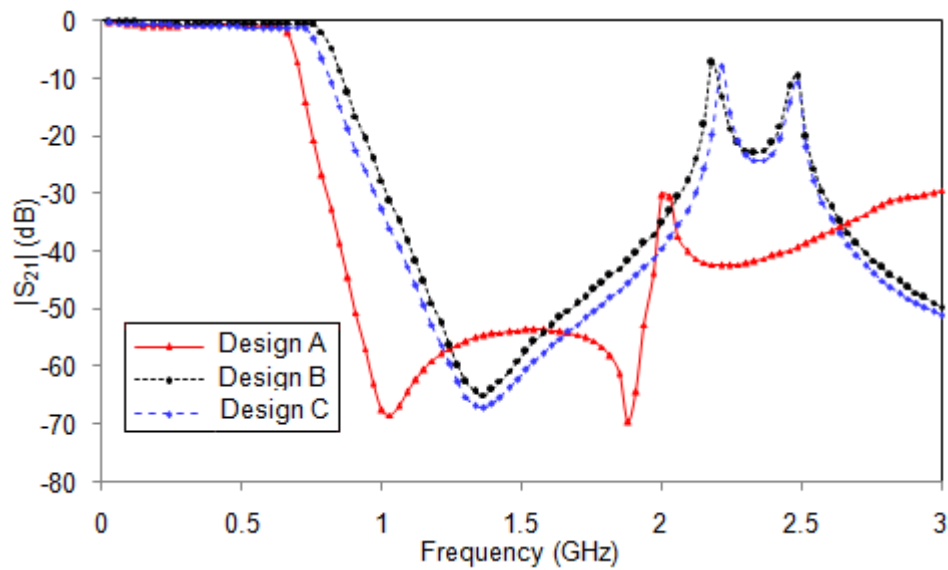


Fig. 2.13 Comparison of filter performance of the three microstrip designs

The performance characteristics of the filter with various structural parameters are depicted in Fig. 2.13. As illustrated in the figure, the performance characteristics of the filter vary with respect to the variation of the dimensions of open circuited stub and width of the transmission line. This is

because, the equivalent L and C components of the filter depend exactly on structural dimensions of each components. As the height of open stubs (h_1 and h_2) increases, the effective reactance of the filter increases that shifts the transmission zero of the filter to the lower frequency range. Thus lowpass filter with Design A performs better roll-off rate by suffering long open circuited stubs size.

Thus, the conventional stepped-impedance and open circuited stubs lowpass filters only provide Butterworth and Chebyshev filter characteristics with a gradual cutoff frequency response. In order to have a sharp transition response, these filters require more number of sections. However, increasing the number of sections increases the physical size of the filter structure together with passband insertion loss. The main shortcoming of conventional method of lowpass filter designs is:

- Limited passband
- Gradual roll-off rate
- Limited stopband
- High insertion loss for higher order filters
- Large layout area

2.5 Survey of Literature

There have been increasing demands for advanced lowpass filters other than conventional Butterworth and Chebyshev filters in order to meet the stringent requirements of modern RF/wireless communication systems such as high performance, small size, light weight, and low cost. Switching characteristics of conventional planar lowpass filters from passband to stopband

is not high enough to meet the application requirements of front-end transceiver of high data rate communication systems. Besides, the filter size must be small to realize overall system miniaturization. Thus, minimizing the dimensions of filter without degrading its performance is a great challenge to the researchers.

Various techniques have been reported in the literature to design and develop high performance compact planar lowpass filters. All the developed methods are classified into two main categories as:

Filter design using

1. Microstrip resonators with defective ground structure (DGS)
2. Microstrip resonators without DGS

2.5.1 Microstrip Resonators with Defective Ground Structure (DGS)

Developing interest in miniaturization of microwave lowpass filters and controlling higher order harmonics by etching the defects in the ground plane of the structure (DGS) are gaining extensive attention in the area of research. Making the defects in the ground plane prohibits propagation of the electromagnetic waves within a certain frequency range. Based on shape, size, pattern and position of etched patterns from the ground plane, various methods have been reported to develop high performance lowpass filters [4–7]. Even though DGS supports designing lowpass filter with enhanced characteristics, the structure itself produces additional radiation and requires a metallic enclosure to mount the structure [8].

2.5.2 Microstrip resonators without DGS

For a lowpass filter with sharp switching characteristics from passband to stopband, for a given number of reactive elements, it is desirable to design

filter structures by introducing infinite attenuation at finite frequencies [1]. Based on this concept, numerous methods have been reported in the literature to develop compact planar lowpass filter with excellent performance characteristics. The designed methods include:

1. Hairpin resonators and stepped impedance hairpin resonators
2. Stub loaded structures
3. Transformed radial stubs
4. Compact microstrip resonant cells (CMRC)
5. Tapered compact microstrip resonator cells
6. Loading multiple patch resonators on high impedance transmission line
7. Symmetric rectangular coupled capacitors
8. Periodic arrangements of complementary split ring resonators
9. Patches and meandered main transmission line
10. Fractal shaped resonators
11. Resonators with external lumped elements

The microstrip hairpin resonators have drawn much attention in lowpass filter design owing to its small size and ease of fabrication. The size reduction of these resonators has been historically achieved from the conventional half-wavelength hairpin resonators to the modified coupled stepped impedance hairpin resonators [9]–[17]. Even though the lowpass filter using stepped impedance hairpin resonators has a finite attenuation pole after cutoff frequency, due to the low capacitance of the coupled line the finite attenuation pole does not locate near the passband. Hence the attenuation characteristics of the filters are gradual. Compact planar and via less composite lowpass filters using folded stepped impedance resonator on liquid crystal polymer substrate

has been reported in [18] to enhance stopband bandwidth, the filter suffers gradual roll-off from passband to stopband. By loading resonant patches inside the free area of a stepped impedance hairpin resonator, a compact microstrip lowpass filter has been reported in [19]. Despite the size reduction in this configuration with enhanced stopband performance, the transition response is not sharp. The stopband can be extended by embedding a pair of coupled stepped impedance resonator in stepped impedance hairpin unit [20–22], still the structure fails to satisfy sharp switching characteristics. Sharp roll-off lowpass filter with wide stopband characteristics is obtained by using stepped impedance resonator with pendulum shaped patch resonator [23]. Wei *et al.* proposed a microstrip lowpass filter featuring compact size and simple structure by using radial stepped impedance hairpin resonators [24]. However, the filter exhibits gradual transition performance.

Lowpass filters with compact size and wide stopband are introduced based on stub-loaded structures. In [25], a sharp roll-off lowpass filter with stub loaded coupled hairpin unit on low cost FR4 has been reported, but its application has been limited up to S-band and generates periodic ripples in the stopband reflection characteristics. Compact, deep, and wide rejection bandwidth lowpass filter using open complimentary split ring resonator and stub loaded hairpin resonator has been reported [26] that still suffers gradual roll-off rate. In [27], a compact lowpass with sharp roll-off is presented, but the insertion loss and the return loss in the passband are not good enough, and the attenuation in the stopband is also weak.

Based on the method of cascading modified semi-circle and semi-ellipse microstrip patch resonators, a microstrip lowpass filter with low insertion loss and sharp roll-off has been proposed in [28]. However, the circuit size and stopband bandwidth still need improvements. To improve the stopband

performance further, Ma and Yeo proposed a lowpass filter by cascading L-C resonant structures and transformed radial stubs. Although better than 13th harmonic suppression was realized, this method increased design complexity and circuit area [29–31]. Recently, compact lowpass filter with excellent stopband rejection performance has been reported by coupled rhombic stubs on taconic TLY-8 substrate with poor roll-off rate [32]. The elliptic-function lowpass filter using elementary rectangular structures provides a wide passband with a sharp cutoff frequency response [33], but the filter provides a narrow stopband performance.

To reduce the filter circuit size, a new group of microstrip lowpass filters utilizing the slow-wave effect has been developed, and they achieve size reduction as compared to the traditional structures [34–36]. In [37], spiral compact microstrip resonance cells are utilized to replace the high-low impedance line in conventional lowpass filters. However the filter does not have good skirt performance and wide stopband. A lowpass filter with 10 dB stopband bandwidth of 128% by using three cells of in-line beeline CMRC has been proposed in [38], but the filter provides only poor transition performance. Lowpass filter with two unsymmetrical T-type compact microstrip resonance cells was utilized with four additional transmission zeros to effectively widen the stopband in [39], but it provides very low stopband suppression levels. A resonator with slow-wave effects is used in the structure of the lowpass filters in order to reduce the size and achieve sharp roll-off [40–42]. But it is hard to achieve a compact size and the good stopband performance. Li *et al.* proposed a lowpass filter featured wide stopband and harmonic response by connecting several CMRC cells with varied dimensions [43]. A method of designing compact lowpass filter with wide stopband characteristics using CMRC and shunt folded open stubs [44], and an extension of double-folded spiral compact

microstrip resonant cell [45] have been introduced to suppress some high-order harmonic frequencies. Hayati and Lotfi have been described a compact lowpass filter design with very good passband characteristics by using front coupled tapered CMRC [46]. The stopband performance of the filter can be improved by introducing slit-loaded tapered CMRC on high impedance transmission line [47]. Since the circuit size of this type of lowpass filter is mainly determined by its basic resonator cells, multiple resonators used in such type of filter will result in a large circuit size and high insertion loss in the passband. The extension of the structure will also increase the design complexity. The filter with multiple patch resonators on high impedance transmission line exhibits an UWB stopband with a high suppression level with better low insertion loss and high return loss characteristics [48–50]. H. Shaman *et al.* reported a filter designed to exhibit a lowpass performance with ultra-wide passband for electronic warfare and radar applications, but the filter fails to achieve sharp roll-off characteristics [51].

A symmetric rectangle with an inter-digital coupled capacitors structure between them for syntheses of the quasi-elliptic function lowpass filter has been proposed in [52]. The utilization of microstrip open-loop resonators allows various filter configurations, including those of elliptic or quasi-elliptic function responses to be realized [53]. In [54], a microstrip lowpass filter with a bulb patch resonator of low roll-off rate has been presented. Compact lowpass filters with very sharp transition bands based on periodic arrangements of open complementary split ring resonators (CSRR) have been reported in [55]. Even though sharp roll-off is achieved, the filter suffers from limited stopband bandwidth and large physical area. A semicircle ended stub resonator, bended transmission line, and a modified radial patch have been used to obtain the sharp frequency response, compact size, low insertion loss, high return loss and

wide stopband characteristics [56]. To achieve a compact design, symmetrically loaded both triangular and polygonal patch resonators and radial shape patches on a meandered main transmission line are adopted [57–58]. Although the size reduction and extended stopband are achieved with these design techniques, the filter suffers from a gradual cutoff and complex structure.

A novel quasi-elliptic lowpass filter with transmission zero close to the transition band, resulting in a sharp roll-off rate by using quasi-lumped elements has been proposed in [59]. In [60], a radial split ring resonator loaded by folded polygon patches to generate multiple transmission zeros is applied to the lowpass filter design, still the filter suffers from a gradual cutoff and fabrication complexity. For expanding the stopband, triangular and radial patch resonators were used by Wang *et al.* [61]. Despite this modification, the return loss in the passband is not good, and the filter suffers from other disadvantages such as gradual cutoff and fabrication complexity. Design methods of high performance lowpass filter with extended stopband characteristics are continuously being extended. R. Gomez-Garcia *et al.* used rat-race directional couplers to extended stopband performance of the lowpass filter [62]. Introduction of circular-shaped patches together with open stub line resonators is another method reported in the literature to enhance the stopband characteristics of the filter [63]. Also miniaturization is achieved with good in-band and out-of band performances by using radial and hexangular shaped resonators [64–65]. Fractal shaped high-low microstrip lowpass filters have been reported in the literature to enhance the passband performances of the filter [66], but its switching characteristics are gradual and the filter provides limited stopband performance. Triangular fractal shaped defects in compact lowpass filter design have been introduced for the generation of transmission zeroes in [67]. Even though the structure is very compact, the stopband performance of the filter is poor. The lowpass filter with

sharp switching and wide stopband suppression characteristics, semi-fractal hairpin resonator with U-shaped resonator has been presented in [68], but the filter possesses high passband losses.

Transmission zeroes within the stopband very close to the cutoff frequency can be generated by using microstrip design with external lumped elements. A compact semi-lumped lowpass filter with coupled capacitor has been proposed in [69]. Tunability can also be achieved by external variable reactive elements. In [70], authors proposed a continuously tunable lowpass filter with five varactor diodes and DC bias voltages. However, by using external lumped elements, the structure does not support the property of ease of integration with other circuit elements of planar structures.

References

- [1] J. S. Hong and M. J. Lancaster, “*Microstrip Filters for RF/ Microwave Applications*,” John Wiley, New York, 2001.
- [2] David M. Pozar, “*Microwave Engineering*,” John Wiley & Sons, 2005.
- [3] M. Makimoto and S. Yamashita, “*Microwave Resonators and Filters for Wireless Communication Theory, Design and Application*,” Springer Series in Advanced Microelectronics, 2001.
- [4] M.K. Mandal, P. Mondal, S. Sanyal, and A. Chakrabarty, “Low Insertion-Loss, Sharp-Rejection and Compact Microstrip Low-Pass Filters,” *IEEE Microw. and Wireless Compon. Lett.*, vol. 16, no. 1, pp. 600–602, 2006.
- [5] S.-W. Ting, K-W. Tan, and R.P Martins, “Miniaturized microstrip lowpass filter with wide stopband using double equilateral U-shaped defected ground structure,” *IEEE Microw. and Wireless Compon. Lett.*, vol. 16, no. 5, pp. 240–242, 2006

- [6] X. Chen, L. Wang, L. Weng, and X. Shi, "Compact lowpass filter using novel elliptic shape DGS," *Microw. Opt. Technol. Lett.* vol. 51, pp. 1088–1091, 2009.
- [7] A.S. Mohra "Microstrip low pass filter with wideband rejection using opened circuit stubs and z-slots defected ground structures," *Microw. Opt. Technol. Lett.*, vol. 53, no. 4, pp. 811–815, 2011.
- [8] Z.Du, K. Gong, J.S. Fu, B. Gao, and Z. Feng, "Influence of a metallic enclosure on the β -parameters of microstrip photonic bandgap structures," *IEEE Trans. on Electromagnetic Compatibility*, vol. 44, no. 2, pp. 324–328, 2002.
- [9] J.S. Won, "Microstrip tapped-line filter design," *IEEE Trans. Microwave Theory Tech.*, vol. 27, pp. 44–50, 1979.
- [10] M. Sagawa, K. Takahashi, and M. Makimot, "Miniaturized hairpin resonator filters and their application to receiver front-end MIC's," *IEEE Trans. Microwave Theory Tech.*, vol. 37, pp. 1991–1997, 1989.
- [11] J.T. Kuo, M.J. Maa, and P.H. Lu, "Microstrip elliptic function filters with compact miniaturized hairpin resonators," in *Proc. of Asia-Pacific Microw. Conf.*, 1999, pp. 860–864.
- [12] D.H. Lee, Y.W. Lee, J.S. Park, D. Ahn, H.S. Kim, and K.Y. Kang, "A design of the novel coupled line low-pass filter with attenuation poles," *IEEE Microwave Theory Tech-Symp. Dig.*, 1999, pp. 1127–1130.
- [13] J. T. Kuo, M. J. Maa, and P. H. Lu, "A microstrip elliptic function filter with compact miniaturized hairpin resonator," *IEEE Microwave Guided Wave Lett.*, vol. 10, pp. 94–95, 2000.
- [14] S.Y. Lee and C.M. Tsai, "New cross-coupled filter design using improved hairpin resonators," *IEEE Trans. Microwave Theory Tech.*, vol. 48, pp. 2482–2490, 2000.

-
-
- [15] L.H. Hsieh and K.Chang, “Compact lowpass filter using stepped impedance hairpin resonator,” *Electron. Lett.*, vol. 37, no. 4, pp. 899–900, 2001.
- [16] L.H. Hsieh and K. Chang, “Compact, broad-stopband elliptic lowpass filters using microstrip stepped impedance hairpin resonators,” *IEEE Microwave Theory Tech-Symp. Dig.*, 2003,1775-1778
- [17] L.H. Hsieh and K. Chang, “Compact elliptic-function low-pass filters using microstrip stepped-impedance hairpin resonators,” *IEEE Trans. Microwave Theory Tech.*, vol. 51, no. 1, pp. 193–199, 2003.
- [18] S. Pinel, R. Bairavasubramanian, J. Laskar, and J. Papapolymerou, “Compact planar and via less composite low-pass filters using folded stepped-impedance resonator on Liquid-Crystal-Polymer substrate,” *IEEE Trans. Microwave Theory Tech.*, vol. 53, pp. 1707–1712, 2005.
- [19] M.H. Yang, and J.Xu, “Design of compact, broad-stopband lowpass filters using modified stepped impedance hairpin resonators,” *Electron. Lett.*, vol. 44, no. 20, pp. 1198–1200, 2008.
- [20] S. Luo and S. Sun, “Stopband-expanded low-pass filters using microstrip coupled-line hairpin units,” *IEEE Microw. and Wireless Compon. Lett.*, vol. 18, pp. 506–508, 2008.
- [21] M.H. Yang, J. Xu, Q. Zhao and X. Sun, “Wide-stopband and miniaturized lowpass filters using sirs-loaded hairpin resonator,” *Jornl. Electromag. Waves Appl*, vol.23, pp. 2385–2396, 2009.
- [22] L. Li, Z.-F Li, and J.-F.Mao, “Compact lowpass filters with sharp and expanded stopband using stepped impedance hairpin units,” *IEEE Microw. and wireless compon. lett.*, vol. 20, no. 6, pp. 310–312, 2010
- [23] K. Dehghani, G. Karimi, A. Lalbakhsh and S.V. Maki, “Design of lowpass filter using novel stepped impedance resonator,” *Electron. Lett.*, vol. 50, no. 1, pp. 37–39, 2014.
-

- [24] X.B. Wei, P. Wang, M.Q. Liu, and Y. Shi, "Compact wide- stopband lowpass filter using stepped impedance hairpin resonator with radial stubs," *Electron. Lett.*, vol. 47, no. 15, pp. 862–863, 2011.
- [25] V.K. Velidi, and S. Sanyal, "Sharp roll-off lowpass filter with wide stopband using stub-loaded coupled-line hairpin unit," *IEEE Microw. and Wireless Compon. Lett.*, vol. 21, no. 6, pp. 301–303, 2011.
- [26] S.S. Karthikeyan and R.S. Kshetrimayum, "Compact, deep, and wide rejection bandwidth lowpass filter using open complimentary split ring resonator," *Microw. Opt. Technol. Lett.*, vol. 53, pp. 845–848, 2011.
- [27] F. Wei, L. Chen, and X.-W. Shi, "Compact lowpass filter based on coupled-line hairpin unit," *Electron. Lett.*, vol. 48, no. 7, pp. 379– 381, 2012.
- [28] M. Hayati, A. Sheikhi, and A. Lotfi, "Compact lowpass filter with wide stopband using modified semi-elliptic and semi-circular microstrip patch resonator," *Electron. Lett.*, vol. 46, no. 22, pp. 1507–1509, 2010.
- [29] K.X. Ma, and K.S. Yeo, "Novel low cost compact size planar low pass filters with deep skirt selectivity and wide stopband rejection," *IEEE MTT-S Int. Microw. Symp. Digest*, 2010, pp. 233–236.
- [30] K.X. Ma, and K.S. Yeo, "New ultra-wide stopband lowpass filter using transformed radial stubs," *IEEE Trans. Microwave Theory Tech.*, 2011, 59, no. 3, pp. 604–611
- [31] K.X. Ma, and K.S. Yeo, and W.M. Lim, "Ultra-wide rejection band lowpass cell," *Electron. Lett.*, 2012, 48, no. 2, pp. 99–100.
- [32] B. Zhang, S. Li and J. Huang, "Compact lowpass filter with wide stopband using coupled rhombic stubs," *Electron. Lett.*, vol. 51, no. 3, pp. 264–266, 2015.
- [33] F. Giannini, M. Salerno, and R. Sorrentino, "Design of low-pass elliptic filters by means of cascaded microstrip rectangular elements," *IEEE Trans. Microwave Theory Tech.*, vol. 30, pp. 1348–1353, 1982.

- [34] C. Jianxin, Y. Mengxia, X. Jun, and X. Quan, “Compact microstrip lowpass filter,” *Electron. Lett.* vol. 40, pp. 674–675, 2004.
- [35] K.F. Chang and K.W. Tam, “Miniaturized cross-coupled filter with second and third spurious responses suppression,” *IEEE Microw. and Wireless Compon. Lett.*, vol. 15, pp. 122–124, 2005.
- [36] J.X. Chen, and Q. Xue, “Compact microstrip low-pass filter with suppression of spurious response,” *IEE Proc. Microw. Antennas Propag.*, vol. 153, no. 5, pp. 432–434, 2006.
- [37] Gu, J., and Sun, X.: “Compact lowpass filter using spiral compact microstrip resonant cells,” *Electron. Lett.*, 2005, 41, no. 19, pp. 1065–1066, 2005.
- [38] F. Zhang, J.Z. Gu, C.Y. Gu, L.N. Shi, C.F. Li, and X.W. Sun, “Lowpass filter with in-line beeline CMRC,” *Electron. Lett.*, vol. 42, no. 8, 472-474, 2006.
- [39] K. Deng, Q. Xue, and W. Che, “Improved compact microstrip resonance cell lowpass filter with wide stopband characteristics,” *Electron. Lett.*, vol. 43, no. 8, pp. 463–464, 2007.
- [40] Z.M. Hejazi, M.C. Scardelletti, F.W. van Keuls, A. A. Omar, and A. S. Al-Zayed, “EM full-wave analysis and testing of novel quasi-elliptic microstrip filters for ultra narrowband filter design,” *Prog. In Electromag. Research*, vol. 85, pp. 261-288, 2008.
- [41] J.-L Li, S.-W Qu, and Q. Xue, “Compact microstrip lowpass filter with sharp roll-off and wide stop-band,” *Electron. Lett.*, vol. 45, no. 2, pp. 110–111, 2009.
- [42] L. Ge, J.P. Wang, and Y.-X Guo, “Compact microstrip lowpass filter with ultra-wide stopband,” *Electron. Lett.*, vol. 46, no.10, pp. 689–691, 2010.
- [43] Li, L., Li, Z.-F., and Wei, Q.-F. “Compact and selective lowpass filter with very wide stopband using tapered compact microstrip resonant cells,” *Electron. Lett.*, vol. 45, no. 5, pp. 267–268, 2009.
-

- [44] X.-B. Wei, P. Wang, Z.-Q. Xu, J.-X. Liao, and Y. Shi, "Compact lowpass filter with wide stopband characteristics," *In: Proc. of ICCP2011, Chengdu, 2011*, pp. 364–365.
- [45] K. Li, M. Zhao, Y. Fan, Z. Zhu, and W. Cui, "Compact lowpass filter with wide stopband using novel double-folded SCMRC structure with parallel open-ended stub," *Progress In Electromag. Research Lett.*, vol. 36, pp. 77–86, 2013.
- [46] M. Hayathi and A. Lotfi, "Compact lowpass filter with high and wide rejection in stopband using front coupled tapered CMRC," *Electron. Lett.*, vol. 46, no. 12, pp. 846–848, 2010.
- [47] M. Hayathi and A. Lotfi, "Elliptic-function lowpass filter with sharp cutoff frequency using slit-loaded tapered compact microstrip resonator cell," *Electron. Lett.*, vol. 46, no. 2, pp. 846–848, 2010.
- [48] M. Mirzaee and B. S. Virdee, "Compact lowpass filter with high out-of-band rejection and superwide stopband performance," *Microw. Opt. Technol. Lett.*, vol. 56, no. 4, pp. 947–950, 2014.
- [49] M. Mirzaee, and B.S. Virdee, "Realization of highly compact planar lowpass filter for UWB RFID applications," *Electron. Lett.*, vol. 49, no. 22, pp. 1396–1398, 2013.
- [50] M. Hayati, A. Abdipour and A. Abdipour, "Compact microstrip lowpass filter with sharp roll-off and ultra-wide stop-band," *Electron. Lett.*, vol. 49, no. 18, pp. 1159–1160, 2013.
- [51] H. Shaman, S. Almorqi, and A. Al-Amoudi, "Composite microstrip lowpass filter with ultra wide stopband and low insertion loss," *Microw. Opt. Technol. Lett.*, vol. 57, no. 4, pp. 871–874, 2015.
- [52] L. Li, and Z.-F, Li, "Compact quasi-elliptic lowpass filter using symmetric rectangular coupled capacitors," *Electron. Lett.*, vol. 44, no. 2, pp. 124–125, 2008.

- [53] J.-S. Hong and M.J. Lancaster, “Theory and experiment of novel microstrip slow-wave open-loop resonator filters,” *IEEE Trans. Microwave Theory Tech.*, vol. 45 pp. 2358–2365, 1997.
- [54] K.R Jha, and M. Rai, “Modification in microstrip lowpass filter using bulb shape patch, ”*Int. Journ. Electron. Commun. (AEÜ)*, vol. 63, pp. 1076–1079, 2009.
- [55] F. Aznar, A. Velez, J. Bonache, J. Martel, and F. Martin, “Compact lowpass filters with very sharp transition bands based on open complementary split ring resonators,” *Electron. Lett.*, vol. 45, 316–317, 2009.
- [56] M. Hayati, H. A.-D. Memari, and H. Abbasi , “Compact microstrip lowpass filter with sharp roll-off and wide stopband using semicircle ended stub resonator,” *Prog. In Electromag. Research Lett.*, vol. 35, pp. 73–81, 2012
- [57] H. Cui, J. Wang, and Zhang, G. “Design of microstrip lowpass filter with compact size and ultra-wide stopband,” *Electron. Lett.*, vol. 48, no. 14, pp. 856–857, 2012.
- [58] J. Wang, L.-J. Xu, S. Zhao and Y.-X. Guo, , and W. Wu, “Compact quasi-elliptic microstrip lowpass filter with wide stopband,” *Electron. Lett.*, vol. 46, no. 20, pp. 1384–1385, 2010.
- [59] C. Miao, J. Xu, and W. Wu “Compact wide stopband quasi-elliptic function lowpass filter using quasi-lumped elements,” *Progress In Electromag. Research Letters*, vol. 39, pp. 151–159, 2013.
- [60] M. Hayati, H. Asadbeigi and A. Sheikhi, “Microstrip lowpass filter with high and wide rejection band,” *Electron. Lett.*, vol. 48, no. 19, 1217–1219, 2012.
- [61] J. Wang, H. Cui, and G. Zhang, “Design of compact microstrip lowpass filter with ultra-wide stopband,” *Electron. Lett.*, vol. 48, no. 14, pp. 854–856, 2012.

- [62] R. Gomez-Garcia, M.-A. Sanchez-Soriano, M. S. Renedo, G. Torregrosa-Penalva and E. Bronchalo, "Extended-stopband microstrip lowpass filter using rat-race directional couplers," *Electron. Lett.*, vol. 49, no. 4, pp. 272–274, 2013.
- [63] G. Karimi, A. Labakhsh, and H. Siahkamari, "Design of sharp roll-off lowpass filter with ultra wide stopband," *IEEE Microw. and Wireless Compon. Lett.*, vol. 23, pp. 303–305, 2013.
- [64] M. Hayati, S. Naderi and F. Jafari, "Compact microstrip lowpass filter with sharp roll-off using radial resonator," *Electron. Lett.*, vol. 50, no. 10, pp. 761–762, 2014.
- [65] M. Hayati, M. Gholami, H.S. Vaziri and T. Zaree, "Design of microstrip lowpass filter with wide stopband and sharp roll-off using hexangular shaped resonator," *Electron. Lett.*, vol. 51, no. 1, pp. 69–71, 2015.
- [66] W-L. Chen, G-M. Wang and Yi-Na Qi, "Fractal-shaped hi-lo microstrip low-pass filters with high passband performance," *Microw. Opt. Technol. Lett.*, vol. 49, no. 10, pp. 2577–2579, 2007.
- [67] J-K Xiao, Q.-X. Chu, and H.-F. Huang, "New microstrip lowpass filter with transmission zero and wide stopband," *Microw. Opt. Technol. Lett.*, vol. 51, no. 3, pp. 830–831, 2009.
- [68] G. Karimi, K. Hamedani, and H. Siahkamari, "Miniaturized microstrip lowpass filter with sharp roll-off and ultra-wide stopband," *Electron. Lett.*, vol. 49, no. 21, pp. 1343–1345, 2013.
- [69] J. W. Sheen, "A compact semi lumped low-pass filter for harmonics and spurious suppression," *IEEE Microw. Guided Wave Lett.*, vol. 10, pp.92–93, 2000.
- [70] J. Ni, and J. Hong, "Compact Continuously Tunable Microstrip Low-Pass Filter," *IEEE Trans. Microwave Theory Tech.*, vol. 61, no. 5, pp. 1793–1800, 2013.

Chapter 3

Compact Lowpass Filter using Funnel and Triangular Patch Resonators

This chapter includes the design and development methods of four low cost, high performance, compact, planar lowpass filters using funnel and triangular patch resonators and their structural modifications: Filter I, Filter II, Filter III, and Filter IV. The filters are designed using FR4 material. The L-C equivalent circuit model of the Filter I has been extracted and the results are validated with full wave EM model structural simulations. Filter I achieves a sharp roll-off rate of 84 dB/GHz at 40 dB attenuation level and relative stopband bandwidth (RSB) of 66.96 % with suppression level (SL) of 15 dB and cutoff frequency (f_c) of 5.55 GHz. After conducting a detailed parametric analysis and by introducing structural modifications in the patch resonators, the RSB of the modified filter, Filter II is enhanced to 113.8% with f_c of 2.5 GHz. The filter structure is further modified by introducing one more resonator near the feed line, Filter III. The measured roll-off rate of Filter III is 125 dB/GHz with same f_c , RSB and SL of Filter II. As the thickness of the substrate material decreases, the impedance offered by the low impedance patch also decreases, which leads to the better approximation of lumped capacitance. This property is made use to design Filter IV. The developed Filter IV achieves a RSB of 134% with stopband suppression level better than 31 dB by suffering its roll-off rate to 60 dB/GHz.

3.1 Introduction

High performance and compact lowpass filters are in great demand for present communication systems to suppress harmonics and spurious signals. Microstrip filters offer low insertion loss in the passband and infinite attenuation in the stopband together with compact size, low cost and ease of fabrication. Filtering of undesired frequencies using microstrip can be accomplished with conventional design techniques such as stepped impedance lines or tuned stubs. However, these filter structures require large layout area in order to obtain sharp frequency characteristics [1]. Recently, different methods have been proposed and developed to implement lowpass filter with good performance utilizing (i) double equilateral U-shaped defected ground structure [2], (ii) Quasi- π -slot resonator and open stubs [3], (iii) open circuited stubs and z-slots defective ground structure [4], (iv) split ring and complementary split ring resonators [5], (v) transformed radial stubs [6], (vi) in-line beeline CMRC [7], (vii) modified stepped impedance hairpin resonators [8], (viii) modified semi-elliptic and semi-circular microstrip patch resonator [9], (ix) compact microstrip resonator cells [10]–[12], (x) cascading multiple resonators on high impedance line [13], (xii) hexangular shaped resonator [14]. Although most of these reported filters are good choice for modern communication systems, they suffer deficiencies such as additional radiation due to defective ground [2]–[5], gradual roll-off near the passband [5]–[12] and large layout area [13–14]. Moreover, the wide stopband characteristics of the reported filters [2]–[14] are due to the material properties such as low loss, low permittivity and small thickness. Compact lowpass filter with sharp roll-off rate using microstrip line resonators on 1.6 mm thickness substrate has been reported in [15]. But, the filter was designed for low frequency applications and exhibits periodic

fluctuation of more than 15 dB of return loss in the stopband. Though various techniques have been reported in the literature to design and develop compact and high performance lowpass filters, loading multiple resonators on high impedance transmission line is an effective method to enhance the filter characteristics.

To realize a lowpass filter with sharp switching from passband to stopband for a given number of reactive elements, it is essential to generate infinite attenuation at finite frequencies. The proposed filters are designed and developed by cascading multiple patch resonators on high impedance transmission line to execute such characteristics. The patch resonators are designed by using high impedance inductive stubs and low impedance capacitive patches, and cascading them will provide series L-C resonator characteristics. This chapter includes the design and analysis of four compact microstrip lowpass filters with sharp roll-off and wide stopband using funnel and triangular patch resonators and their structural modifications named as Filter I, Filter II, Filter III and Filter IV. Filter I is designed by loading funnel patch resonator (FPR) in between two triangular patch resonators (TPR) symmetrically about the centre of 96Ω impedance microstrip line. The L-C equivalent circuit of the filter has been extracted and validated with full wave EM model simulation results. The measured cutoff frequency of Filter I is at 5.55 GHz with a relative stopband bandwidth (RSB) of 66.96 %. The filter achieves sharp roll-off of 84 dB/GHz at 40 dB attenuation level with an ultra compact size of 9.4 mm x 8 mm. As there exists an inverse relation between frequency and size of the filter structure, the cutoff frequency can be lowered by increasing its physical size of the resonant patch within the filter structure. But, as the size of the patch elements increases its characteristic impedance

decreases, that may introduce transverse resonance in the operating frequency range. So, the funnel and triangular patches are modified for the new filter structure, Filter II. The cutoff frequency of Filter II is at 2.5 GHz. Moreover, the Filter II achieves a roll-off of 85 dB/GHz at 20 dB level and an ultra wide stopband with suppression level (SL) better than 23 dB from 2.73 GHz to 9.95 GHz. Filter II has a compact circuit size of about $0.04478 \lambda_g^2$, where λ_g is the guided wave length at 2.5 GHz. The filter structure is further modified by introducing one more resonator near the feed line, named as Filter III. Filter III achieves a sharp roll-off of 125 dB/GHz at 40 dB attenuation level and a wide stopband with SL better than 23 dB from 2.72 GHz to 10 GHz. The physical size of Filter III is 17.6 mm x 12.8 mm.

As the thickness of the substrate decreases, the characteristics impedance of the microstrip line also decreases for material having same dielectric constant, that leads to better approximation of lumped capacitance of the open circuited patch. Thus, the low impedance patches are shorted to ground at high frequencies and provide high level of attenuation at transmission zero frequencies. This property of microstrip line is used for the design of Filter IV. Besides, the length of the transmission line is increased without expanding the physical size by introducing corrugations in the transmission line and U-shaped high impedance short circuited stubs. The 3 dB cutoff frequency of the Filter IV is at 2.04 GHz. Filter IV achieves a roll-off of 60 dB/GHz at 40 dB attenuation level and a wide stopband with suppression level better than 31 dB from 2.65 GHz to 13.4 GHz. The normalized circuit size of the developed filter is $0.02867 \lambda_g^2$, where λ_g is the guided wavelength at 2.04 GHz.

3.2. Basic Characteristics of Microstrip Line

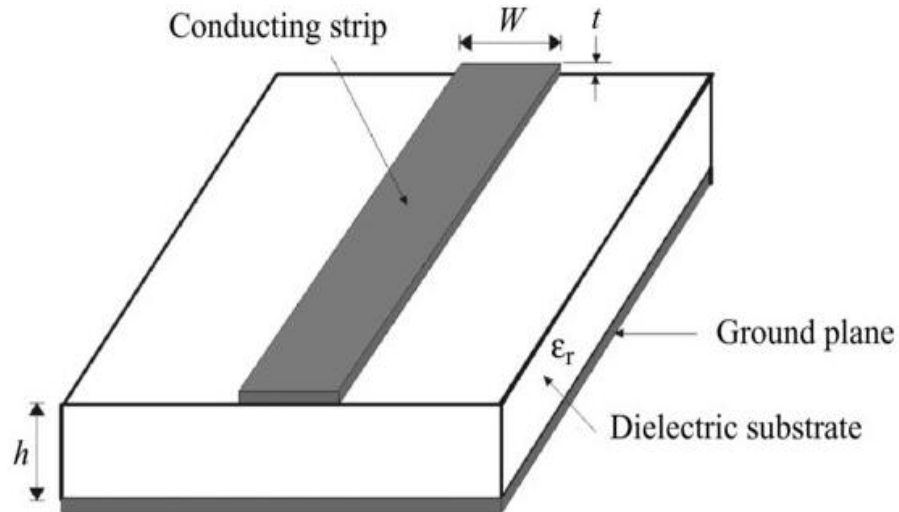


Fig. 3.1 General microstrip structure

The transmission characteristics of microstrip line basically depend on the properties of the substrate material such as its permittivity, thickness and dielectric loss tangent and inversely proportional to its strip line width [1]. Fig. 3.1 demonstrates the structural configuration of a microstrip line. Since microstrip is an inhomogeneous transmission media, the wave propagation through the microstrip not only depends on its substrate properties but also on the physical dimensions of the strip conductor. As the width of the strip conductor increases, the impedance offered by the transmission line decreases. The substrate having same thickness with different permittivity possesses different impedance characteristics.

A homogeneous dielectric material with an effective dielectric permittivity can replace the inhomogeneous dielectric-air media of microstrip.

The wave propagation characteristics of microstrip are expressed by two important parameters, such as the effective permittivity, ϵ_{re} and characteristic impedance Z_0 . Generally the characteristic impedance Z_0 of the microstrip line can be determined by the formula, (3.1) to (3.6), that relate the width of the strip conductor, W and the parameters such as permittivity, ϵ_r and thickness, h of the substrate material [1].

$$Z_0 = \frac{\eta}{2\pi\sqrt{\epsilon_{re}}} \ln \left[\frac{F}{u} + \sqrt{1 + \left(\frac{2}{u}\right)^2} \right] \quad (3.1)$$

where ϵ_{re} is the effective permittivity of the substrate,

$$u = \frac{W}{h}, \quad \eta = 120\pi \Omega, \quad (3.2)$$

and

$$F = 6 + (2\pi - 6) \exp \left[- \left(\frac{30.666}{u} \right)^{0.7528} \right] \quad (3.3)$$

The expression for effective dielectric constant ϵ_{re} is

$$\epsilon_{re} = \frac{\epsilon_r + 1}{2} + \frac{\epsilon_r - 1}{2} \left(1 + \frac{10}{u} \right)^{-ab} \quad (3.4)$$

where,

$$a = 1 + \frac{1}{49} \ln \left(\frac{u^4 + \left(\frac{u}{52}\right)^2}{u^4 + 0.432} \right) + \frac{1}{18.7} \ln \left[1 + \left(\frac{u}{18.1}\right)^3 \right] \quad (3.5)$$

and

$$b = 0.564 \left(\frac{\epsilon_r - 0.9}{\epsilon_r + 3} \right)^{0.053} \quad (3.6)$$

As demonstrated in Fig. 3.2, the material having lower permittivity possesses higher impedance characteristics even though the substrate thickness remains same. Also, as illustrated in Fig. 3.3, as the thickness of the substrate increases with same dielectric constant, the impedance of the microstrip line also increases.

Usually lowpass filters are designed by using multiple resonators either by using line resonators or by patch resonators to generate transmission zeroes in the stopband. So, for high performance compact filter design using low impedance patches and high impedance stubs, the researchers commonly prefer the substrate having low permittivity and very low thickness with extremely low loss tangent for better approximation of lumped inductance and capacitance. Materials having such properties bear very high costs. Also the design of the inductive stub requires very high impedance for better performance, its fabrication becomes extremely difficult as narrow line.

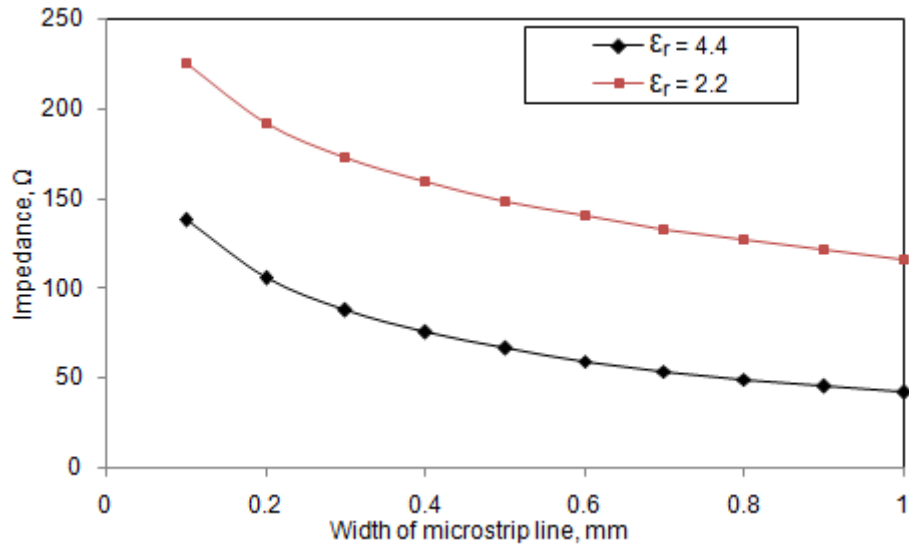


Fig. 3.2 Impedance characteristics of microstrip line as a function of permittivity, ϵ_r of the substrate for the thickness $t = 1.6$ mm

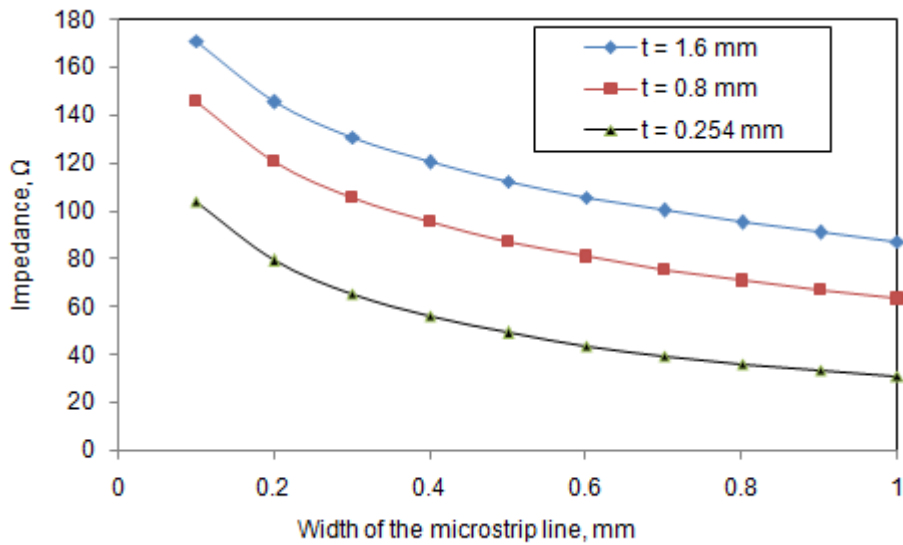


Fig. 3.3 Impedance characteristics of microstrip line as a function of thickness, t of the substrate for permittivity $\epsilon_r = 4.4$

3.3 Filter I- Compact Lowpass Filter using Funnel and Triangular Patch Resonators

Based on the concept of impedance characteristics of planar microstrip transmission line, the compact microstrip lowpass filter is designed and investigated by selecting high impedance stubs and low impedance patches. Since patch resonators possess high power handling capacity and lower conductor loss than narrow line resonators, patch resonators are used for the design of proposed filters. The physical dimensions of individual elements of the resonators are less than $\lambda_g/8$ to approximate lumped components, and they together form a series L-C resonator without considering fringe and parasitic capacitance [1]. The material selected for the design is low cost, lossy FR4 substrate having permittivity 4.4, thickness 1.6 mm with loss tangent 0.02.

3.3.1. Filter Design Considerations

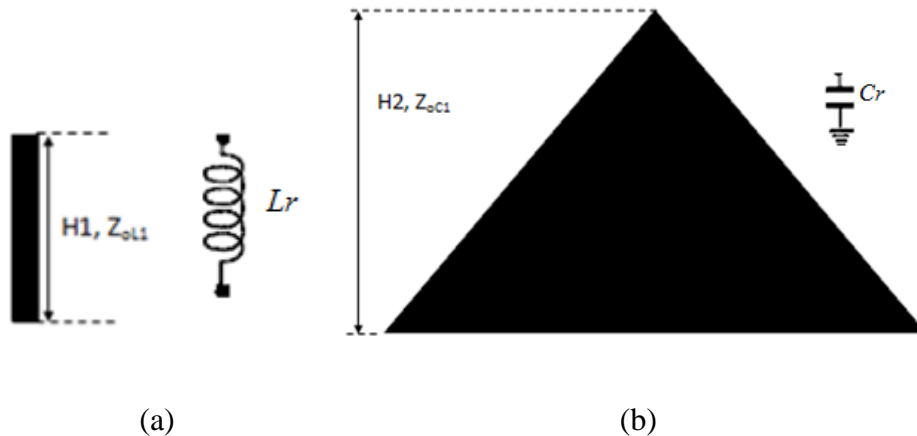


Fig. 3.4 (a) High impedance short circuited stub, (b) Low impedance open circuited patch

Fig. 3.4 shows the layout of the high impedance stub and low impedance triangular patch that used to design the triangular patch resonator (TPR). The high impedance stub is approximated as lumped inductance, L_r , and its value can

be extracted using (3.7) and the low impedance triangular patch as lumped capacitance, C_r is extracted using Eqs. (3.8) - (3.9).

$$L_r = \frac{Z_{OL1} \tan(\beta H1)}{2\pi fc} \quad (3.7)$$

where β is the propagation constant, $H1$ is the electrical length of short circuited high impedance stub connected to the main transmission line, and fc is the 3 dB cutoff frequency.

$$C_r = \frac{-1}{2\pi fc(\text{img}(Z_{in}))} \quad (3.8)$$

where,

$$Z_{in} = 50 \left[\frac{1 + S_{11}}{1 - S_{11}} \right] \quad (3.9)$$

3.3.2 Design of Patch Resonators

The high impedance short circuited stub loaded with low impedance inverted triangular shaped patch forms a series L-C resonator named as funnel patch resonator (FPR). L_{r1} and C_{r1} are the equivalent circuit component values of FPR. The triangular patch resonator (TPR) is also designed with a high impedance short circuited stub and low impedance triangular shaped patch, cascading to form a series L-C resonator with L_{r2} and C_{r2} component values. The geometry of FPR and TPR with equivalent circuit is demonstrated in Figs. 3.5 and 3.6 respectively.

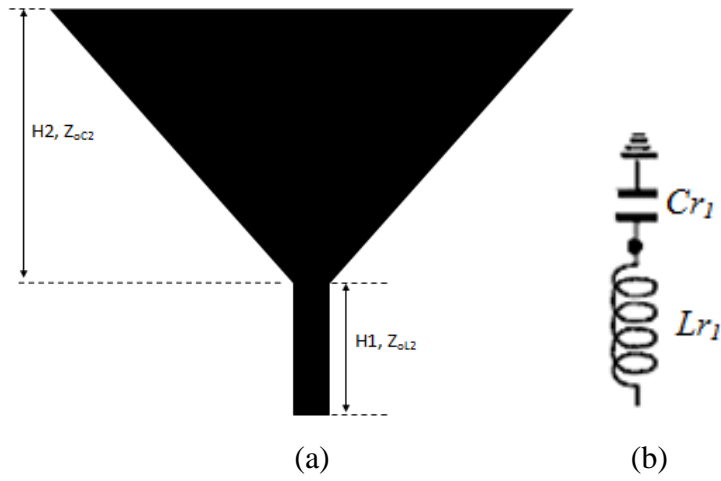


Fig. 3.5 (a) Geometry of FPR, (b) L-C model equivalent circuit of FPR

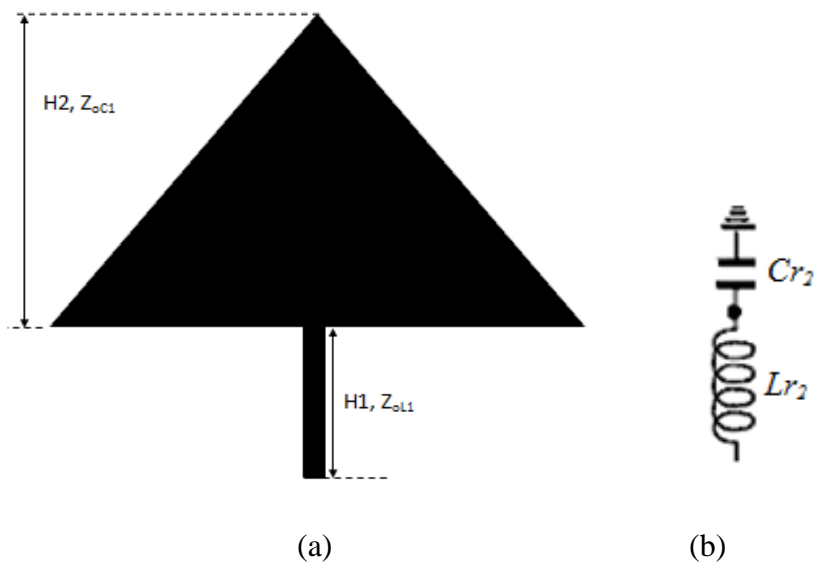


Fig. 3.6(a) Geometry of TPR, (b) L-C model equivalent circuit of TPR

For sharp roll-off and wide stopband lowpass filter characteristics, the impedance of the short circuited stubs of the two resonators is selected in such a way that a narrowband design for the central resonator and wideband design for

side resonators [16]. These stubs perform as short and open circuit with respect to frequency. Thus the stopband bandwidth is enhanced by changing the frequencies satisfying the short circuit condition between high impedance stub of FPR and TPRs. In the proposed filter design, FPR is loaded as the centre resonator and TPRs as side resonators. The stub impedance for FPR is optimized as 106Ω and that of TPRs as 146Ω both having a physical length of 1.6 mm.

3.3.3 S-Parameter Calculations

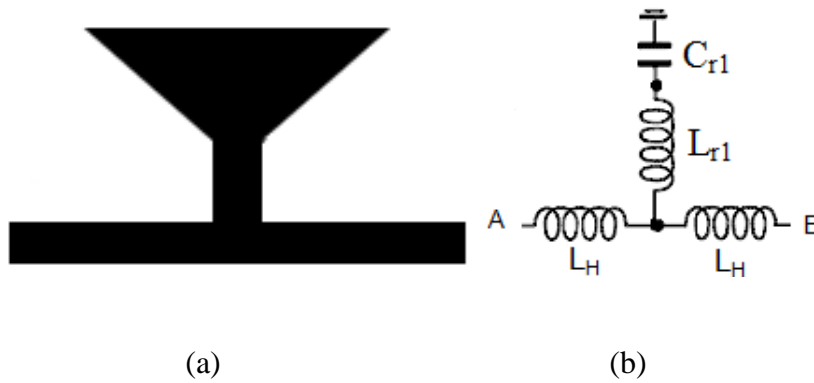


Fig. 3.7(a) Layout of FPR on high impedance line, (b) Equivalent Circuit

The transmission characteristics of a resonator can be easily extracted from its scattering parameters (S-parameters). Figure 3.7(a) demonstrates the layout of the FPR on high impedance line, which is equivalent to a two port T-network of m-derived lowpass filter as shown in Fig. 3.7(b). The S-parameters of a symmetrical network can be determined by using ABCD matrix [17].

The extracted ABCD parameters are:

$$A = D = 1 - \frac{\omega^2 L_H C_{r1}}{(1 - \omega^2 L_{r1} C_{r1})} \quad (3.10)$$

$$B = 2j\omega L_H - \frac{j\omega^3 L_H^2 C_{r1}}{(1 - \omega^2 L_{r1} C_{r1})} \quad (3.11)$$

$$C = \frac{j\omega C_{r1}}{(1 - \omega^2 L_{r1} C_{r1})} \quad (3.12)$$

Relations between ABCD parameters and S-parameters are:

$$S_{11} = \frac{A + B/Z_0 - CZ_0 - D}{A + B/Z_0 + CZ_0 + D} \quad (3.13)$$

$$S_{12} = \frac{2(AD - BC)}{A + B/Z_0 + CZ_0 + D} \quad (3.14)$$

$$S_{21} = \frac{2}{A + B/Z_0 + CZ_0 + D} \quad (3.15)$$

$$S_{22} = \frac{-A + B/Z_0 - CZ_0 + D}{A + B/Z_0 + CZ_0 + D} \quad (3.16)$$

The transmission parameter $|S_{21}|$ of the proposed FPR on high impedance microstrip line from ABCD parameters is:

$$S_{21} = \frac{2Z_0(1 - \omega^2 L_{r1} C_{r1})}{2Z_0(1 - \omega^2 L_{r1} C_{r1} - \omega^2 L_H C_{r1}) + j\omega(2L_H + C_{r1} Z_0^2) - j\omega^3 L_H C_{r1}(2L_{r1} + L_H)} \quad (3.17)$$

The condition for the existence of transmission zero is $|S_{21}| = 0$, then we can deduce the transmission zero frequency, f_Z from Eq.(3.17) as:

$$f_Z = \frac{1}{2\pi\sqrt{L_{r1}C_{r1}}} \quad (3.18)$$

Eqn.(3.18) is validated with L-C Equivalent circuit simulation model analysis using Zeland IE3D software as illustrated in Fig. 3.8. As shown in the figure, the transmission zero corresponds to the value of L_{r1} and C_{r1} , which can be controlled by properly optimizing the dimensions of the resonator.

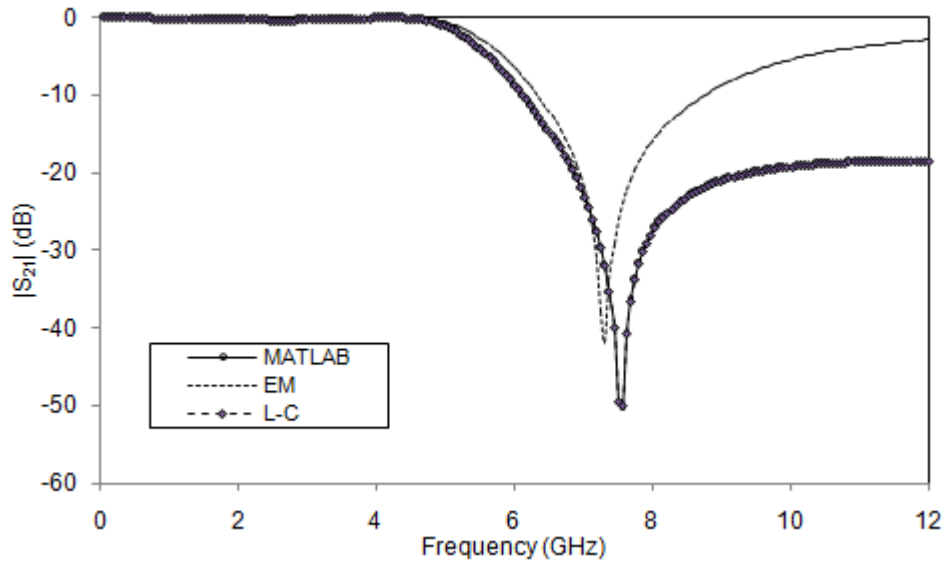


Fig. 3.8 EM, L-C and MATLAB coded simulated $|S_{21}|$ characteristics of FPR on high impedance line

An in-house MATLAB code is written for determining the transmission parameter $|S_{21}|$ of the proposed resonator by using extracted ABCD matrix which also possesses the same response characteristics as illustrated in Fig. 3.8. Moreover, the full-wave EM structural model analysis is also carried out and the result shows good agreement with equivalent circuit model results.

3.3.4 Design of Symmetrical FPR

Fig. 3.9 shows the layout of FPR symmetrically loaded on a high impedance transmission line. As shown in Fig. 3.10, the transmission zero of the resonator can be adjusted by changing the resonator component values without changing the passband insertion and reflection characteristics of the resonator. The response shows a single transmission zero, which can be tuned with the width of the high impedance stub, $W1$ and the height of the stub, $H1$. Since the patch has multiple dimensional parameters, the parametric analyses are mostly conducted on high impedance stub parameters.

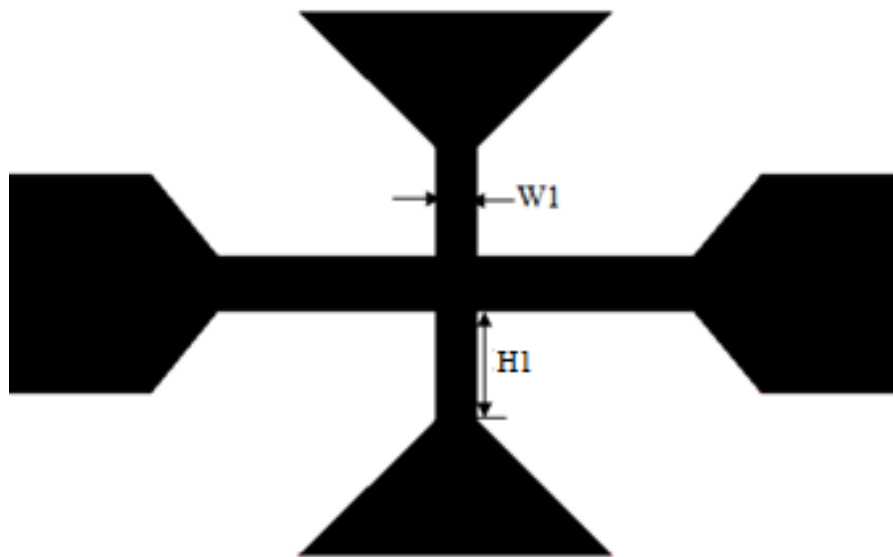


Fig. 3.9 Geometry of FPR on transmission line ($W1 = 0.6$ mm, $H1 = 1.6$ mm)

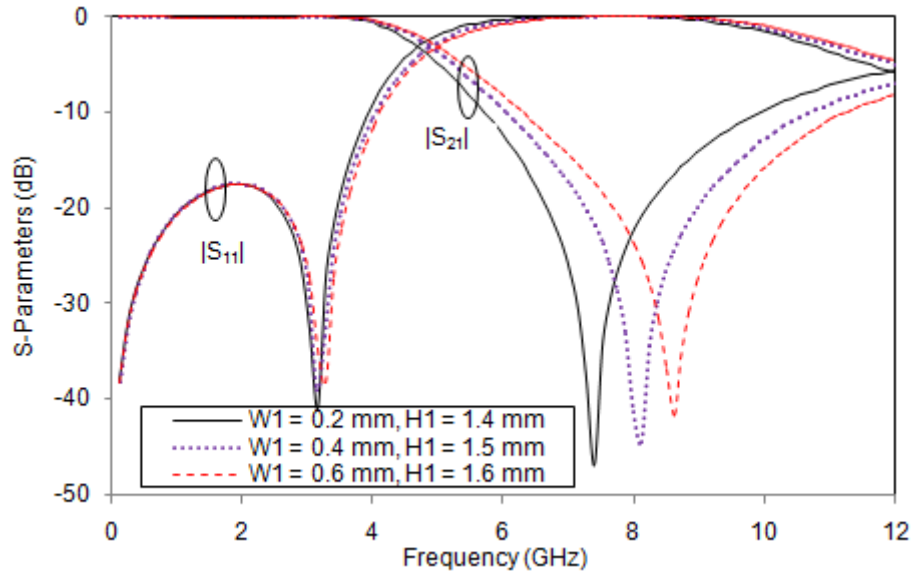


Fig. 3.10 Simulated S-Parameter characteristics of FPR as a function of $W1$ and $H1$ (Optimized dimensions are: $W1 = 0.6$ mm, $H1 = 1.6$ mm)

3.3.5 Design of symmetrical TPR

Fig. 3.11 shows the geometry of symmetrical TPR loaded on high impedance transmission line. TPR also possesses a single transmission zero, T_z at 8.364 GHz corresponds to the inductance and capacitance associated with the 146 Ω impedance stub and low impedance patch respectively. The frequency corresponds to the transmission zero, T_z is independent of the position of TPR on the transmission line as demonstrated in Fig. 3.12. However, the quality factor of the resonator improves with an offset from the centre. In Fig. 3.12, the solid line denotes the S-Parameters characteristics of symmetrical TPR loaded at the centre of the transmission line and the dotted line shows the characteristics at an offset of 2.4 mm from the centre.

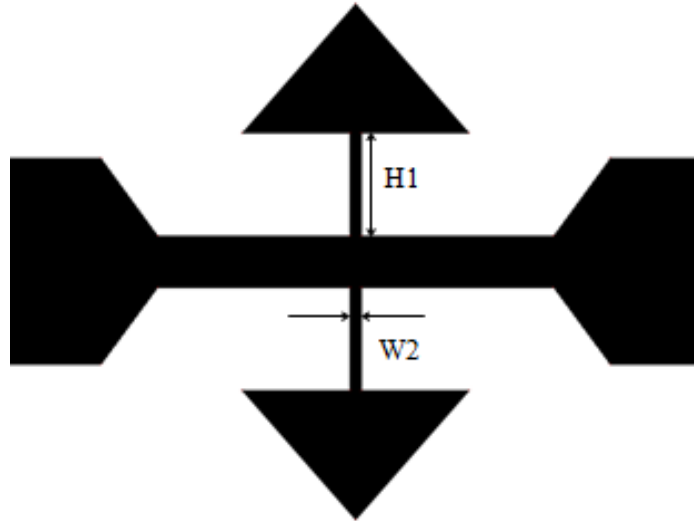


Fig. 3.11 Geometry of symmetrical TPR on high impedance transmission line ($W2 = 0.2$ mm, $H1 = 1.6$ mm)

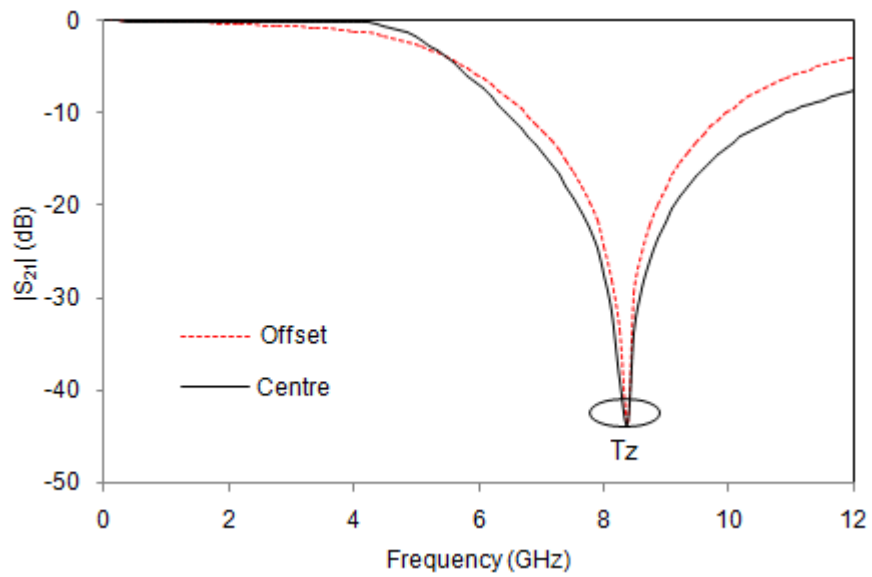


Fig. 3.12 Simulated S-Parameters of symmetrical TPR as a function of position along the transmission line

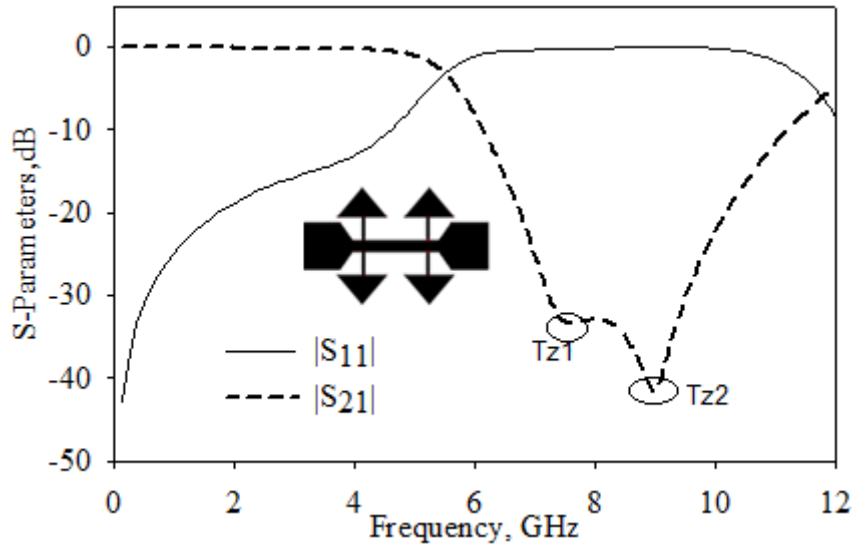


Fig. 3.13 Simulated S-parameters characteristics with two TPRs

Fig. 3.13 shows the simulated characteristics with two TPRs loaded on the 96Ω transmission line, which improves the stopband performance with two transmission zeroes and better roll-off rate by the presence of two resonators. Moreover, the stopband bandwidth is also enhanced by the presence of Tz1 and Tz2 in the stopband, which are located at 7.63 GHz and 8.97 GHz respectively. As shown in figure, the passband performance can also be improved by the effect of 146Ω narrow stub connected to the triangular patch and central microstrip line. However, an ideal lowpass filter has a sharp transition from passband to stopband, the responses of the above mentioned resonator should be modified to a great extent.

By suitably combining both resonators in a filter as shown in Fig. 3.14, we can achieve sharp roll-off rate as well as wide stopband performance. The sharp transmission zero near the cutoff frequency is due to the presence of low impedance patches in both FPR and TPRs and the tight coupling between them,

which enhances the shunt capacitance experienced between the resonators and main transmission line. The wide stopband performance is achieved under the combined effect of the three resonators.

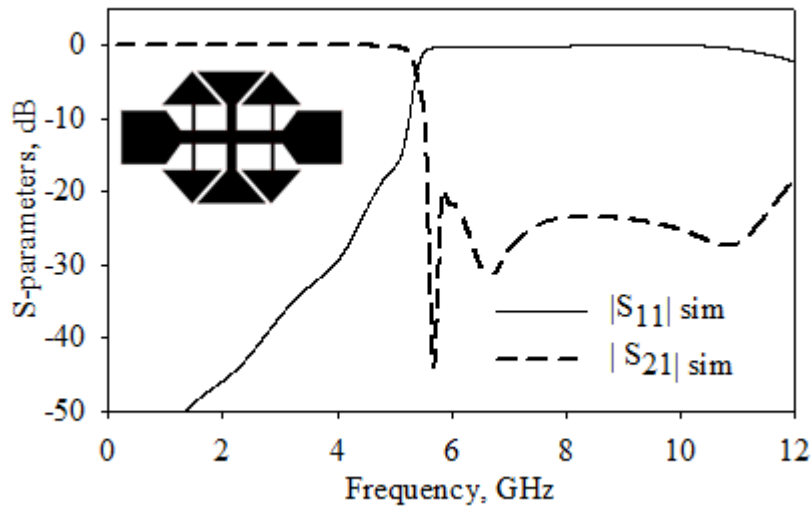


Fig. 3.14 Simulated S-parameters with FPR and two TPRs

Cascading the separate resonators on high impedance transmission line also increases the effective inductance and capacitance of the structure. The insertion loss and return loss in the passband are eliminated to a great extent by using the tapered microstrip feed line. The tapered section acts as an impedance matching transformer and it provides a good coupling between the 50 Ω feed line and the 96 Ω impedance main transmission line. The filter has been designed and fabricated on a low cost FR4 substrate with relative permittivity 4.4 and thickness 1.6 mm.

3.3.6 Parametric Analysis of Filter I

The proposed Filter I consists of low impedance patches and high impedance stubs that together form FPR and TPRs. The size and shapes of patches of TPRs should be compatible with that of FPR in order to enhance the maximum coupling. Many structural parameters are involved in the filter design. A detailed parametric analysis has been conducted to optimize the dimensions of the parameters of the filter.

Fig. 3.15 illustrates the transmission characteristics of the proposed Filter I as a function of stub height (HI) from the 96Ω impedance transmission line. As HI increases, the effective inductance of the resonators increases, that decreases the transmission zeroes in the lower frequency range. The frequency corresponding to the first transmission zero plays an important role to determine the selectivity of the filter. The transmission zero is shifted from 5.212 GHz to 5.93 GHz as HI increases from 1.4 mm to 2 mm. The optimum height of the stubs from the microstrip line is 1.6 mm which corresponds to $0.053 \lambda_g$. Similarly, the width of the gap, W between the resonant patches also has a significant role in the filter design. The decrease in gap width (W) between the resonators causes the tight coupling between the patches that also causes the downward shift in the transmission zero frequency. The first null frequency moves from 5.455 GHz to 5.939 GHz as W varies from 0.2 mm to 0.6 mm as shown in Fig. 3.16.

Fig. 3.17 shows the variation of insertion loss, $|S_{21}|$ with respect to the first transmission zero frequency of Filter I for different values of W and HI by keeping all other parameters constant. The filter achieves a parallel resonance with maximum attenuation of 49 dB at 5.697 GHz, that corresponds to an optimum value of $W = 0.4$ mm and $HI = 1.6$ mm.

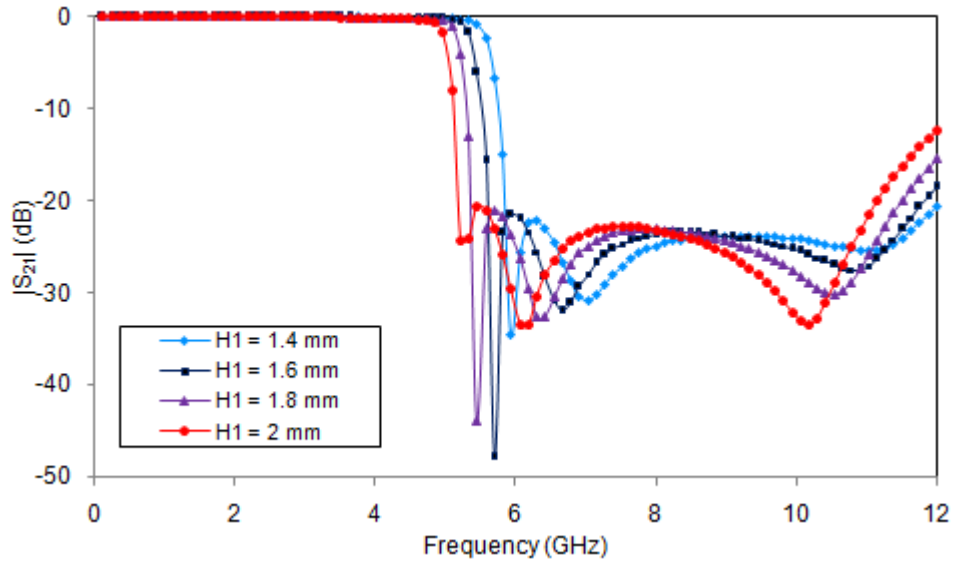


Fig. 3.15 Simulated $|S_{21}|$ characteristics of the Filter I as a function of stub height ($H1$) from the microstrip line

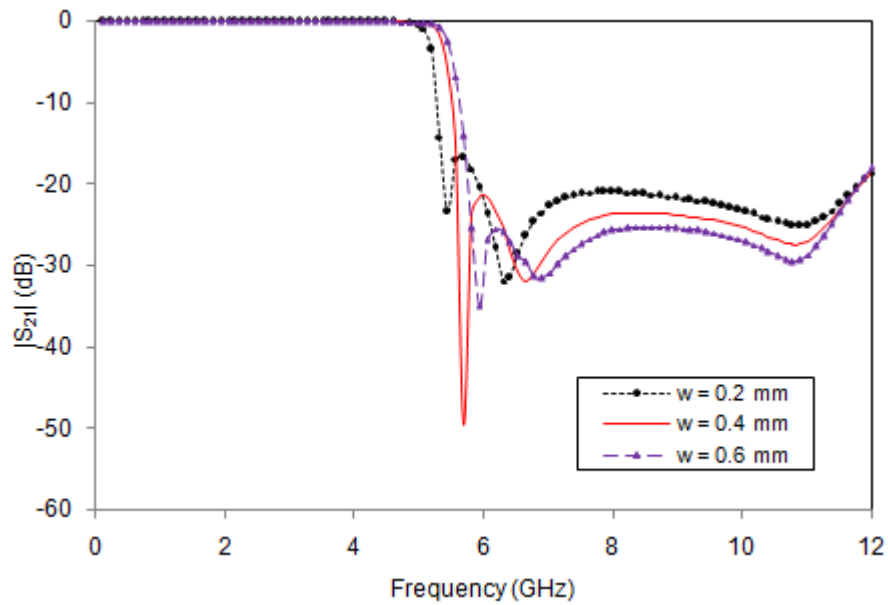


Fig. 3.16 Simulated $|S_{21}|$ characteristics of the Filter I as a function of gap size (W) between the low impedance patches

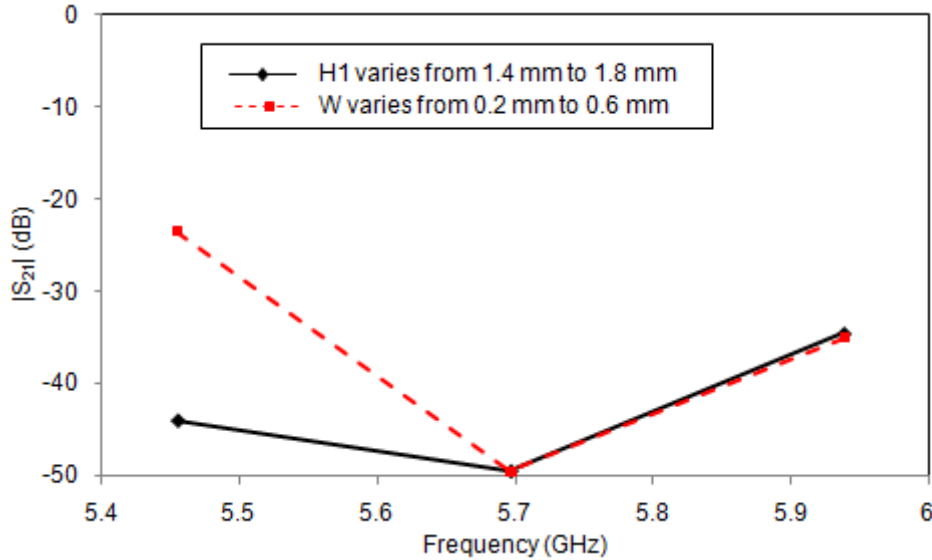


Fig. 3.17 First Null frequency variation of the Filter I as a function of $H1$ and W

3.3.7 L-C Equivalent Circuit Analysis

Figs. 3.18 and 3.19 show the layout and L-C equivalent circuit model of proposed Filter I respectively. As illustrated in Fig. 3.19, the equivalent circuit of Filter I characterizes the elliptic function response. Filter I consists of series L-C resonators in parallel with the inductance associated with the high impedance transmission line, that short out the transmission at their resonant frequencies which contribute an elliptic function response. The equivalent L component values can be extracted by the method demonstrated in [1]. L_1 , L_2 , L_3 and L_4 are the inductance of the transmission line with characteristic impedance 96Ω of length L_2 , L_3 , L_4 and L_5 respectively, which block the transmission at high frequencies due to their high series impedance at high frequencies. The optimum values are: $L_1 = 0.44511$ nH, $L_2 = 1.48148$ nH, $L_3 = 1.4156$ nH and $L_4 = 0.44511$ nH. L_{r1} and L_{r2} are the inductance of the high

impedance stub of the centre resonator and the side resonators respectively. The extracted value of $L_{r1} = 0.864$ nH, and $L_{r2} = 1.35$ nH.

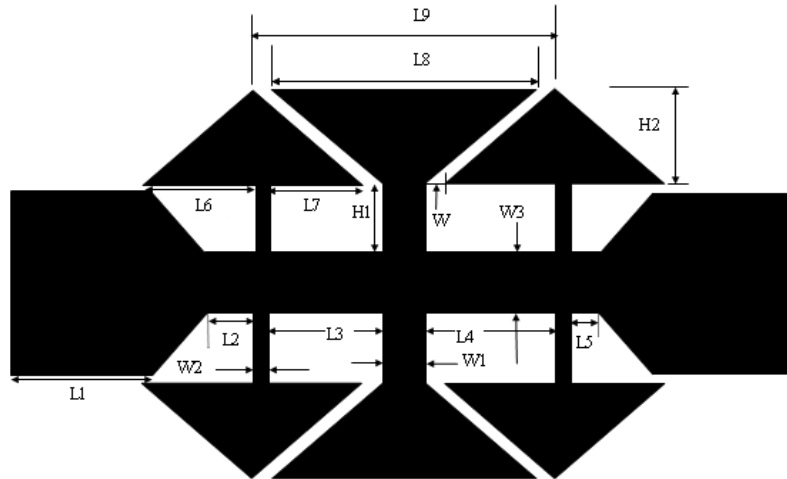


Fig. 3.18 The layout of the proposed Filter I. The optimum dimensions are $L1 = 3$ mm, $L2 = 0.8$ mm, $L3 = 2.2$ mm, $L4 = 2.4$ mm, $L5 = 0.6$ mm, $L6 = 2$ mm, $L7 = 1.8$ mm, $L8 = 4.6$ mm, $L9 = 5.4$ mm, $W = 0.4$ mm, $W1 = 0.6$ mm, $W2 = 0.2$ mm, $W3 = 0.8$ mm, $H1 = 1.6$ mm and $H2 = 2$ mm.

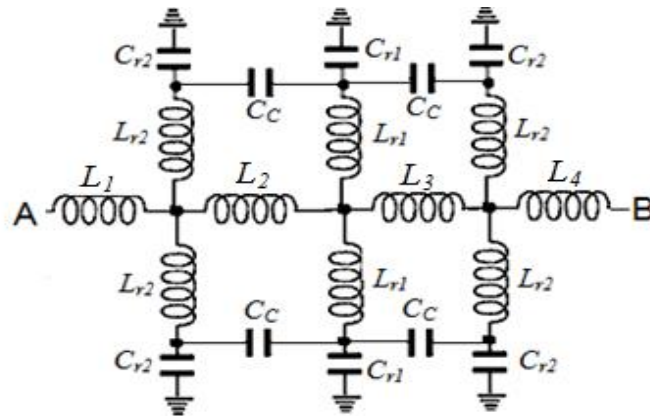


Fig. 3.19 L-C model equivalent circuit of the Filter I. The optimum values are: $L1 = 0.44511$ nH, $L2 = 1.48148$ nH, $L3 = 1.4156$ nH, $L4 = 0.44511$ nH, $L_{r1} = 0.864$ nH, and $L_{r2} = 1.35$ nH. $C_{r1} = 0.41697$ pF, $C_{r2} = 0.28$ pF, and $C_c = 0.035$ pF.

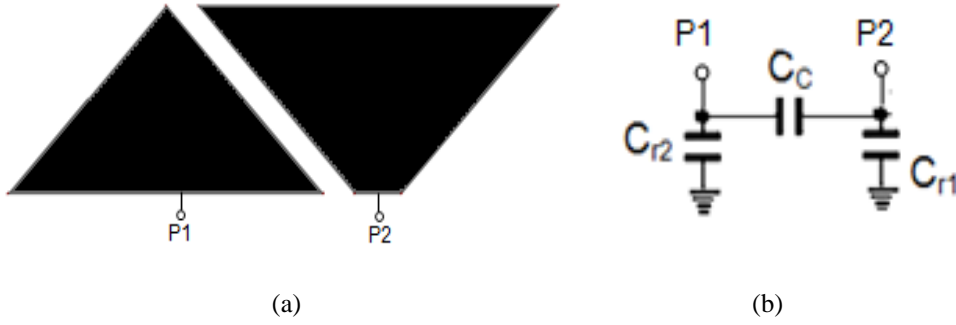


Fig. 3.20(a) Configuration to calculate the capacitance of resonant patch, (b) Equivalent circuit

The capacitance of the low impedance centre and side patches can be determined by the two-port circuit analysis as shown in the configuration depicted in Fig. 3.20. The capacitances C_{r1} and C_{r2} can be extracted through two-port Z-parameters using (3.19). As shown in Fig. 3.20(b), C_c is the equivalent capacitance associated with the coupling between patches. The values of C_c can be extracted through two port admittance parameter using Eq. (3.20).

$$C_{ri} = \frac{-1}{2\pi fc(\text{imag}(Z_{ii}))}, i = 1, 2 \quad (3.19)$$

$$C_c = \frac{-1}{2\pi fc \left(\frac{1}{\text{imag}(Y_{ij})} \right)}, j = 1, 2 (i \neq j), \quad (3.20)$$

where f_c is the 3 dB cutoff frequency, Z_{ii} is the input impedance seen looking into port i when other port is open circuited, and Y_{ij} is the input admittance between port i and port j . The extracted values of capacitance are: $C_{r1} = 0.41697$ pF, $C_{r2} = 0.28$ pF and $C_C = 0.035$ pF.

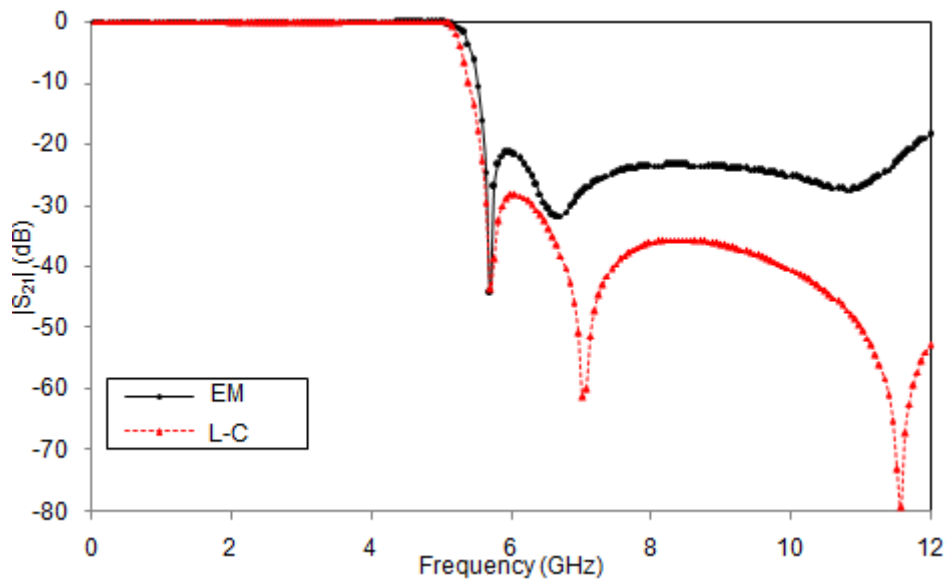


Fig. 3.21 EM and L-C simulation results of Filter I

Fig. 3.21 compares the EM and L-C simulated transmission characteristics of the proposed filter. Both results show a good agreement in the entire passband and up to first transmission pole after cutoff frequency. The difference in zero locations and attenuation level in the higher frequency range is acceptable because of three main reasons. Firstly, the equivalent lumped circuit model may be beyond the constraint conditions in the high-frequency range where the electric length may be larger than a quarter-wave length and the high-order parasitic effects become dominant. Secondly, referring to the ideal

model results in Figs. (3.24–3.26); the zeros in the stopband are quite sensitive to the value of L_{ri} and C_{ri} , especially for C_{ri} . A smaller change in C_{r1} and C_{r2} , the zeros change dramatically and make the model difficult to accurately represent the stopband zeros. Finally in L-C model, only values of L and C are the dependent parameters for the transmission analysis, whereas in EM model all the substrate details and loss parameters come in the picture [6]. Practically, when the resonators are connected together on a high impedance transmission line they form a compound resonator. The transmission zeroes are contributed by the combined effect of all resonators and the coupling between them.

3.3.8 Equivalent Circuit Parametric Analysis

Since the size and shape of resonant patches of FPR and TPRs are one to one compatible, it is very difficult to conduct full wave structural parametric analysis of the patch resonators individually. So, to analyze the contribution of individual components within the filter structure, we conducted a detailed equivalent circuit parametric analysis. The equivalent circuit was realized using Zeland IE3D simulation software.

3.3.8.1 Transmission line inductance, (L_1/L_2)

As illustrated in Fig. 3.19, L_1 , L_2 , L_3 and L_4 are the inductance of the transmission line with characteristic impedance 96Ω of length L_2 , L_3 , L_4 , and L_5 respectively. As demonstrated in Figs. 3.22 and 3.23, the position of transmission zeroes is independent of inductance of main transmission line. Since the transmission zero frequencies depend exactly on the resonator parameters, small change in inductance of main transmission line (L_1 or L_2) does not have much significance in the characteristics of the filter.

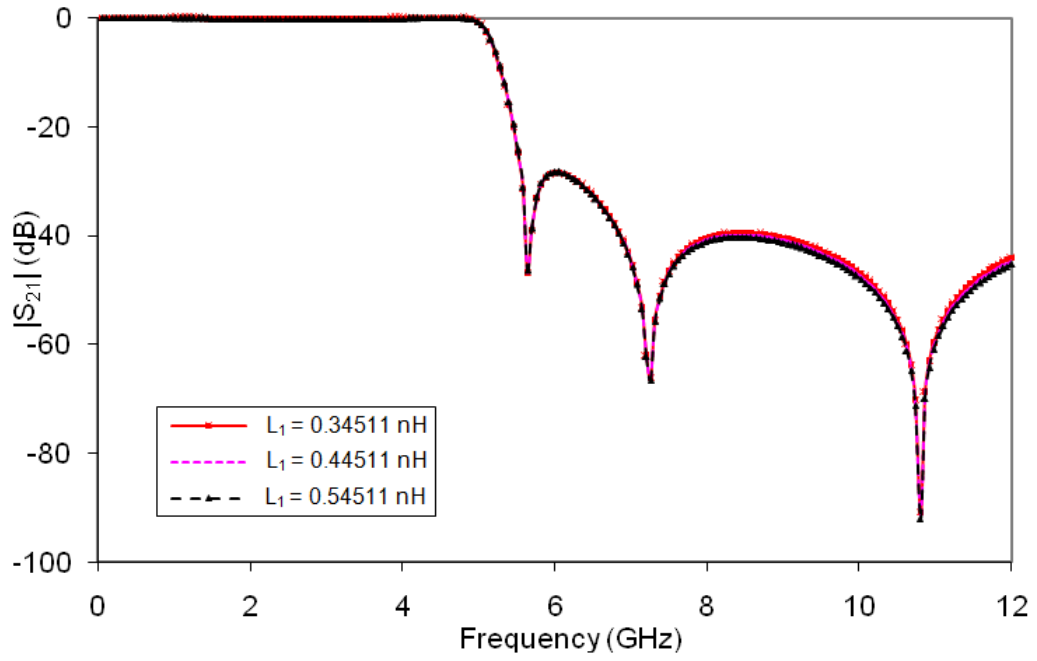


Fig. 3.22 $|S_{21}|$ Characteristics of the Filter I as a function of L_1

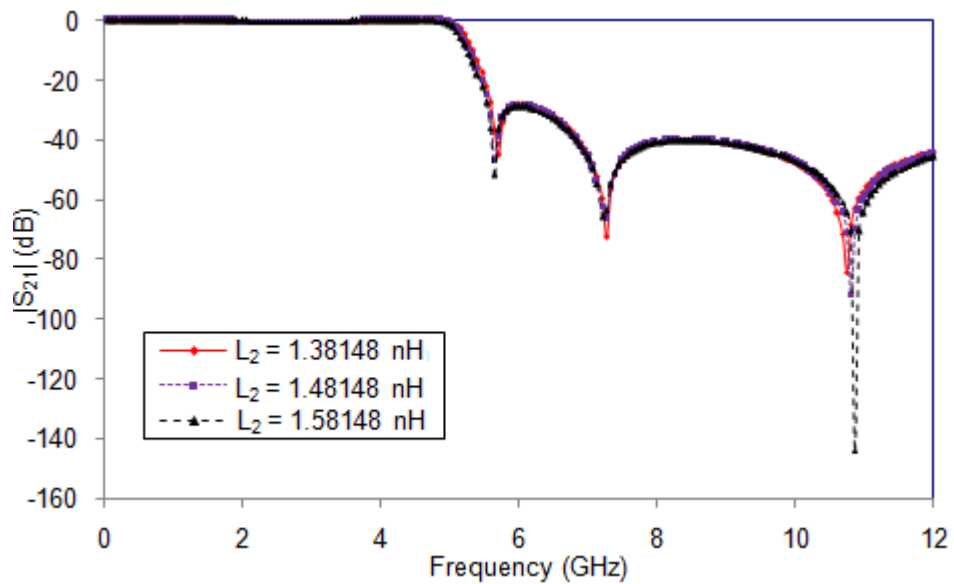


Fig. 3.23 $|S_{21}|$ Characteristics of the Filter I as a function of L_2

3.3.8.2 Inductance of high impedance stub, (L_{r1}/L_{r2})

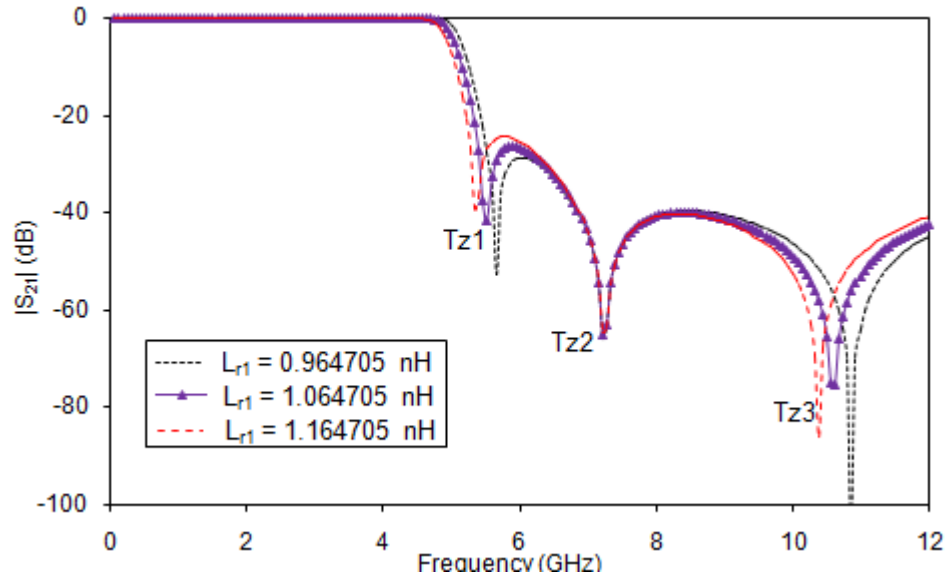


Fig. 3.24 $|S_{21}|$ Characteristics of the Filter I as a function of L_{r1}

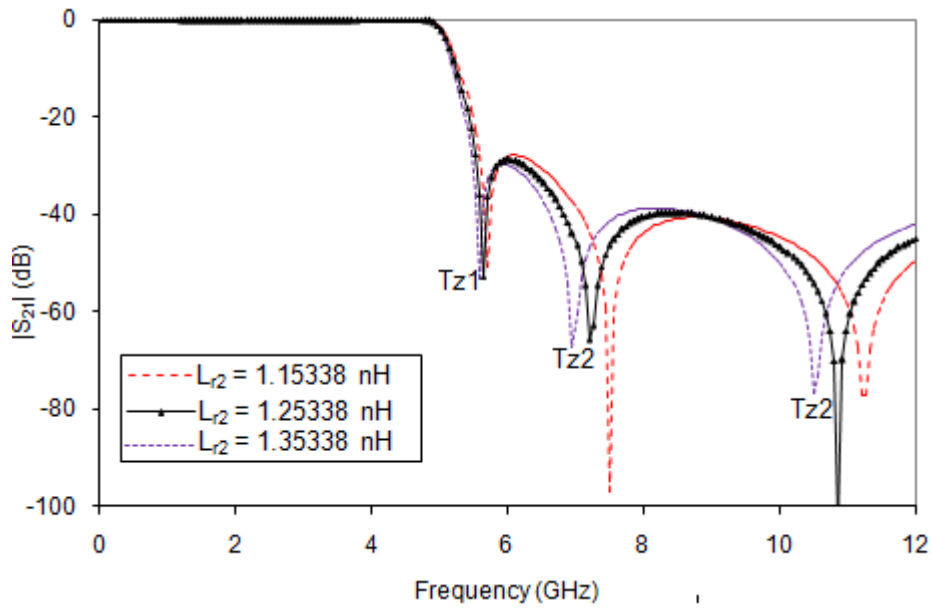
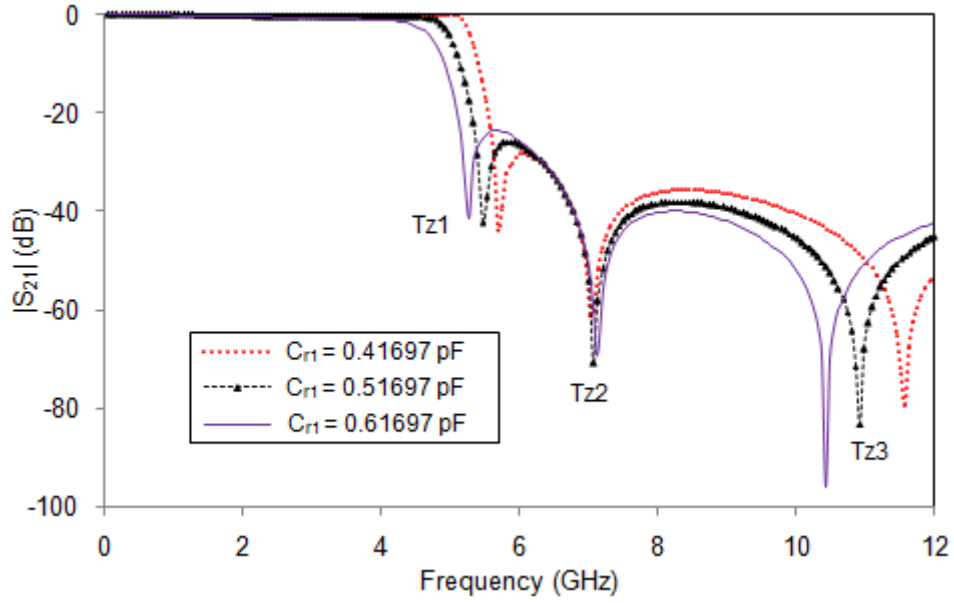


Fig. 3.25 $|S_{21}|$ Characteristics of the Filter I as a function of L_{r2}

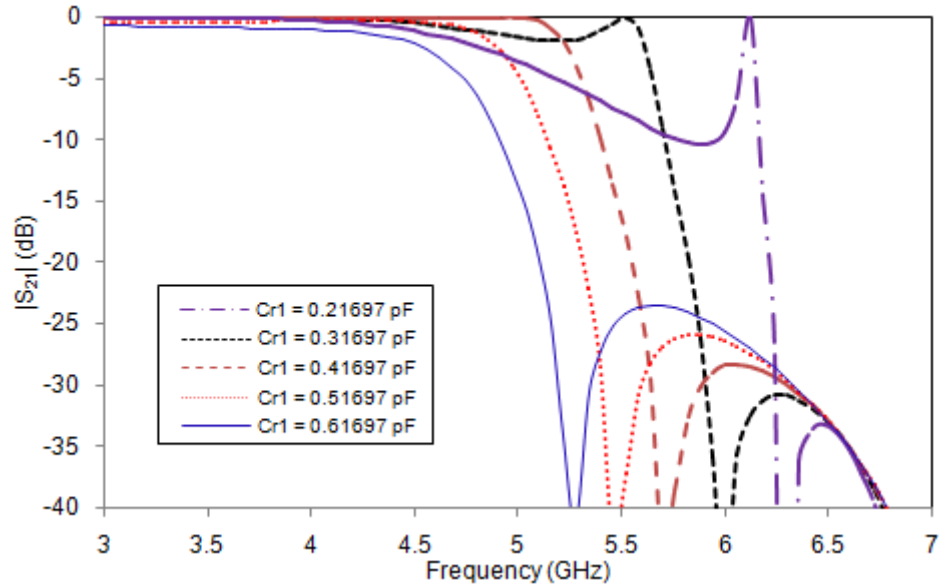
Figs. 3.24 and 3.25 demonstrate the transmission characteristics of Filter I as a function of inductance of high impedance stub of centre and side resonators L_{r1} and L_{r2} respectively. As shown in Fig. 3.24, the second transmission zero Tz2 is independent of change in L_{r1} , whereas the position of Tz1 and Tz3 changes with L_{r1} . The second transmission zero, Tz2 is contributed by the effect of side resonators, which can be tuned by adjusting the side resonator structural parameters. However, the positions of Tz1, Tz2 and Tz3 affect evenly with the change in inductance of high impedance stub of side resonators L_{r2} as depicted in Fig. 3.25.

3.3.8.3 Capacitance of low impedance patch, (C_{r1}/C_{r2})

Fig. 3.26(a) shows the simulated $|S_{21}|$ characteristics of the filter as a function of capacitance of FPR patch, C_{r1} where the contribution of Tz2 is independent of the variation of C_{r1} , which is again proved by the characteristics. Also, the selectivity and passband insertion loss of the filter can be controlled by the value of C_{r1} . Fig. 3.26(b) shows the passband insertion loss characteristics of Filter I as a function of C_{r1} . As shown in the same figure, for lower values of C_{r1} , there exists a ripple near the cutoff frequency with sharp switching characteristics. The amount of ripple level and selectivity of the filter decreases as the C_{r1} increases, which can be achieved by increasing the size of the centre resonator patch. The passband ripples are mainly due to the anti-resonance contributed by very low impedance of FPR patch, since as capacitance C_{r1} increases, the impedance offered by the patch decreases.

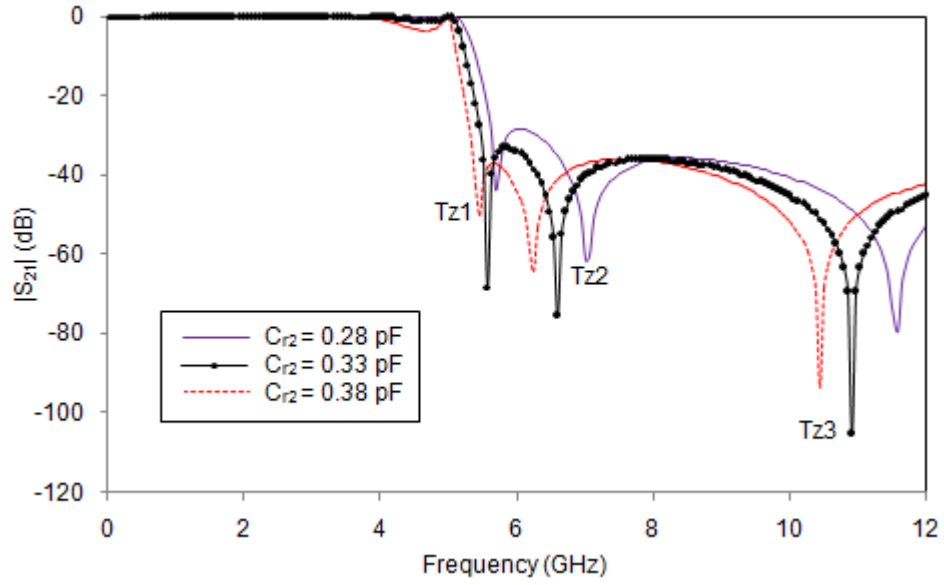


(a)

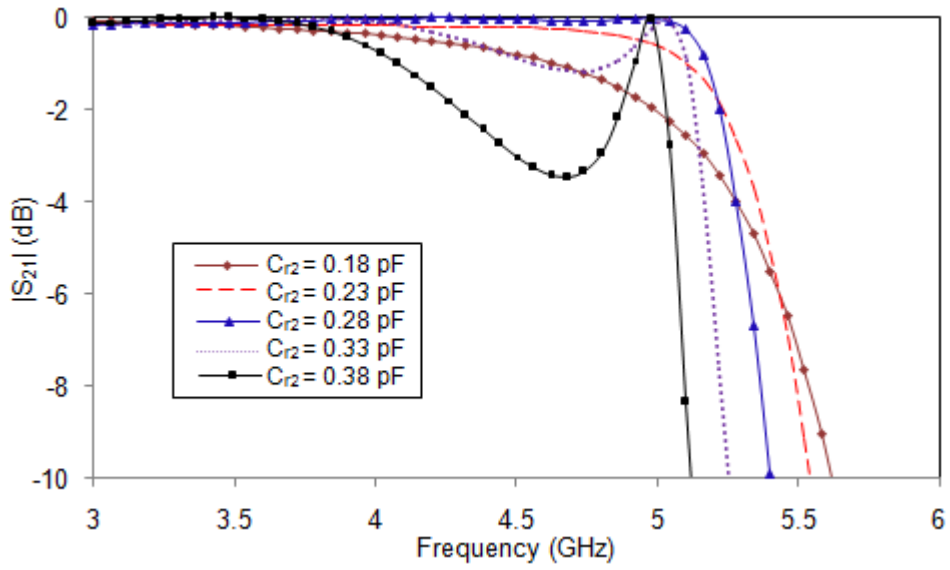


(b)

Fig. 3.26 (a) $|S_{21}|$ Characteristics of Filter I as a function of C_{r1} , (b) passband performance of Filter I as a function of C_{r1}



(a)



(b)

Fig.3.27(a) $|S_{21}|$ Characteristics of Filter I as a function of C_{r2} , (b) passband performance of Filter I as a function of C_{r2}

Fig. 3.27 illustrates the transmission characteristics of Filter I as a function of C_{r2} , the capacitance of open circuited patch of side resonators. As shown in the figure, C_{r2} has an inverse effect in the filter characteristics as compared to the role of C_{r1} . The filter achieves sharp elliptic function response for high values of C_{r2} . As the value of C_{r2} increases, the ripple level in the passband also increases. Thus for designing filter with sharp roll-off rate and minimum insertion loss in the passband, it is desirable to design the capacitive patches having high value of C_{r1} and low values of C_{r2} . Thus we can transform the filter response from elliptic function response to Chebyshev response by tuning the values of C_{r1} and C_{r2} . The designed optimum values of $C_{r1} = 0.41697$ pF and $C_{r2} = 0.28$ pF.

3.3.8.4 Coupling Capacitance, (C_c)

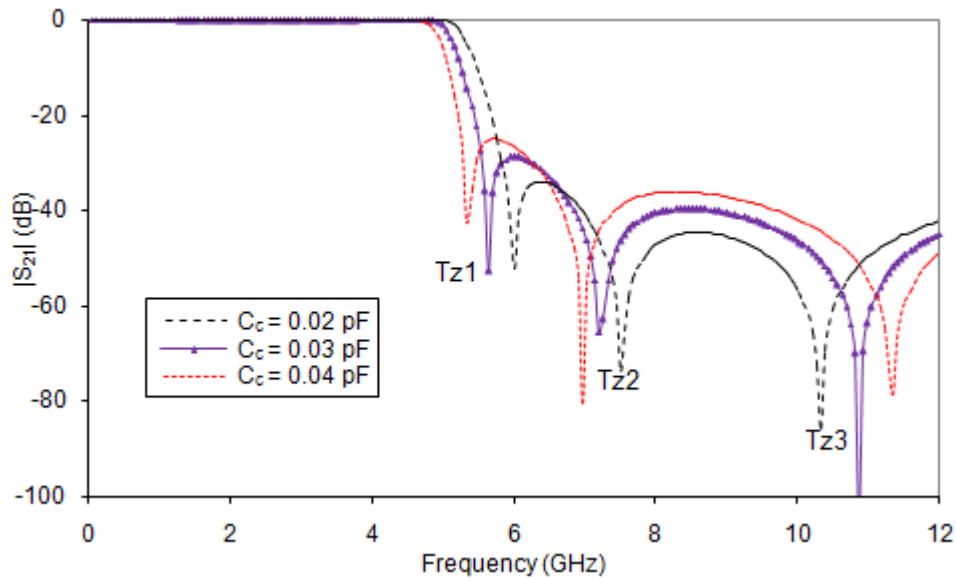


Fig. 3.28 $|S_{21}|$ Characteristics of Filter I as a function of coupling capacitance C_c

The coupling capacitance, C_C between the resonant patches has an important role in the filter design. Changing the value of C_C affects all the transmission zero frequencies and the cutoff frequency, as shown in Fig.3.28. As C_C increases, cutoff frequency and the position of transmission zeroes Tz1 and Tz2 are shifted to low frequency range, whereas Tz3 is shifted to higher range that enhances the stopband of the filter.

3.3.9 Measurement results of Filter I

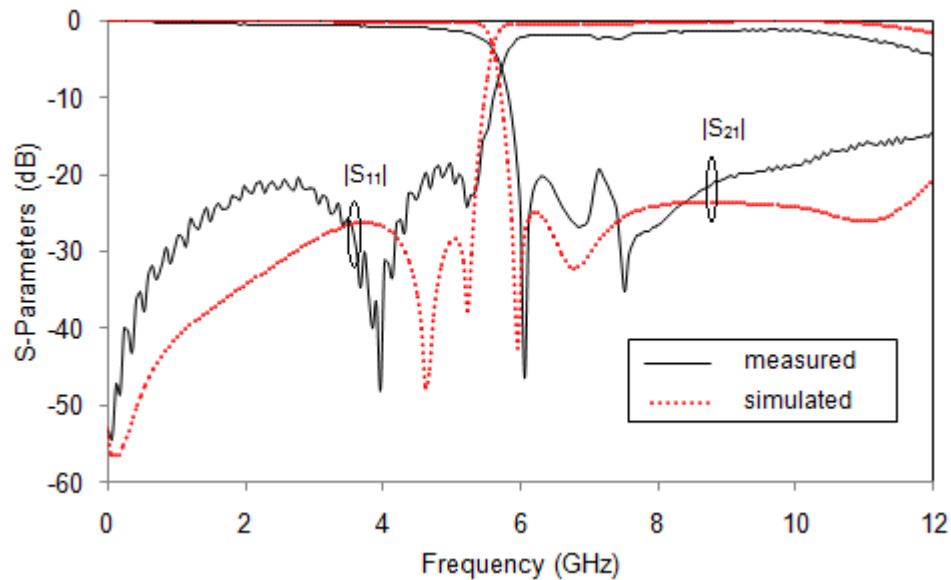


Fig.3.29 Measured and simulated results of proposed Filter I

The layout of the proposed Filter I is depicted in Fig. 3.18. The simulation has been accomplished using Electromagnetic simulation software Zeland IE3D and fabricated using photolithographic process. The measurement was carried out using R&S ZVL 13 Vector Network Analyzer. As shown in

Fig. 3.29, the measured results of Filter I are in good agreement with the simulated results. The result shows that Filter I has an insertion loss less than 0.7 dB in the passband up to 4 GHz, with a cutoff frequency of 5.55 GHz. The filter achieves a stopband suppression level (SL) better than 15 dB from 5.88 GHz to 11.8 GHz. The measured return loss of the filter is less than 20 dB in the passband and close to 2 dB at the end of the stopband. The relative stopband frequency of the filter is 66.96%. The filter has a compact size of about 9.4 mm x 8 mm, which corresponds to the normalized circuit size of $0.3174\lambda_g \times 0.27016\lambda_g$ where λ_g is the guided wavelength at 5.55 GHz. As illustrated in Fig. 3.30, each of the measured frequency components in the passband experiences nearly same delay so that their phase relative to one another is maintained. The filter exhibits a very small group delay variation of 0.15 ns (0.2 ns to -0.35 ns) throughout the passband.

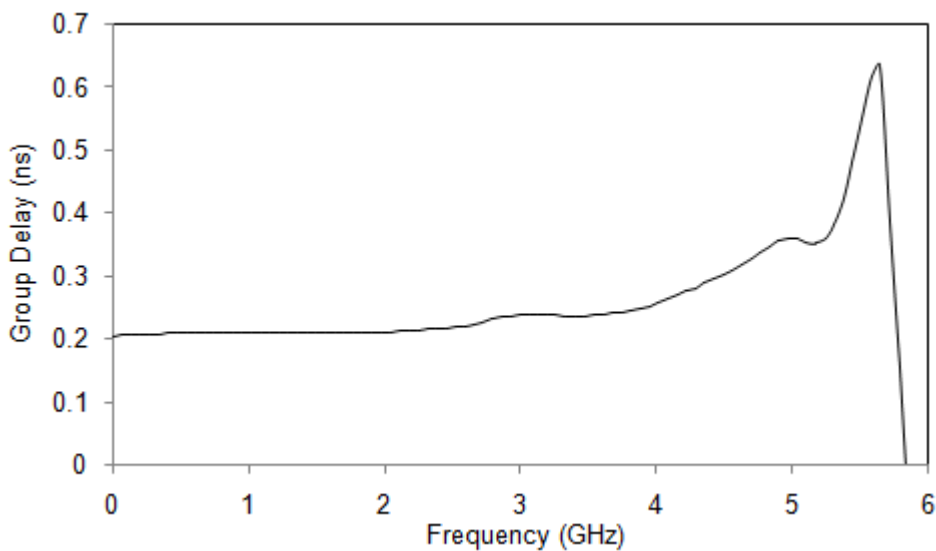


Fig.3.30 Measured group delay characteristics of Filter I

Fig. 3.31 shows the photograph of the fabricated filter. A comparison of designed filter with the previous works is shown in Table 3.1. From the table it is clear that, the proposed filter is made of low cost FR4 substrate and gives high roll-off rate among the quoted filters. The proposed filter passband includes two major ISM bands.

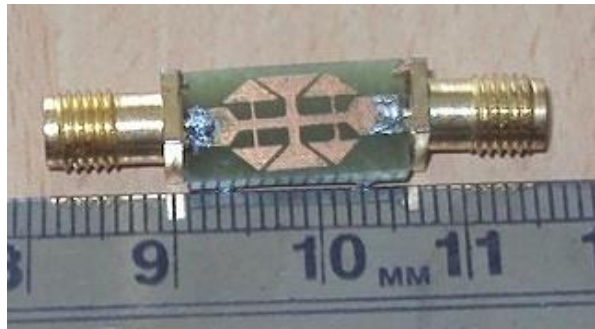


Fig. 3.31 Photograph of prototype of Filter I

Table 3.1 Comparison between performance of Filter I and other published works in the literature

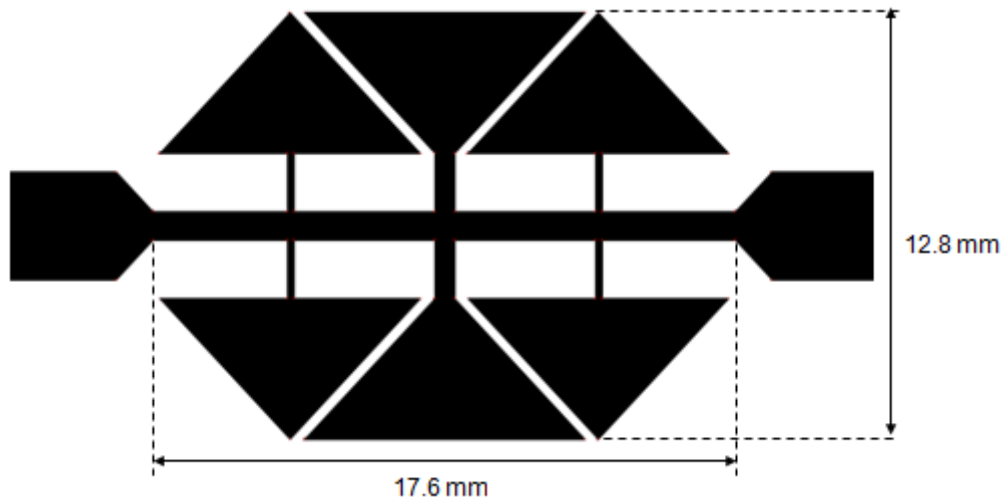
| <i>Ref</i> | <i>fc</i> (GHz) | ξ (dB/GHz) | <i>Material used</i> |
|------------|--------------------|-------------------|----------------------|
| [6] | 6.3 | 12 | RT/duroid 5880 |
| [7] | 1.5 | 30.8 | RT/duroid 5880 |
| [8] | 1.3 | 36 | RT/duroid 5870 |
| [10] | 0.85 | 23 | Roger RO4003 |
| [13] | 6 | 30 | RT/duroid 5880 |
| [Filter I] | 5.55 | 84 | FR4 |

f_c = cutoff frequency, ξ = roll-off rate

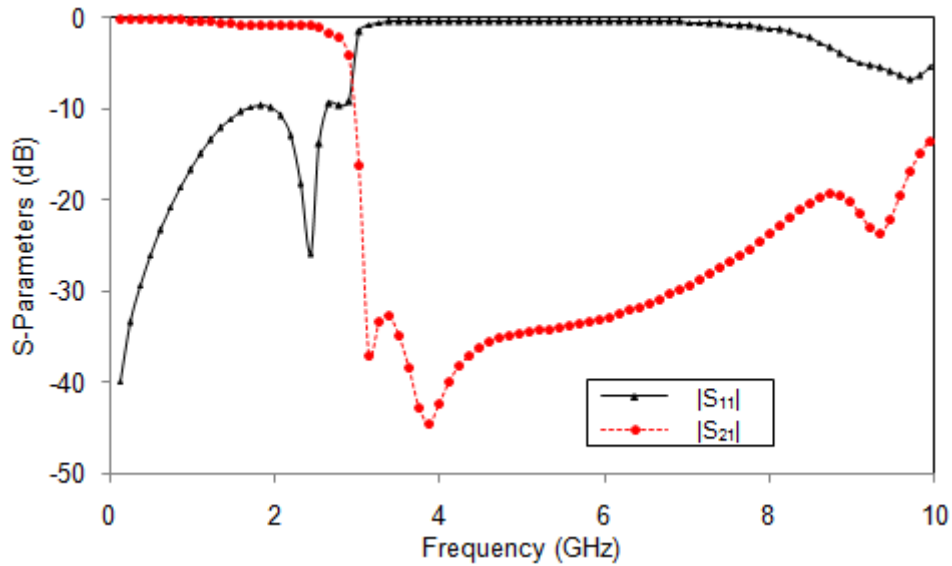
This work has been published in *Microwave. and Optical Technology Letters* Vol. 56, No. 11, Nov. 2014.

3.4 Filter II- Compact Planar Lowpass Filter with modified FPR and TPRs

3.4.1. Filter Design Considerations



(a)



(b)

Fig. 3.32(a) Layout of Filter I with enhanced length of transmission line and patch size, (b) Simulated S-Parameters

The fractional stopband bandwidth as well as the circuit size of Filter I can be enhanced by scaling up the geometrical dimensions of the filter as illustrated in Fig. 3.32. (The physical size of Filter I is 9.4 mm x 8 mm). As physical size increases, the effective inductance and capacitance increase that decreases the cutoff frequency of the filter. But, as the size of the patch capacitance increases, the impedance offered by the open circuited patches decreases, which increases the capacitance of the side resonators and thereby leads to introduce high ripples in the passband insertion loss characteristics as shown in Fig. 3.32(b). So, mere scaling up of Filter I will introduce transverse resonance, that contributes high level of ripples in the passband and high insertion loss as demonstrated in Figs. 3.33. Increasing the impedance of TPRs by modifying its shape will reduce the passband losses and that property is used in the design of Filter II.

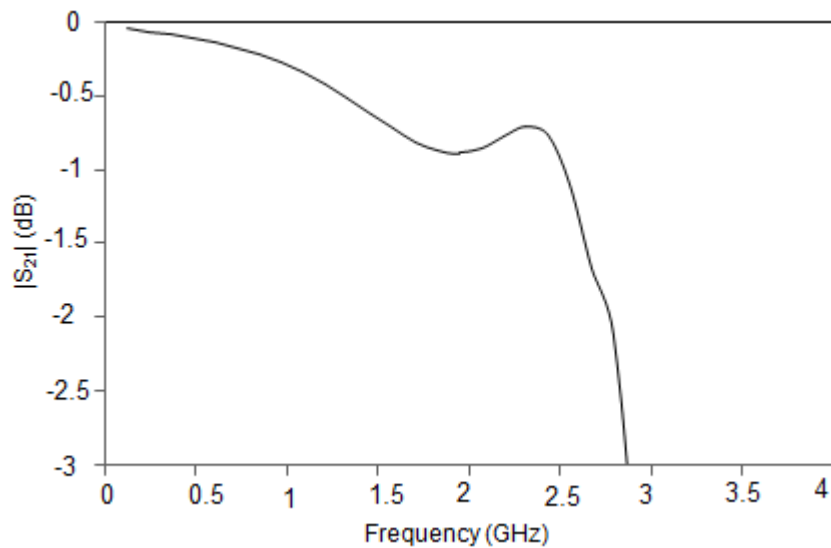


Fig. 3.33 Passband insertion loss characteristics of enhanced size of Filter I

The structure of the proposed Filter II is derived from TPRs and FPR by cutting the base corner of TPRs symmetrically. The inner corner portion is attached to the FPR on both sides as shown in Fig. 3.34, and the outer corner is eliminated. The impedance of the connecting stub of the centre resonators is 106Ω and that of modified TPRs is 146Ω . Table 3.2 compares the performance of enhanced size of Filter I with and Filter I with modified FPR and TPRs. As demonstrated in the table, by modifying the structure we can reduce the passband insertion loss of the filter by 0.3 dB.

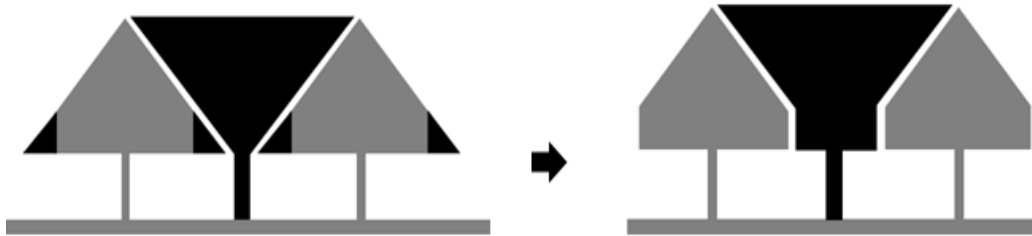


Fig. 3.34 Equivalent relation between TPRs and FPR with modified TPRs and FPR

Table 3.2 IL Comparison between filter shown in Fig. 3.32 (a) and Filter II

| <i>Filter</i> | <i>f_c</i> (GHz) | <i>f_s</i> (GHz) | <i>IL in PB</i> (dB) |
|-----------------------------------|-------------------------------|-------------------------------|-------------------------|
| Low <i>f_c</i> Filter I | 2.87 | 2.95 | 0.9 |
| Modified FPR & TPR | 3.05 | 3.18 | 0.6 |

f_c = cutoff frequency, *f_s* = 20 dB attenuation frequency, IL in PB = insertion loss in the passband

3.4.2 Parametric Analysis of Filter II

Since various parameters influence the performance characteristics of the proposed filter, a detailed analysis has been conducted to optimize the structure of Filter II.

3.4.2.1 Stub Height, ($H1$)

Figs. 3.35 and 3.36 demonstrate the transmission and reflection characteristics of Filter II with respect to variation of height $H1$ of the high impedance short circuited stubs connected to patches. As the value of $H1$ increases, the transmission zeroes are shifted to the lower frequency range because of the increase in the effective inductance of the structure as illustrated in Fig. 3.36. As shown in Fig. 3.37, short length high impedance stub produces better reflection characteristics with wide stopband performance.

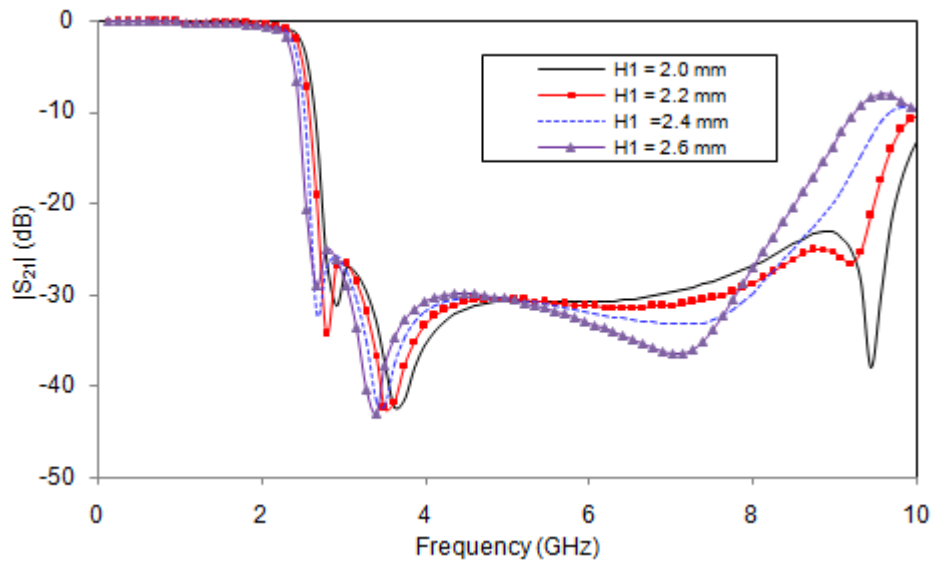


Fig. 3.35 $|S_{21}|$ Characteristics of Filter II as a function of stub height $H1$

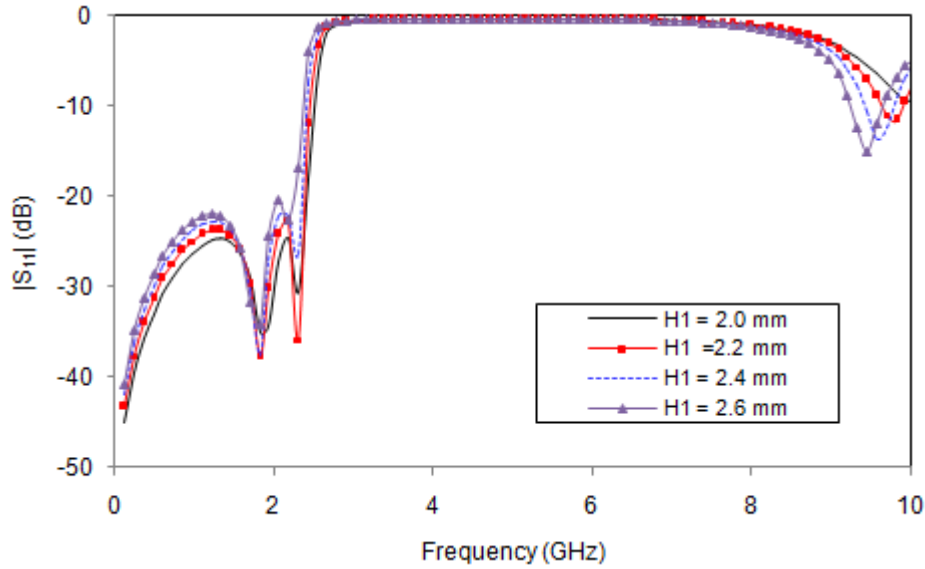


Fig. 3.36 $|S_{11}|$ Characteristics of Filter II as a function stub height $H1$

3.4.2.2 Width of the Transmission Line, ($W3$)

Figs. 3.37 and 3.38 illustrate the characteristics of the filter with the effect of width of the high impedance transmission line $W3$. The high impedance transmission line performs as lumped inductance and, that offers high impedance in the high frequency range. As $W3$ decreases, the impedance of the transmission line increases that enhances the stopband bandwidth of the filter. The stopband suppression level also increases with decrease in $W3$. However, the first two transmission zero frequencies, $Tz1$ and $Tz2$ of the filter characteristics are moreover same for all the values of $W3$. The position of $Tz1$ and $Tz2$ depends exactly on the resonator parameters.

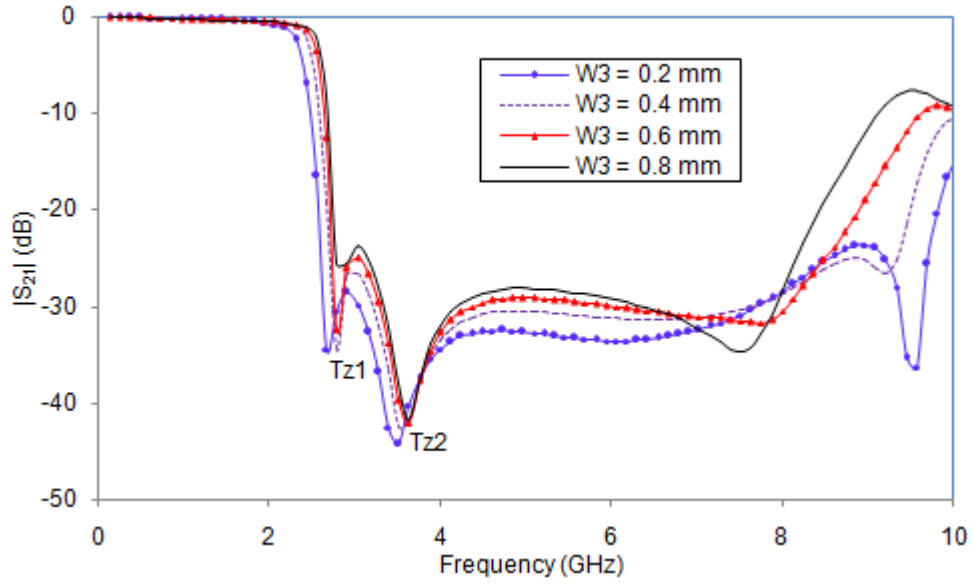


Fig. 3.37 $|S_{21}|$ Characteristics of Filter II as a function transmission line width, W_3

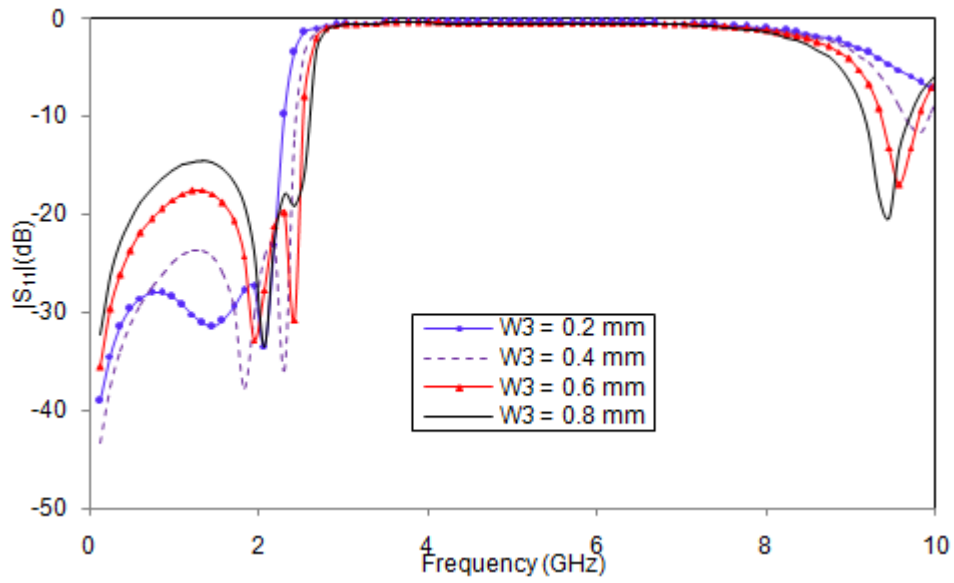


Fig. 3.38 $|S_{11}|$ Characteristics of Filter II as a function transmission line width, W_3

3.4.2.3 Position of high impedance stub of TPRs relative to the patch, ($L4$)

The position of high impedance stub of side resonators (TPRs) relative to the patch, $L4$ also plays an important role for optimizing the filter structural dimensions. As demonstrated in Fig. 3.39, as $L4$ increases, the selectivity of the filter decreases with increase in stopband suppression level. Also, the stopband bandwidth decreases with increasing $L4$. Conversely, as the position of high impedance stub moves towards the edge of the capacitive patch near the feed line, the stopband bandwidth of the filter can be enhanced to a great extent due to the existence of asymmetrical step discontinuity between stub and patch. However, as $L4$ increases, the reflection characteristics of the filter feel poor in passband, as demonstrated in Fig. 3.40.

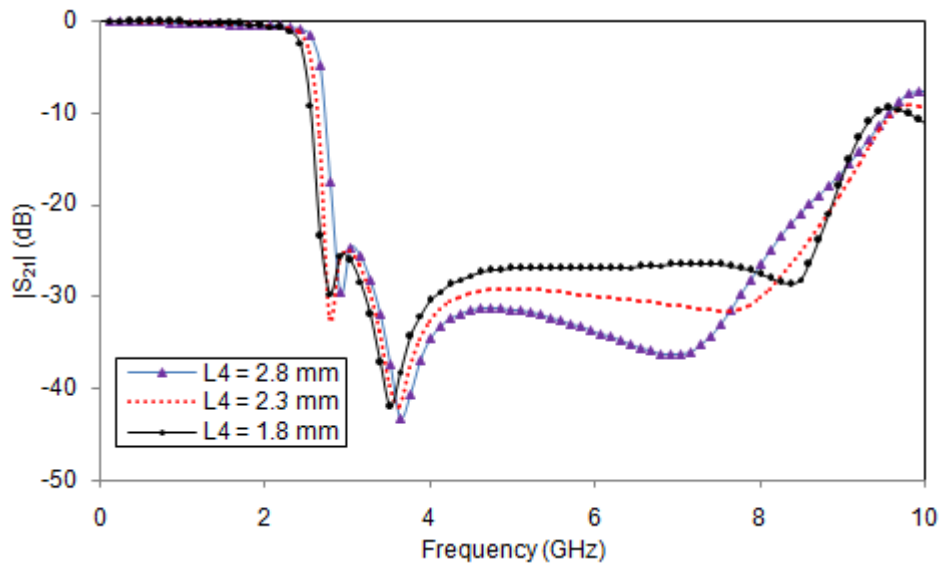


Fig. 3.39 $|S_{21}|$ Characteristics of Filter II as a function of position of high impedance stub TPRs relative to the patch, $L4$

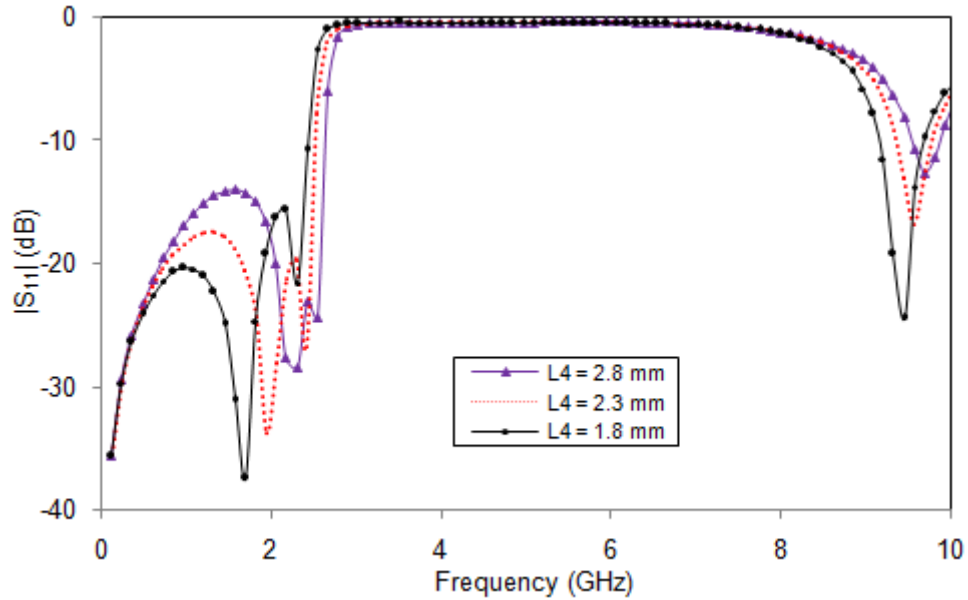


Fig. 3.40 $|S_{11}|$ Characteristics of Filter II as a function of position of high impedance stub TPRs relative to the patch, L_4

3.4.3 Measurement Results of Filter II

Fig. 3.41 shows the layout of the proposed Filter II with modified FPR and TPRs, which are placed symmetrically on the high impedance central microstrip line. The optimum dimensions are: $L_1 = 1.3$ mm, $L_2 = 1.3$ mm, $L_3 = 4.7$ mm, $L_4 = 2.3$ mm, $L_5 = 3.3$ mm, $L_6 = 1$ mm, $L_7 = 8.2$ mm, $W_1 = 0.4$ mm, $W_2 = 0.2$ mm, $W_3 = 0.4$ mm, $H_1 = 2.2$ mm, $H_2 = 1$ mm, $H_3 = 2.9$ mm, and $G_1 = G_2 = G_3 = 0.4$ mm.

As shown in Fig. 3.42, the measured results are in good agreement with the simulated results. A photograph of prototype Filter II is depicted in Fig. 3.43. The measured result shows that the proposed filter has an insertion loss less than 0.6 dB in the passband up to 2 GHz, with a cutoff frequency of 2.5

GHz and stopband attenuation better than 23 dB from 2.73 GHz to 9.95 GHz. Thus the filter achieves RSB of 113.8 % at 23 dB suppression level.

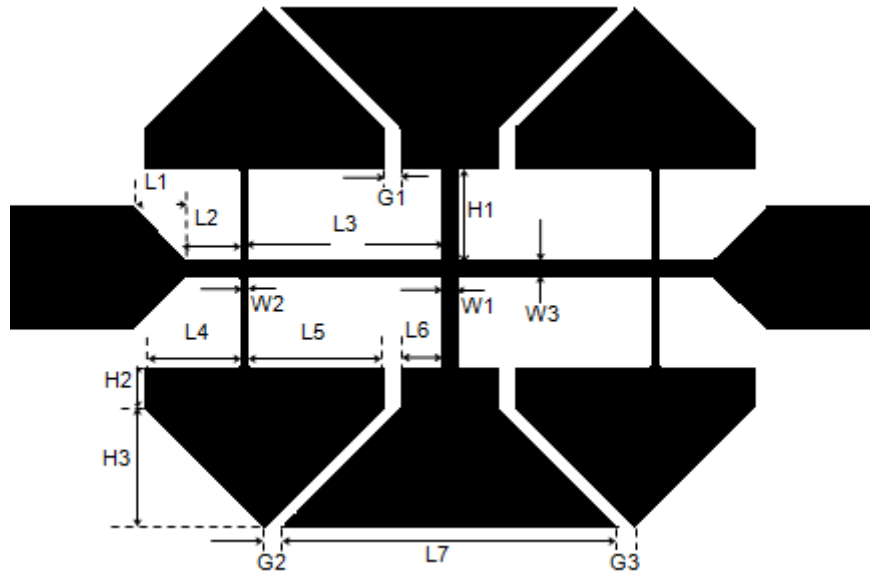


Fig. 3.41 Layout of proposed Filter II

The return loss of the filter is less than 18 dB in the passband and close to 5 dB at 9.5 GHz. The high value of insertion loss in the passband and return loss in the stopband of the measured filter is due to the inherent dielectric losses associated with FR4 material (loss tangent 0.02). The measured 20 dB roll-off rate of the proposed filter is 85 dB/GHz (20 dB attenuation frequency is 2.7 GHz). The measured group delay characteristics of the proposed filter are depicted in Fig. 3.44. As shown in the figure, the filter achieves a flat passband group delay of less than 0.4 ns up to 2 GHz. Moreover, the filter performs very good reflection characteristics with approximately unity VSWR in the entire

passband of the filter as illustrated in Fig. 3.45. Excluding the size of microstrip feed line, the filter has a size of 15.4 mm x 12.6 mm, which corresponds to the NCS of $0.23395 \lambda_g \times 0.191415 \lambda_g$, where λ_g is the guided wavelength at 2.5 GHz.

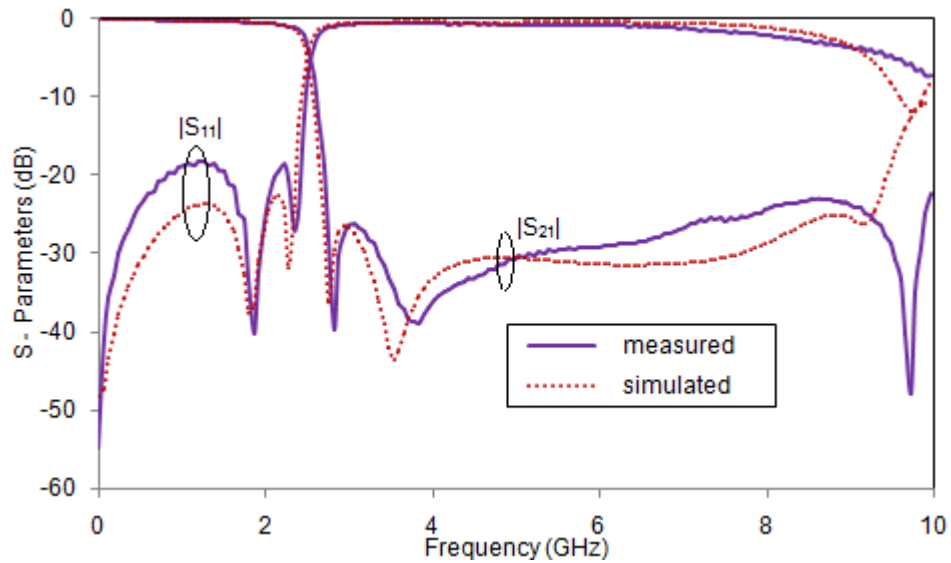


Fig. 3.42 Simulated and measured results of Filter II

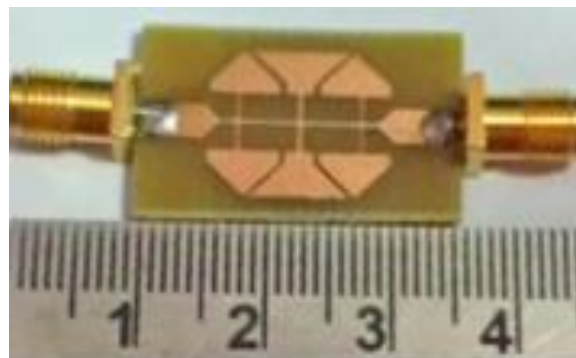


Fig. 3.43 Photograph of prototype of Filter II

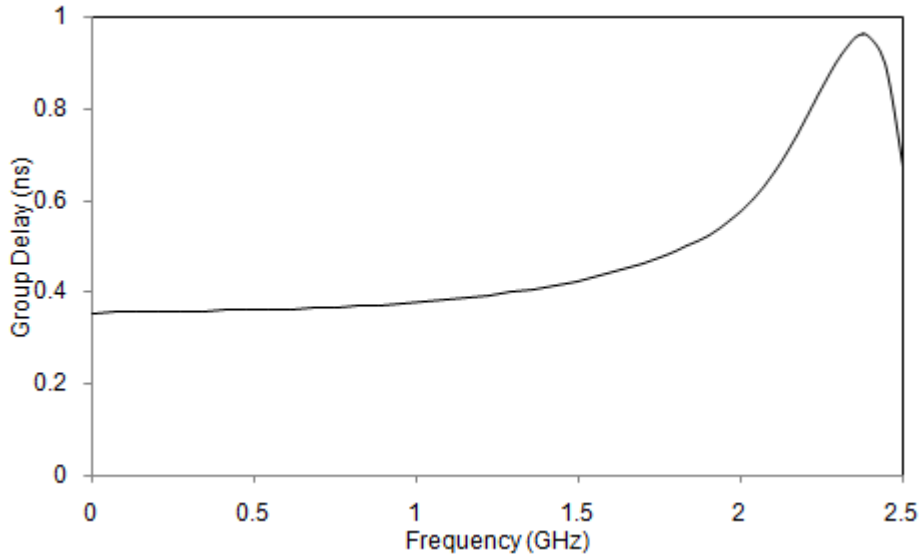


Fig. 3.44 The measured group delay characteristics of Filter II

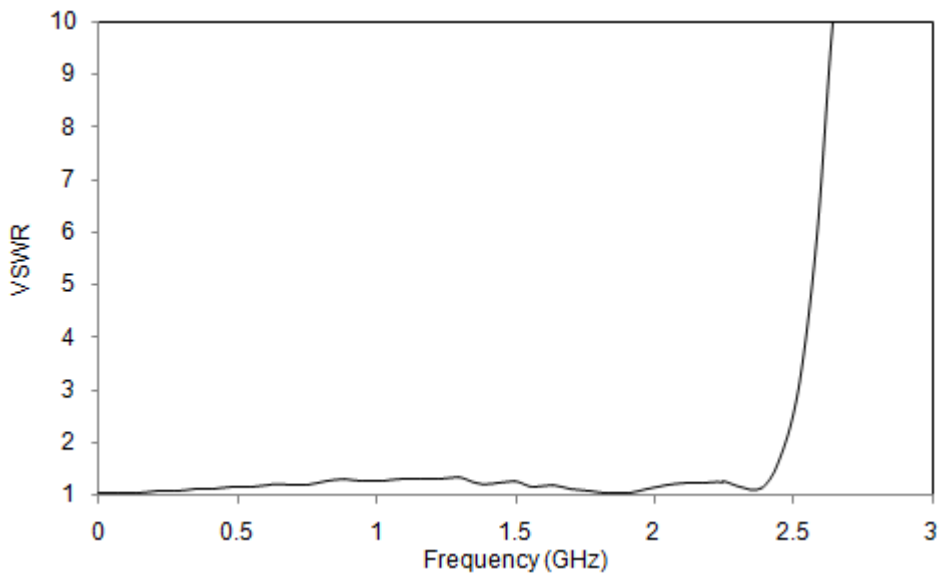


Fig. 3.45 The measured VSWR Characteristics of Filter II

This work has been published in *Proceeding of International Symposium on Antennas & Propagation, APSYM 2014*, Conducted by Cochin University of Science and Technology, Kerala, India.

3.5 Filter III- Compact Lowpass Filter with sharp roll-off and wide stopband using modified FPR and TPRs and suppressing cells

3.5.1 Filter Design Considerations

We can enhance the roll-off rate of the filter for the same f_c and RSB of Filter II by introducing one more resonator near the feed line symmetrical about the transmission line as shown in Fig. 3.46. The additional resonator has also possessed semi-lumped element characteristics with wider stopband bandwidth, which acts as a suppressing cell for high frequencies. The width and height of high impedance stubs used for the third resonator are same as that of side resonators of Filter II. The roll-off rate of the filter is enhanced by the introduction of additional transmission zeroes that are contributed by the third resonator and the combined action of all the resonators. The optimized structure dimensions are: $l_1 = 0.8$ mm, $l_2 = 1.8$ mm, $l_3 = 5.8$ mm, $l_4 = 0.8$ mm, $l_5 = 0.6$ mm, $l_6 = 4$ mm, $l_7 = 1.4$ mm, $l_8 = 0.6$ mm, $l_9 = 8.2$ mm, $w_1 = 0.6$ mm, $w_2 = 0.2$ mm, $w_3 = 0.4$ mm, $h_1 = 2$ mm, $h_2 = 1.6$ mm, $h_3 = 2.5$ mm, $g_1 = g_2 = 0.4$ and $g_3 = 0.2$ mm.

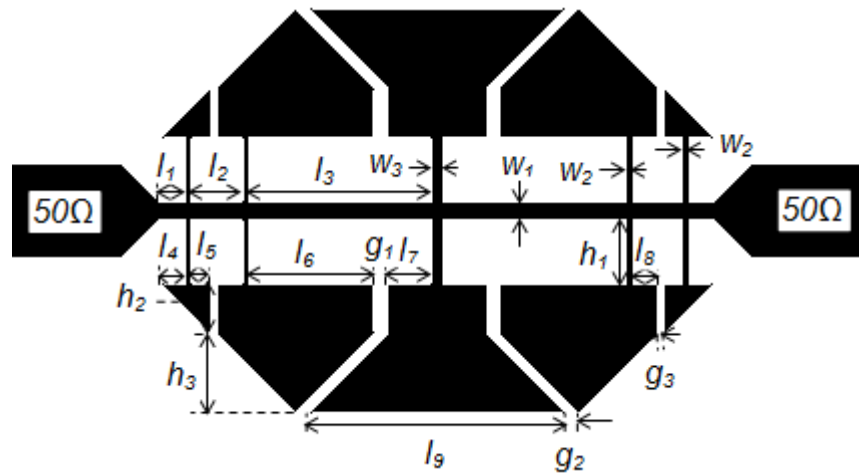


Fig. 3.46 Layout of the proposed Filter III

3.5.2 Simulated and Measured Results of Filter III

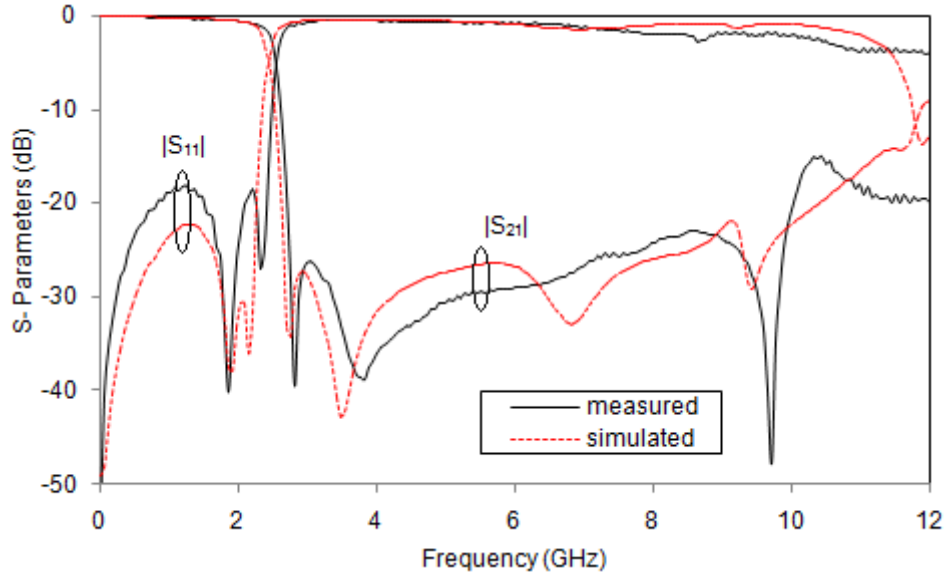


Fig. 3.47 Simulated and measured results of Filter III

The simulated results are validated with experimental results as shown in Fig. 3.47. The measured 3 dB cutoff frequency of the filter is at 2.5 GHz and 40 dB roll off rate is 125 dB/GHz (40 dB attenuation point is at 2.82 GHz). The measured stopband bandwidth of Filter III is from 2.72 GHz to 10 GHz with suppression level better than 23 dB. The measured insertion loss of the filter is less than 0.5 dB in the passband at 1.9 GHz. The maximum return loss in the passband of the filter is 19 dB, and in stopband is less than 2 dB up to 8 GHz. The filter shows a uniform group delay of 0.5 ns up to 1.9 GHz in passband as illustrated in Fig. 3.48.

Excluding the 50 Ω microstrip feed line; the filter has a compact size of 17.6 mm x 12.8 mm, which corresponds to the NCS of $0.2669 \lambda_g \times 0.1941 \lambda_g$, where λ_g is the guided wavelength at cutoff frequency.

Fig. 3.49 shows the photograph of the fabricated filter. Table 3.3 presents the performance comparison of the proposed lowpass filter with previous works. As shown in Table 3.3, the proposed filter exhibits sharp roll-off rate and high stopband suppression level among the quoted filters.

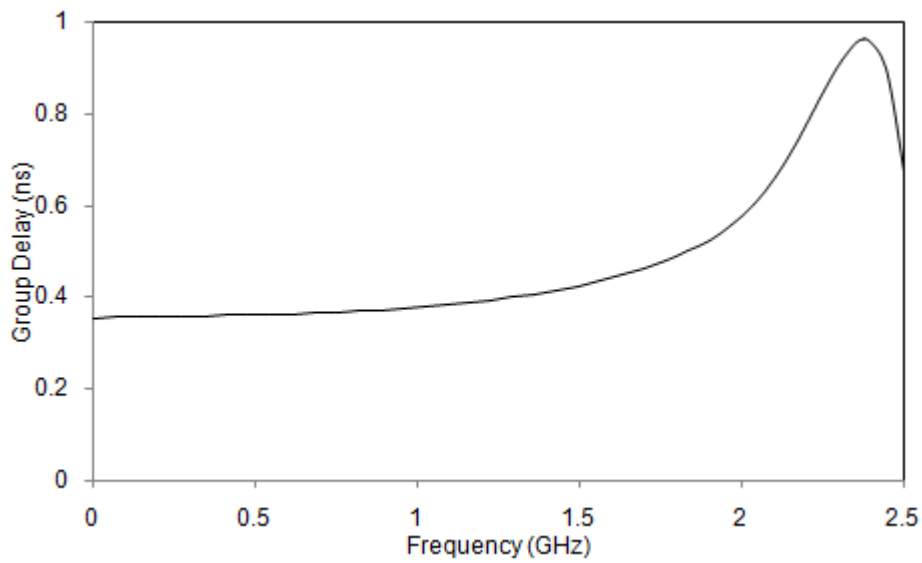


Fig. 3.48 Measured group delay characteristics of Filter III

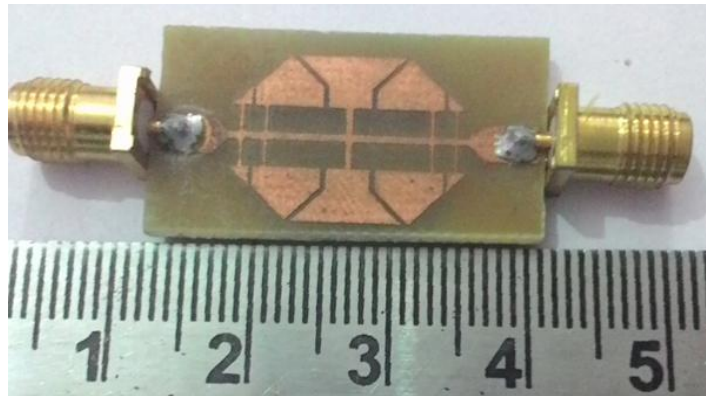


Fig. 3.49 Photograph of prototype of Filter III

Table 3.3. Comparison between performance of Filter III and similar reported work

| <i>Ref</i> | <i>fc</i> (GHz) | ξ (dB/GHz) | α_{max} (dB) | <i>SBW</i> (GHz) | <i>SSL</i> (dB) |
|--------------|--------------------|-------------------|------------------------|---------------------|--------------------|
| [7] | 1.5 | 30.8 | 40 | 2.00–15.0 | 10 |
| [10] | 0.85 | 30 | 40 | 1.57–12.6 | 15 |
| [14] | 2.97 | 84.69 | 60 | 3.32–21 | 20 |
| [15] | 0.5 | 95 | 40 | 0.8–4.6 | 20 |
| [Filter I] | 5.55 | 84 | 40 | 5.58–11.8 | 15 |
| [Filter III] | 2.5 | 125 | 40 | 2.72–10 | 23 |

fc = cutoff frequency, ξ = roll-off rate, α_{max} = roll-off attenuation level, SBW = stopband bandwidth, SSL = stopband suppression level

This work has been published in *Proceedings of International Conference IEEE RADIO 2015*, September 2015, Belle Mare, Mauritius.

3.6 Filter IV-Compact wide stopband lowpass filter with high suppression level

Compact lowpass filters with wide stopband bandwidth and high suppression level are in great demand for modern communication systems to suppress harmonics and spurious signals. As demonstrated in Figs. 3.2 and 3.3, as the thickness of the substrate decreases the characteristics impedance of the microstrip line also decreases, that leads to the better approximation of lumped capacitance of the open circuited patch. Thus, the low impedance patches are shorted to ground at high frequencies and provide high level of attenuation at transmission zero frequencies. This property is used for the design of Filter IV. The stopband bandwidth and the suppression level of the filter are further enhanced by the use of FR4 material with 0.8 mm thickness. The length of transmission line is increased without expanding the physical size by

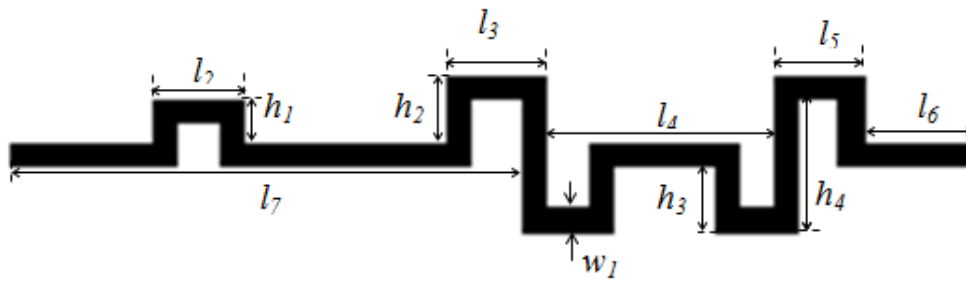
introducing corrugations in the transmission line. The length of high impedance stub of modified TPRs of Filter III is increased and a U-shape is introduced to make the structure compact. The 3 dB cutoff frequency of the filter is at 2.04 GHz. The filter provides a roll-off of 60 dB/GHz at 40 dB attenuation level and a wide stopband with suppression level better than 31 dB from 2.65 GHz to 13.4 GHz. The normalized circuit size of the developed filter is $0.02867 \lambda_g^2$, where λ_g is the guided wavelength at cutoff frequency.

3.6.1 Design of Filter IV

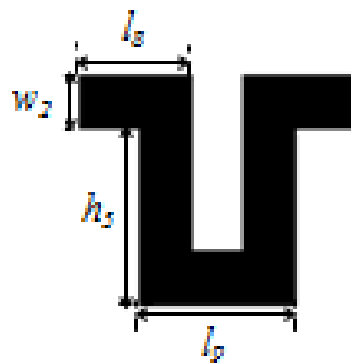
Filter IV is designed by introducing structural modifications in main transmission line, high impedance stubs of side resonators and resonator patch size. The length of high impedance short circuited stub of the side resonators of Filter III is increased and modified to U-shape to enhance the effective inductance of the filter. The size of centre patch and associated side patches are modified to enhance the lumped element characteristics. The patch resonators are loaded as $\lambda_g/2$ stepped impedance resonators on a corrugated main transmission line with characteristic impedance of 120Ω .

Fig. 3.50 (a) and (b) shows the layout of the corrugated transmission line symmetrical about longitudinal axis and U-shaped high impedance stub of resonator 2 respectively. The optimum dimensions selected are: $l_1 = 0.75$ mm, $l_2 = 0.8$ mm, $l_3 = 0.9$ mm, $l_4 = 2.1$ mm, $l_5 = 0.8$ mm, $l_6 = 1$ mm, $l_7 = 4.7$ mm, $l_8 = 0.45$ mm, $l_9 = 0.6$ mm, $h_1 = 0.4$ mm, $h_2 = 0.65$ mm, $h_3 = 0.65$ mm, $h_4 = 1.3$ mm, $h_5 = 0.65$ mm, $w_1 = 0.2$ mm and $w_2 = 0.2$ mm. Figs. 3.51 and 3.52 show the geometry of unit cell model of modified funnel and triangular patch resonators. The open circuited capacitive patches are short circuited to the ground at its

transmission zero, and produce a high attenuation level in the stopband. The selected dimensions are: $l_{10} = 1.4$ mm, $l_{11} = 8.2$ mm, $l_{12} = 1.65$ mm, $l_{13} = 3.35$ mm, $h_6 = 1.1$ mm, $h_7 = 1.6$ mm and $w_3 = 0.4$ mm.



(a)



(b)

Fig. 3.50 (a) Layout of the corrugated high impedance transmission line, (b) Layout of U- shaped high impedance stub of resonator 2

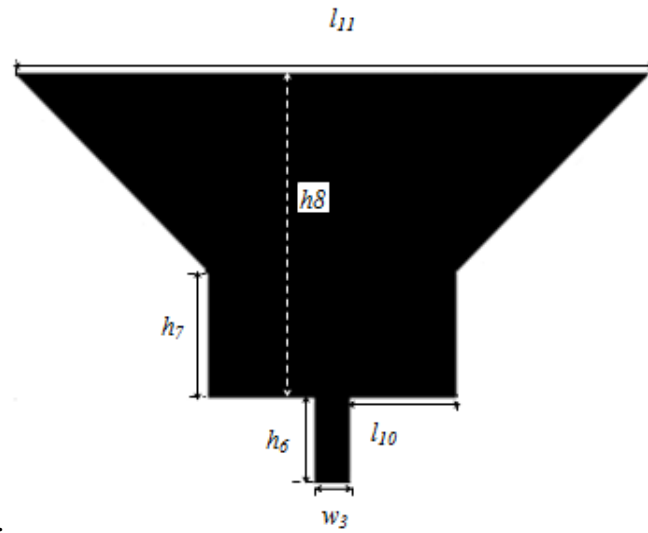


Fig. 3.51 Geometry of unit cell model of modified funnel patch resonator

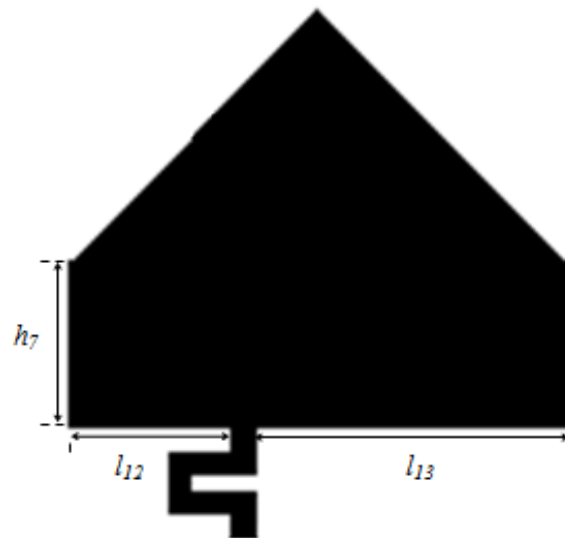


Fig. 3.52 Geometry of unit cell model of modified triangular patch resonator

3.6.2 Simulated and Measured Results of Filter IV

Fig. 3.53 illustrates the geometry of Filter IV. The simulated results are validated with experimental results as shown in Fig. 3.54. The measured 3 dB cutoff frequency of the filter is at 2.04 GHz with a roll off rate of 60 dB/GHz. The filter exhibits high suppression level better than 31 dB with a wide stopband bandwidth from 2.65 GHz to 13.4 GHz. The measured insertion loss of the filter is less than 0.7 dB in the passband at 1.5 GHz. The maximum return loss in the passband of the filter is 13 dB and in the stopband is less than 1.2 dB up to 8.5 GHz and -3dB in the upper end of the stopband. Excluding the tapered feed line, the filter has a compact size of 17.6 mm x 10.6 mm which corresponds to the normalized circuit size of $0.21824 \lambda_g \times 0.1314 \lambda_g$, where λ_g is the guided wavelength at cutoff frequency.

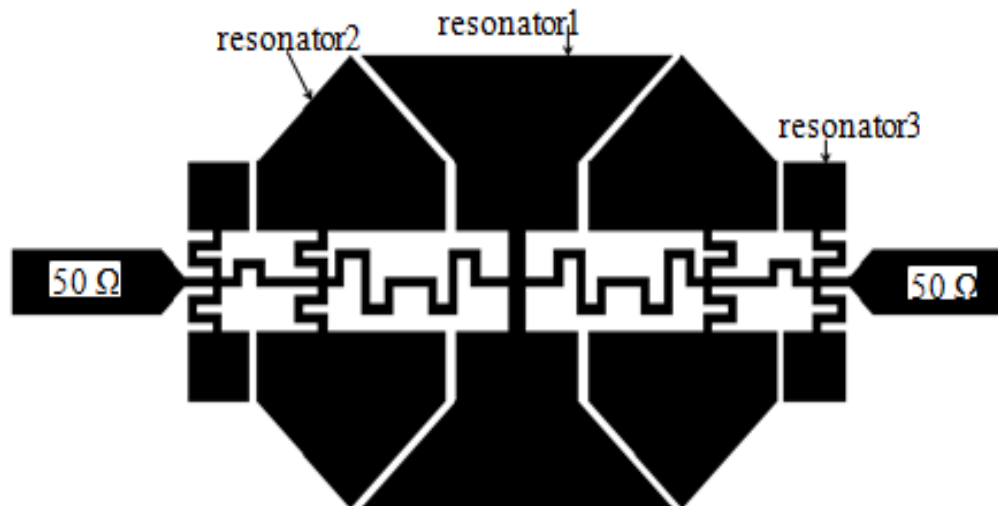


Fig. 3.53 Schematic structure of the proposed Filter IV

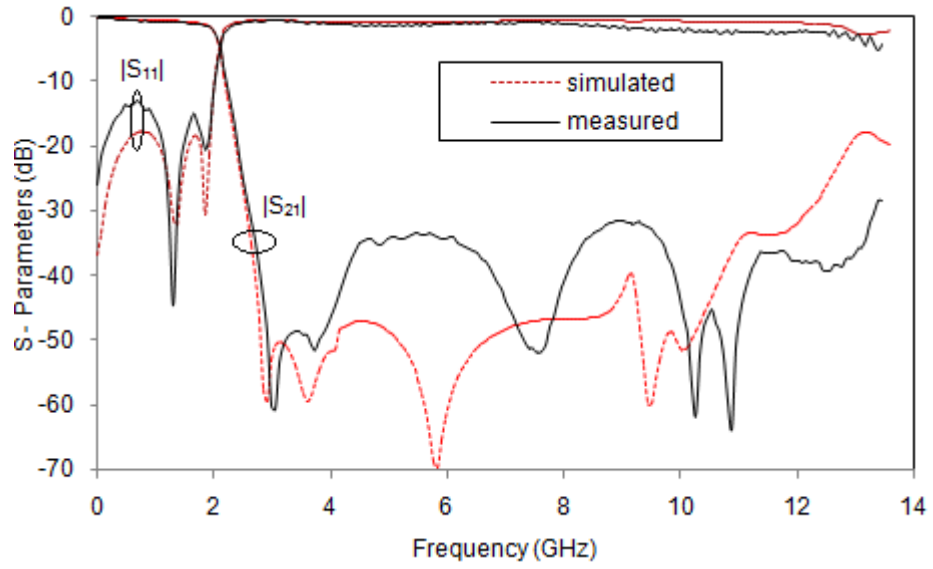


Fig. 3.54 Simulated and measured results of of Filter IV

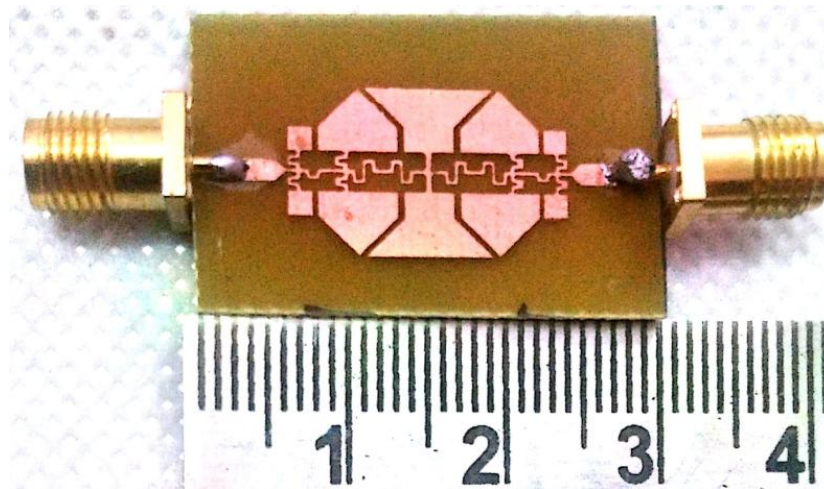


Fig. 3.55 Photograph of prototype Filter IV

Fig. 3.55 shows the photograph of the fabricated filter. Table 3.4 presents the performance comparison of the proposed filter with similar works reported in the literature. As shown in the table, the proposed filter exhibits compact size and wide stopband with high suppression level among the quoted filters.

Table 3.4 Comparison between performance of Filter IV and similar work reported in the literature

| <i>Ref</i> | <i>f_c</i> (GHz) | <i>SBW</i> (GHz) | <i>SSL</i> (dB) | <i>NCS</i> (λg ²) | <i>ε_r & t</i> (mm) |
|--------------|-------------------------------|---------------------|--------------------|----------------------------------|--------------------------------------|
| [15] | 0.5 | 0.8–4.6 | 20 | 0.022 | 4.4, 1.58 |
| [12] | 1.26 | 1.37–16 | 20 | 0.036 | 3.38, 0.508 |
| [9] | 3.12 | 3.68–19 | 20 | 0.056 | 2.2, 0.787 |
| [Filter I] | 5.55 | 5.58–11.8 | 15 | 0.085 | 4.4, 1.6 |
| [Filter III] | 2.5 | 2.72–10 | 23 | 0.052 | 4.4, 1.6 |
| [Filter IV] | 2.04 | 2.65–13.6 | 31 | 0.029 | 4.4, 0.8 |

This work has been published in *IOP Conference Series: Material Science and Engineering* Vol. 120, No.1, March 2016.

3.7 Conclusions

To realize a lowpass filter with sharp switching from passband to stopband for a given number of reactive elements, it is essential to generate infinite attenuation at finite frequencies. Four such filters are designed and developed by cascading multiple resonators on high impedance microstrip line. Patch resonators offer high power handling capability and lower conductor loss, as compared to line conductors. The patch resonators are designed using high impedance short circuited stubs and low impedance open circuited patches, and

by cascading these components form L-C series resonators. In the first stage of filter design, a compact lowpass filter, by loading FPR as the centre resonator and TPR as side resonators symmetrically on a 96Ω transmission line. The L-C equivalent circuit model has established with component values and the results are validated with full wave EM model structural simulation results. The filter, Filter I achieves a sharp roll-off rate of 84 dB/GHz and relative stopband bandwidth (RSB) of 66.6 %. The cutoff frequency f_c of the filter is at 5.55 GHz. After conducting a detailed parametric analysis, the filter characteristics have been enhanced with modified FPR and TPRs. RSB of the modified filter, Filter II is enhanced to 113 % with f_c at 2.5 GHz. The filter structure is further modified by introducing one more resonator near the feed line as Filter III, the roll-off rate of the filter is enhanced to 125 dB/GHz at same f_c . All the above mentioned filters are designed and developed using FR4 substrate having permittivity 4.4, thickness 1.6 mm with loss tangent of 0.02. As the thickness of the substrate material decreases, the impedance offered by the low impedance patch decreases, that leads to better approximation of lumped capacitance that will produce high attenuation level at each transmission zero frequencies. This property is used to design Filter IV, with corrugated transmission line on FR4 of 0.8 mm thickness. The filter has achieved RSB of 134% with stopband suppression level better than 31 dB by suffering its roll-off rate to 60 dB/GHz. Also the NCS of the Filter IV is reduced to 50% compared to that of Filter III. Table 3.5 demonstrates the performance characteristics of the developed filters.

Table 3.5. Comparison between Proposed Filters using FPR and TPRs

| Filter | f_c GHz | ξ dB/GHz | SIZE ₂ mm | NCS ₂ λ_g | RSB % | SL dB | PB IL dB | RL in PB/SB |
|------------|--------------|-----------------|-------------------------|---------------------------------|----------|----------|------------------|---------------------------------|
| Filter I | 5.55 | 84 (40) | 9.4 x 8 | 0.085 | 67 | 15 | 0.7 (4GHz) | < 20 in PB < 2 in SB |
| Filter II | 2.5 | 85 (20) | 15.4x12.6 | 0.044 | 113 | 23 | 0.6 (2 GHz) | < 18 in PB < 5 in SB |
| Filter III | 2.5 | 125 (40) | 17.6x12.8 | 0.051 | 114 | 23 | 0.5 (1.9 GHz) | < 19 in PB < 2 in SB |
| Filter IV | 2.04 | 60 (40) | 17.6x10.6 | 0.028 | 134 | 31 | 0.7 (1.5 GHz) | < 13 in PB <1.2 up to 8.5 |

References

- [1] J.S. Hong and M.J. Lancaster, *Microstrip Filters for RF/ Microwave Applications*, John Wiley, New York, 2001.
- [2] S.W. Ting, K.W. Tam, and R.P. Martins, "Miniaturized microstrip lowpass filter with wide stopband using double equilateral U-shaped defected ground structure," *IEEE Microw. Wireless Compon. Lett.*, vol.16, no. 5, pp. 240–242, May 2006.
- [3] C.J. Wang, and C.H. Lin, Compact lowpass filter with sharp transition knee by utilizing a quasi- π -slot resonator and open stubs, *IET Microwaves, Antennas and Propagation*, vol. 4, pp. 512–517, 2010.

- [4] A.S. Mohra, Microstrip lowpass filter with wide rejection using opened circuit stubs and z-slots defective ground structure, *Microwave Opt. Technol. Lett.*, vol. 53, 811–815, 2011.
- [5] Y. Yang, X. Zhu and N.C. Karmakar, “Microstrip lowpass filter based on split ring and complementary ring resonators,” *Microwave Opt. Technol Lett.*, vol. 54, pp. 1723–1726, 2012.
- [6] K.Ma and K.S. Yeo, “New ultra-wide stopband low-pass filter using transformed radial stubs,” *IEEE Trans. Microw. Theory Tech.*, vol. 59, no. 3, pp. 604–611, 2011.
- [7] F. Zhang, J.Z. Gu, C.Y. Gu, L.N. Shi, C.F. Li and X.W. Sun, “Lowpass filter with in-line beeline CMRC, ” *Electron. Lett.*, vol. 42, pp. 472–474, 2006.
- [8] M.H. Yang and J. Xu, “Design of compact broad-stopband lowpass filters using modified stepped impedance hairpin resonators, ” *Electron. Lett.*, vol. 44, pp.1198–1200, 2008.
- [9] Hayati M, Sheikhi A, and Lotfi A, “Compact lowpass filter with wide stopband using modified semi-elliptic and semi-circular microstrip patch resonator, ” *Electron. Lett.*, vol. 46, no. 22, pp 1507–1509, 2010.
- [10] L. Ge, J.P. Wang, and Y-X Guo, “Compact microstrip lowpass filter with ultra-wide stopband, ” *Electron. Lett.*, vol. 46, pp.689 – 691, 2010.
- [11] H. Cui, J. Wang and G. Zhang, “Design of microstrip low pass filter with compact size and ultra-wide stopband, ” *Electron. Lett.*, vol.48, pp. 856–857, 2012.
- [12] Karimi G. and Lalbaksh A., “Design of Sharp Roll-off Lowpass Filter with Ultra Wide Stopband,” *IEEE Microw. Wireless Compon. Lett.*, vol. 23, no. 6, pp.303–305, 2013.
- [13] M. Mirzaee and B.S. Virdee, “Compact lowpass filter with high out-of-band rejection and super wide stopband performance, ” *Microwave Opt. Technol. Lett.* vol. 56, pp. 947–950, 2014.

- [14] M. Hayati, M. Gholami, H.S. Vaziri and T. Zaree, “Design of microstrip lowpass filter with wide stopband and sharp roll-off using hexangular shaped resonator,” *Electron. Lett.* vol. 51, no. 1, pp. 69–71, 2015.
- [15] V.K. Velidi and S. Sanyal, “Sharp roll-off lowpass filter with wide stopband using stub-loaded coupled-line hairpin unit,” *IEEE Microw. and wireless Compon. Lett.*, vol. 21, no. 6, pp. 301–303, 2011.
- [16] Makimoto, M. and S. Yamashita, *Microwave Resonators and Filters for Wireless Communications Theory, Design and Application*, Springer Series in Advanced Microelectronics, 2001.
- [17] David, M.P., *Microwave Engineering*, 3rd Edition, New York, 2005.

Compact Lowpass Filter with Sharp 20 dB Roll-off Rate and Wide Stopband using Stepped Impedance Patch Resonators

In this chapter, the design techniques to enhance the sharp switching characteristics of the lowpass filter by using stepped impedance patch resonators are discussed. The developed filter achieves a sharp roll-off of 90 dB/GHz at 20 dB attenuation level and RSB of 93.52 % with stopband suppression level 16 dB. The L-C equivalent circuit model of the filter is extracted with component values and the results are validated with EM structural simulation results. After executing various parametric analysis and optimization techniques, the filter performances are improved to a great extent, which is included in the second section. In the third section, the techniques to enhance the roll-off characteristics of the filter using stepped impedance polygonal patch resonator (SI-PPR) are described. Furthermore, an additional resonator is introduced and investigated to enhance the stopband bandwidth and suppression level of the filter without increasing the overall physical dimension, which is also demonstrated in this chapter with experimental results.

4.1 Introduction

Lowpass filters are commonly used with RF front-end circuit in modern communication systems to suppress harmonics and spurious signals. Sharp transition from passband to stopband near the cutoff frequency and wide stopband bandwidth are important characteristics of a lowpass filter to suppress the unwanted signals captured by the RF front-end circuits in high data rate communication systems. Since patch resonators possess high power handling capacity and lower conductor loss compared to line resonators [1], the proposed filters are designed and developed by using multiple stepped impedance patch resonators.

Recently various methods have been reported in the literature to develop high performance lowpass filters by multiple resonators without external lumped elements [2–11]. Since the performance characteristics of the lowpass filters depend mainly depends on size and shape of the patch resonator, we tried to enhance both the selectivity and stopband performance of the filter with stepped impedance patch resonators. The proposed filters consist of different types of resonators, one as centre resonator and the others as side resonators. The centre resonator is designed with a symmetrically loaded stepped impedance patch resonator (SI-PR). In order to provide better selectivity and improved coupling, the shape and size of the side resonator patches are exactly matched with that of the centre resonator patch. The L-C equivalent circuit model has been developed with component values and compared the results with full wave EM model simulation results. The filter achieves a sharp roll-off of 90 dB/GHz at 20 dB attenuation level and RSB of 93.52 % with stopband suppression level 16 dB. After executing various parametric analysis, the filter performance is enhanced to a great extend by the modified SI-PRs. Finally, the

stopband bandwidth and suppression level of the filter is very much improved with stepped impedance polygonal patch resonator (S-PPR) as the centre resonator and two more resonators as side resonators. The modified lowpass filter achieves a RSB of 126% with suppression level of 23 dB.

4.2. Design of Stepped Impedance Patch Resonators (SI-PRs)

The proposed compact microstrip lowpass filters are designed and investigated by cascading multiple resonators on high impedance microstrip line [HIML]. It consists of a centre resonator and multiple side resonators, where each resonator is designed by $\lambda_g/2$ stepped impedance patch resonators (SI-PR). The patch resonators are designed with high impedance inductive stub (HIIS) and low impedance capacitive patches (LICP). The physical dimensions of these individual components are less than $\lambda_g/8$ to approximate these components as lumped elements, and they together form a series L-C resonator without considering fringe and parasitic capacitance [1].

4.2.1 Design of SI-PR1

The basic structure and L-C equivalent circuit unit cell model of SI-PR1 are shown in Fig. 4.1. The structure is designed with HIIS of impedance Z_{HI} and LICP of impedance Z_{CI} , connected together to form a $\lambda_g/4$ SI-PR, where λ_g is the guided wavelength at cutoff frequency. For better performance Z_{HI} should be greater than Z_0 and Z_{CI} less than Z_0 , where Z_0 is the characteristic impedance of the feed line. The resonant condition of the unit cell is determined by the impedance ratio $R_z = Z_{CI}/Z_{HI}$ and the dimensions of HIIS and LICP [12].

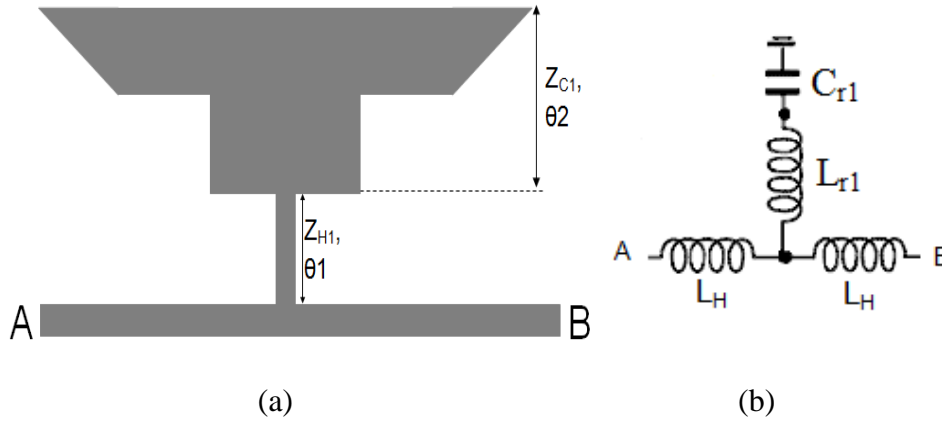


Fig. 4.1 Unit cell model of SI-PR1, (a) Structure of unit cell, (b) L-C equivalent circuit

The impedance and dimensions of HIIS and LICP is computed by the conventional design procedure [1]. Generally the characteristic impedance Z_0 of the microstrip line can be determined using (3.1) to (3.6) that relate the width of the strip W and the parameters such as permittivity ϵ_r and thickness h of the substrate material.

The substrate used for the design of proposed filter is low cost lossy FR4 material with permittivity $\epsilon_r = 4.4$, thickness $h = 1.6$ mm and loss tangent = 0.02. Fig. 4.1(b) illustrates the equivalent circuit of the unit cell model of SI-PR1, where the inductance L_{r1} of the HIIS can be determined by Eq. (3.7) and the capacitance C_{ri} and C_c of low impedance capacitive patches can be determined by two port S-parameter using Eqs. (3.19) and (3.20). L_H is the inductance associated with the corresponding HIML element.

As explained in Eq. (3.18) of Chapter 3, the transmission zero frequency, f_Z of the resonator depends exactly on HIIS inductance L_{r1} , LICP capacitance C_{r1} , so that f_Z can be controlled by adjusting the impedance HIIS and LICP and their electrical dimensions. As per Fig. 4.1, Z_{H1} and Z_{C1} are the

impedances of HIIS and LICP respectively that depend on the width of the corresponding strips. The impedance of LICP can be lowered by increasing the size of the patch. Fig. 4.2 shows the structural configuration of the LICP where patch 1, patch 2 and patch 3 are the elements separately added to study the response characteristics of the LICP together with HIIS. The design of LICP is optimized by avoiding transverse resonance [1].

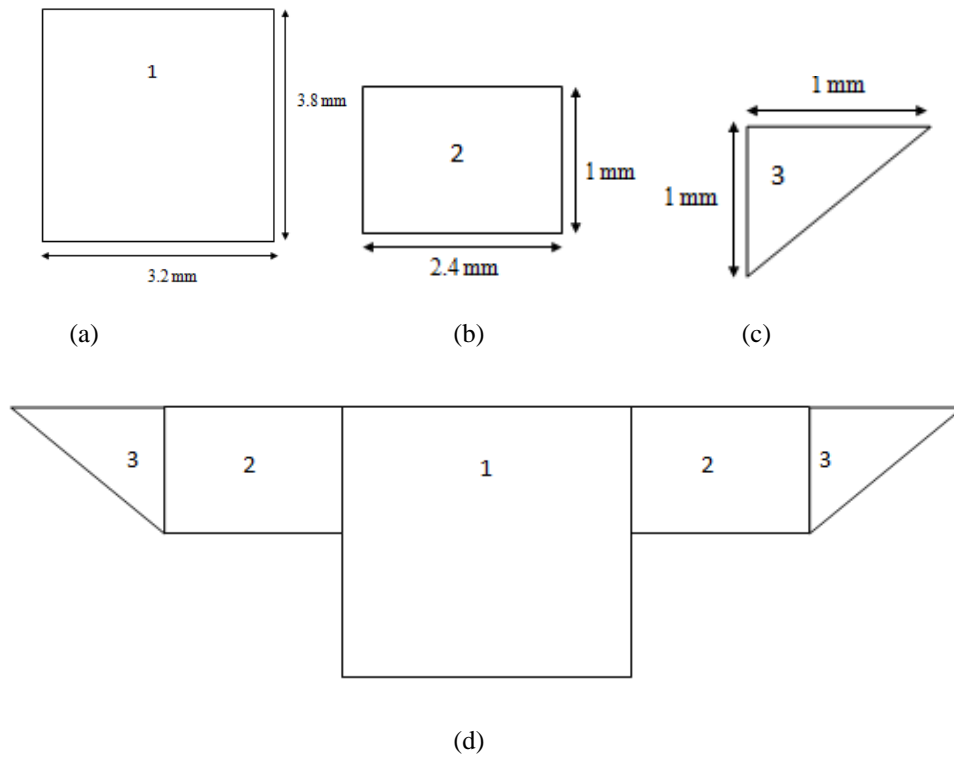


Fig. 4.2 Configuration of the LICP of SI-PR1, (a) Patch 1, (b) Patch 2, (c) Patch 3, (d) Proposed LICP of SI-PR1

Fig. 4.3 depicts the response characteristics of the unit cell of SI-PR1 as a function of LICP size. Adding each patch elements, patch 1, patch 1 & 2 and

patch 1, 2, & 3, the effective impedance of the patch decreases that increases the capacitance C_{rl} , which decreases the transmission zero, f_z of the resonator.

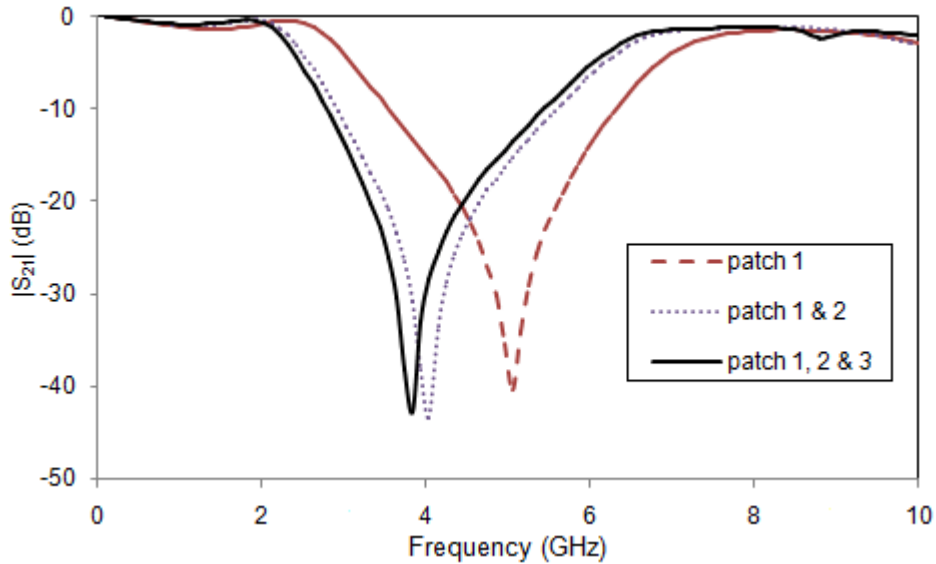


Fig. 4.3 Frequency response characteristics of unit cell model of SI-PR1 as a function of patch size

Table 4.1 Response of SI-PR1 related to the size of LICP

| <i>Patch</i> | f_c (GHz) | f_z (GHz) | $f_z - f_c$ (GHz) | 10 dB Bandwidth (GHz) |
|--------------|----------------|----------------|----------------------|--------------------------------------|
| 1 only | 2.9 | 5.05 | 2.15 | 2.8 |
| 1 & 2 | 2.4 | 4 | 1.6 | 2.7 |
| 1, 2 & 3 | 2.3 | 3.8 | 1.5 | 2.6 |

f_L - lower 3 dB cutoff frequency, f_z – transmission zero frequency

As shown in Fig. 4.3, the frequency response of the resonator follows bandstop filter characteristics with a single transmission zero, where the passband characteristics of the filter is improved by increasing the size of the

patches with a small decrease in 10 dB bandwidth. Table 4.1 demonstrates the effect of patch size on the transmission zero frequency f_z , and the difference in frequency between f_c and f_z . As patch size increases the difference in frequency between f_c and f_z decreases.

The characteristics of $\lambda g/4$ SI-PR1 is greatly improved by loading SI-PR1 symmetrically on HIML, so that it becomes a $\lambda g/2$ SI-PR1 as shown in Fig.4.4(a). Fig. 4.4(b) shows the equivalent circuit model of $\lambda g/2$ SI-PR1, where the two series L-C circuits are in parallel that decreases the overall impedance of the structure. As shown in Fig. 4.5, the transmission zero of $\lambda g/4$ SI-PR1, Tz1 is at 3.838 GHz and that of $\lambda g/2$ SI-PR1, Tz2 is at 4.44 GHz. The 10 dB stopband bandwidth is enhanced to 4.2 GHz and the return loss is also improved by the symmetrical structure.

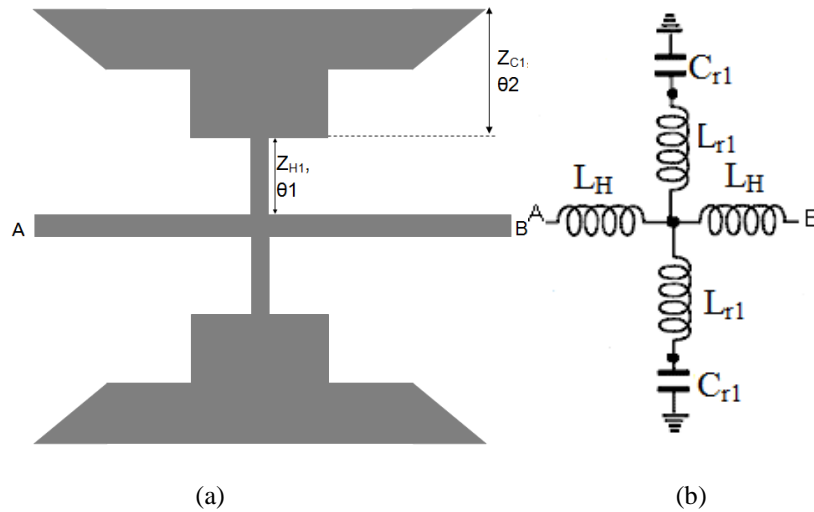


Fig. 4.4 Geometry of $\lambda g/2$ SI-PR1 with L-C equivalent circuit and performance characteristics, (a) Geometry, (b) L-C equivalent circuit

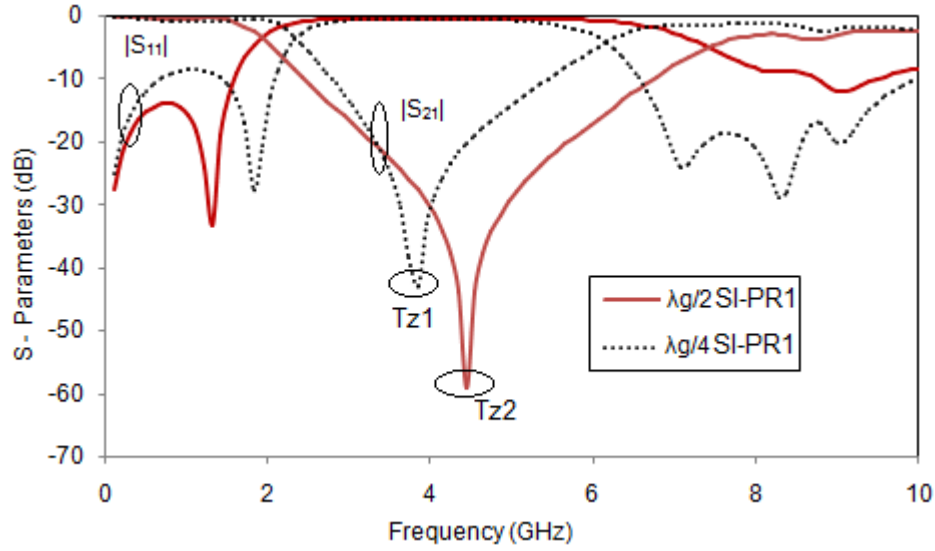


Fig. 4.5 Simulated S-Parameter characteristics of $\lambda_g/2$ SI-PR1

4.2.2 Design of SI-PR2

Fig. 4.6(a) demonstrates the layout of unit cell model of SI-PR2 and its L-C equivalent circuit. It is also designed with HIIS of impedance Z_{H2} and LICP of impedance Z_{C2} with electrical length θ_1 and θ_2 respectively. The inductance L_{r2} and capacitance C_{r2} of these elements are also computed by Eqs. (3.7-3.9) with appropriate parameters. The dimensions and the shape of the LICP of SI-PR2 are designed to make the whole structure compact to provide better approximation of lumped capacitance [1]. Figs. 4.6(b) and 4.6(c) show the geometry and response characteristics of SI-PR2 with its f_z depend on L_{r2} and C_{r2} .

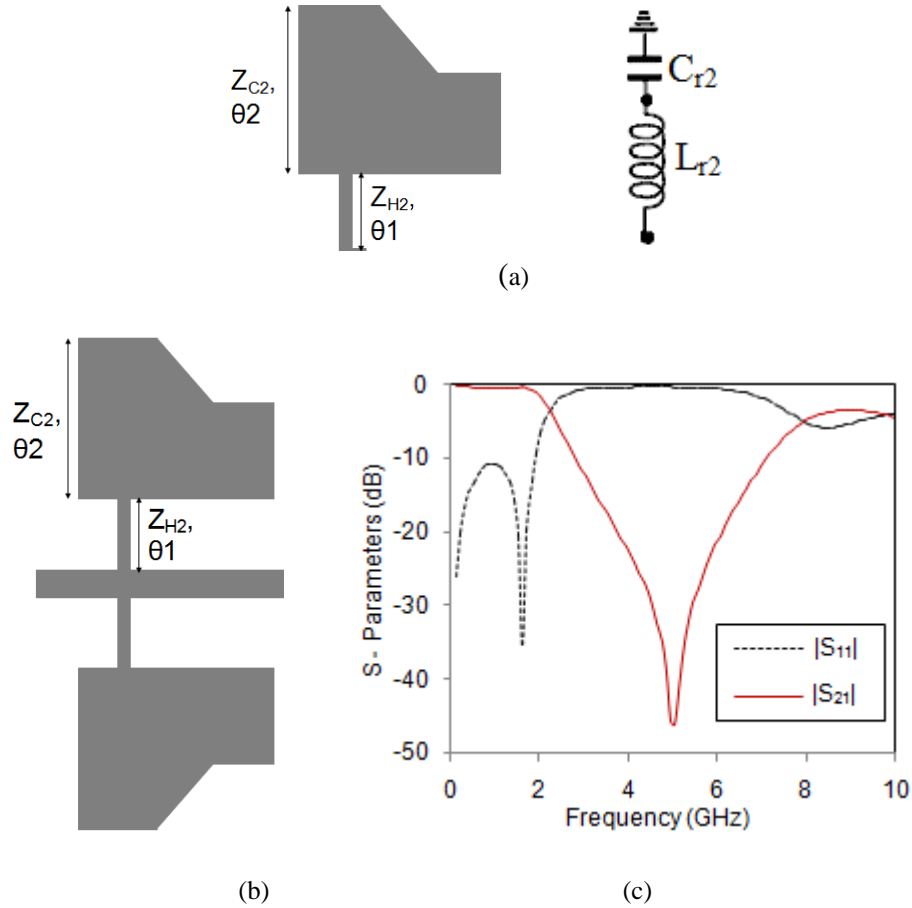


Fig.4.6 Unit cell model, geometry and frequency response characteristics of SI-PR2. (a) Unit cell model and L-C equivalent circuit, (b) Geometry of SI-PR2, (c) Frequency response characteristics SI-PR2

4.3 Compact Elliptic Function Lowpass Filter Design using SI-PRs

Observing the frequency response of individual resonators shown in Fig. 4.5 and Fig. 4.6(c), the attenuation level of each resonator increases after cutoff frequency and reaches its maximum level at transmission zero frequency, f_z and starts decreasing just after the resonance. By suitably combining both resonators

in a filter as shown in Fig. 4.7, we can enhance the characteristics of the filter towards the ideal response. Fig. 4.8 demonstrates the transmission characteristics of the filter as a function of resonators. As shown in the characteristics, the filter with SI-PR1 shows single transmission zero located at 4.38 GHz, far from its cutoff frequency 1.96 GHz by 2.42 GHz, whereas the filter with SI-PR2 shows first transmission zero at 4.26 GHz with its cutoff frequency 2.36 GHz by 1.9 GHz. Moreover the SI-PR2 consists of two sets of resonant components, so that the filter with SI-PR2 shows better roll-off and stopband performance than the filter with SI-PR1.

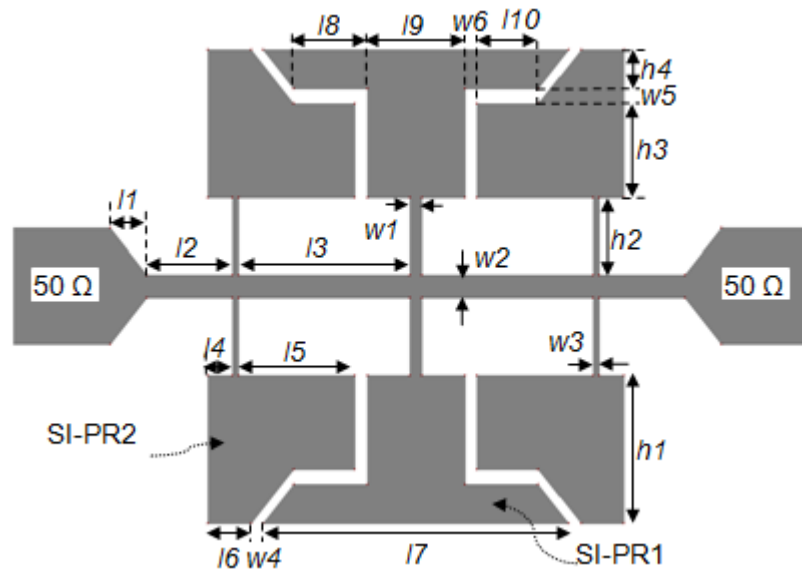


Fig. 4.7 Layout of compact lowpass filter with SI-PRs

As illustrated in Fig. 4.8, the first transmission zero generated by the filter with SI-PR1 and SI-PR2 is at 2.7 GHz, which is very near to its cutoff frequency 2.4 GHz by 0.3 GHz that improves the roll-off rate as well as the

stopband performance. The sharp skirt very close to the f_c is achieved due to the simultaneous effect of series and parallel resonance caused by the patch resonators and high impedance central microstrip line. Moreover, the series and parallel combination short out transmission at their resonant frequencies and thus gives three finite attenuation poles together with wide stopband performance. Cascading separate resonators also increases the effective reactance of the circuit. The structural dimensions of the filter have been optimized using simulation software Ansoft HFSS and Zeland IE3D.

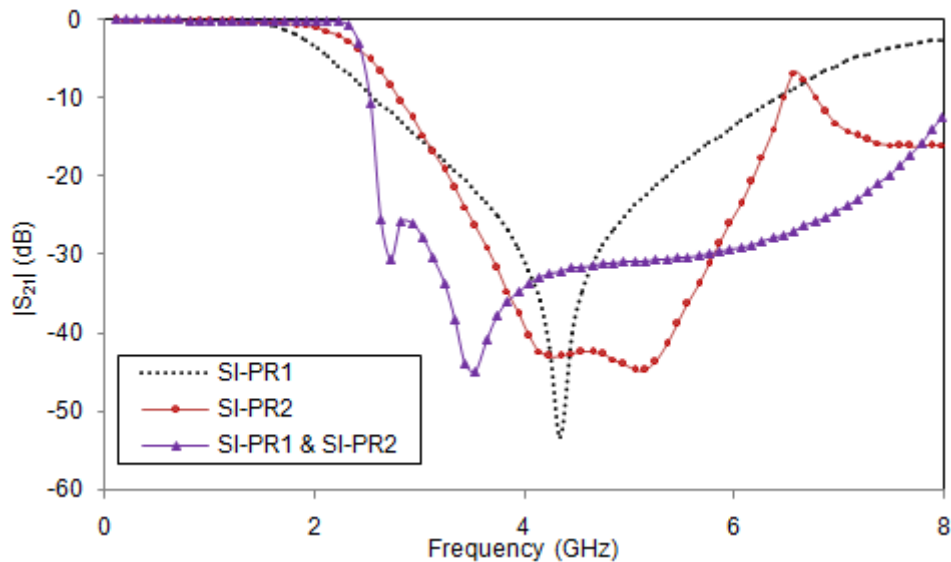


Fig. 4.8 Simulated transmission characteristics as a function of resonators

4.3.1 Equivalent Circuit Analysis

Fig. 4.9 shows the equivalent circuit model of compact lowpass filter with SI-PRs, which is exactly similar to the circuit of an elliptic function lowpass filter where L_{H1} and L_{H2} are the effective inductance contributed by the corresponding HIML element. The circuit component values L and C are

determined by the methods demonstrated in Section 3.3.7 of Chapter 3. The extracted L and C values are $L_{H1} = 1.977$ nH, $L_{H2} = 3.7373$ nH, $L_{r1} = 1.4584$ nH, $L_{r2} = 1.7744$ nH, $C_{r1} = 0.74521$ pF, $C_{r2} = 0.66074$ pF and $C_C = 0.13046$ pF.

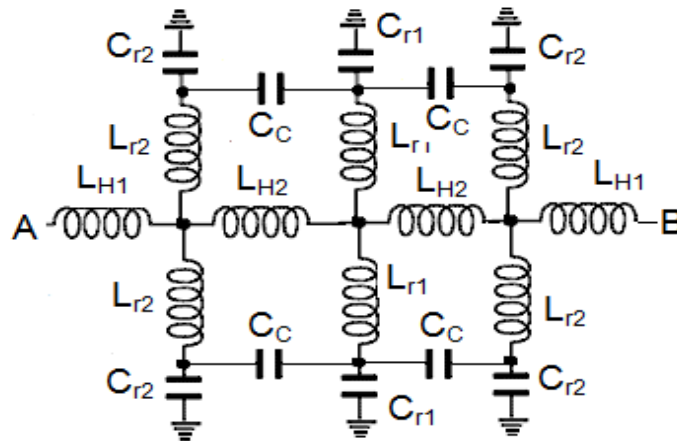


Fig. 4.9 Equivalent circuit of compact elliptic function lowpass filter using SI-PRs

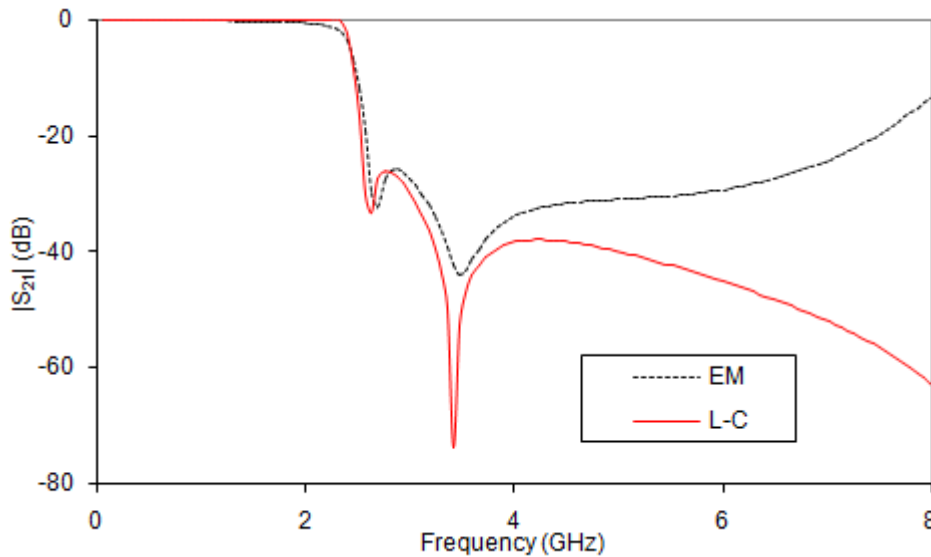


Fig. 4.10 EM and L-C model transmission characteristics of compact elliptic function lowpass filter using SI-PRs

As shown in Fig. 4.10, the simulated L-C passband characteristics of the filter is validated with the full-wave EM model structural simulation results. The difference in characteristics in the high frequency range is because of two reasons. Firstly, the equivalent parameters are approximated to lumped elements at the cutoff frequency and guided wavelength and phase velocity may change with change in frequency. Secondly, L-C analysis depends purely on equivalent L and C values whereas EM simulation result depends on the characteristics of substrate material and loss parameters [13].

4.3.2 Parametric Analysis

Since many variables are involved in the filter design, a detailed full-wave EM model parametric analysis has been conducted to optimize the dimensions of the filter.

4.3.2.1 Stub Position of SI-PR2, (l_4)

There are many variables involved in the design of the polygonal patches of the SI-PR1 and SI-PR2. The roll-off rate of the proposed filter mainly depends on the size and shapes of patches of the resonators and the coupling between them. The position of the connecting stub of the SI-PR2 with its patch also affects the cutoff frequency and the position of the transmission zeroes due to the asymmetrical step discontinuity at the junction the of connecting stub and the polygonal patch of SI-PR2 [14]. Fig. 4.11 shows the simulated frequency characteristics of the proposed filter as a function of the connecting stub position of SI-PR2, l_4 . As shown in figure, as l_4 increases from 0.4 mm to 0.8 mm, the null frequencies in the stopband and stopband bandwidth are shifted to the higher range due to the asymmetric excitation of the patch. The reflection loss in the passband also increases with the change in stub

position.

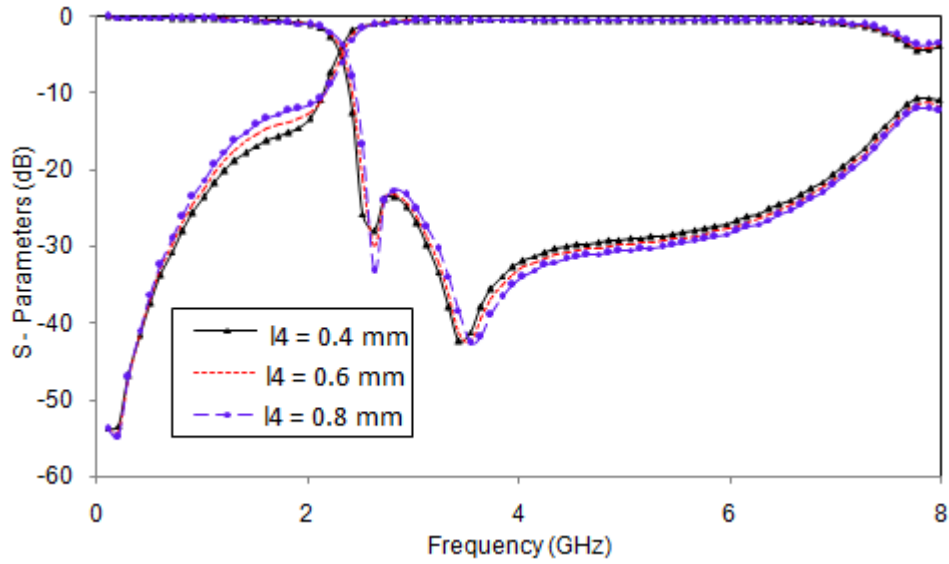


Fig. 4.11 Simulated S-Parameters of the proposed filter as a function of the connecting stub position of SI-PR2, (l_4)

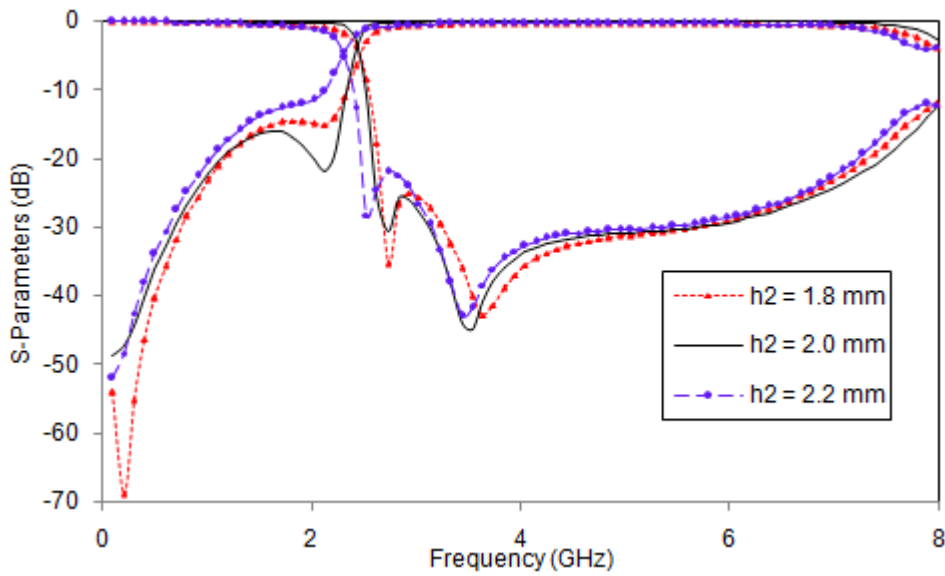


Fig. 4.12 Simulated S-Parameters of the proposed filter as a function of the connecting stub height, (h_2)

4.3.2.2 Stub Height, (h_2)

Fig. 4.12 illustrates the frequency response characteristics of the filter as a function of connecting stub height, h_2 . Since the transmission zero frequency f_z of the individual resonators mainly depends on their stub inductance L and patch capacitance C , the HIRS height and width of the resonators play an important role in the filter design. As shown in Fig. 4.12, both the transmission and reflection characteristics of the filter affect the filter performance. The optimum value of $h_2 = 2$ mm.

4.3.2.3 Width of High Impedance Transmission Line, (w_2)

Figs. 4.13 and 4.14 demonstrate the effect of width w_2 and characteristic impedance Z_C of HIML on 3 dB cutoff frequency f_c and first transmission zero frequency f_z of the filter. As the inductance of HIML is directly related to its impedance, f_c increases as w_2 increases from 0.6 mm to 1.4 mm. Since the value of f_z depends exactly on the resonator parameters as expressed in Eq. (3.18), f_z remains constant throughout the variation of w_2 . However the characteristic impedance Z_C of HIML follows an inverse relationship with the width w_2 of HIML. As Z_C varies from 75 Ω to 110 Ω , the filter passband increases as Z_C whereas f_z remains constant at 2.727 GHz as shown in Fig. 4.15.

As all the individual circuit elements contribute to the performance of the filter, we can tune either the cutoff frequency or the transmission zero frequency by changing dimensions of individual components. Several degrees of freedom exist for adjusting the response of the filter. The exact dimensions are adjusted to optimize the performance of the filter.

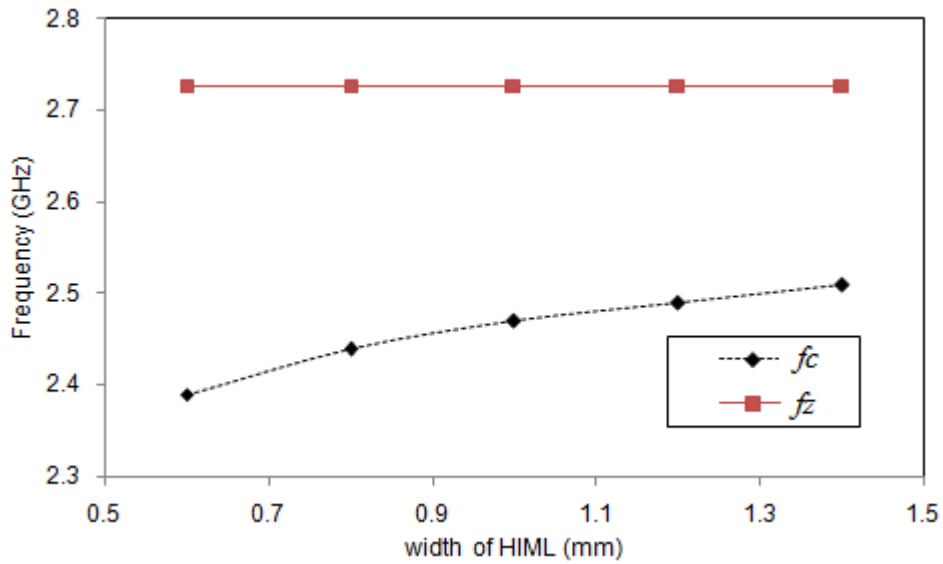


Fig. 4.13 The effect of width of HIML w_2 on 3 dB cutoff frequency, f_c and first transmission zero frequency, f_z of the compact filter with SI-PRs

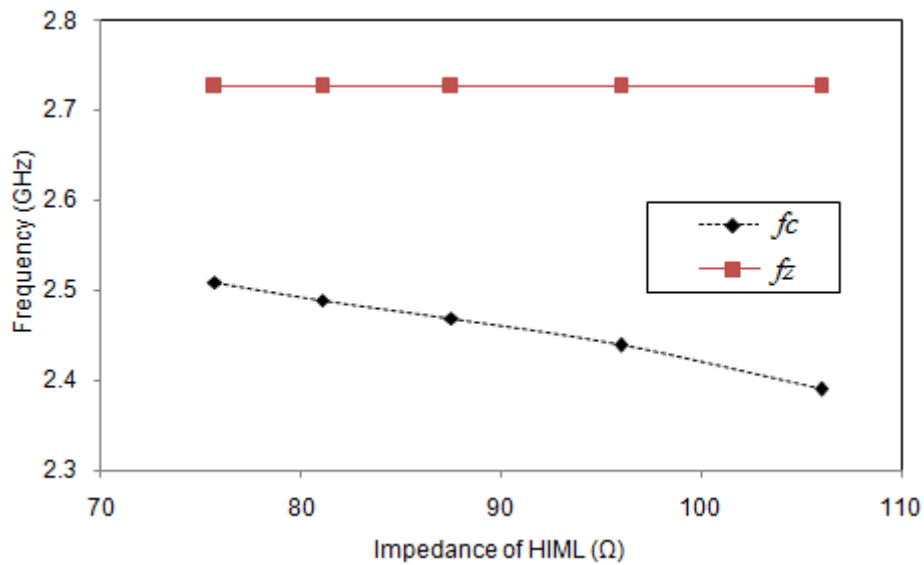


Fig. 4.14 The effect of characteristic impedance Z_C on 3 dB cutoff frequency f_c and first transmission zero frequency, f_z of the compact filter with SI-PRs

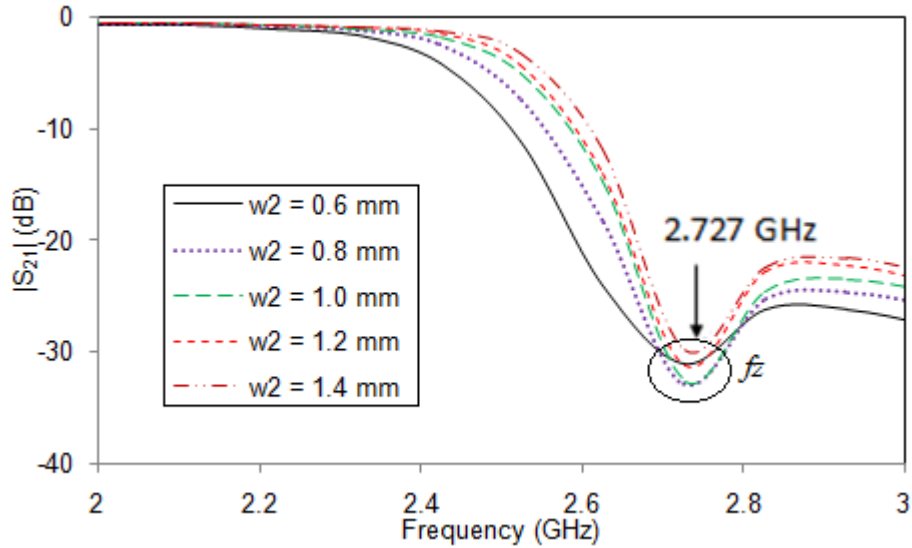


Fig. 4.15 Simulated $|S_{21}|$ characteristics of compact filter with SI-PRs as a function of width, w_2 of HIML

4.3.3 Simulation and Measurement Results of Filter using SI-PRs

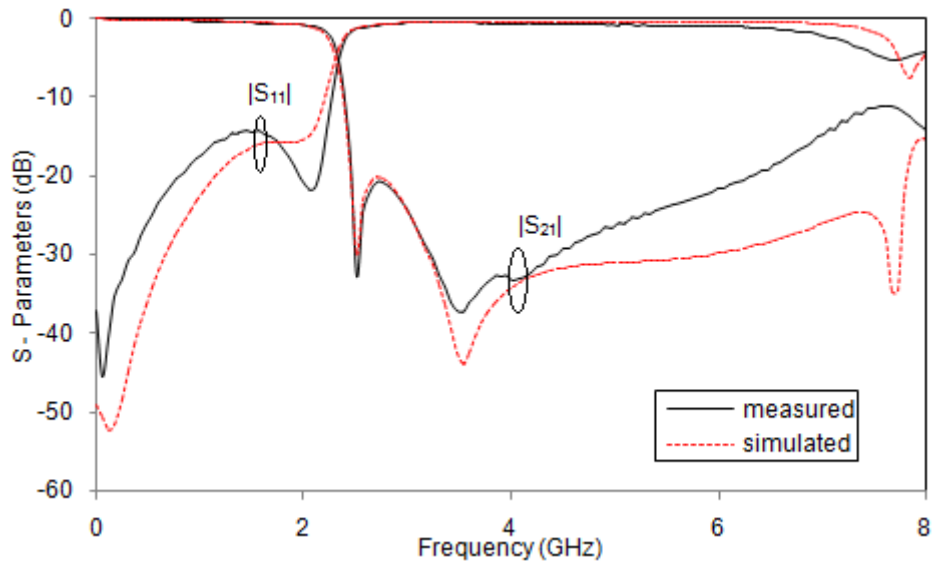


Fig. 4.16 Simulated and measured result of compact elliptic function lowpass filter with SI-PRs

The layout of the proposed compact filter with SI-PRs is illustrated in Fig. 4.7. The optimized filter dimensions are: $l1 = 1.2$ mm, $l2 = 2.8$ mm, $l3 = 5.6$ mm, $l4 = 0.8$ mm, $l5 = 3.8$ mm, $l6 = 1.4$ mm, $l7 = 10$ mm, $l8 = 2.4$ mm, $l9 = 3.2$ mm, $l10 = 2$ mm, $h1 = 3.8$ mm, $h2 = 2$ mm, $h3 = 2.4$ mm, $h4 = 1$ mm, $w1 = 0.4$ mm, $w2 = 0.6$ mm, $w3 = 0.2$ mm, $w4 = 0.4$ mm, and $w5 = 0.4$ mm. Good agreement between experimental and simulated results is achieved in passband as well as in stopband as shown in Fig. 4.16. The measured results show that the filter has an insertion loss less than 0.7 dB in the passband at 2.03 GHz and the 3 dB cutoff frequency, f_c at 2.4 GHz. The filter achieves a sharp roll-off of 90 dB/GHz (20 dB stopband frequency is 2.58 GHz) and wide stopband bandwidth of 4.48 GHz, from 2.55 GHz to 7.03 GHz with a suppression level better than 16 dB in the upper end of the stopband. The measured RSB of the filter is 93.52%. The filter has a compact size of 17.6 mm x 12.2 mm with NCS of $0.0414\lambda_g^2$, where λ_g is the guided wavelength at cutoff frequency.

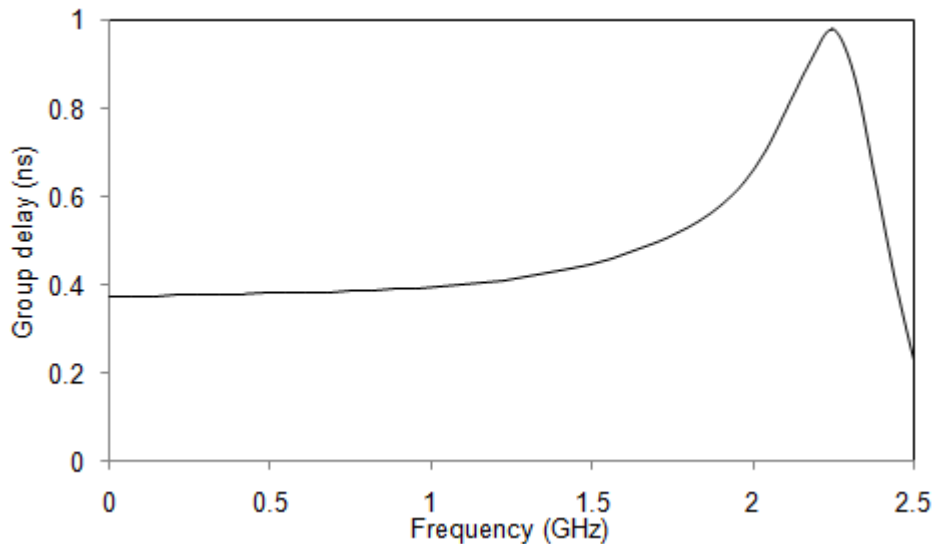


Fig. 4.17 Measured group delay characteristics of the compact elliptic function lowpass filter with SI-PRs

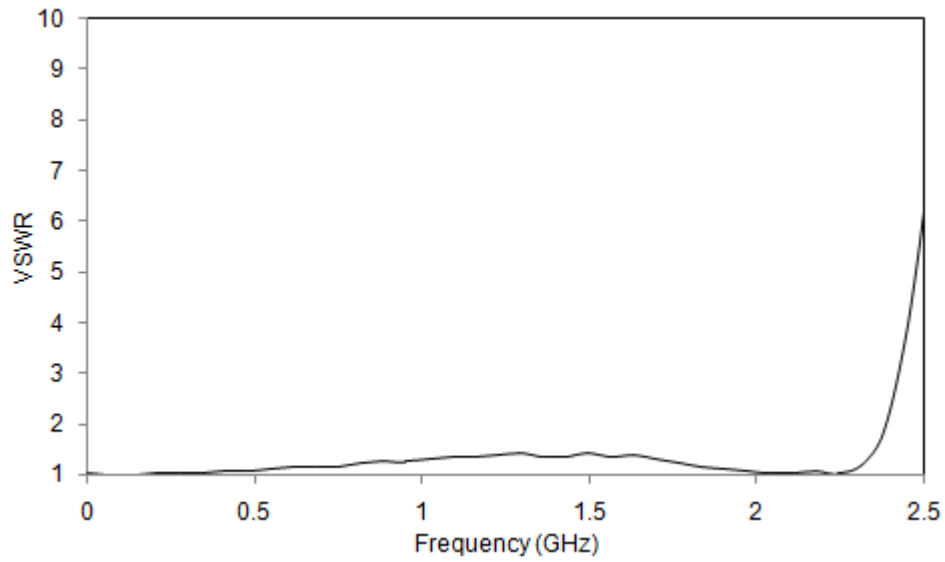


Fig. 4.18 Measured VSWR characteristics of the compact lowpass filter with SI-PRs

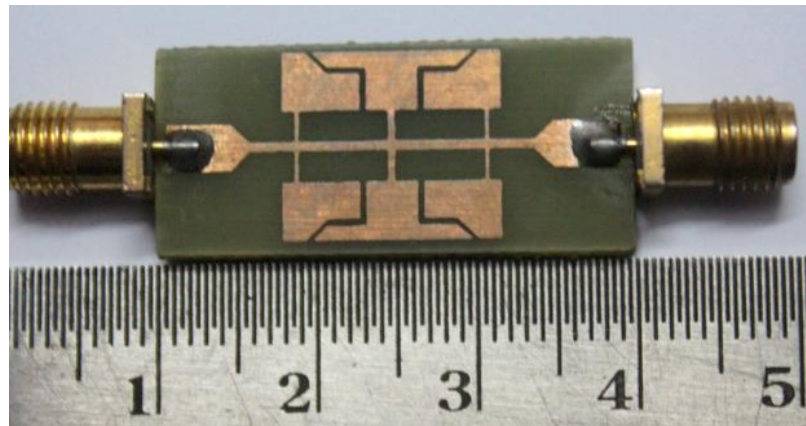


Fig. 4.19 Photograph of the proposed compact lowpass filter with SI-PRs

As shown in Fig. 4.16, the measured return loss in the passband is better

than 15.5 dB and close to 1dB at 6.3 GHz and 2 dB in the upper end of the stopband. The measured group delay characteristics of the filter are depicted in Fig. 4.17. The filter achieves almost constant group delay of 0.4 ns up to 1.5 GHz in the passband. The measured VSWR characteristics of the filter are depicted in Fig. 4.18.

Photograph of the fabricated filter is shown in Fig. 4.19. Table 4.2 compares the performance characteristics of lowpass filters which referred in the introduction and the proposed filter. From the table it is clear that the proposed filter is made of low cost FR4 substrate and gives high roll-off rate among the quoted filters.

Table 4.2 Comparison between performance of filter with SI-PRs and other published work in the literature.

| <i>Ref</i> | ξ (dB/GHz) | <i>Material used</i> | <i>f_c</i> (GHz) |
|-------------------------|-------------------|----------------------|-------------------------------|
| [2] | 17 | RT/duroid 5880 | 6.2 |
| [3] | 18 | RT/duroid 5880 | 1.5 |
| [4] | 20 | RT/duroid 5870 | 1.3 |
| [5] | 18 | Rogers RO4003 | 0.85 |
| [6] | 24 | RT/duroid 5880 | 6 |
| [7] | 63 | FR4 | 0.5 |
| [Filter with SI-PRs] | 90 | FR4 | 2.4 |

This work has been published in *Proc. of IEEE International Microwave & RF Conference(IMaRC), Bangalore, 2014, pp. 316–319*

4.4 Compact Elliptic Function lowpass Filter Design using modified SI-PRs

One of the important characteristics of lowpass filter is the sharp transition from passband to stopband, and is defined in terms of roll-off rate ξ as in (2.6) as:

$$\xi = \frac{\alpha_{\max} - \alpha_{\min}}{f_s - f_c} \text{ dB/GHz},$$

where α_{\max} is 20 dB attenuation point, α_{\min} is the 3 dB attenuation point, f_s is 20 dB stopband frequency and f_c is the 3dB cutoff frequency.

Basically roll-off rate is a measure of the switching characteristics of the filter from passband to stopband, and is inversely proportional to the difference between the 3 dB cutoff frequency f_c and specified attenuation frequency f_s . The roll-off rate can be improved by shifting the attenuation frequency close to the f_c , so as to maintain the difference in frequencies to a minimum level. Efforts to enhance the roll-off rate of the filter with SI-PRs are continuously being extended to minimize the difference between these two frequencies. Since the filter characteristics after f_c depend very much on the resonator parameters, the attenuation level frequency, f_s can be decreased to a great extent by modifying the centre resonator as well as the position of high impedance stub of side resonators.

One of the methods to improve the roll-off rate of the filter is by modifying the dimensions of centre resonator, thereby enhancing the inductance and capacitance associated with HIIS and LICP of SI-PR1 without changing the dimensions of SI-PR2. By increasing the height of HIIS and decreasing the height of LICP, we can modify the roll-off rate to a great extent without modifying the overall filter dimensions. Fig. 4.20 illustrates the layout of compact lowpass filter with modified SI-PR1.

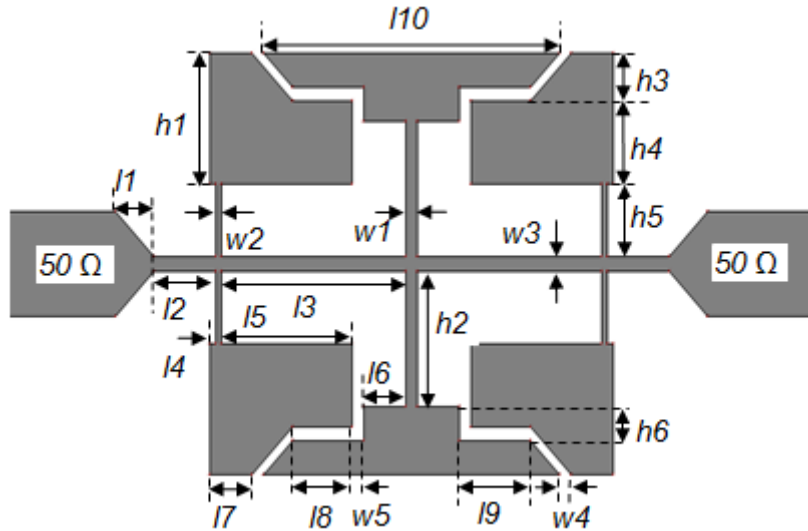


Fig. 4.20 Layout of compact lowpass filter modified SI-PR1

4.4.1 Parametric Analysis

Various parametric analyses have been conducted to optimize the filter dimensions. The major analysis includes the height of HIIS of SI-PR1, h_2 and the position of the HIIS of SI-PR2, l_4 with respect to the low impedance patch.

4.4.1.1 Height of HIIS of SI-PR1, (h_2)

Figs. 4.21 and 4.22 show the transmission and reflection characteristics of the filter as a function of height of HIIS of SI-PR1 respectively. As shown in Fig. 4.21, as h_2 increases, the attenuation level of transmission zero frequency after cutoff and the stopband suppression level also increases. Moreover, as shown in Fig. 4.22, the reflection characteristics in the passband are also enhanced by increasing h_2 . The optimized value of $h_2 = 3.9$ mm.

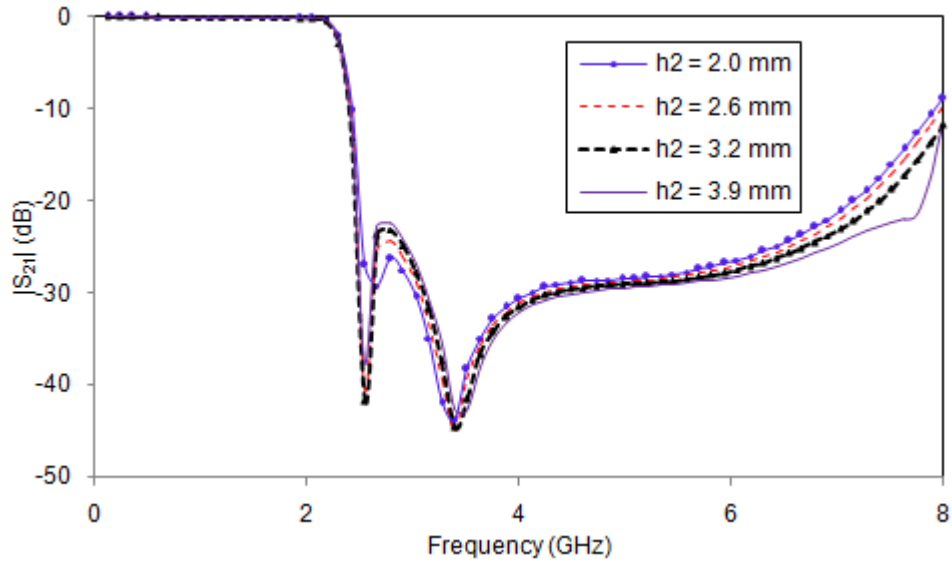


Fig. 4.21 Transmission characteristics of filter as a function of height of HIIS of SI-PR1, h_2

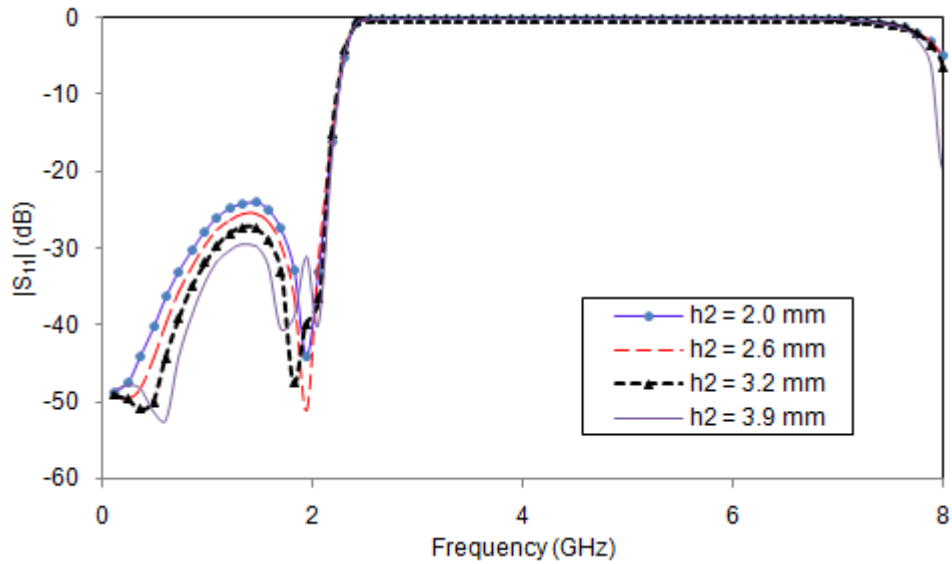


Fig. 4.22 Reflection characteristics of filter as a function of height of HIIS of SI-PR1, h_2

4.4.1.2. Position of HIIS of SI-PR2, (l_4)

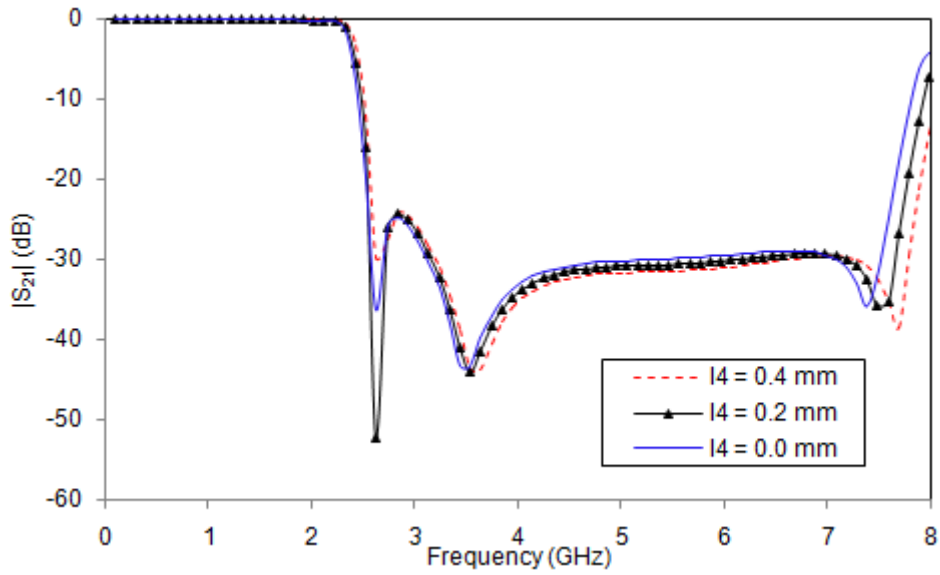


Fig. 4.23 Transmission characteristics of filter as a function of position of HIIS of SI-PR2, l_4

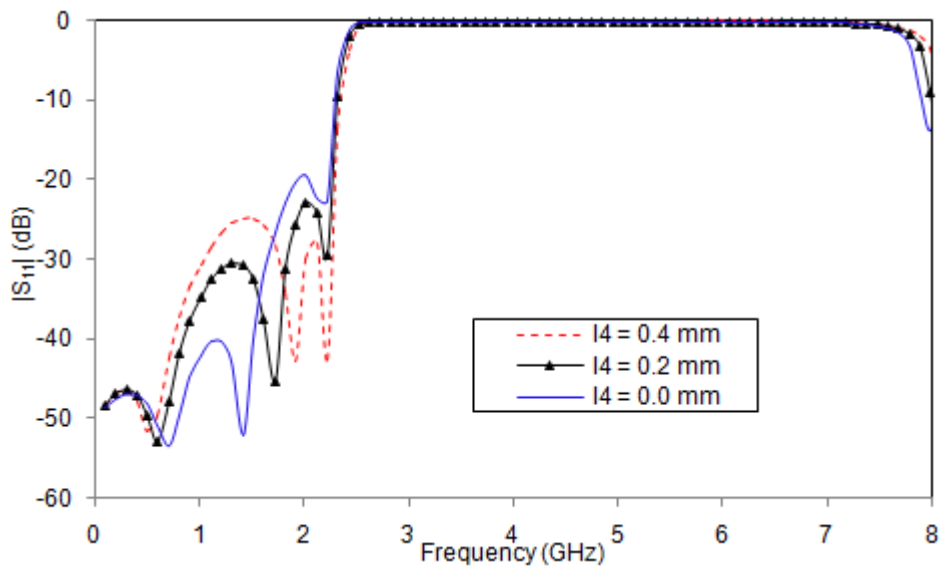


Fig. 4.24 Reflection characteristics of filter as a function of position of HIIS of SI-PR2, l_4

Figs. 4.23 and 4.24 show the transmission and reflection characteristics of the compact lowpass filter as a function of position of HIIS of SI-PR2 respectively. Even though there is no significant change in the passband transmission characteristics of the filter with respect to the small change in $l4$, the passband reflection characteristics improve with increasing $l4$. The stopband bandwidth and attenuation level are also increased with increase in $l4$. The optimized value of $l4 = 0.4$ mm.

4.4.2 Simulation and Measurements Results of Compact Lowpass Filter with Modified SI-PR1

The layout of the filter with modified SI-PRs is illustrated in Fig. 4.20. The filter dimensions are optimized with the simulation software Zeland IE3D. The optimized filter dimensions are: $l1 = 1.3$ mm, $l2 = 2.1$ mm, $l3 = 6.2$ mm, $l4 = 0.4$ mm, $l5 = 4.4$ mm, $l6 = 1.4$ mm, $l7 = 1.4$ mm, $l8 = 2$ mm, $l9 = 2.4$ mm, $l10 = 10$ mm, $h1 = 3.8$ mm, $h2 = 3.9$ mm, $h3 = 1.4$ mm, $h4 = 2.4$ mm, $h5 = 2.1$ mm, $h6 = 1$ mm, $w1 = 0.4$ mm, $w2 = 0.2$ mm, $w3 = w4 = w5 = 0.4$ mm. As shown in Fig. 4.25, the measurements results are in good agreement with the simulated results. The measured results show that the filter has an insertion loss less than 0.4 dB in the passband at 1.5 GHz and the 3 dB cutoff frequency is at 2.21 GHz. The filter achieves a wide stopband from 2.38 GHz to 6.7 GHz with a suppression level better than 18 dB in the upper end of the stopband. The return loss is better than 19.5 dB in the passband and close to 1.4 dB at 6.7 GHz. As shown in Fig. 4.26, the filter achieves almost constant group delay in the lower frequencies in the passband and gradually increases as the frequency approaches the cutoff frequency. A photograph of the prototype filter is depicted in Fig. 4.27.

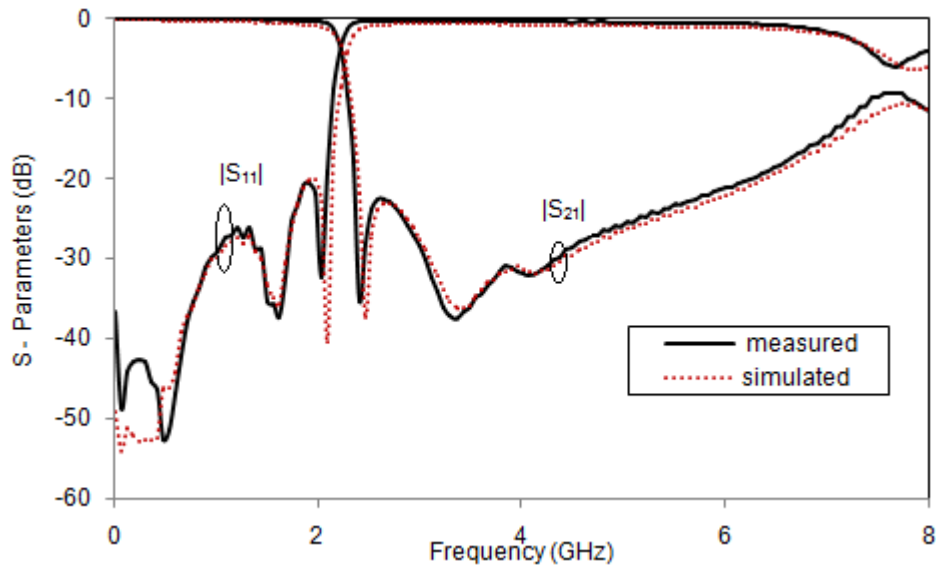


Fig. 4.25 Measured and simulated results of compact lowpass filter with modified SI-PR1

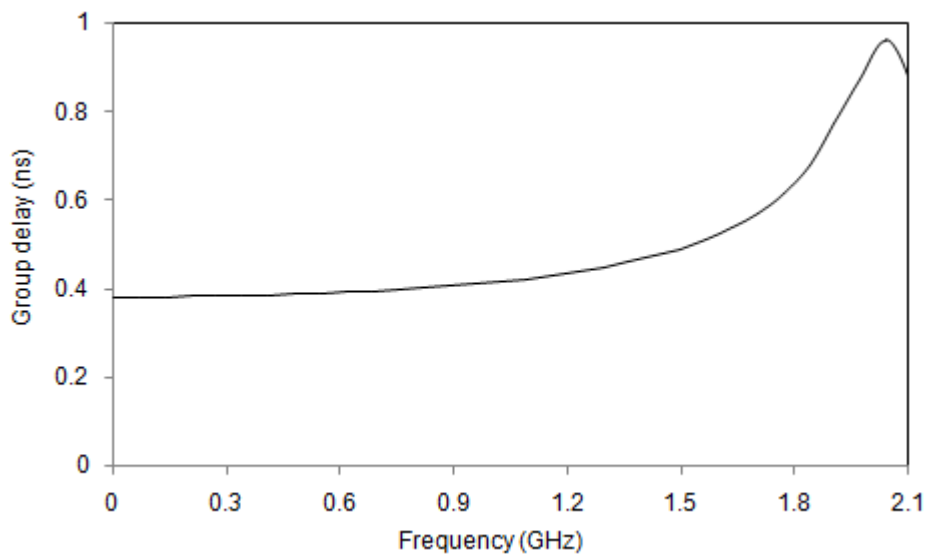


Fig. 4.26 Measured group delay characteristics of the compact lowpass filter with modified SI-PR1

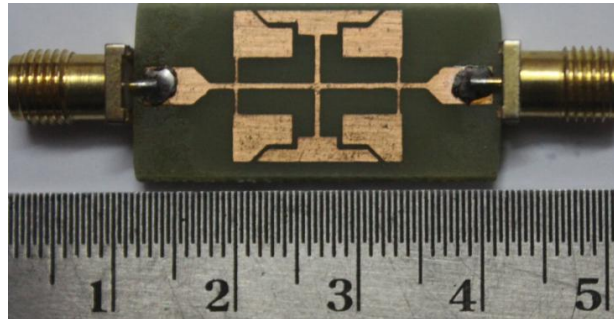


Fig. 4.27 A photograph of prototype compact filter with modified SI-PRs

This work has been published in *Proceedings of Asia Pacific Microwave Conference (APMC) 2014, Sendai, Japan, pp. 1229-1231.*

4.5 Compact Elliptic Function lowpass Filter Design using SI-PPR

The second method to enhance the performance of SI-PR1 (discussed in Section 4.3) is by modifying its LICP of centre resonator. The centre resonator of the filter is replaced by a stepped impedance polygonal patch resonator (SI-PPR). SI-PPR is designed by cascading low and high impedance sections Z_{C1} and Z_{H1} respectively and a polygonal patch as shown in Fig. 4.28.

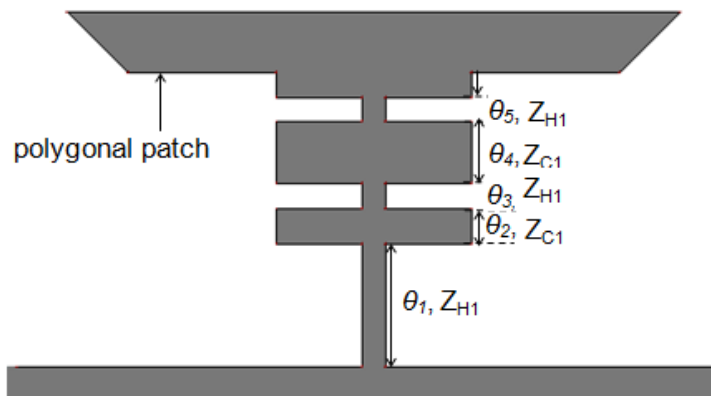


Fig. 4.28 Unit cell model of proposed SI-PPR

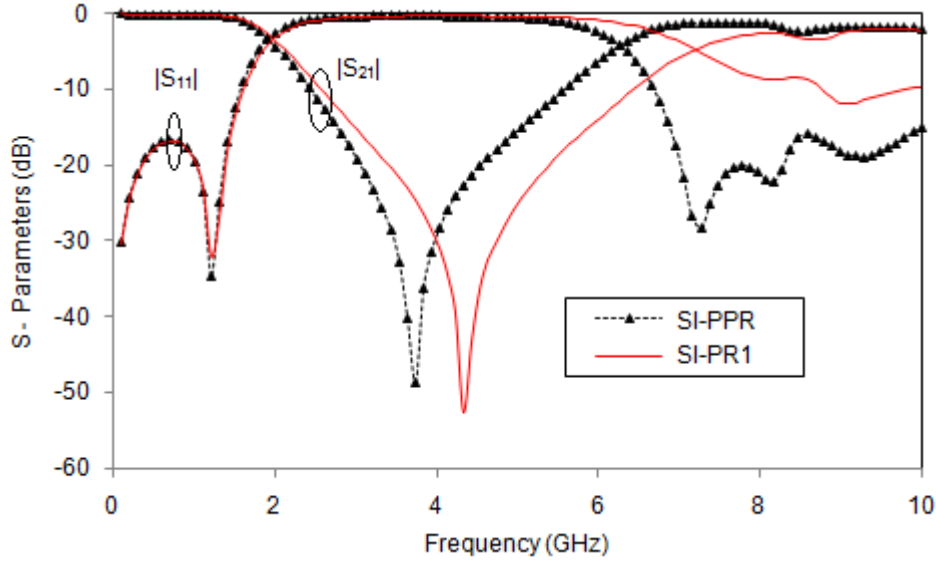


Fig.4. 29 Simulated S–Parameters of SI-PPR and SI-PR1

Fig. 4.29 demonstrates the simulated S-Parameters of SI-PPR. By introducing stepped impedances within the patch, the effective impedance enhances which shifts the transmission zero to a lower frequency without any change in passband performance. Fig. 4.30 shows the layout of the modified compact lowpass filter by replacing SI-PR1 with SI-PPR. Parameters of the filter are optimized using EM simulation. The optimized dimensions in millimeters are: $l_1 = 1.2$, $l_2 = 2.8$, $l_3 = 5.6$, $l_4 = 0.8$, $l_5 = 3.8$, $l_6 = 1.4$, $l_7 = 10$, $l_8 = 2.4$, $l_9 = 3.2$, $l_{10} = 2$, $h_1 = 3.8$, $h_2 = 2$, $h_3 = 2.4$, $h_4 = 1$, $h_5 = 0.6$, $h_6 = 1.0$, $w_1 = 0.4$, $w_2 = 0.6$, $w_3 = 0.2$, $g_1 = g_2 = g_3 = g_4 = 0.4$.

Fig. 4.31 shows the photograph of the fabricated filter using modified SI-PPR. The simulated results are validated with experimental results. Fig.4.32 shows the simulated and measured results of the proposed filter with SI-PPR. The roll off rate of the filter is improved to 106 dB/GHz of f_c at 2.3 GHz and the measured 20 dB attenuation level frequency is at 2.46 GHz. We can achieve

17% increase in the roll-off rate by the introduction of SI-PPR. The measured stopband bandwidth of the filter is from 2.4 GHz to 7 GHz with a suppression level of 16 dB and insertion loss less than 0.5 dB in the passband at 2 GHz. The return loss in the stopband is 1 dB at 6.4 GHz and 2 dB at upper end of the stopband. Excluding the microstrip feed line, the filter has a size of $0.24384 \lambda_g \times 0.16902 \lambda_g$, where λ_g is the guided wavelength at cutoff frequency.

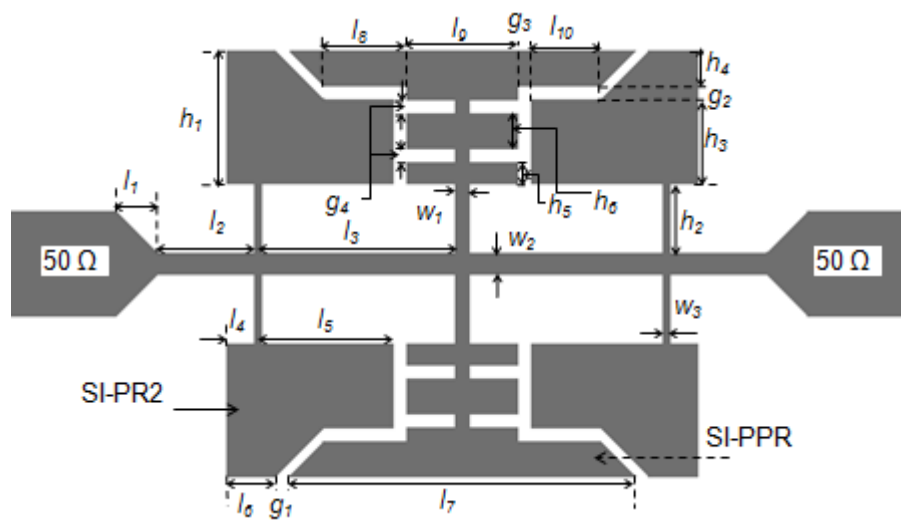


Fig. 4.30 Layout of the proposed Filter with SI-PPR

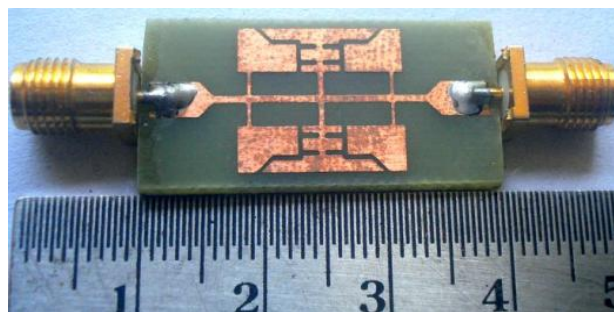


Fig. 4.31 Photograph of compact lowpass filter with SI-PPR

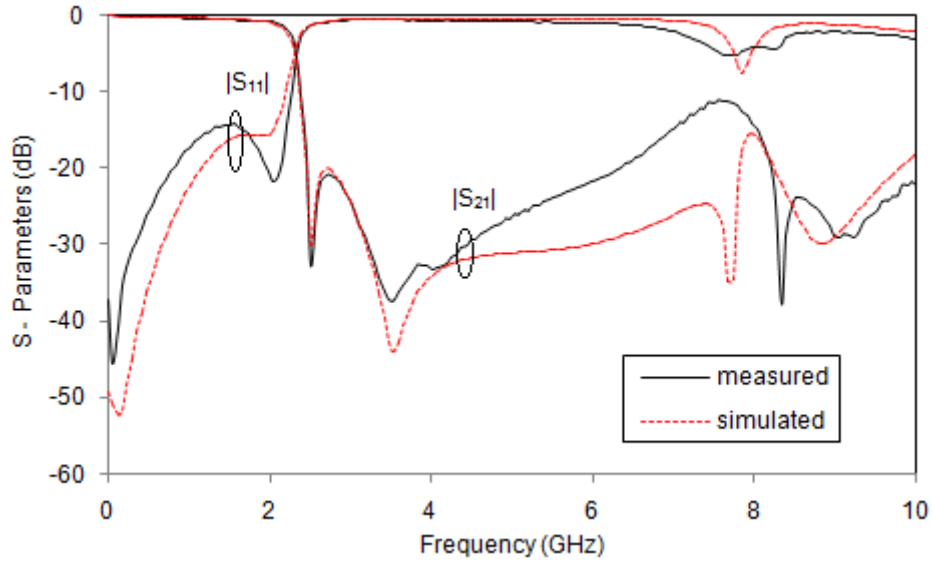


Fig. 4.32 Simulated and measured result of proposed Filter with SI-PPR

4.6 Compact and Wide Stopband Lowpass Filter Design using SI-PPR

The stopband bandwidth of the Filter with SI-PPR is further enhanced by loading one more resonator, SI-PR3 on both sides of SI-PR2 without any change in the overall physical dimensions of the filter. Addition of SI-PR3 provides substantial improvement in stopband bandwidth by 4.35 GHz with 16 dB suppression level by short outing the transmission pole at 7.56 GHz. It also provides the impedance matching at the passband, thereby minimizing the insertion loss to 0.5 dB in 80% of the passband.

Fig. 4.33 shows the layout of the optimized structure of modified filter. Optimized dimensions of the filter in millimeters are: $l_1 = 1.2$, $l_2 = 0.8$, $l_3 = 1.8$, $l_4 = 5.6$, $l_5 = 0.8$, $l_6 = 3.8$, $l_7 = 1.4$, $l_8 = 1.8$, $l_9 = 1.4$, $l_{10} = 10$, $l_{11} = 2.4$, $l_{12} = 3.2$, $l_{13} = 2$, $w_1 = 0.4$, $w_2 = 0.6$, $w_3 = 0.2$, $w_4 = 0.2$, $w_5 = 4.8$, $h_1 = 2$, $h_2 = 1$, $h_3 = 1.8$, $h_4 = 3.8$, $h_5 = 2.4$, $h_6 = 0.6$, $h_7 = 1$, $g_1 = 0.4$, $g_2 = 0.2$, $g_3 = g_4 = g_5 = g_6 = 0.4$.

Fig. 4.34 shows the photograph of the proposed filter. The experimental results are in very good agreement with the simulated results as shown in Fig. 4.35.

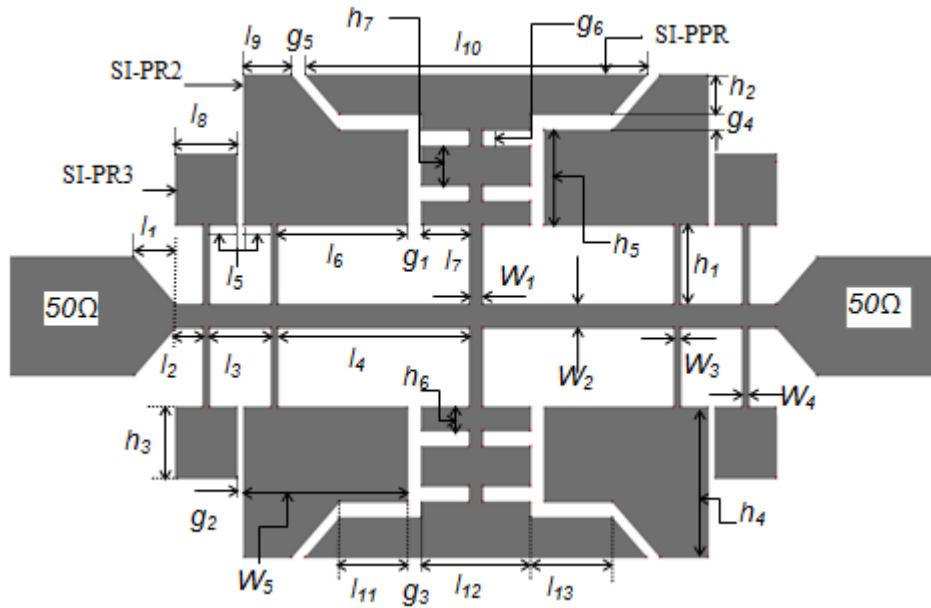


Fig. 4.33 Layout of the proposed compact and wide stopband lowpass filter using SI-PPR

The measured insertion loss of the filter is less than 0.5 dB in the passband up to 1.8 GHz with f_c of 2.28 GHz and 20 dB attenuation at 2.46 GHz. The filter achieves a wide stopband from 2.49 GHz to 11 GHz with a suppression level better than 23 dB and a sharp roll-off rate ζ of 94 dB/GHz. The measured fractional stopband bandwidth of the filter is 126%. The return loss is better than 16 dB for the entire passband and close to 4 dB in the upper end of the stopband. The high value of insertion loss in the passband and return loss in the stopband of the measured filter is due to the inherent dielectric losses associated with FR4 material. Even though the filter designed by cascading

multiple resonators, the filter performs uniform group delay characteristics in the passband as shown in Fig. 4.36.

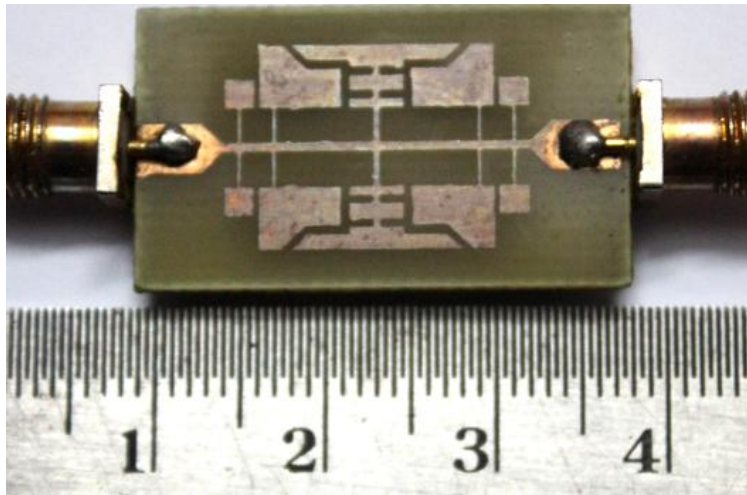


Fig. 4.34 The photograph of the proposed filter with SI-PPR

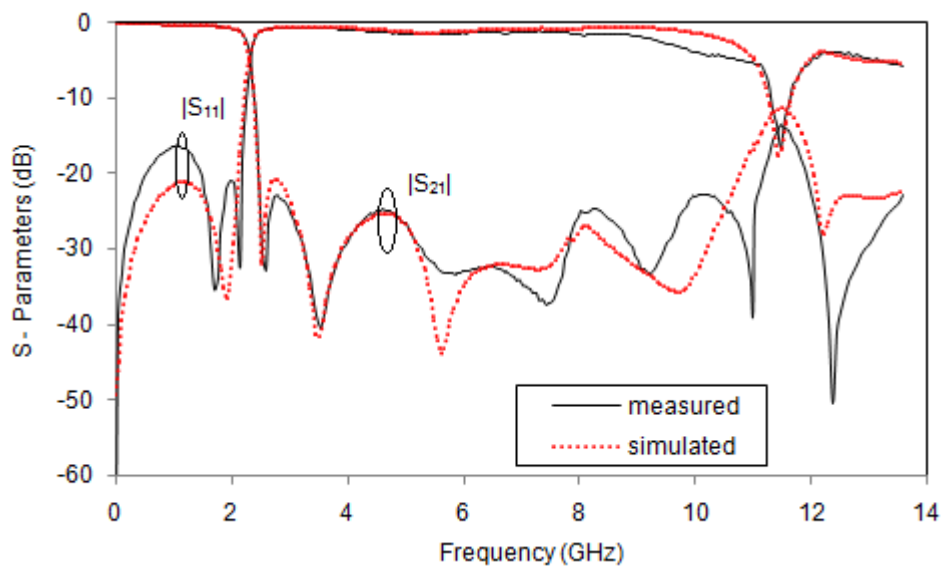


Fig.4.35 Simulated and measured results of proposed compact lowpass filter with wide stopband

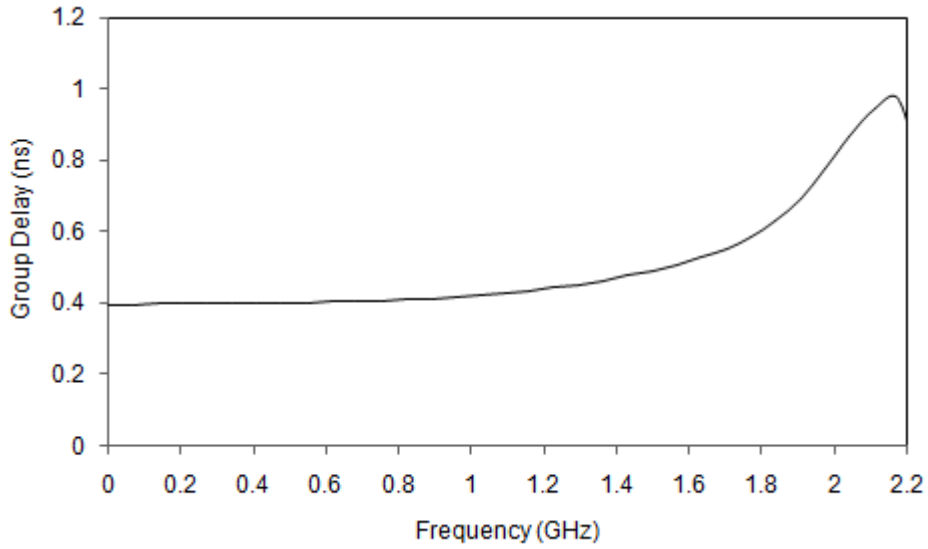


Fig. 4.36 Measured group delay characteristics of proposed compact lowpass filter with wide stopband

Table 4.3 Performance comparison of proposed filter with SI-PPR and similar published work in the literature

| <i>Ref.</i> | ξ (dB/GHz) | <i>SB</i> (GHz) | <i>SSL</i> (dB) | <i>fc</i> (GHz) | ϵ_r | <i>t</i> (mm) |
|-------------|-------------------|--------------------|--------------------|--------------------|--------------|------------------|
| [7] | 63 | 0.80 - 4.60 | 20 | 0.53 | 4.4 | 1.58 |
| [8] | 45 | 1.38-5.5 | 20 | 1 | 2.65 | 1 |
| [9] | 46 | 1.5 - 6.6 | 20 | 1.08 | 4.4 | 1.6 |
| [10] | 81 | 1.21 - 26.35 | 20 | 1 | 3.38 | 0.508 |
| [11] | 50 | 3.32 - 21 | 20 | 2.97 | 2.2 | 0.254 |
| This work | 94 | 2.49 - 11.0 | 23 | 2.28 | 4.4 | 1.6 |

ξ = roll-off rate, SB = Stopband Bandwidth, SSL = Suppression Level, $f_c = 3$ dB cutoff frequency, ϵ_r & t = permittivity and thickness of the substrate

Table 4.3 summarizes the performance of proposed lowpass filters in comparison with previous published work. From the table it is clear that the proposed filter shows the highest roll-off at 20 dB attenuation level and wide stopband bandwidth with high suppression level of 23 dB.

This work has been published in *Microwave & Optical Technology Letters*, vol. 58, Issue 1, pp. 133-136, January 2016.

4.7 Conclusions

In this chapter, compact elliptic function lowpass filters with very sharp 20 dB roll-off rate near cutoff frequency with wide stopband and high suppression level are designed and proposed. The filter is designed by loading multiple stepped impedance patch resonators on high impedance transmission line. The patch resonators are designed with cascading high impedance short circuited stub with low impedance stepped impedance open circuited patch. The stepped impedance patch resonators provide high capacitance effects that lead to enhance the roll-off rate of the filter. The equivalent circuit model of the filter has been developed and the results are validated with EM structural simulation results. By modifying the shape of centre patch resonator as stepped impedance polygonal patch resonator, the filter response has been improved to a great extent. Moreover, by introducing one more resonator near the feed line, the stopband bandwidth and suppression level improved greatly. Performance comparison of all the filters discussed in this chapter is summarized in Table 4.4. The compact size, wide stopband, sharp roll-off and good suppression level of the proposed lowpass filters make them suitable for applications in modern communication systems.

Table 4.4 Performance comparison of compact lowpass filters using SI-PRs and SI-PPR

| Filter | f_c GHz | ξ dB/GHz | SIZE ² mm ² | NCS ² λ_g^2 | RSB % | SL dB | PB IL dB | RL in PB/SB |
|--------|--------------|-----------------|--------------------------------------|-----------------------------------|----------|----------|-------------------|----------------------------------|
| I | 2.4 | 90 | 17.6x12.2 | 0.041 | 93.52 | 16 | 0.7 (2.03 GHz) | < 15.5 in PB < 2 in SB |
| II | 2.21 | 94 | 17.4x12.2 | 0.038 | 95.15 | 18 | 0.4 (1.5 GHz) | < 19.5 in PB < 1.4 in SB |
| III | 2.3 | 106 | 17.6x12.2 | 0.042 | 97 | 16 | 0.6 (1.7 GHz) | < 14.5 in PB < 1.3 in SB |
| IV | 2.28 | 94 | 17.6x12.2 | 0.041 | 126 | 23 | 0.5 (1.8 GHz) | < 16 in PB < 1.2 up to 8.5 |

- I Compact elliptic function lowpass filter using SI-PRs
- II Compact elliptic function lowpass filter using modified SI-PRs
- III Compact elliptic function lowpass filter using SI-PPR
- IV Compact and wide stopband lowpass filter using SI-PPR and suppressing cells

References

- [1] J. S. Hong and M. J. Lancaster, “*Microstrip Filters for RF/ Microwave Applications*,” John Wiley, New York, 2001.
- [2] F. Zhang, J.Z. Gu, C.Y. Gu, L.N. Shi, C. F.Li and X.W. Sun, “Lowpass filter with in-line beeline CMRC,” *Electronics Lett.*, vol. 42, no. 8, pp. 472-474, 2006.
- [3] M.H. Yang and J. Xu, “Design of compact broad-stopband lowpass filters using modified stepped impedance hairpin resonators,” *Electronics Lett.*, vol. 44, no. 20, pp. 1198–1200, 2008.
- [4] L. Ge, J.P. Wang and Y-X Guo, “Compact microstrip lowpass filter with ultra-wide stopband,” *Electronics Lett.*, vol. 46, no. 10, pp. 689 – 691, 2010.
- [5] H. Cui, J. Wang and G. Zhang, “Design of microstrip low pass filter with compact size and ultra-wide stopband,” *Electronics Lett.*, vol. 48, no. 14, pp. 856 – 857, 2012.
- [6] M. Mirzaee and B.S. Virdee, “Compact lowpass filter with high out-of-band rejection and super wide stopband performance,” *Microwave and Opt. Technology Lett.*, vol. 56, no. 4, pp. 947-950, 2014.
- [7] V.K. Velidi and S. Sanyal, “Sharp roll-off lowpass filter with wide stopband using stub-loaded coupled-line hairpin unit,” *IEEE Microw. and Wireless Compon. Lett.*, vol. 21, no. 6, 2011.
- [8] Lin Li, Zheng-Fan Li, and Jun-Fa Mao, “Compact lowpass filters with sharp and expanded stopband using stepped impedance hairpin units,” *IEEE Microw. Wireless Compon. Lett.* vol. 20, pp. 310–312, 2010.
- [9] S.S. Karthikeyan and R.S. Kshetrimayum, “Compact, deep, and wide rejection bandwidth lowpass filter using open complimentary split ring resonator,” *Microwave Opt. Technol. Lett.* vol. 53, pp. 845–848, 2011.
- [10] G. Karimi, F.K. Hamedani, H. Siahkamari, “Ultra-wide stopband lowpass filter using symmetrical cascaded modified hairpin resonators,”

International Journal of RF and microwave Computer-Aided Engg. vol. 24, 314–321, 2014.

- [11] M. Hayati, M. Gholami, H.S. Vaziri and T. Zaree, “Design of microstrip lowpass filter with wide stopband and sharp roll-off using hexangular shaped resonator, ” *Electron. Lett.* vol. 51, pp. 69–71, 2015.
- [12] Makimoto, M. and S. Yamashita, “*Microwave Resonators and Filters for Wireless Communications Theory, Design and Application,* ” Springer Series in Advanced Microelectronics, 2001.
- [13] K. Ma and K.S. Yeo, “New ultra-wide stopband low-pass filter using transformed radial stubs,” *IEEE Trans. Microw. Theory Tech.* vol. 59, no. 3, pp. 604–611, 2011.
- [14] L. Zhu and K. Wu, “Short–Open Calibration Technique for Field Theory-Based Parameter Extraction of Lumped Elements of Planar Integrated Circuits,” *IEEE Trans. Microwave Theory and Techniques,* vol. 50, no. 8, pp. 1861-1869, 2002.

Chapter 5

Compact Lowpass Filter with High Suppression Level using Octagonal and Heptagonal Patch resonators

This chapter deals with, the design procedure of a compact lowpass filter with high suppression level on lossy FR4 material (loss tangent 0.02) by octagonal and heptagonal patch resonators. The role of loss tangent of the substrate to determine the performance characteristics of the filter is studied and compared the results with a low loss material having same substrate properties such as permittivity and thickness. The designed filter is developed on low cost ceramic filled PTFE substrate CMET/LK-4.3 with loss tangent 0.0018. The experimental results are validated with EM simulation results. The filter achieves a sharp roll-off of 137 dB/GHz at 40 dB attenuation level with suppression level better than 30 dB.

5.1 Introduction

In this chapter, a microstrip lowpass filter with sharp roll-off rate and excellent stopband performance up to C-band using symmetrical octagonal patch resonators (OPR) using FR4 substrate is proposed. The filter characteristics are further enhanced by modifying the shape of centre OPR as heptagonal patch resonator (HPR) to increase effective capacitance of the structure. The characteristics of the filter are further enhanced by developing the same filter structure on a low loss ceramic filled PTFE substrate having the properties of FR4 material with loss tangent of 0.0018. The equivalent circuit of the filter is extracted with component values using simulation software Zeland IE3D and the results are compared with full wave EM simulation results. A detailed parametric analysis has been conducted in both L-C model and EM model. The current distribution characteristics of the structure are analyzed for different transmission zero frequencies. The filter achieves a high value suppression level, which is contributed by the effect of very low impedance resonant patches and tight coupling between them. The prototype filter is fabricated on a 1.6 mm thick CMET/LK4.3 substrate of dielectric constant 4.3 with loss tangent 0.0018 and the filter achieves a sharp roll-off rate of 137 dB/GHz with suppression level more than 30 dB.

5.2 Compact Lowpass Filter Design using Octagonal Patch Resonators

The geometric structure of the proposed lowpass filter using octagonal patch resonator is shown in Fig. 5.1. The filter consists of two types of OPRs symmetrically loaded on 120 Ω transmission line. Each resonator is designed with high impedance short circuited stubs and low impedance open circuited octagonal shaped patches.

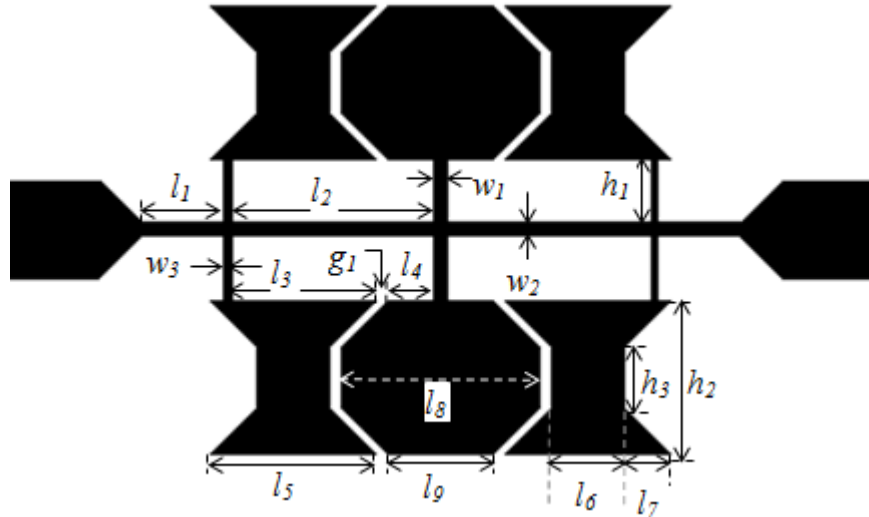


Fig. 5.1 Geometric structure of the proposed lowpass filter using OPRs

To illustrate the design of the proposed filter, frequency responses caused by loading of centre and side resonators on the transmission line are separately studied. Fig. 5.2 demonstrates the performance characteristics of centre OPR. The centre OPR is designed with a symmetrical octagonal shaped patch and 120Ω impedance stubs, which is designed for narrow band rejection near transmission zero with high level of attenuation. Fig. 5.3 shows the performance characteristics of side resonators, which also consists of octagonal shaped capacitive patch with 146Ω impedance short circuited stubs. The size and shapes of side resonators are fully compatible with the size and shape of the centre resonator, so as to enhance maximum coupling between them.

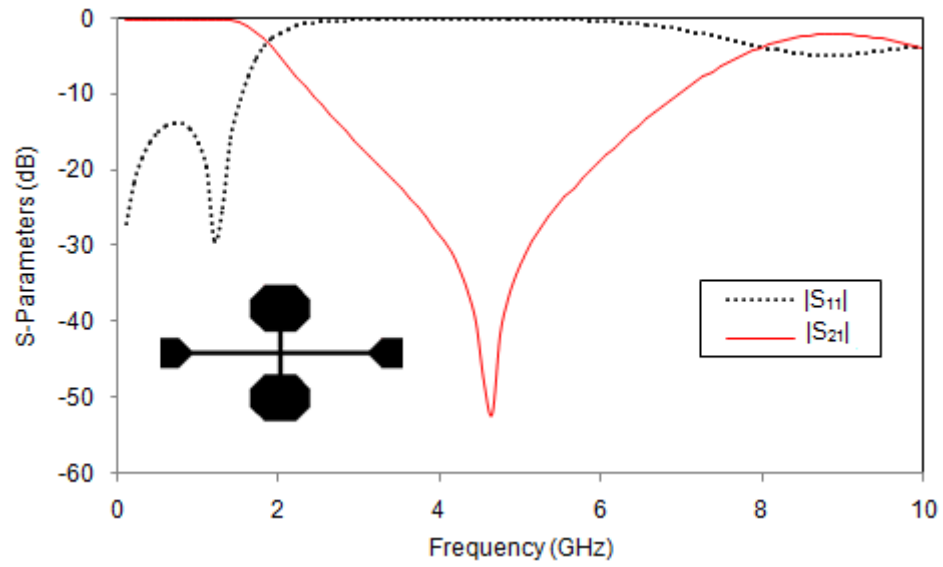


Fig. 5.2 Simulated S-Parameters of proposed filter with centre OPR

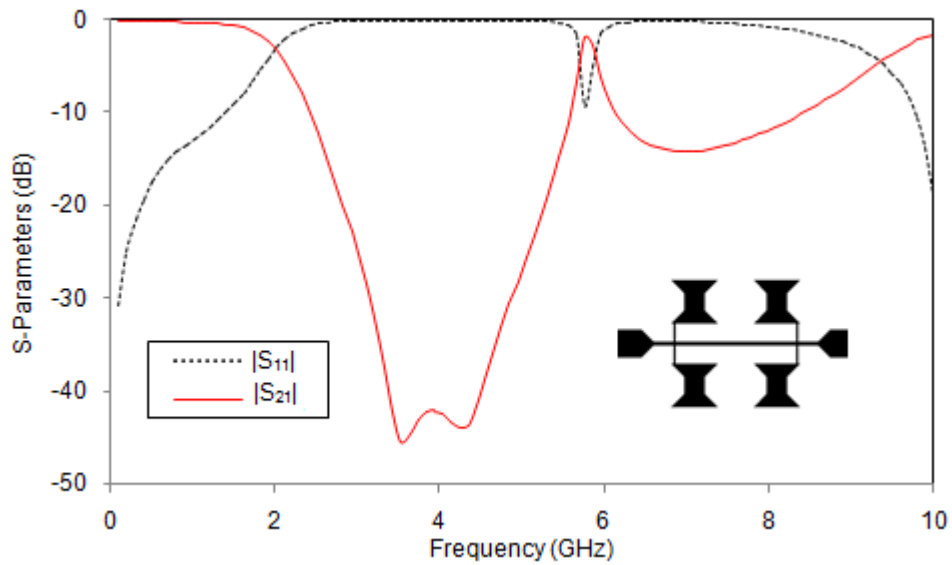


Fig. 5.3 Simulated S-Parameters of filter response with side OPRs

Since both resonators possess high attenuation level at their transmission zeroes, by suitably loading these two resonators we can develop a wide

stopband lowpass filter with high suppression level as shown in Fig 5.4. The filter is designed and developed on glass epoxy FR4 material having permittivity 4.4, thickness 1.6 and loss tangent 0.02. The filter parameters are optimized using Zeland IE3D simulation software. The optimized filter dimensions are: $l_1 = 2.1$ mm, $l_2 = 6.6$ mm, $l_3 = 4.8$ mm, $l_4 = 1.4$ mm, $l_5 = 5$ mm, $l_6 = 2.2$ mm, $l_7 = 1.4$ mm, $l_8 = 6$ mm, $w_1 = 0.4$ mm, $w_2 = 0.4$ mm, $w_3 = 0.2$ mm, $h_1 = 2$ mm, $h_2 = 4.7$ mm, $h_3 = 1.6$ mm, $h_4 = 1.9$ mm and $g_1 = 0.4$ mm.

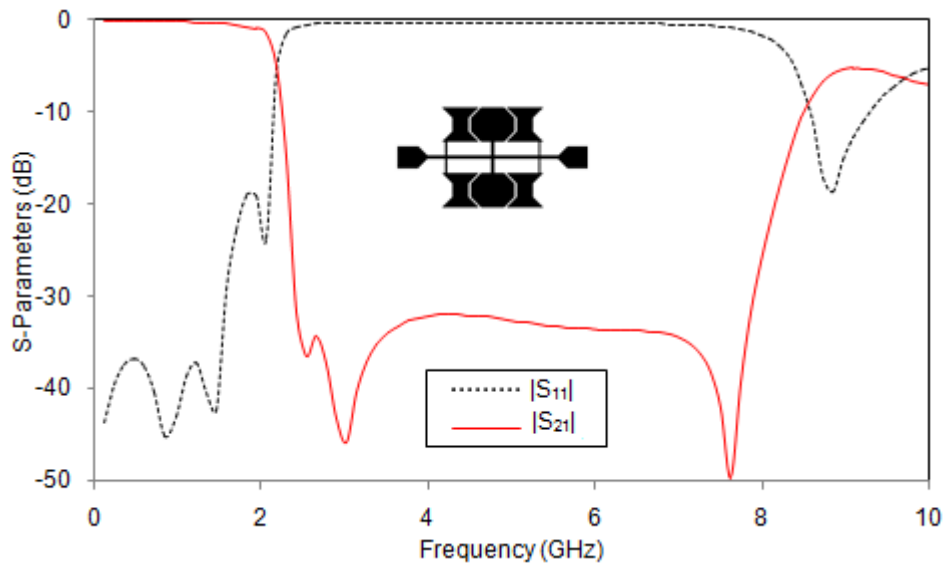


Fig. 5.4 Simulated S-Parameters characteristics of filter with two types of OPRs

Fig. 5.5 demonstrates the simulated and measured results of the proposed filter with two types of OPRs. The measured 3 dB cutoff frequency of the filter is at 2.16 GHz with roll-off rate 119 dB/GHz (40 dB level). The developed filter achieves a stopband bandwidth of 2.4 GHz to 5.2 GHz with SL better than 30 dB and 2.368 GHz to 9 GHz with SL better than 20 dB. Fig. 5.6 shows the photograph of the fabricated filter with OPRs.

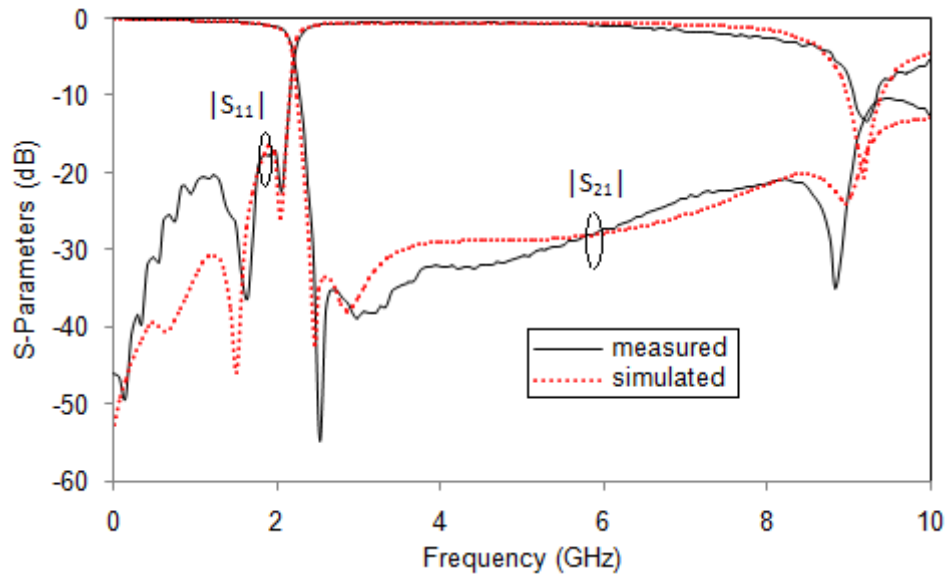


Fig. 5.5 Simulated and measured results of the filter with OPRs

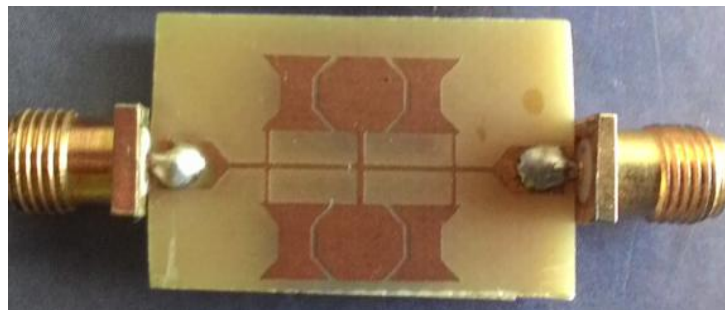


Fig. 5.6 Photograph of the fabricated filter with OPRs

5.3 Compact Lowpass Filter Design using Heptagonal Patch Resonator

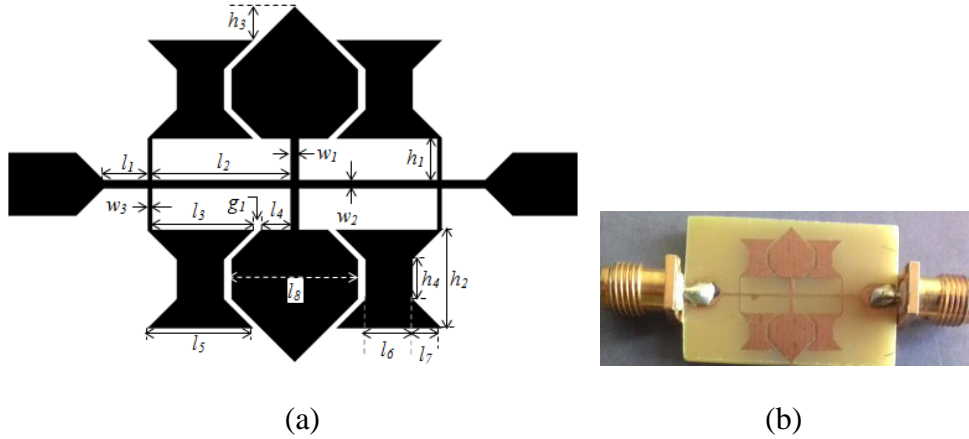


Fig. 5.7 Layout and photograph of compact lowpass filter with HPR and OPRs
(a) Layout, (b) Photograph

The stopband suppression level of the filter with OPR can be further improved by replacing the octagonal shaped centre patch resonator with heptagonal shaped patch. As impedance of the patch decreases, the effective capacitance increases and that enhances the stopband suppression level of the filter. However, the stopband bandwidth of the filter decreases as effective capacitance increases. Fig. 5.7 shows the layout of the modified filter with OPR as side resonator and heptagonal patch resonator (HPR) as centre resonator. The position of the high impedance stub of side resonator has been optimized to achieve maximum impedance matching and thereby reducing the passband insertion loss in the minimum level. All other structural dimensions remain the same. The optimum dimensions are: $l_1 = 2.1$ mm, $l_2 = 6.6$ mm, $l_3 = 4.8$ mm, $l_4 = 1.4$ mm, $l_5 = 5$ mm, $l_6 = 2.2$ mm, $l_7 = 1.4$ mm, $l_8 = 6$ mm, $w_1 = 0.4$ mm, $w_2 = 0.4$ mm, $w_3 = 0.2$ mm, $h_1 = 2$ mm, $h_2 = 4.7$ mm, $h_3 = 1.6$ mm, $h_4 = 1.9$ mm and $g_1 = 0.4$ mm.

Fig. 5.8 shows the comparison of the measured results of the filter with OPRs discussed in Section 5.2 and filter with centre HPR and side OPRs, where the 3 dB cutoff frequency of the filter with HPR is shifted to 2.06 GHz. The roll-off rate of the proposed filter decreases with the increase in capacitance of the centre patch. The measured roll-off rate of the filter with HPR is 108 dB/GHz (40 dB level). As shown in Fig. 5.8, the stopband bandwidth of the filter with HPR is 2.323 GHz to 8.3 GHz with SL better than 26 dB.

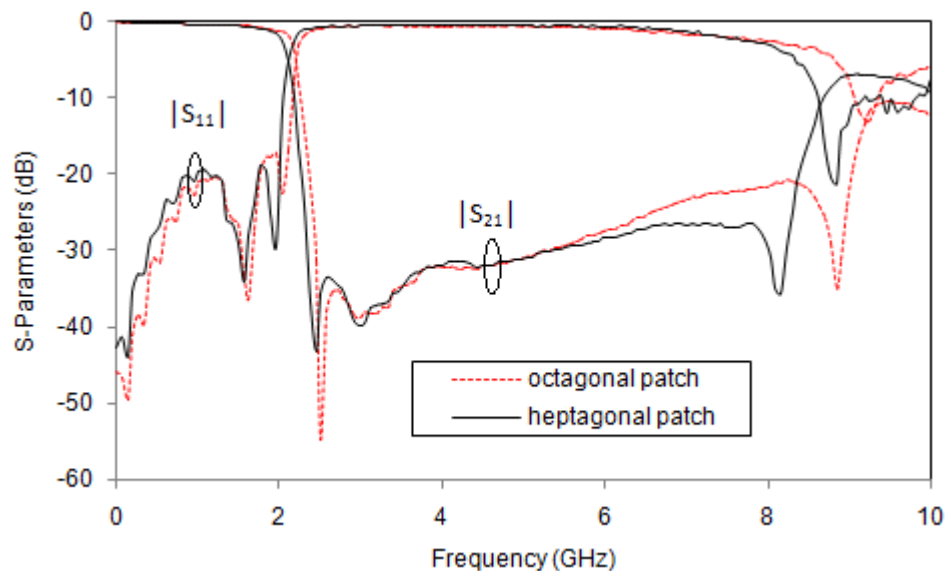


Fig. 5.8 Measured S-Parameters characteristics of lowpass filter using OPR and HPR discussed in Sections 5.2 and 5.3

The loss tangent of the material is a parameter that introduces losses in transmitted power owing to imperfect dielectric [1]. A lossy dielectric is a partial conducting medium (imperfect dielectric or imperfect conductor) with $\sigma \neq 0$, as distinct from lossless dielectric (perfect or good dielectric) in which $\sigma = 0$.

The loss tangent of a medium is calculated by Eq. (5.1) as:

$$\tan \theta = \frac{\sigma}{\omega \epsilon_r}, \quad (5.1)$$

where,

σ , ϵ_r are the conductivity and permittivity of the medium and

$$\omega = 2\pi f, \quad (5.2)$$

where ,

f is the frequency of operation.

Equation (5.1) demonstrates that the loss tangent of the dielectric medium is frequency dependent. As frequency increases, loss tangent of the medium increases and that will lead to make the dielectric as a partial conductor and the signals get attenuated. Since the proposed filters are designed and developed using lossy FR4 material with loss tangent of 0.02, the filter exhibits magnitude response of transmission and reflection characteristics as shown in Fig. 5.9. We can enhance the response characteristics of the filter by using the low loss material having same material properties such as permittivity and thickness as demonstrated in Fig. 5.10. The designed filter with centre HPR and side OPRs is designed using a low loss, low cost ceramic filled PTFE substrate, C-MET/LK4.3 of $\epsilon_r = 4.3$, $t = 1.6$ mm with loss tangent 0.0018. As shown in Fig.5.10, the proposed filter with new substrate material possesses a flat passband characteristics with $|S_{21}|$ is approximately unity.

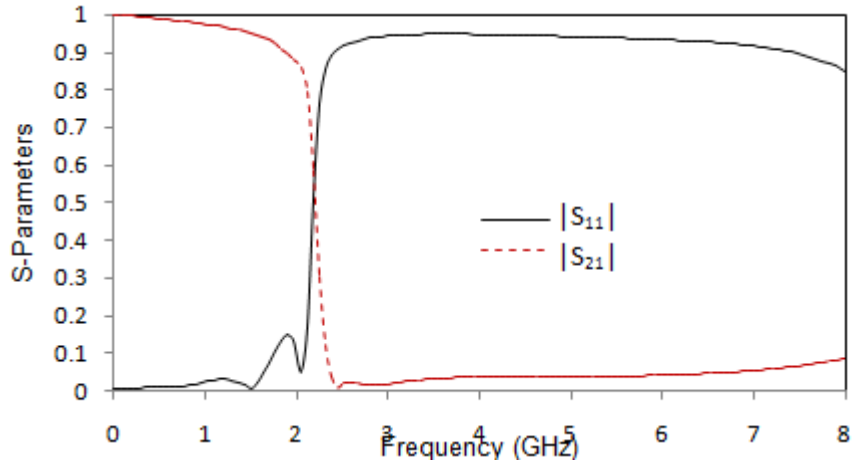


Fig. 5.9 Simulated magnitude response of the lowpass filter with centre HPR and side OPRs designed on FR4 material with loss tangent of 0.02

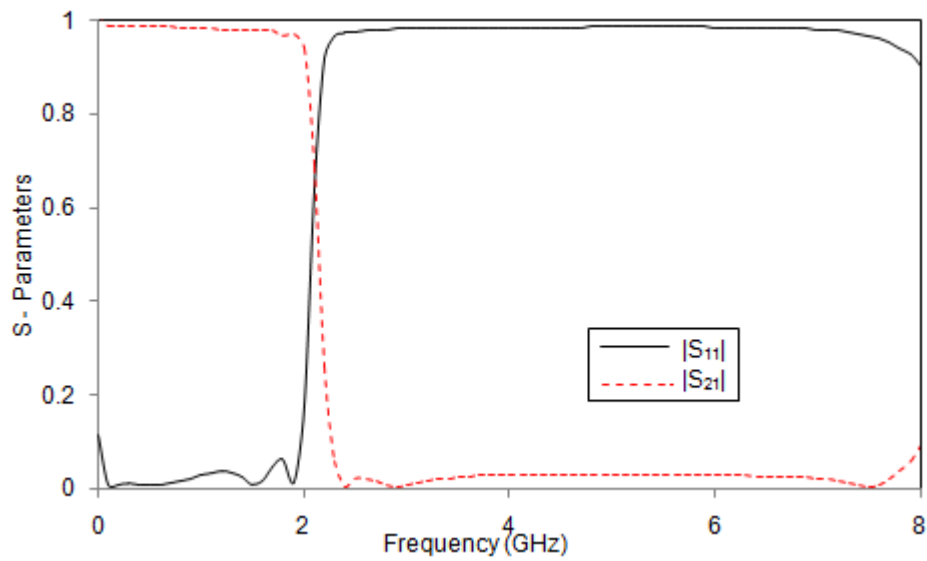


Fig. 5.10 Simulated magnitude response of the lowpass filter with centre HPR and side OPRs designed on C-MET/LK4.3 material with loss tangent of 0.0018

5.4 Equivalent Circuit Analysis

As demonstrated in Chapter 3 and Chapter 4, the L-C model equivalent circuit of the filter with HPR and OPRs is shown in Fig. 5.11, which characterizes the elliptic function response. The two types of resonators are modeled as six shunt connected series L-C branches that short out transmission at their resonant frequencies which enhances the slope of transition. L_{H1} and L_{H2} are the inductance of the transmission line with characteristic impedance 120Ω and length l_1 and l_2 respectively, which block the transmission at higher frequencies due to their infinite series impedance. L_{r1} and L_{r2} are the inductance of the high impedance stub of the centre resonator and the side resonators respectively and the value of equivalent L and C components is calculated by using the method demonstrated in Eqs. (3.7, 3.19 and 3.20).

The calculated values of inductance are: $L_{H1} = 1.46 \text{ nH}$, $L_{H2} = 4.41 \text{ nH}$, $L_{r1} = 1.39 \text{ nH}$, and $L_{r2} = 1.66 \text{ nH}$. The extracted values of capacitance are: $C_{r1} = 1.127 \text{ pF}$, $C_{r2} = 0.716 \text{ pF}$ and $C_C = 0.12 \text{ pF}$. The equivalent circuit was realized using Zeland IE3D simulation software. Fig. 5.12 shows the simulated L-C model transmission characteristics of the filter with HPR and OPRs that are validated with full wave EM structural simulated results.

The filter exhibits wide stopband including three transmission zeroes which is verified as shown in Fig. 5.12. The difference of the zero locations and attenuation level in the higher frequency range is mainly due to two reasons. Firstly, the equivalent circuit is extracted with respect to the cutoff frequency f_c , so that the electric length which may be larger than a quarter-wave length as frequency increases and the high-order parasitic effects become dominant [2]. Secondly, in L-C model analysis, only values of L and C components are

dominant parameters, but in EM analysis, all the structural parameters including loss factors are involved.

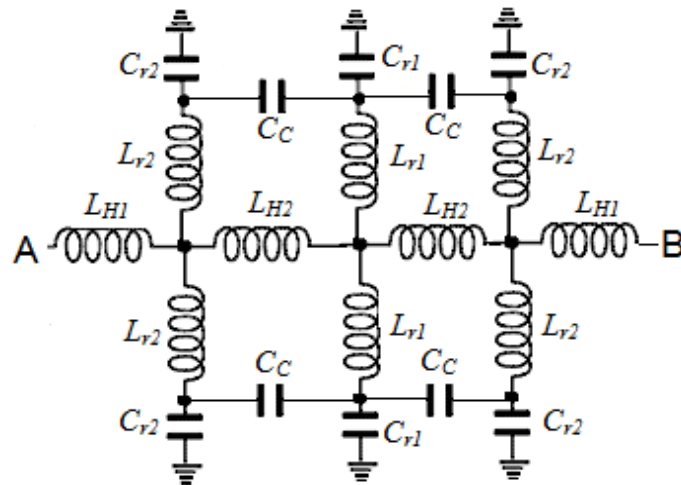


Fig. 5.11 L-C Equivalent circuit model of the filter with HPR and OPRs

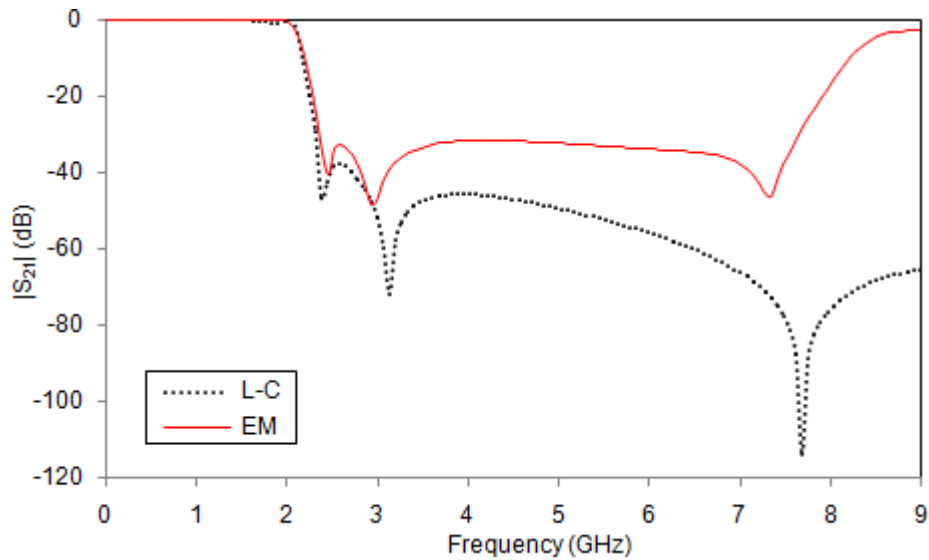


Fig. 5.12 L-C and EM simulation results of the filter HPR and OPRs

5.5 Parametric Analysis

There are many variables involved in the design of the filter. A detailed parametric study has been conducted by utilizing the effect of different component values in both equivalent circuit model and in EM model simulation. Practically, when the resonators are connected together on a high impedance transmission line, they form the compound resonator and transmission zeroes are contributed by the combined effect of all resonators and coupling between them.

5.5.1 HPR Parameters

Fig. 5.13 illustrates the simulated transmission characteristics of the filter corresponding to the change in the width of high impedance stub of HPR, w_1 . As shown in the figure, the position of the transmission zeroes has significant effect in changing w_1 .

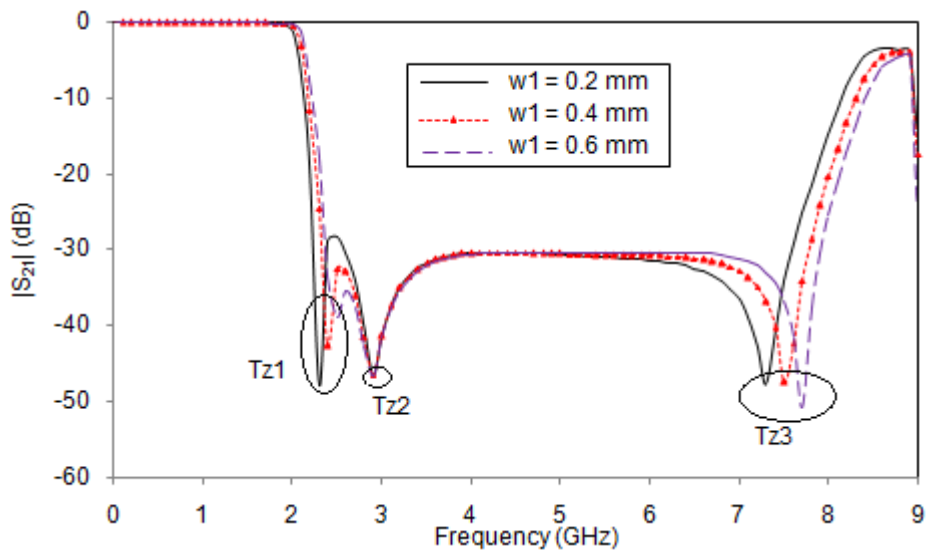


Fig. 5.13 $|S_{21}|$ characteristics of the filter as a function of width of high impedance stub of HPR, w_1

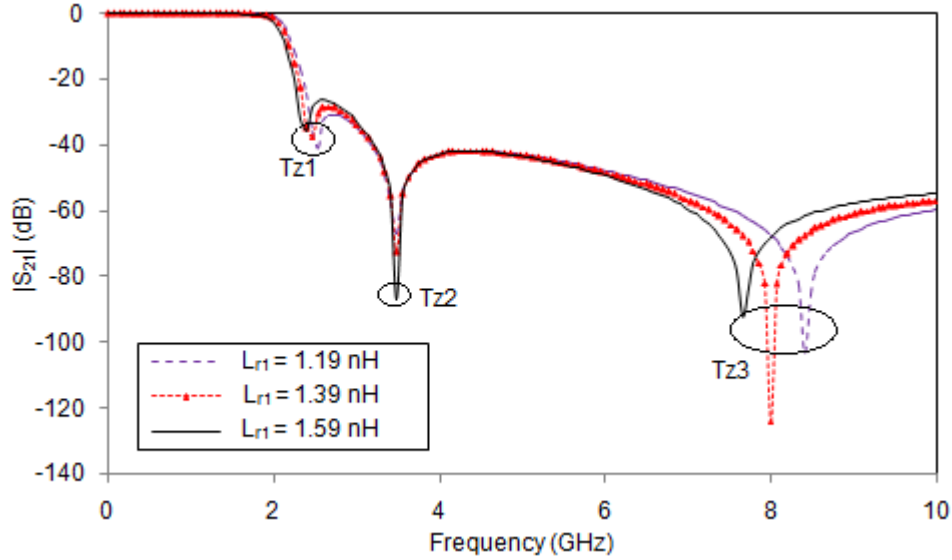


Fig. 5.14 $|S_{21}|$ characteristics of the filter as a function of inductance of high impedance stub of HPR, L_{r1}

As w_l varies from 0.2 mm to 0.6 mm, T_{Z1} shifts from 2.3 GHz to 2.5 GHz, and T_{Z3} shifts from 7.3 GHz to 7.7 GHz, whereas T_{Z2} remains at 2.9 GHz. This is because T_{Z1} is contributed by the combined effect of all resonators and the coupling between them and (5.3) is extracted as its resonant frequency f_{Z1} . Whereas T_{Z2} is contributed by the side resonators and its coupling with the centre resonator, and the resonant frequency f_{Z2} at T_{Z2} can be extracted as (5.4). Moreover, by changing w_l , the stopband suppression level of the filter in between T_{Z2} and T_{Z3} remains constant. This concept is proved by change in L_{r1} as demonstrated in Fig. 5.14. The calculated resonant frequencies corresponding to T_{Z1} and T_{Z2} are at $f_{Z1} = 2.362$ GHz and $f_{Z2} = 3.02$ GHz.

$$f_{Z1} = \frac{1}{2\pi\sqrt{2(L_{r2}C_{r2}+L_{r2}Cc)+L_{r1}C_{r1}+L_{r1}Cc}} \quad (5.3)$$

and

$$f_{Z2} = \frac{1}{2\pi\sqrt{2(L_{r2}C_{r2}+L_{r2}Cc)}}. \quad (5.4)$$

As shown in Fig. 5.15, the position of second transmission zero is also independent of HPR patch capacitance C_{r1} . However, the values of C_{r1} have a significant role in the design of the filter to achieve sharp roll-off rate with minimum passband insertion loss. Fig. 5.16 shows the passband insertion loss characteristics of the filter for different values of C_{r1} . As shown in the figure, for the decreasing values of C_{r1} , the transmission characteristics of the filter transforms to sharp elliptic function filter response with sharp roll-off rate and high passband ripple level. The optimum value of C_{r1} is 1.127 pF.

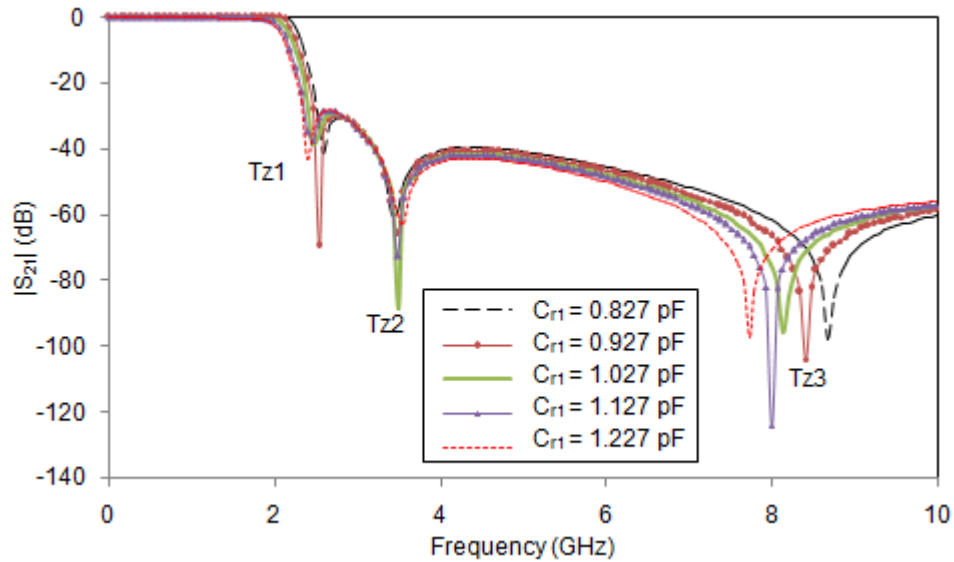


Fig. 5.15 $|S_{21}|$ characteristics of the filter as a function of HPR patch capacitance, C_{r1}

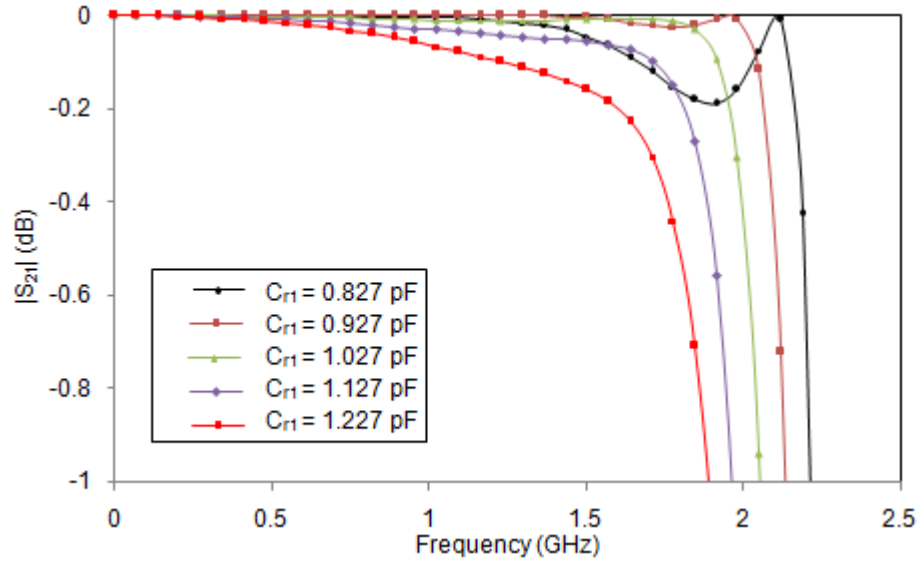


Fig. 5.16 Passband insertion loss characteristics of the filter as a function of HPR patch capacitance, C_{r1}

5.5.2 OPR Parameters

The dependence of the position of transmission zeroes with respect to the side resonator, OPR parameters is also verified and demonstrated with Figs. 5.17 and 5.18. Fig. 5.17 shows the simulated $|S_{21}|$ characteristics of the filter as a function of side resonator, OPR stub width, w_3 . As shown in the figure, the frequency of all the transmission zeroes T_{Z1} , T_{Z2} , and T_{Z3} is related to the side resonator (OPR) parameters. By increasing the value of w_3 , the impedance offered by the shorted stub of OPR decreases that decreases the effective inductance of the structure, which in turn shifts the transmission zero frequencies to a higher range. Also the same was proved by changing the OPR patch capacitance C_{r2} as shown in Fig. 5.18.

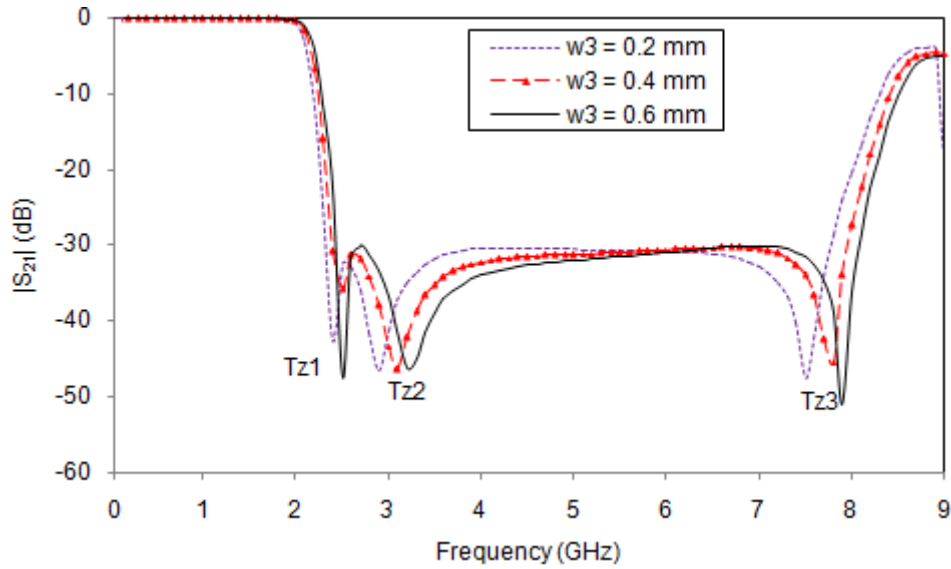
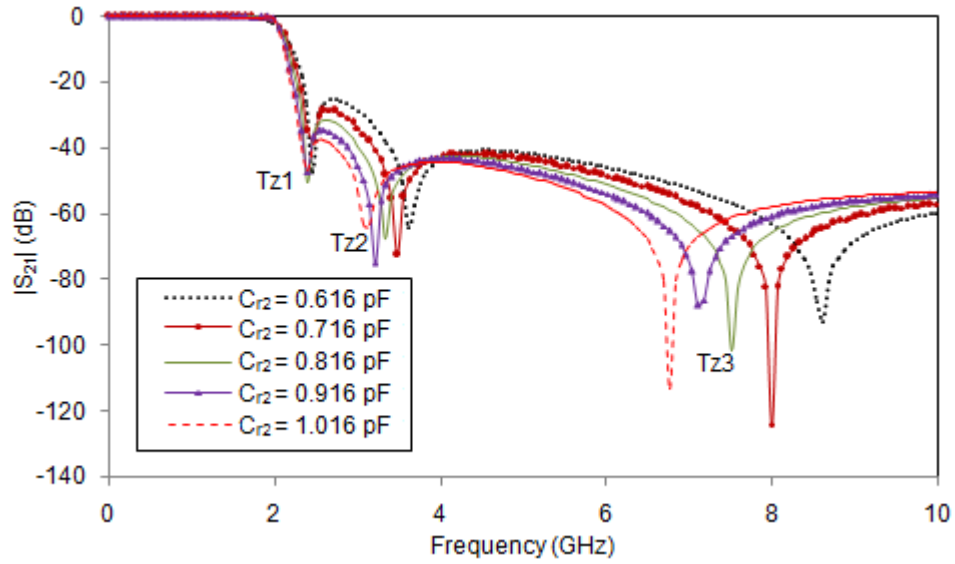
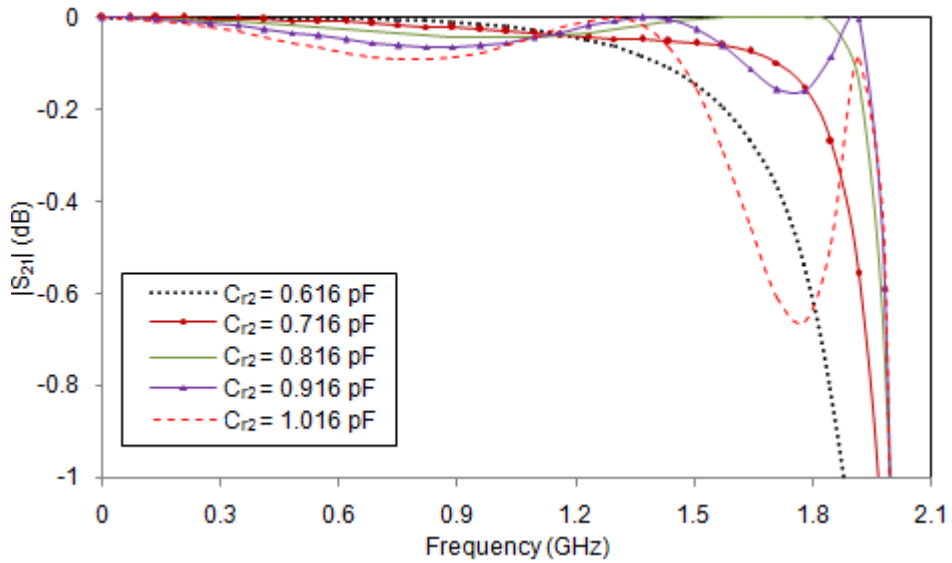


Fig. 5.17 $|S_{21}|$ characteristics of the filter as a function of width, w_3

Fig. 5.18 shows the insertion loss characteristics of the filter for different values of C_{r2} . As shown in Fig. 5.18(a), the stopband transmission zeroes are critically more affected the side resonator patch capacitance C_{r2} than centre resonator patch capacitance C_{r1} . Also, these figures demonstrate that the change in the capacitance is more severely affected by the position of T_{Z2} and T_{Z3} than the change in inductance. A 0.4 pF difference in C_{r2} produces a frequency difference of 1.845 GHz in T_{Z3} . Moreover, as shown in Fig. 5.18(b), the dependence of patch capacitance, C_{r2} on the selectivity and passband insertion loss has an inverse relation with the values of C_{r1} . The selectivity of the filter critically increases with increasing the value of C_{r2} , where the passband ripple approaches to a maximum level.



(a)



(b)

Fig. 5.18 $|S_{21}|$ characteristics of the filter as a function of OPR patch capacitance, C_{r2} , (a) Passband and stopband characteristics (b) Passband characteristics

Since a tradeoff exists between the roll-off rate or selectivity and passband insertion loss characteristics of the filter, by suitably selecting the capacitance of HPR and OPR resonant patches as $C_{r1} = 1.127$ pF and $C_{r2} = 0.716$ pF, we can design a compact lowpass filter with sharp roll-off rate of 137 GHz with very low passband insertion loss of 0.2 dB up to 1.7 GHz. The 3 dB cutoff frequency of the designed filter is at 2.07 GHz.

Figs. (5.19-5.21) show the current distribution characteristics of the filter at T_{Z1} , T_{Z2} and T_{Z3} respectively. As shown in Fig. 5.20, at T_{Z2} , the current is exactly concentrated at the side resonator, whereas at T_{Z1} and T_{Z3} the current is distributed among the centre and side resonators as shown in Figs. 5.19 and 5.21 respectively.

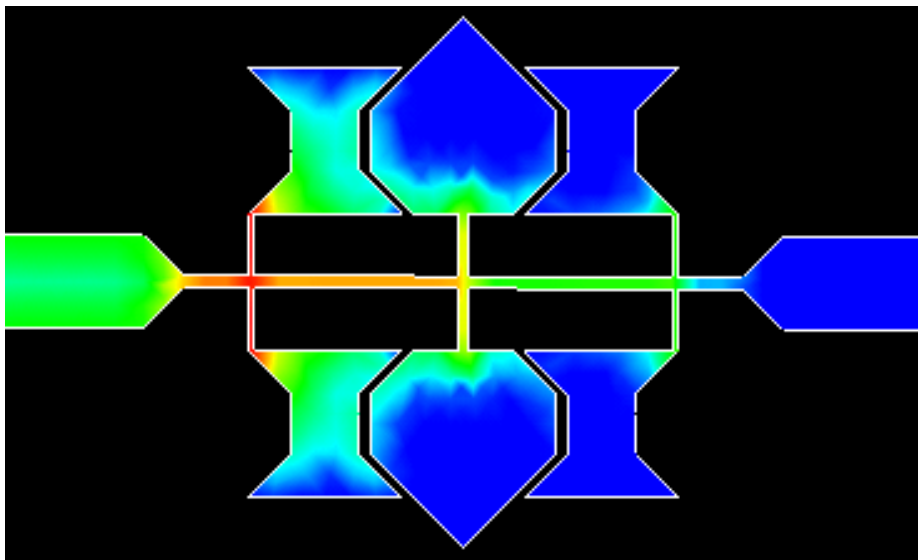


Fig. 5.19 Current distribution characteristics of the filter at $T_{Z1} = 2.32$ GHz

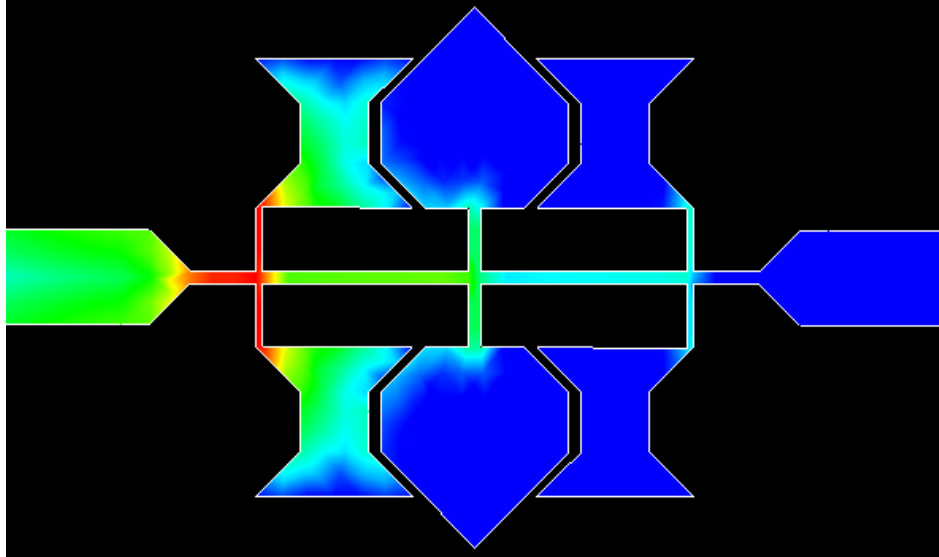


Fig. 5.20 Current distribution characteristics of the filter at $T_{Z2} = 2.9$ GHz

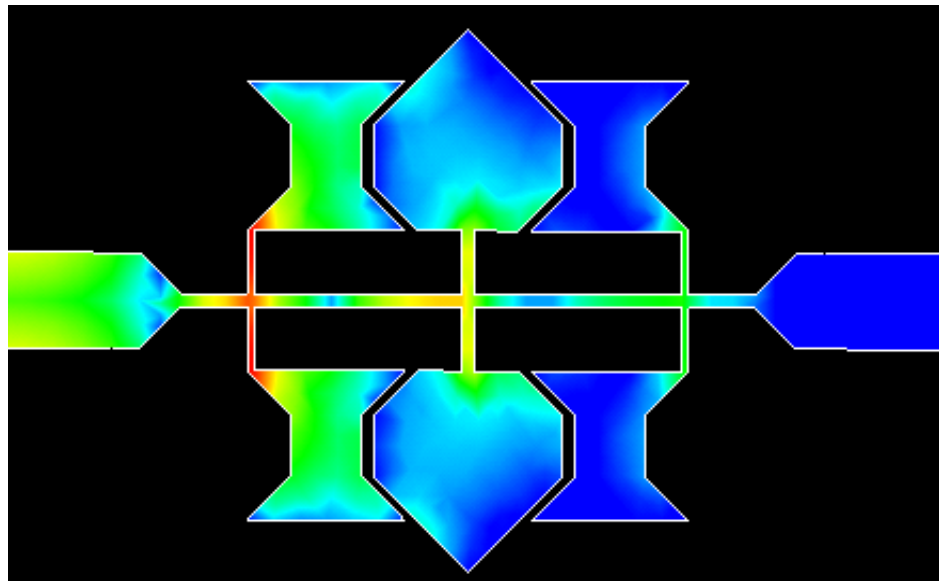


Fig. 5.21 Current distribution characteristics of the filter at $T_{Z3} = 7.75$ GHz

5.5.3 Width of Gap Size between HPR and OPR Patches, (g_1)

The selectivity, suppression level and stopband bandwidth of the filter can be tuned by adjusting the coupling gap g_1 between the HPR and OPR patches as demonstrated in Table 5.1. As g_1 increases, coupling between the resonant patches decreases and that deteriorates the roll-off rate of the filter with increase in the stopband suppression level. Also the stopband bandwidth of the filter decreases with the increase in the gap size.

Table 5.1 Filter characteristics as a function of g_1

| g_1 (mm) | f_L (GHz) | f_H (GHz) | SL (dB) | SSB (dB) | ξ (dB/GHz) | f_C (GHz) |
|---------------|----------------|----------------|--------------|---------------|-------------------|----------------|
| 0.2 | 2.11 | 8.22 | 27 | 6.11 | 126 | 1.975 |
| 0.4 | 2.27 | 8.02 | 30.3 | 5.75 | 94.4 | 2.09 |
| 0.6 | 2.37 | 7.88 | 33 | 5.51 | 79 | 2.16 |
| 0.8 | 2.43 | 7.79 | 36 | 5.36 | 70.8 | 2.19 |

g_1 = gap size, f_L = 20 dB lower cutoff frequency, f_H = 20 dB higher cutoff frequency, SL = Suppression Level, SSB = 20 dB Stopband Bandwidth, ξ = roll-off rate (20 dB), f_C = 3 dB cutoff frequency.

5.5.4 Width of High Impedance Transmission Line, (w_2)

Width of the transmission line plays an important role in the design of the filter structure. As the width of the line w_2 decreases, the impedance offered by the line increases, so that the cutoff frequency of the filter decreases together with an increase in the stopband bandwidth.

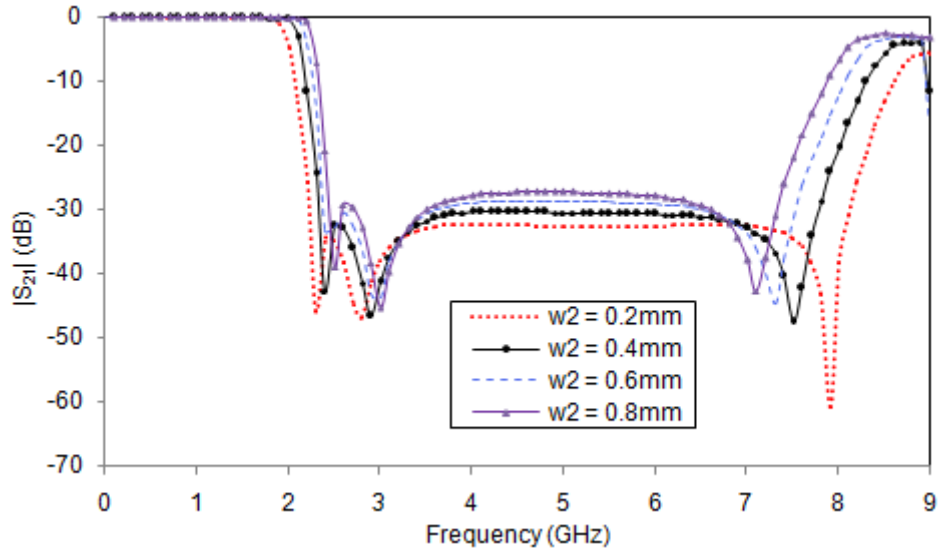


Fig. 5.22 $|S_{21}|$ Characteristics of the filter as a function of width of the transmission line, w_2

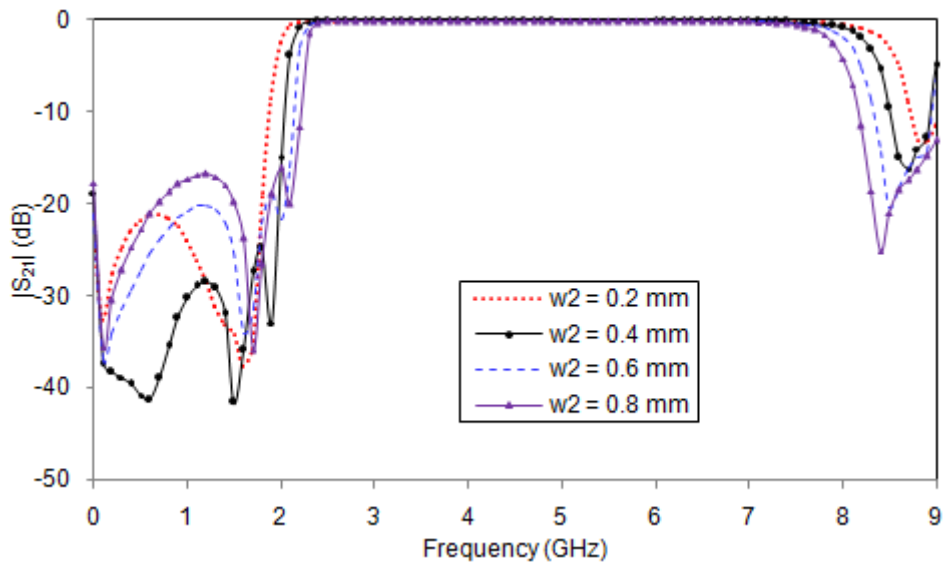


Fig. 5.23 $|S_{11}|$ Characteristics of the filter as a function of width of the transmission line, w_2

The stopband suppression level as well as the selectivity of the filter also increases with decrease in w_2 as demonstrated in Fig. 5.22. The width of the transmission line also affects the reflection characteristics as shown in Fig. 5.23. The optimum selected dimension of width of the transmission medium is $w_2 = 0.4$ mm corresponding to an impedance of 120Ω .

5.6 Measurement Results of Filter using OPR and HPR

As shown in Fig. 5.24, the measured results are in good agreement with simulated results. The filter achieves a stopband from 2.3 GHz to 7.77 GHz with suppression level better than 30 dB. Even though the filter consists of multiple resonators, the measured insertion loss of the filter is less than 0.2 dB in the passband up to 1.7 GHz with a 3 dB cutoff frequency of 2.07 GHz. Measured return loss of the filter is better than 19.5 dB in the entire passband and close to 1 dB in the upper end of the stopband. As illustrated in Fig. 5.25, the filter shows a constant group delay of 0.4 ns up to 1 GHz in the passband. Moreover, the filter achieves almost unity VSWR characteristics throughout the passband of the filter as demonstrated in Fig. 5.26. Fig. 5.27 shows the photograph of fabricated filter.

Excluding 50Ω feed line, normalized circuit size of the filter is $0.041207 \lambda_g^2$, where λ_g is the guided wavelength at cutoff frequency. Table 5.2 demonstrates the characteristics of the proposed filter and some published work in the literature. As shown in Table 5.2, the proposed filter shows the highest roll-off rate with suppression level 30 dB, even though the substrate is having highest thickness. The circuit size is slightly larger compared to the reported work in the literature due to the high permittivity and thickness of the substrate material.

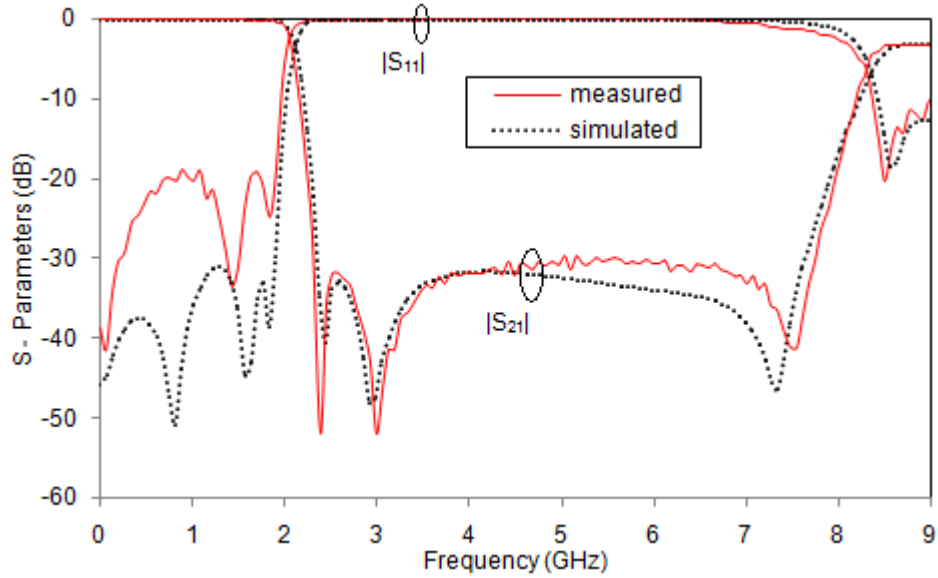


Fig. 5.24 Simulated and measured results of the proposed lowpass filter centre HPR and side OPRs

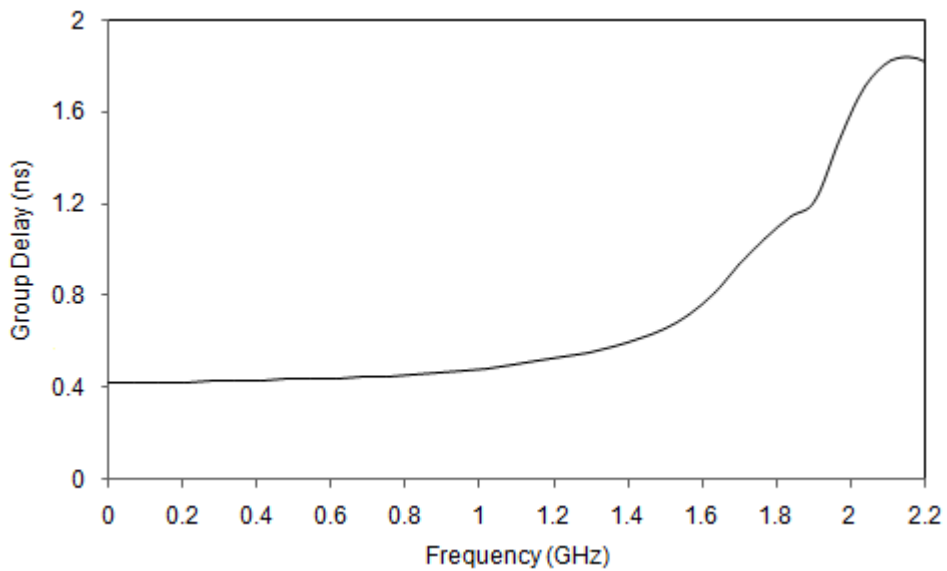


Fig. 5.25 Measured group delay characteristics the lowpass filter centre HPR and side OPRs

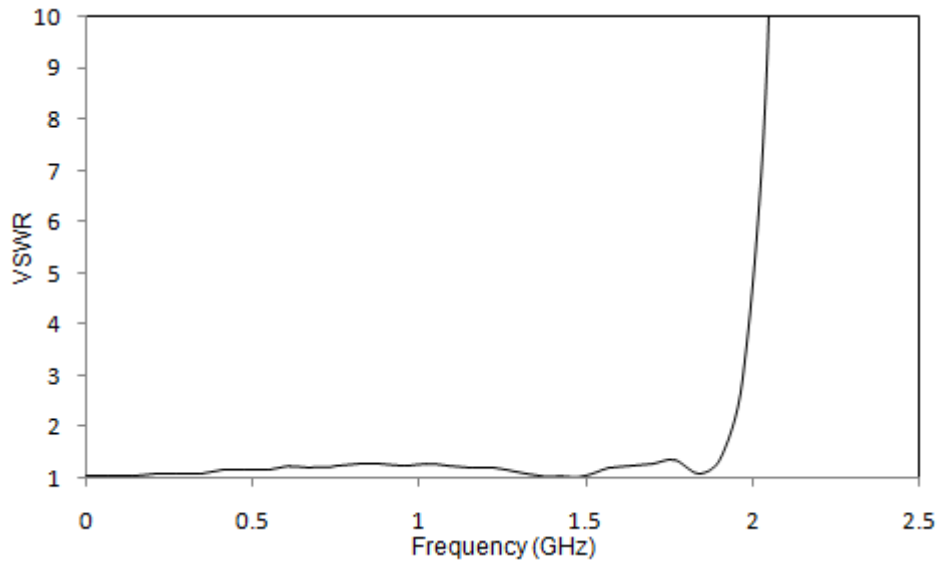


Fig. 5.26 Measured VSWR characteristics the lowpass filter centre HPR and side OPRs

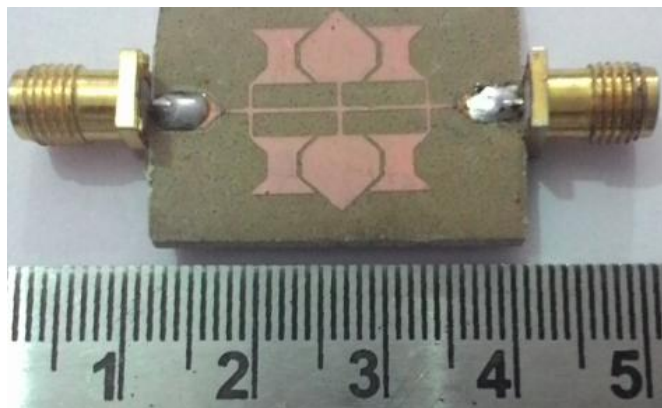


Fig. 5.27 Photograph of the proposed lowpass filter centre HPR and side OPRs

Table 5.2: Comparison of compact lowpass filter using centre HPR and side OPRs with previous work reported in the literature

| Ref. | ξ (dB/GHz) | SB (GHz) | SSL (dB) | ϵ_r, t (mm) |
|------------------|-------------------|------------------|-------------|-------------------------|
| [3] | 18 | 1.57–12.6 | 15 | 3.38, 0.508 |
| [4] | 94.9 | 2.06–18.83 | 23 | 2.2, 0.508 |
| [5] | 92.5 | 2.8–14.8 | 30 | 2.33, 0.784 |
| [6] | 63 | 3.32–21 | 20 | 2.2, 0.254 |
| [7] | 84 | 5.58–11.8 | 15 | 4.4, 1.6 |
| [8] | 90 | 2.55–7.03 | 16 | 4.4, 1.6 |
| [9] | 95 | 0.80–4.6 | 20 | 4.3, 1.58 |
| This work | 137 | 2.32–7.77 | 30 | 4.4, 1.6 |

ξ = roll-off rate at 40 dB attenuation level, SB = Stopband Bandwidth, SSL = Stopband Suppression Level, ϵ_r, t = permittivity and thickness of the substrate material, f_c = 3 dB cutoff frequency.

This work has been submitted to *IEEE Microwave and Wireless Component Letters* on April 2016 after second revision.

5.7 Conclusions

Compact planar elliptic function lowpass filter with sharp roll-off rate and very high stopband suppression level using different types of symmetrical octagonal shaped patch resonators has been designed and demonstrated. The suppression level and selectivity of the filter are enhanced by replacing the centre patch resonator with a heptagonal patch resonator. The filter structures are designed and developed on lossy FR4 substrate. The transmission and

reflection characteristics are further enhanced by using low loss, low cost ceramic filled PTFE substrate C-MET/LK4.3 having properties of FR4 with loss tangent 0.0018. The L-C equivalent circuit of the filter has been analyzed and validated with EM structural simulation results. The roll-off rate of the filter can be tuned to a specific range by adjusting the gap between the resonant patches. The prototype filter has the cutoff frequency of 2.07 GHz with passband insertion loss less than 0.2 dB. The filter exhibits a sharp roll-off of 137dB/GHz with stopband suppression level better than 30 dB. With these attractive results, the proposed filter has potential applications in modern communication systems.

Table 5.3. Comparison between performance of the filters discussed in this chapter

| Filter | f_c GHz | ξ dB/GHz | SIZE ₂ mm | NCS ₂ λg | RSB % | SL dB | PB IL dB | RL in PB/SB |
|--------|--------------|-----------------|-------------------------|---------------------------------|----------|----------|-------------------|------------------------------|
| I | 2.4 | 119 | 18.2x13.8 | 0.0385 | 72 | 30 | 0.7 (2.03 GHz) | < 17 in PB < 3 in SB |
| II | 2.07 | 108 | 18.2x17 | 0.0489 | 112.5 | 26 | 0.6 (1.7 GHz) | < 18 in PB < 2 in SB |
| III | 2.07 | 137 | 18.2x17 | 0.0412 | 108 | 30 | 0.2 (1.7 GHz) | < 19.5 in PB < 1 in SB |

- I Compact lowpass filter design using OPRs
- II Compact lowpass filter design using centre HPR and side OPRs using FR4 material having $\epsilon_r = 4.4$, $t = 1.6$ mm and $\tan\delta = 0.02$
- III Compact lowpass filter design using centre HPR and side OPRs using C-MET/LK 4.3 material having $\epsilon_r = 4.4$, $t = 1.6$ mm and $\tan\delta = 0.0018$

Table 5.3 demonstrates the performance characteristics of the developed compact lowpass filters discussed in this chapter.

References

- [1] Matthew N.O. Sadiku, *Principles of Electromagnetics*, Oxford University Press, New Delhi, India 2009.
- [2] K. Ma and K.S. Yeo, “New ultra-wide stopband low-pass filter using transformed radial stubs,” *IEEE Trans. Microw. Theory Tech.* vol. 59, no. 3, pp. 604–611 March 2011.
- [3] H. Cui, J. Wang and G. Zhang, “Design of microstrip low pass filter with compact size and ultra-wide stopband,” *IET Electron. Lett.*, vol. 48, no. 14, pp. 856 – 857, 2012.
- [4] M. Hayati, H. Asadbeigi, and A. Sheikhi, “Microstrip lowpass filter with high and wide rejection band,” *IET Electron. Lett.*, vol. 48, no. 19, pp. 1217–1219, 2012.
- [5] J. L. Li, S. W Qu and Q. Xue, “Compact microstrip lowpass filter with sharp roll-off and wide stop-band,” *IET Electron. Lett.*, vol. 45, no. 2, pp. 110–111, 2009.
- [6] M. Hayati, M. Gholami, H.S. Vaziri, and T. Zaree, “Design of microstrip lowpass filter with wide stopband and sharp roll-off using hexangular shaped resonator,” *IET Electron. Lett.*, vol. 51, no. 1, 2015.
- [7] P. M. Raphika, P. Abdulla, and P. M. Jasmine, “Compact lowpass filter with a sharp roll-off using patch resonators,” *Microw. and Opt. Tech. Lett.*, vol. 56, no. 11, pp. 2534–2536, 2014.
- [8] P.M. Raphika, P. Abdulla, and P.M. Jasmine, “Compact microstrip elliptic function lowpass filter with sharp roll-off and wide stopband by cascading multiple patch resonators,” in *Proc. IEEE International Microwave & RF Conference*, 2014, pp. 316–319.

- [9] V.K Velidi, S. Sanyal, “Sharp roll-off lowpass filter with wide stopband using stub-loaded coupled-line hairpin unit,” *IEEE Microw. Wireless Compon. Lett.*, vol. 21, no. 6, pp. 301–303, 2011.

Chapter 6

Compact Lowpass Filter with Ultra Sharp Roll-Off rate using Elliptical Patch Resonators

A compact elliptic function microstrip lowpass filter with ultra-sharp roll-off and wide stopband bandwidth using multiple stepped impedance patch resonators is presented. The structure consists of elliptical and modified rectangular shaped patch resonators, placed symmetrically on a high impedance central microstrip line. The 3 dB cutoff frequency of the filter is at 1.98 GHz. The measured results validate the simulated characteristics and exhibit an ultra-sharp roll-off of 289 dB/GHz and a wide stopband with an attenuation level better than 20 dB from 2.06 GHz to 13.6 GHz.

6.1. Introduction

In this chapter, a compact elliptic function lowpass filter with ultra-sharp roll-off rate and wide stopband bandwidth using multiple stepped impedance patch resonators is designed and developed for low cost applications. The structure consists of elliptical and modified rectangular shaped patch resonators, placed symmetrically on a high impedance central microstrip line. The filter is designed and fabricated using 1.6 mm thick PTFE ceramic filled substrate with a dielectric constant of 4.3 and loss tangent of 0.0018. The results demonstrates that the filter has a very sharp roll-off of 289 dB/GHz at 40 dB attenuation level and a wide stopband from 2.06 GHz to 13.6 GHz with a suppression level better than 20 dB. The 3 dB cutoff frequency of filter is at 1.98 GHz and has a compact size of 24 mm x 12.8 mm, which corresponds to the normalised circuit size of $0.2882\lambda_g \times 0.15375\lambda_g$, where λ_g corresponds to the guided wavelength at cutoff frequency.

6.2. Design of Stepped Impedance Patch Resonators

The proposed compact elliptic function lowpass filter is designed and investigated by loading multiple stepped impedance patch resonators (SI-PRs) on a high impedance microstrip line (HIML). The filter consists of an elliptical shaped centre patch resonator and multiple side patch resonators, where each resonator is designed by cascading high impedance short circuited stub and low impedance open circuited patches. The physical dimensions of these individual

components are shorter than the associated guided wavelength to approximate as semi-lumped elements and they together form a series L-C resonators [1].

6.2.1 Design of Elliptical Patch Resonator

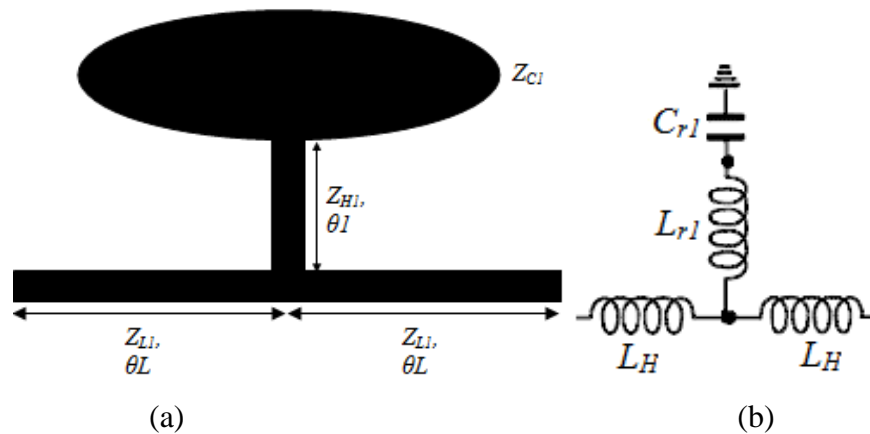


Fig. 6.1 (a) Geometry of the unit cell model of EPR, (b) L-C equivalent circuit

The unit cell model of centre patch resonator with its L-C equivalent circuit is shown in Fig. 6.1. The structure is designed with high impedance short circuited stub and low impedance elliptical shaped open circuited patch of characteristic impedances Z_{H1} and Z_{C1} respectively. The stub and patch are connected together to form a $\lambda_g/4$ elliptical patch resonator (EPR). For better performance, Z_{H1} should be greater than Z_0 and Z_{C1} less than Z_0 , where Z_0 is the characteristic impedance of the feed line. The resonance condition of the unit cell is determined by the impedance ratio $R_Z = Z_{C1}/Z_{H1}$ and the electrical length of the components [2].

Fig. 6.1(b) illustrates the equivalent circuit model of EPR, where the inductance, L_{r1} can be determined by Eq. (6.1) as:

$$L_{r1} = \frac{Z_{H1} \sin(\theta_1)}{2\pi fc} \quad (6.1)$$

where θ_1 is the electrical length of short circuited high impedance stub connected to the main transmission line and fc is the 3 dB cutoff frequency.

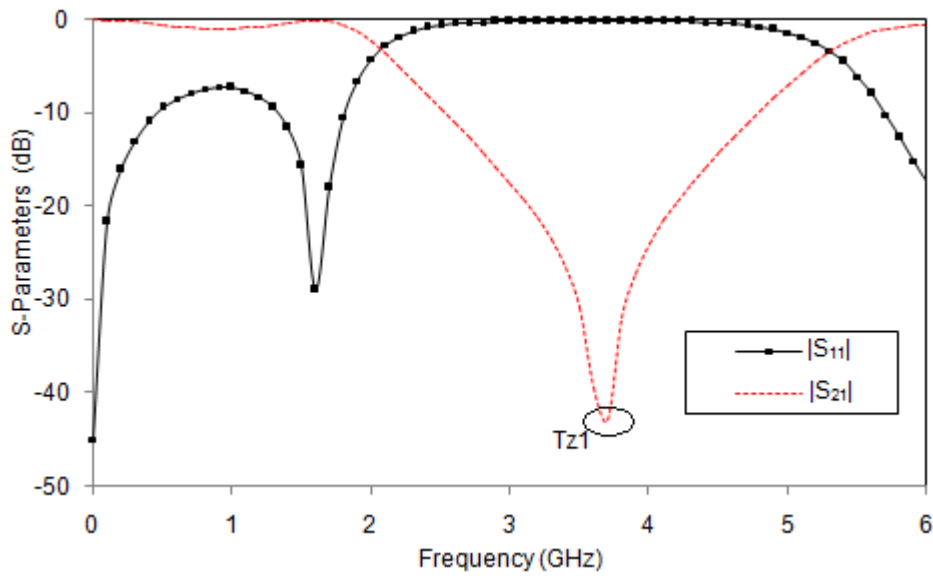


Fig. 6.2 Simulated S-Parameters of unit cell model of EPR

The capacitance, C_{r1} can be determined by one port S-Parameter using Eqs. (6.2)–(6.3) [3]. L_H is the inductance associated with the corresponding transmission line element.

$$C_{r1} = \frac{-1}{2\pi fc(\text{imag}(Z_{in}))} \quad (6.2)$$

where Z_{in} can be calculated as:

$$Z_{in} = 50 \left[\frac{1+S_{11}}{1-S_{11}} \right] \quad (6.3)$$

As shown in Fig. 6.2, the resonator possesses a single transmission zero, T_{Z1} located at 3.705 GHz.

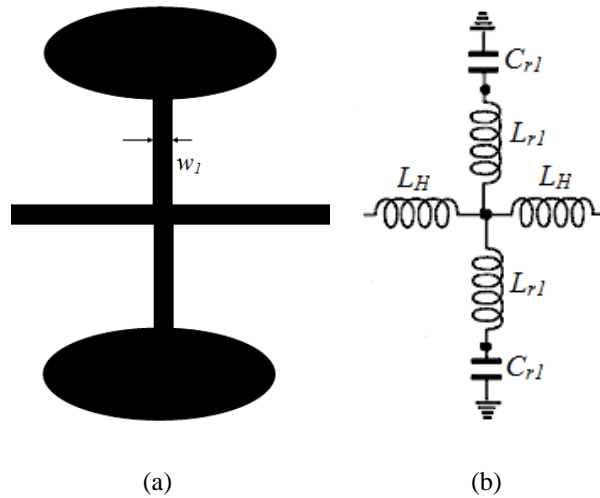


Fig. 6.3 (a) Geometry of $\lambda g/2$ EPR, (b) L-C equivalent circuit

The characteristics of the unit cell of EPR are greatly improved by loading symmetrically on HIML, that becomes a $\lambda g/2$ EPR as shown in Fig. 6.3(a). Fig. 6.3(b) shows the equivalent circuit model, where the two series L-C circuits are in parallel that decreases the overall impedance of the structure. The transmission zero T_{Z1} , shown in Fig. 6.2, can be adjusted by varying the width of the short circuited stub, w_1 without changing passband characteristics of the resonator. Fig. 6.4 illustrates the simulated S-Parameters of $\lambda g/2$ EPR as a function of w_1 .

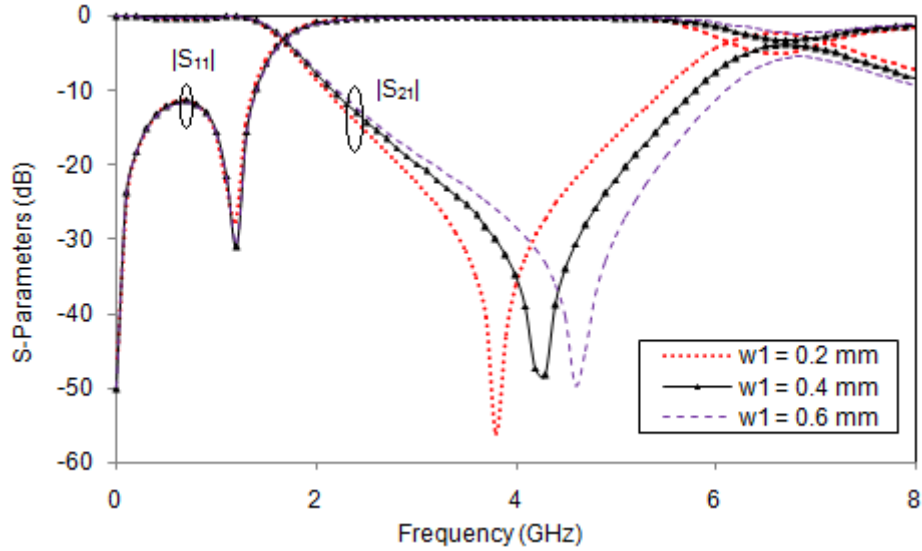


Fig. 6.4 Simulated S-Parameters of $\lambda g/2$ EPR as a function of the width of high impedance short circuited stub, w_1

6.2.2 Design of Modified Rectangular Patch Resonators

Figs. 6.5(a) and 6.5(b) demonstrate the layout of $\lambda g/4$ modified rectangular patch resonator (MRPR) and its L-C equivalent circuit. It is also designed with short circuited stubs and modified rectangular patches of characteristic impedance Z_{H2} and Z_{C2} with electrical lengths θ_1 and θ_2 respectively. The inductance L_{r2} and capacitance C_{r2} of these elements are also computed by Eqs. (6.1)–(6.3) with appropriate parameters. The dimensions and shape of the low impedance capacitive patches of MRPR are designed to make the whole structure compact and to provide better approximation of lumped capacitance [1].

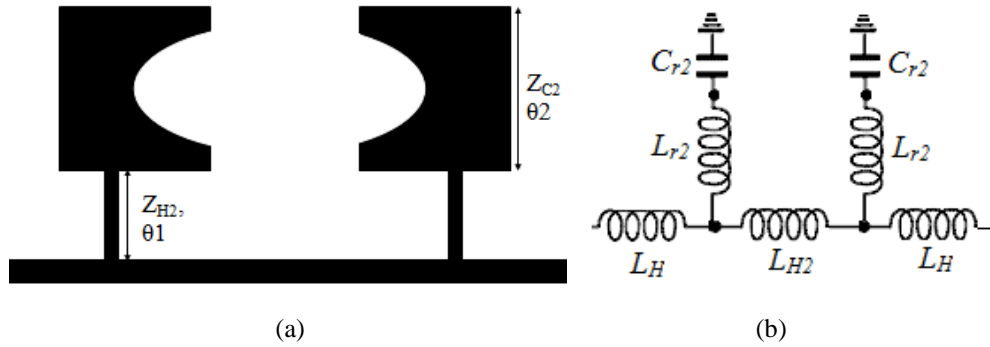


Fig. 6.5 (a) Geometry of unit cell model of MRPR, (b) L-C equivalent circuit

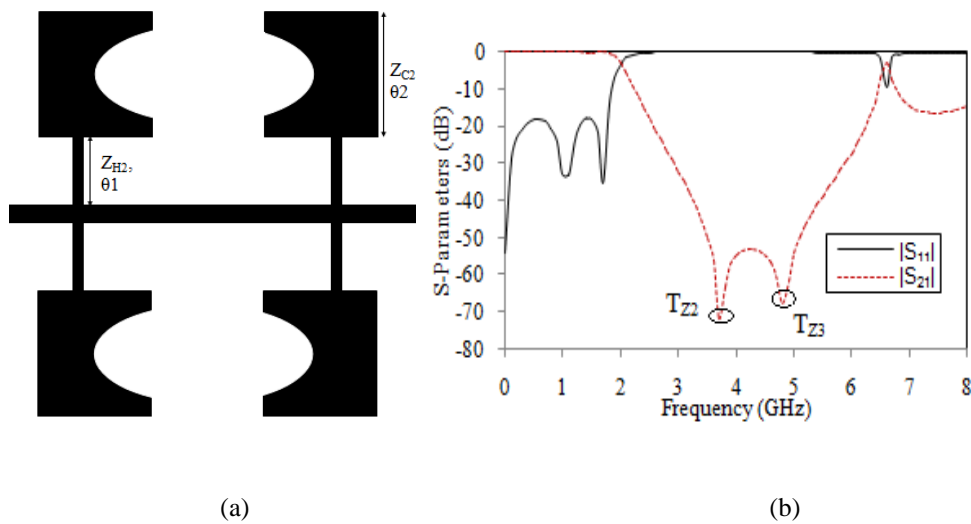


Fig. 6.6 (a) Geometry of $\lambda/2$ MRPR, (b) Simulated S-Parameters

The position of the high impedance stub loaded to the rectangular patch of MRPR will affect the response characteristics of the filter [4]. Figs. 6.6(a) and 6.6(b) illustrate the geometry and S-Parameter characteristics of $\lambda/2$ MRPR. As shown in Fig. 6.6(b), the filter with $\lambda/2$ MRPR shows two

transmission zeros, T_{Z2} at 3.7 GHz and T_{Z3} at 4.8 GHz. It also shows a better roll-off and high suppression level than with $\lambda_g/2$ EPR.

6.3. Design of Compact Lowpass Filter with Sharp Roll-off using SI-PRs

Observing the transmission characteristics of the individual resonators shown in Fig. 6.4 and Fig. 6.6(b), the attenuation level of each resonator increases after cutoff frequency and reaches the maximum at transmission zero frequency and starts decreasing just after the resonance. Investigations depict that by suitably loading EPR and MRPR on HIML as shown in Fig. 6.7(a), we can transform the resonator characteristics to an elliptic function lowpass filter with sharp roll-off of 242 dB/GHz at 20 dB attenuation level. The combined structure achieves a stopband bandwidth from 2.13 GHz to 6.66 GHz with a suppression level of 20 dB as shown in Fig. 6.7(b). The attenuation sustained at these frequencies is due to the multiple resonances contributed by the individual resonators and the coupling between them. As shown in the L-C equivalent circuit of both resonators as illustrated in Figs. 6.1(b) and 6.2(b), there exist series resonant branches in shunt that short out transmission at their resonant frequencies and contribute the elliptic function response with sharp attenuation pole near the cutoff frequency.

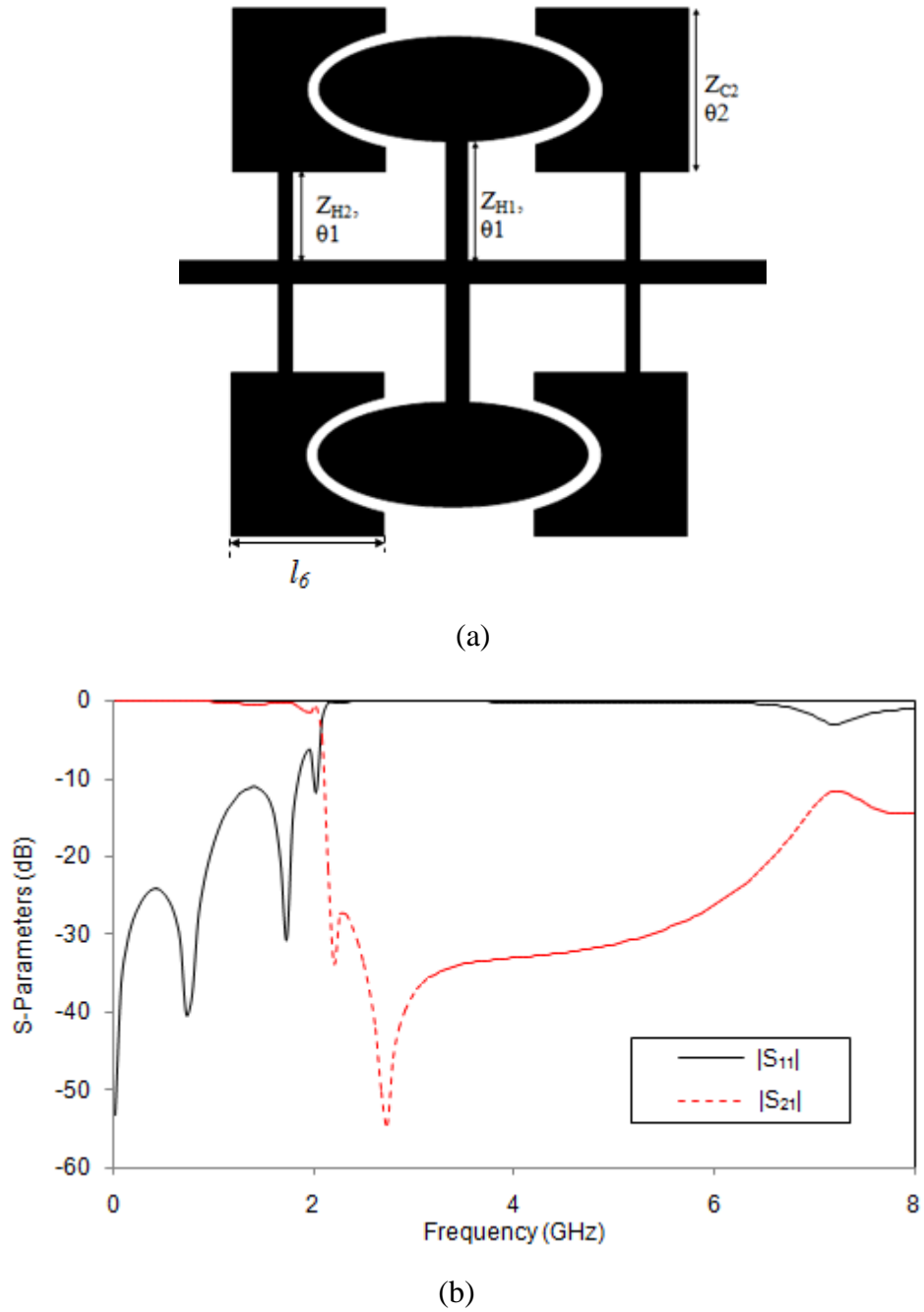


Fig. 6.7 (a) Configuration of lowpass filter with EPR and MRPR, (b) Simulated S-Parameters characteristics

The ripple level in the passband of the filter can be eliminated by suffering its roll-off rate by adjusting the size of capacitive patch of the MRPR. Fig. 6.8 demonstrates the effect of patch size that contributes the ripple level of the filter. As shown in the figure, as MRPR patch length l_6 decreases the selectivity of the filter increases, by suffering its passband ripple level. The roll-off rate at 20 dB attenuation level of the filter for $l_6 = 5.5$ mm is at 377.77 dB/GHz, and the same for $l_6 = 6.5$ mm is 283 dB/GHz.

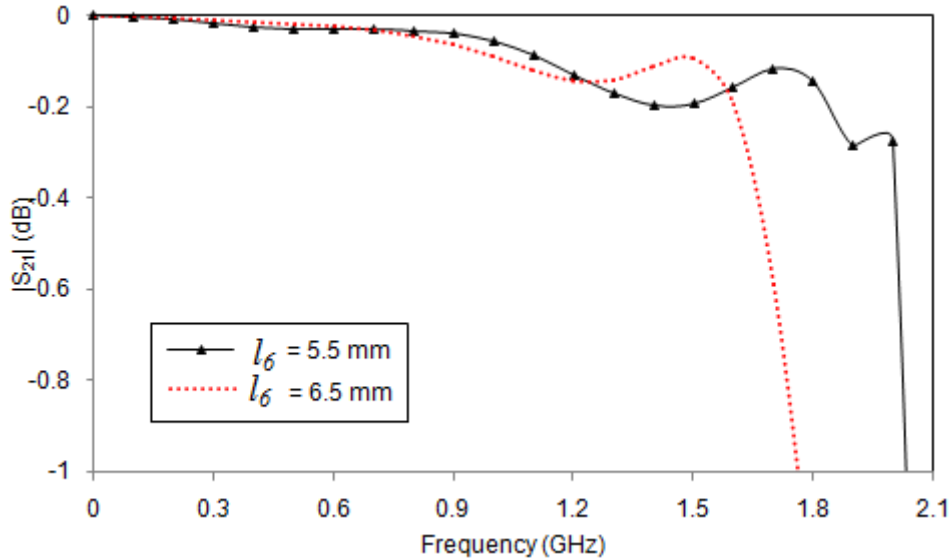


Fig. 6.8 Passband insertion loss characteristics of the filter as a function of MRPR patch length l_6

The stopband bandwidth of the filter can be enhanced to a great extent by introducing another resonator, square patch resonator (SPR), symmetrically to the HIML without increasing the overall filter dimensions. As shown in Fig. 6.9, the SPR also consists of high impedance short circuited stubs loaded with

square patches. SPR acts as suppressing cells that block high frequencies which enhances the stopband bandwidth. Cascading the patch resonators on HIML enhances the effective reactance of the circuit. The 50Ω feed lines are connected to 120Ω HIML via a tapered microstrip line that provides a good impedance matching and also reduces the parasitic effect due to the step discontinuity.

6.4. Simulation and Measurement Results of Proposed Filter

The proposed filter is designed and developed using 1.6 mm thick PTFE ceramic filled substrate having dielectric constant of 4.3 and loss tangent of 0.0018. Parameters of the filter are optimized using EM simulation software, Ansoft HFSS. The optimized dimensions in millimeters are: $l_1 = 1.7$, $l_2 = 4.2$, $l_3 = 5.5$, $l_4 = 2.1$, $l_5 = 4.2$, $l_6 = 6.5$, $l_7 = 1.4$, $l_8 = 9.24$, $l_9 = 0.7$, $h_1 = 4$, $h_2 = 2.2$, $h_3 = 2.84$, $h_4 = 1.4$, $h_5 = 2.72$, $h_6 = 0.41$, $h_7 = 2.1$, $w_1 = 0.4$, $w_2 = w_3 = 0.2$, $w_4 = 0.4$ and $g = 0.35$. Photograph of the prototype filter is depicted in Fig. 6.10. As shown in Fig. 6.11, simulated transmission characteristics are validated with experimental results obtained from R&S ZVL 13 vector network analyzer.

The measured 3 dB cut-off frequency of the filter is at 1.98 GHz and 40 dB attenuation frequency is at 2.108 GHz. The filter achieves a very sharp roll off of 289 dB/GHz at 40 dB attenuation level. It also possesses a wide stopband from 2.06 GHz to 13.6 GHz with a suppression level better than 20 dB. Since elliptic function filter has inherent ripples in the passband, the measured maximum ripple level in the passband is -2.2 dB at 1.8 GHz and -1.8 dB at 1.9 GHz. As shown in Fig. 6.12, the measured return loss in the passband is 12.2

dB at 1GHz and 5.6 dB at 1.8 GHz. The measured return loss in the stopband is 1.3 dB at 9.5 GHz and up to 5 dB in the upper end of the stopband.

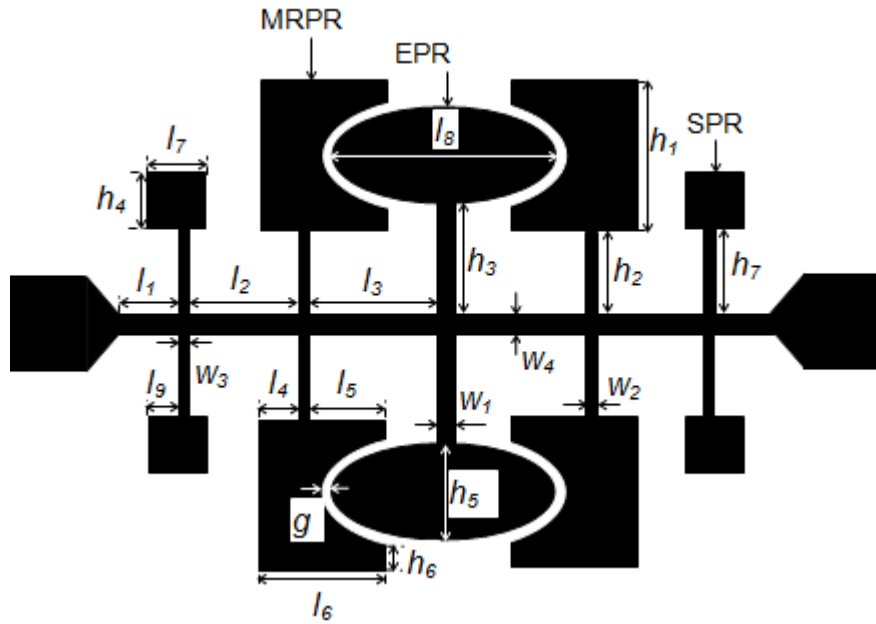


Fig. 6.9 Layout of the proposed lowpass filter using EPR with MRPR and SPR

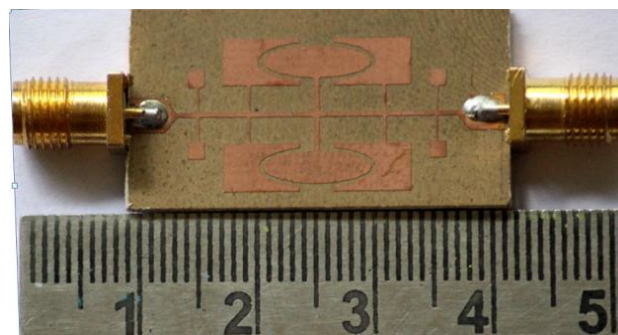


Fig. 6.10 Photograph of the prototype filter using EPR with MRPR and SPR

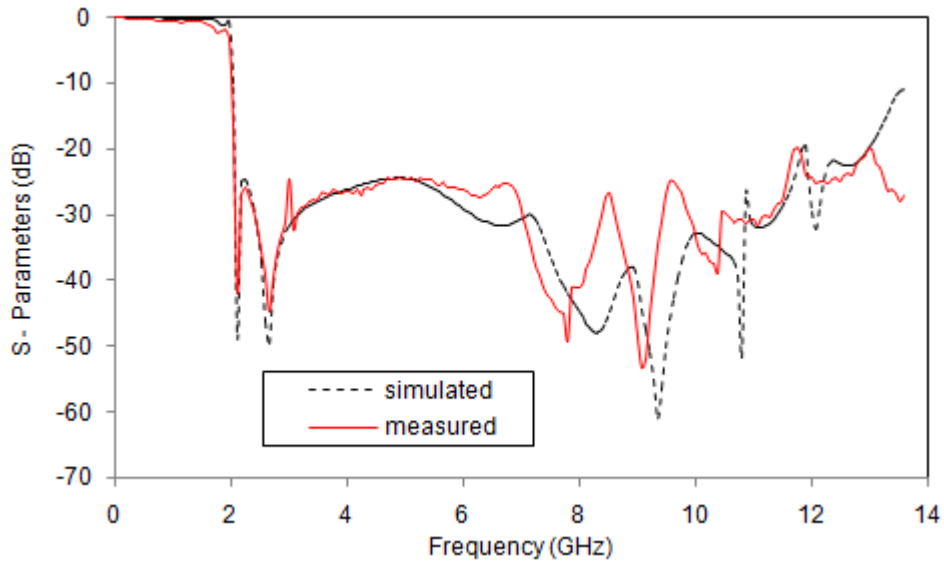


Fig. 6.11 Measured and simulated transmission characteristics of the filter using EPR with MRPR and SPR

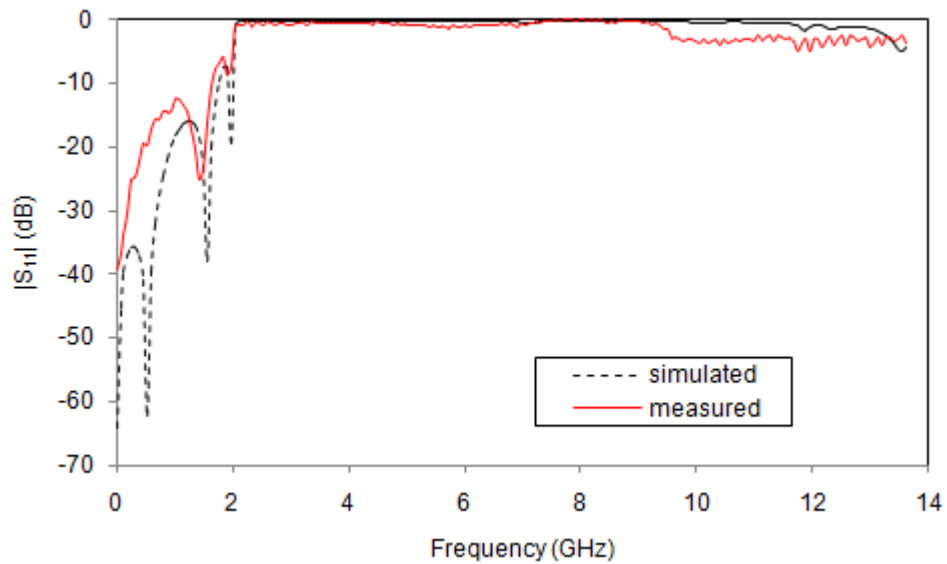


Fig. 6.12 Measured and simulated reflection characteristics of the filter using EPR with MRPR and SPR

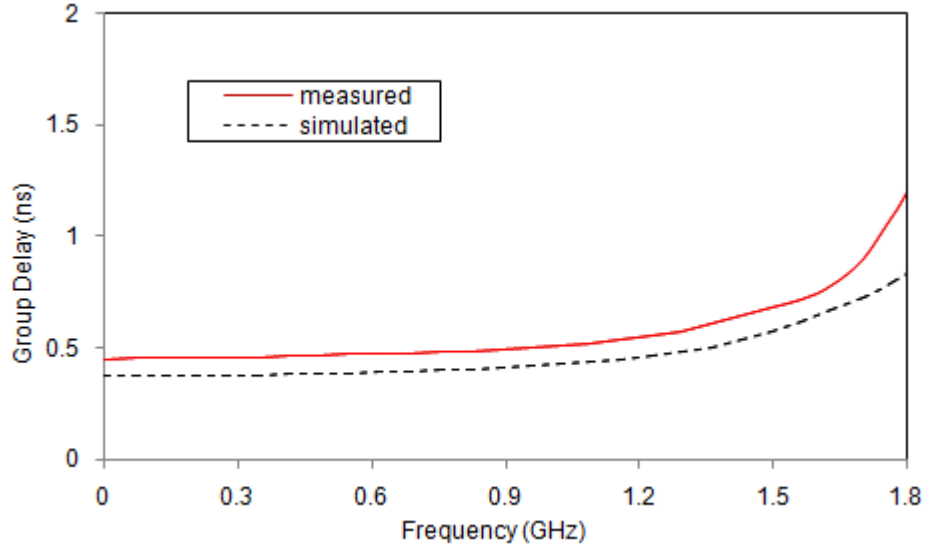


Fig. 6.13 Measured and simulated passband group delay characteristics of the filter using EPR with MRPR and SPR

Table 6.1 Performance comparison of performance of proposed lowpass filter with previously reported high performance lowpass filters.

| Refs. | ξ (dB/GHz) | RSB | NCS (λg^2) | SF | AF | FOM |
|-----------|-------------------|-------|--------------------------|-----|----|-------|
| [3] | 62 | 1.72 | 0.062 | 3 | 1 | 5160 |
| [5] | 130 | 0.933 | 0.0202 | 2 | 2 | 6004 |
| [6] | 92.5 | 1.355 | 0.0372 | 3 | 1 | 10106 |
| [7] | 36.3 | 1.323 | 0.0062 | 1.5 | 1 | 11543 |
| [8] | 95 | 1.407 | 0.022 | 2 | 1 | 12151 |
| [9] | 56.6 | 1.43 | 0.0242 | 2.5 | 1 | 8657 |
| [10] | 84.69 | 1.51 | 0.0223 | 2 | 1 | 11625 |
| This Work | 289 | 1.47 | 0.0443 | 2 | 1 | 19049 |

As illustrated in Fig. 6.13, each of the measured signal frequency components in the passband experiences nearly same delay, so that their phase relative to one another is maintained. The filter exhibits a uniform group delay of less than 0.5 ns up to 1 GHz in the passband. Excluding the microstrip feed line; the filter has a normalized circuit size of $0.2882 \lambda_g \times 0.15375 \lambda_g$, where λ_g is the guided wavelength at cutoff frequency.

Table 6.1 demonstrates the comparison results of the proposed work with similar works recently reported in the literature. In this table, ξ is the roll-off rate, RSB is the relative stopband bandwidth, NCS is the normalized circuit size, and these parameters can be determined using Eqs. (2.6-2.9) discussed in the Section 2.2 of Chapter 2. SF is the suppression factor, which is of 10 % of stopband suppression level in dB. AF is the architecture factor which is equal to one when the design is two dimensional and two when the design is three dimensional [10]. FOM is the figure of merit of the filter, which is defined as:

$$FOM = \frac{\xi \times RSB \times SF}{NCS \times AF} \quad (6.4)$$

As observed in the table, the proposed filter exhibits superior roll-off rate (289 dB/GHz) and high figure of merit (19049) among the quoted filters.

6.5. Conclusions

An elliptic function lowpass filter with ultra-sharp roll-off rate and wide stopband using multiple stepped impedance patch resonators has been studied and demonstrated. Both simulations and measurement results have been

presented and good agreement between them is achieved. The filter exhibits an ultra-sharp roll-off rate of 289 dB/GHz and a wide stopband with an attenuation level better than 20 dB from 2.06 GHz to 13.6 GHz. The cutoff frequency of the filter is 1.98 GHz and has a simple planar topology. The proposed lowpass filter with these specifications is a good candidate for modern day to day communication systems where the sharp switching characteristics and wide stopband are the main factors.

References

- [1] Hong, J.S. and M.J. Lancaster, *Microstrip Filters for RF/Microwave Applications*, Wiley, New York, 2001.
- [2] Makimoto, M. and S. Yamashita, *Microwave Resonators and Filters for Wireless Communications Theory, Design and Application*, Springer Series in Advanced Microelectronics, 2001.
- [3] Ma, K and K.S. Yeo, "New ultra-wide stopband low-pass filter using transformed radial stubs," *IEEE Transactions on Microwave Theory and Techniques*, Vol. 59, No. 3, 604–611, 2011.
- [4] L. Zhu and K. Wu, "Short–Open Calibration Technique for Field Theory-Based Parameter Extraction of Lumped Elements of Planar Integrated Circuits," *IEEE Trans. MTTs*, vol. 50, no. 8, 2002.
- [5] Mandal, M.K., Mondal, P., Sanyal, S. and A. Chakrabarty, "Low insertion-loss sharp-rejection and compact microstrip low-pass filters", *IEEE Microw. Wirel. Compon. Lett.*, vol. 16, no. 11, pp. 600–602, 2006.
- [6] J.L Li, Qu, S.W. and Xue, Q. "Compact microstrip lowpass filter with sharp roll-off and wide stop-band", *Electron. Lett.*, vol. 45, no. 2, pp.

110– 111, 2009.

- [7] J. Wang, L.J. Xu, Zhao, S. Guo, Y.X., and Wu, W.B.: “Compact quasi-elliptic microstrip lowpass filter with wide stopband”, *Electron. Lett.*, vol. 46, no. 20 , pp. 1384–1385, 2010.
- [8] V.K. Velidi, and S. Sanyal, “Sharp roll-off lowpass filter with wide stopband using stub-loaded coupled-line hairpin unit”, *IEEE Microw. Wirel. Compon. Lett.*, vol. 21, no. 6, pp. 301-303, 2011.
- [9] M. Mirzaee, and B.S. Virdee, “Realization of highly compact lowpass filter for UWB RFID applications”, *Electron. Lett.*, vol. 49, no. 22, pp. 1396–1398, 2013.
- [10] Hayathi, M., Gholami, M., Vaziri, H.S. and Zaree, T.: “Design of microstrip lowpass filter with wide stopband and sharp roll-off using hexangular shaped resonator”, *Electron. Lett.*, vol. 51, no. 1, pp. 69–71, 2015.

Chapter 7

Conclusions and Scope of Future Developments

This chapter highlights the results and achievements of the developed compact lowpass filter and discusses the scope of future works. Most of the proposed design techniques have been published in International Journals and Conferences.

7.1 Summary of Achievements

High performance compact lowpass filters with sharp roll-off rate and high suppression level are of great demand in modern communication system to suppress harmonics and spurious signals. Planar lowpass filter offers good electrical characteristics such as low insertion loss in the passband and high attenuation level in the stopband together with low cost, light in weight and ease of fabrication that make it suitable for RF and wireless applications. Prime objectives of the work are to design and develop planar compact lowpass filters with sharp roll-off rate and wide stopband bandwidth using low cost substrate materials. Since FR4 material offers good performance characteristics at low frequencies, most of the proposed filters in the thesis are designed and developed using glass epoxy FR4 material.

To realize a lowpass filter with sharp switching from passband to stopband for a given number of reactive elements, it is essential to generate infinite attenuation at finite frequencies. The proposed filters were designed and developed by cascading multiple patch resonators on high impedance microstrip line to execute such characteristics. Patch resonators offer high power handling capability and lower conductor loss compared to line resonators. The patch resonators were designed using high impedance short circuited stubs and low impedance open circuited patches; cascading these components form L-C series resonators. In the first stage of the filter design, we have designed and developed a compact lowpass filter (Filter I) by loading funnel patch resonator as the centre resonator and triangular patch resonator as side resonators symmetrically on a 96Ω transmission line. The L-C equivalent circuit model of the filter has been established with component values and the results were

validated with full wave EM model simulation results. Filter I achieves a sharp roll-off rate of 84 dB/GHz and relative stopband bandwidth (RSB) of 66.6 %. The cutoff frequency (f_c) of the filter is at 5.55 GHz. After conducting a detailed parametric analysis and by introducing some modifications in the filter structure, RSB of the filter (Filter II) is enhanced to 113 % with $f_c = 2.5$ GHz. The filter structure is further modified by introducing one more resonator near the feed line. The roll-off rate of the modified filter (Filter III) is enhanced to 125dB/GHz at the same cutoff frequency of Filter II. All the above mentioned filters were designed and developed on 1.6 mm thick FR4 substrate having permittivity 4.4 and loss tangent 0.02. As the thickness of the substrate material decreases, the impedance offered by the patch decreases which leads to a better approximation of lumped capacitance and produces high attenuation level at each transmission zero frequencies. This property is made to use in designing Filter IV with corrugated transmission line on FR4 substrate of 0.8 mm thickness. The RSB of the filter is 134% with stopband suppression level better than 31 dB by suffering its roll-off rate to 60dB/GHz.

Efforts to enhance the selectivity of the lowpass filter lead to the design of another class of compact lowpass filters using stepped impedance patch resonators (SI-PR) with very sharp attenuation near f_c . The design of the filter is started with two different types of SI-PRs as centre resonator and side resonators. The filter achieves a sharp roll-off rate of 90 dB/GHz at 20 dB attenuation level and RSB of 93.52% with stopband suppression level 16 dB. The L-C equivalent circuit model has extracted with component values and the results are validated with EM simulation results. After executing various parametric analyses, the centre resonator stub and patches are modified and

thereby improved the filter performances to a great extent. The filter structure is further reshaped with additional resonators and achieved the RSB of 126% with suppression level 23 dB.

Sharp selectivity with more than 25 dB suppression level is the demandable criteria for a lowpass filter used in modern practical communication systems. In light of this, we have developed another class of filters with octagonal patch resonator (OPR) as center and side resonators, with 30 dB suppression level 72% RSB. By replacing centre OPR with heptagonal shaped patch resonator (HPR), RSB of the filter is enhanced to 112% with suppression level 26 dB. The effect of loss tangent of the substrate plays an important role to determine the transmission and reflection characteristics of the filter, both in passband and stopband. We have studied the filter performance on a low loss material having same material properties with very low loss tangent. We obtained a passband insertion loss of 0.2 dB with sharp roll-off of 137dB/GHz by using a low loss, low cost PTFE ceramic filled substrate developed by CMET Trissur, Kerala, India. The RSB of the filter is 108% with suppression level better than 30 dB.

Finally, we have developed compact lowpass filter with an ultra-sharp roll-off of 289dB/GHz with RSB of 146% using elliptical shaped patch resonator (EPR) as centre resonator and modified rectangular patch resonator as the side resonator on ceramic filled PTFE substrate. The performance of all the developed filters is compared with the similar works reported in the literature. The filters presented in this thesis have much greater achievement than the same designed with high cost substrate materials.

7.2 Scope of Future Developments

Following is a list of several possible fields and problems related to the present work which can be investigated further.

- The present filters are designed and developed by loading multiple patch resonators on high impedance transmission line. The patch resonators are designed with high impedance stubs and low impedance patches. Higher the impedance of the stub, better the approximation of lumped inductance and that provides good performance characteristics. But, the impedance must not be so high that its fabrication becomes inordinately difficult to normal photolithographic process.
- Various studies demonstrate that, as the impedance of the transmission line increases, the roll-off rate and RSB of the filter get increased. In the present works, the gap between the centre and side resonators contributes the coupling capacitance, which also has a significant contribution for the selectivity of the filter. The performance of the filter can be improved to a great extent by decreasing the gap size. So we can further improve the filter performance for too narrow stub and lines with very small gap size by employing micro-machining technology.
- In the present works, the filters are designed using substrate material with permittivity of 4.4 and thickness of 1.6 mm. As we experienced in Chapter 3, the RSB and stopband suppression level of the filter can be improved by using substrate having 0.8 mm thickness. If we further

reduce the substrate thickness to a very small value (approximately 0.254 mm), we can enhance the stopband bandwidth in millimeter wave frequency range.

List of Publications and Honors

Publications

Related to the work reported in the thesis

1. **Raphika P.M.**, Abdulla P., and Jasmine P.M., "Compact wide stopband lowpass filter with high suppression using corrugated transmission line", *IOP Conference Series: Material and Engineering*, Vol. 120, No. 1, March 2016.
2. **Raphika P.M.**, Abdulla P., Jasmine P.M., "Planar Elliptic Function Lowpass Filter with Sharp Roll-off and Wide Stopband" *Microwave and Optical Technology Letters*. Vol. 58, No. 1, pp. 133-136, January 2016.
3. **Raphika P.M.**, Abdulla P., Jasmine P.M., "Compact Lowpass Filter with sharp roll-off using Funnel Patch Resonator" *Microwave and Optical Technology Letters*. Vol. 56, No. 4, pp. 2534-2536, 2014
4. **Raphika P.M.**, P. Abdulla and P.M. Jasmine," Compact Lowpass Filter with Extended Stopband Bandwidth", Accepted for Publication in *International Symposium on Antennas & Propagation, APSYM 2016*.
5. **Raphika P.M.**, P. Abdulla and P.M. Jasmine, "Planar Lowpass Filter with Sharp Roll-off Using Patch Resonators on High Impedance Microstrip Line," *IEEE RADIO 2015 International Conference*, Mauritius, Sept. 21-24, 2015, pp. 1-2.
6. **Raphika P.M.**, Abdulla P., Jasmine P.M., "Compact Microstrip Elliptic function Lowpass Filter with Sharp Roll-off and Wide Stopband by Cascading Multiple Patch Resonators," *Proc. of IEEE International Microwave & RF Conference (IMaRC)*, Bangalore, Dec. 2014, pp. 316-319.
7. **Raphika P.M.**, P. Abdulla and P.M. Jasmine, "Compact Planar Lowpass Filter with sharp roll-off and wide stopband using multiple patch resonators," *Proc. of International Symposium on Antennas & Propagation APSYM 2014*, Dec. 17-19, pp. 347-350.
8. **Raphika P.M.**, P. Abdulla and P. M. Jasmine, "Compact Microstrip Lowpass Filter with sharp roll-off and wide stopband using multiple resonators," *Proceedings of Asia Pacific Microwave Conference*, Sendai, Japan , Nov. 4-7, 2014, pp. 1229-1231.

-
-
9. **Raphika P.M.**, P. Abdulla and P.M. Jasmine, "Compact Planar Lowpass Filter with Sharp Roll-off using Patch Resonators," *SPECTRUM 2014, UGC Sponsored National Seminar on Future of Electromagnetic Communication and Materials, Govt. College, Palakkad.*
 10. Divya Mohan, Abdulla P., **Raphika P.M.**, Arya, "Planar Lowpass Filter With Razor- Sharp Roll-off Using Patch Resonators," *UGC Sponsored National Conference on Recent Advances in Microwave Communication NCMWC2015, 11-12 August 2015.*

Related to the work reported in the thesis

1. A.R Anu, P. Abdulla, P.M. Jasmine and **Raphika P.M.**, "Semicircular Aperture Coupled Hemispherical Dielectric Resonator Antenna", *International Journal of Advances in Microwave Technology*, VOL.1, No. 2, pp..53-57, 2016.
2. P.M. Jasmine, P. Abdulla and **P.M. Raphika**, "Coupling Enhancement of Waveguide fed HDRA using Steps" *International Journal of Scientific Progress and Research*", Vol. 25, No. 2, pp. 78-80, July 2016.
3. Ami Iqbal, Abdulla P., Rekha T.K., Anu A.R. P.M. Jasmine, **P.M. Raphika**, " A Novel Bandpass Filter using dual mode chamfered square Patch Resonator with diamond shaped slots", *Accepted for Publication in International Symposium on Antennas & Propagation, APSYM 2016.*
4. P.M. Jasmine, P. Abdulla, and **P.M. Raphika**, "Tapered Waveguide fed Cylindrical Dielectric Resonator Antenna," *Accepted for Publication in Loughborough Antennas and Propagation Symposium, LAPC 2016.*
5. P.M. Jasmine, P. Abdulla and **P.M. Raphika**, "Analysis and experiment of stair shaped waveguide fed dielectric resonator antenna", *IET Microwaves Antennas and Propagation*, Vol. 10, No. 4, pp. 453-458, 2016.
6. P.M. Jasmine, P. Abdulla and **P.M. Raphika**, "Rectangular Waveguide fed DRA Using Tapered Waveguide Section" *Microwave and Optical Technology Letters*. Vol. 57, No. 9, pp. 2025-2028, 2015.

7. P.M. Jasmine, P. Abdulla and **P.M. Raphika**, "Double step junction coupled waveguide fed dielectric resonator antenna", *IEEE International Conference on Advances in computing and Communications, (ICACC)*, Kochi, Sept. 2015, pp. 297-300.
8. P.M. Jasmine, P. Abdulla, and **P.M. Raphika**, "Theoretical Analysis of Double Step Junction Coupled Waveguide fed DRA," *International Symposium on Antennas & Propagation, APSYM 2014*, Dec. 17-19, pp-241-242.
9. Abdulla P, Jasmine P.M. and **Raphika P.M.**, "Waveguide-fed Cylindrical DRA: Wide-Band Design" *IEEE International Symposium on Antennas and Propagation (ISAP), Kaohsiung, Taiwan Dec.2014*, pp. 241-242.
10. P.M. Jasmine, P. Abdulla, and **P.M. Raphika**, "Coupling Enhancement of waveguide fed Dielectric Resonator Antenna using Tapered Section of waveguide," *Poceedia Computer Science (ICICT)* Dec. 2014, Vol. 46, 2015, pp. 1278-1284.
11. P.M. Jasmine, P. Abdulla, and **P.M. Raphika**, " A Novel Technique of Coupling Enhancement of Waveguide fed Dielectric Resonator Antenna," *SPECTRUM 2014,UGC Sponsored National Seminar on Future of Electromagnetic Communication and Materials, Govt. College, Palakkad.*
12. P.M. Jasmine, **P.M. Raphika**, P. Abdulla, "MoM Analysis of Waveguide fed Dielectric Resonator Antenna," *UGC Sponsored National Seminar*, Sree Ayyappa College, Eramallikkara, Alappuzha December 2013.

Honors

- Third Prize for the Best Student Paper Award in IEEE Radio and Antenna Days of Indian Ocean 2015, (IEEE RADIO 2015), 21-24 September 2015, Belle Mare, Mauritius.
- In the board of reviewers of Frequenz Journal. ISSN: 0016-1136 (Print), 2191-6349 (Online)
- In the board of reviewers of IETE Journal of Research ISSN: 0377-2063 (Print), ISSN: 0974-780X (Online)

